UNIVERSITÀ DI PARMA

UNIVERSITA' DEGLI STUDI DI PARMA

Ph.D in Biotechnology and Life Sciences

XXXI cycle

Identification of cellular targets and molecular action mechanism of newly synthesized metal complexes

Coordinator of the Ph.D Program:

Prof. Simone Ottonello

Scientific Tutor:

Dr. Annamaria Buschini

Ph.D student: **Serena Montalbano**

2015-2018

Table of contents

Abstract

The end goal of this project is the study of the biological activity of newly synthesized compounds, members of the class of thiosemicarbazones. They are widely studied for their pharmaceutical properties and possess antitumor, antibacterial, antifungal and antiviral activities.

This research can be divided into two sections.

In the first one, the aim was to identify thiosemicarbazone derivates as antifungal agents. This part belongs to the "Aflatox project", which purpose is the design and the synthesis of new types of inhibitors of proliferation and aflatoxins production of *Aspergillus flavus*. In this context, we studied the cytotoxic and genotoxic activities of antimycotoxigenic molecules on human healthy cell lines.

In the second one, the aim was to identify thiosemicarbazone derivates as anticancer agents. In particular, we focused on the biological activity of citronellal thiosemicarbazones coordinated with three different metals: nickel, platinum and copper. We performed *in vitro* studies on human cancer cell lines and on primary tumour samples to identify metal complex cytotoxic and genotoxic activities. In addition, we analysed specific cellular pathways after the treatment with the compounds in order to identify their cellular targets and molecular action mechanisms.

Furthermore, all the results were used to evaluate their structure/activity relationships.

1. Introduction

1.1 Strategies for drug design and synthesis

The first aim of medicinal chemistry is the design, synthesis and development of new drugs with improved properties and diminished side-effects for the treatment of human diseases. This is a complicated and lengthy process involving other disciplines, such as organic chemistry, biology, pharmacology, drug metabolism, and clinical research.

The advent of molecular biology and genomic sciences is having a profound impact on drug discovery: the knowledge about molecular mechanism involved in a specific disease could help the conventional methods of drug discovery.

The Food and Drug Administration (FDA) defines a drug as "a substance recognized by an official pharmacopoeia or formulary and intended for use in the diagnosis, cure, mitigation, treatment, or prevention of disease". Biological products are also included within this definition. Molecules for pharmacological applications are most often small organic compounds, that are complementary in shape and charge to the biomolecular target with which they interact and therefore will bind to it. In the recent years, also inorganic and organometallic compounds are used in drug discovery processes (Polêto *et al*., 2018).

The activity of a molecule varies by its structure. It is necessary to draw attention to properties such as lipophilicity, solubility, and permeability, that can ensure optimal potency, in addition to selecting the candidate compounds with appropriate physicochemical properties (Arnott *et al*., 2013).

The lipophilicity of a molecule is a key property, that refers to its affinity in a lipophilic environment. It drives the transport of drugs, including intestinal absorption, membrane permeability, protein binding, and distribution among different tissues. One of the most reliable methods in medicinal chemistry to improve *in vitro* activity is to incorporate properly positioned lipophilic groups. On the contrary, it is generally difficult to improve *in vitro* potency by manipulation of the polar groups. In the drugs, polar groups can be modified only when they are not required for the receptor binging. Too many hydrogen bond acceptor groups also hinder permeability across a membrane bilayer (Lipinski *et al*., 2001).

Evaluation of druglikeness is based on Lipinski's rules (Lipinski *et al*., 2004), that describe molecular properties of a compound required for estimating important pharmacokinetic ADME (Absorption, Distribution, Metabolism and Excretion)parameters, such as molecular weight; Log P; the number of H-bond donors and the number of H-bond acceptors. The cut-

offs for each of the these parameters were all close to 5 or a multiple of 5. Poor absorption or permeation are more likely when:

- There are more than 5 H-bond donors (expressed as the sum of OHs and NHs);
- The molecular weight is over 500;
- The Log P is over 5;
- There are more than 10 H-bond acceptors and donors.

Compound classes that are substrates for biological transporters are exceptions to the rule (Lipinski *et al*., 2001).

The rule is useful during lead optimization to increase the activity and selectivity of a likely drug candidate (Ertl *et al*., 2000). Other molecular properties like number of rotatable bonds, number of heavy atoms, can also be calculated.

Heterocyclic compounds bearing nitrogen and sulphur atoms have been the major molecules in organic chemistry because of their remarkable pharmaceutical activities, especially their anticancer properties.

The biological activity of a ligand enhances after the coordination with transition metals. One efficient strategy to improve complex stability is to incorporate strong donor ligands that generate stable metal-ligand bonds resistant to physiological reductants and nucleophiles (e.g. -SH, $-NH_2$).

Furthermore, chirality is an important tool in modern drug development since the molecular recognition of chiral biological targets can provide insight into the design of new active drugs. This is not valid for organic drugs and for metal-based drugs in which the enantiomeric resolution becomes necessary for their medicinal applicability. Metal compounds are isomeric. There are two or more structures sharing the same molecular composition but with a different spatial orientation (Wang *et al*., 2018).

QSAR modeling is an important approach in drug discovery that correlates molecular structure with biological and pharmaceutical activities.

Despite the accessibility of several anticancer drugs, common problems like multi-drug resistance, less therapeutic efficacy, solubility, adverse side effects, and/or poor bioavailability issues necessitate the development of new anticancer agents. There is an increased demand for newer and safer anticancer agents.

1.2 Transition metals as anticancer agents

There is a strong relationship between metals and cancer given that metals can play a dual role in the cells. Some, such as zinc, copper, iron and manganese, are essential cellular components and are involved in several biological processes; others, such as nickel, cadmium and chromium, are considered as mutagenic and carcinogenic and are associated with tumour induction and progression (Marloye *et al*., 2016).

Since cisplatin discovery, different metal compounds have demonstrated efficacy in cancer treatment and their therapeutic potential has attracted a lot of interest. Metals used in cancer therapy are elements of periodic table *d* block, including groups III-XII. Elements of platinum (Pt) and copper (Cu) groups are the most studied, followed by palladium (Pd), gold (Au), iron (Fe), zinc (Zn), cobalt (Co), nickel (Ni), and osmium (Os) (Marloye *et al*., 2016). All of these elements represent the group of noble metals in oncology therapy.

The therapeutic potentials of metal-based compounds are due to chemical characteristics of metals, such as redox activity, Lewis acid properties and charge.

First, chemical reactivity is determined by the oxidation state ranging from +1 to +8. Inside cells, transition metals can take part in oxidation and reduction reactions. Furthermore, oxidation state allows the participation in biochemical redox catalysis and endows prodrug effects (Thompson *et al*., 2003; Frezza *et al*., 2010). The metal reduction to a lower oxidation state by biological molecules can lead to several active chemical species co-existing in cells, with different mechanism of action. Studies demonstrate that platinum (Wu *et al*., 2015), ruthenium (Harris *et al*., 2009), cobalt (Munteanu *et al*., 2015) and gold (Graf *et al*., 2012) can have prodrug effects (Marloye *et al*., 2016).

Electronic and magnetic properties of transition metal complexes depend on the number of electrons in *d* shell orbitals (Haas *et al*., 2010). In aqueous solution, metal ions exist as positively charged species but can generate cationic, anionic or neutral species as a result of coordination with several ligands (Haas *et al*., 2010; Ndagi *et al*., 2017).

With regards to the coordination with the ligand, metal-based anticancer drugs present two important features. On the one hand, metals can coordinate several organic and inorganic ligands in a three-dimensional configuration and in a wide range of coordination geometries that give them unique shapes. The metal and its oxidation state define the bond length, bond angle and coordination site (Haas *et al*., 2010). On the other hand, the ligands can be used to maximise metal pharmacological and physicochemical properties. In some

cases, this can lead to improved specificity and greater control of drug release (Frezza *et al*., 2010). The hydrophilic or lipophilic features of the ligands affect their ability to cross the plasmatic membrane and the blood brain barrier (Duncan *et al*., 2012; Hambley, 2007). Sometimes, it could be difficult to distinguish among the effects of the metal or of the ligand or their synergic activity. In order to overcome this issue, ligands and complexes should be tested separately (Marloye *et al*., 2016).

All of these properties have allowed the design and the synthesis of metal based compounds with therapeutic and, in particular, anticancer activity. Metal complexes can interact with several biological targets: nucleic acid, such as DNA and RNA, amino acids and proteins, especially enzymes and cytoskeletal proteins, mitochondria and their membrane proteins. Targets may also be several biological processes, such as cell cycle, gene expression regulation, cellular metabolism and cell death mechanisms (Marloye *et al*., 2016) (Fig.1).

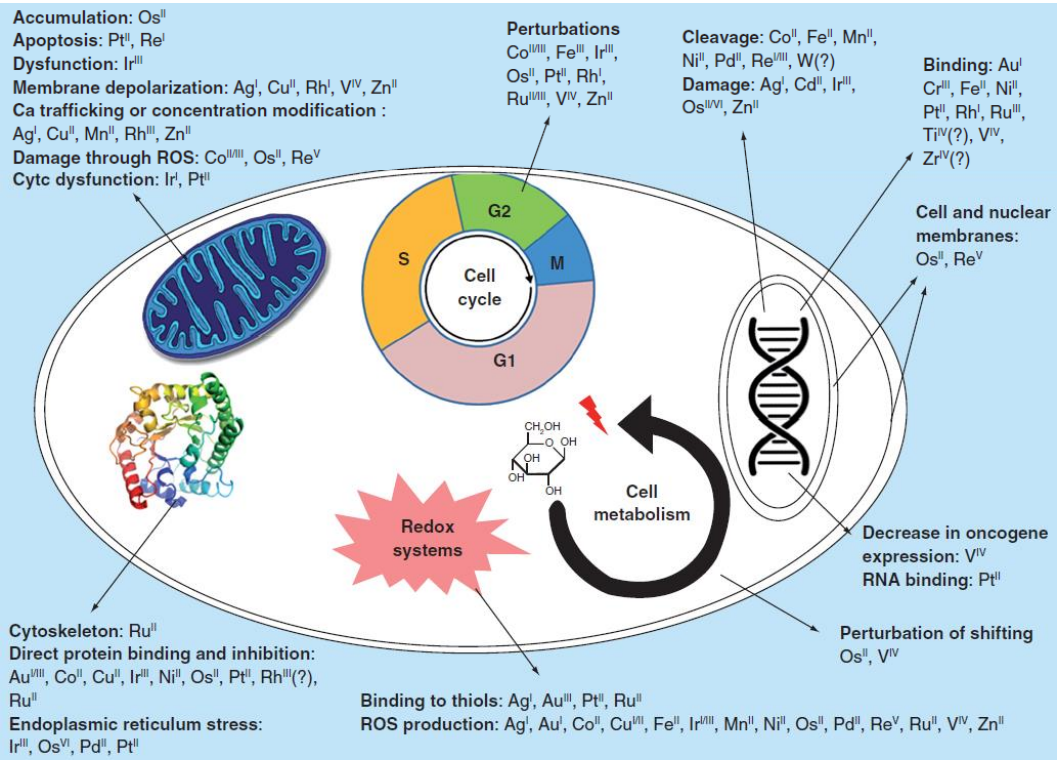

Figure 1. Main targets of transition metals (Marloye *et al*., 2016).

1.2.1 Platinum-based anticancer agents

Platinum (Pt) is the 78th element in the periodic table and belongs to the group 10 transition metals along with nickel and palladium. It was the first metal used in a coordination compound with anticancer activity: the *cis*-diamminedichloroplatinum(II) ($Cl_2H_6N_2Pt$) (cisplatin), that consists of one atom of platinum, two chloride ions and two molecules of ammonia (Fig. 2).

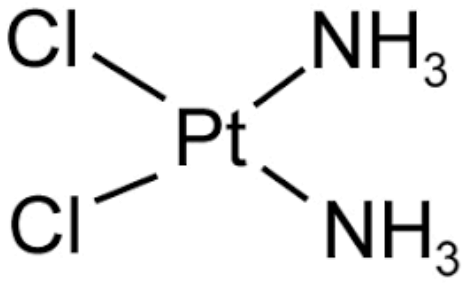

Figure 2. Cisplatin.

It was first synthesized by Peyrone in 1844 and its chemical structure was first clarified by Werner in 1893 (Dasari *et al*., 2014). Subsequently, Rosenberg and co-workers discovered that in the presence of an electrical field generated by platinum electrodes *Escherichia coli* failed to divide but formed long filamentous strands (Rosenberg *et al*., 1965; Muggia *et al*., 2015). Cisplatin inhibited bacterial cell division but induced cell growth. Further studies in sarcoma-180 mice model showed a strong tumor regression (Kelland, 2007; Rosenberg *et al*., 1969).

Cisplatin was approved by Food and Drug Administration (FDA) in 1978 (Kelland, 2007) and today can be administered alone or in combination with radiotherapy or other antineoplastic agents for several malignant solid cancers, such as testicular, ovarian, lung, oesophageal, stomach, prostate, cervical and colorectal cancers, squamous cell and head-neck carcinoma, non-Hodgkin lymphoma, multiple myeloma, neuroblastoma, melanoma and mesothelioma (Markowska *et al*., 2015).

After intravenous injection, cisplatin is a neutral molecule in the bloodstream as a result of high chloride concentration (100 mM) and can bind plasma proteins, such as albumin, gammaglobulin and transferrin (De Conti *et al*., 1973; Visacri *et al*., 2017).

For a long time, passive diffusion across the plasmatic membrane had been regarded as a main mechanism of cisplatin uptake but now cellular influx seems to involve multiple mechanisms, such as passive diffusion, ion channels and active or receptor-mediated transports. Several studies showed a relationship between cisplatin uptake and other Pt(II) drugs and copper transport system proteins (Öhrvik *et al*., 2014). The copper transporter 1 (CTR1) is involved in cisplatin uptake (Song *et al*., 2004; Kuo *et al*., 2012); while copper-extruding P-type ATPases, ATP7A and ATP7B, promote the cisplatin efflux and are responsible for drug resistance (Tadini-Buoninsegni *et al*., 2014). ATP7A is able to sequester the drug away from its targets (Zhu *et al*., 2017), and ATP7B is responsible for bringing out the drug from the cell (Nakayama *et al*., 2002; Spreckelmeyer *et al*., 2014). In addition, some studies recently showed that Cox17, a copper chaperone protein, promotes cisplatin accumulation in mitochondria and is involved in cisplatin cytotoxicity pathways (Li *et al*., 2016) (Fig. 3).

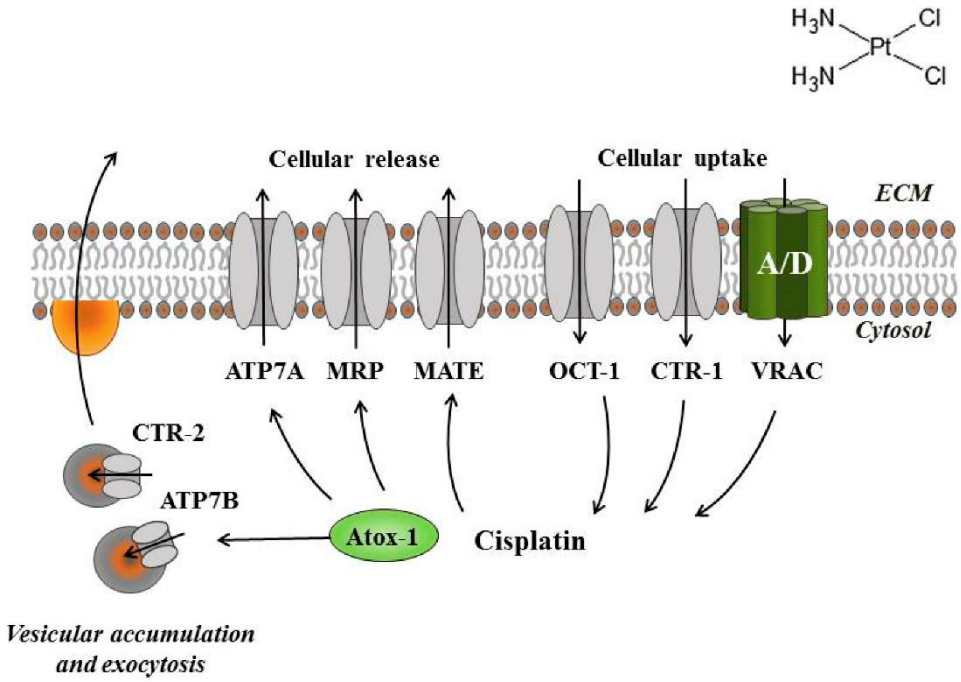

Figure 3. Cisplatin transporters involved in cisplatin accumulation. Cu transporters: CTR1, CTR2, ATP7A, and ATP7B. ABC transporters: MRP. Chaperone protein: Atox-1. Organic cation transporters: OCT1. Multidrug and toxin extrusion family members: MATE. Volume sensitive, LRRC8A/D-containing proteins: VRAC (Lambert *et al*., 2018).

Inside cells, chloride concentration is lower (4–10 mM) than in the extracellular environment, and cisplatin is hydrolysed generating monohydrate $[Pt(NH_3)_2Cl(H_2O)]^+$ and dihydrate $[Pt(NH_3)_2(H_2O)_2]_2^+$ complexes. These species are electrophiles and can react with

nucleophilic species in the cytoplasm and in the nucleus. The main target is N7 reactive center on purine residues (guanine and adenine): this leads to DNA damage, in particular 1,2-intrastrand crosslinks (60-65% of d(GpG) and 20-25% of d(ApG) adducts), and to a lesser extent 1,3-intrastrand crosslinks or interstrand crosslinks (Wang *et al.*, 2005). The intrastrand crosslinks represent about 90% of total DNA adducts and cause a significant distortion in the DNA double helix recognized by DNA repair proteins, transcription factors and other proteins involved in apoptosis (Fig. 4).

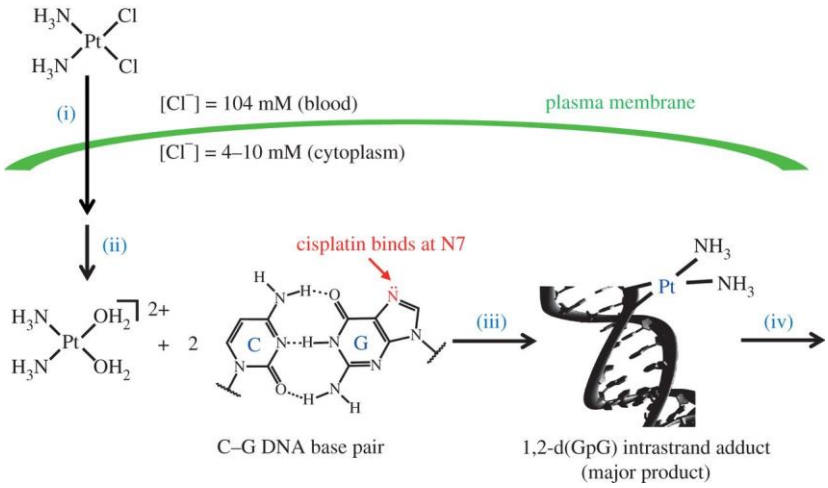

Figure 4. Mechanism of action of cisplatin comprising (i) cellular uptake, (ii) aquation/activation, (iii) DNA platination, and (iv) cellular processing leading to apoptosis (Johnstone *et al.*, 2015).

The genotoxic stress induces the inhibition of DNA replication and transcription and triggers the activation of a signaling cascade, which may lead to phosphorylation of ATM (ataxia telangiectasia mutated) and ATR (ataxia telangiectasia and Rad3-related), followed by recruitment and activation of other signaling proteins, such as checkpoint kinase 1 (Chk1) and checkpoint kinase 2 (Chk2), inducing cell cycle arrest or apoptosis (Zhao *et al.*, 2016), and by activation of a signaling pathway marked by histone 2AX (H2AX) phosphorylation. On the one hand, apoptosis can trigger cytochrome c release from mitochondria and activation of caspase-3 and -9 due to calcium ions increase; on the other hand, apoptosis can involve also the activation of calpain, a protein involved in apoptosis activation in addition to caspases and cathepsins. Calpain leads the cleavage of Bid, a member of the Bcl-2 family, and the modulation of Bak, a proapoptotic mitochondrial Bcl-2 family protein (Mandic *et al.*, 2002).

Cisplatin hydrolysed reactive species can react with glutathione (GSH), methionine, metallothioneins and other cysteine-rich proteins and lead to oxidative stress and cytoplasmic antioxidant reserves depletion (Dilruba *et al*., 2016). Furthermore, reactive species can interact with phospholipids and phosphatidylserine in membranes and can disrupt the cytoskeleton and actin polymerization (Szczepański *et al*., 2010).

Cisplatin long-term treatment leads to development of acquired or intrinsic resistance in cancer cells and occurrence of several toxic effects for the organism, including nephrotoxicity, neurotoxicity and ototoxicity (Karasawa *et al*., 2017).

Various cisplatin resistance mechanisms have been identified (Dilruba *et al*., 2016; Galluzzi *et al*., 2012) (Fig. 5).

- Pre-target resistance mechanisms. These effects involve two main mechanisms.
  The first one involves copper transporter (CTR): CTR1 down-regulation reduces cisplatin uptake, intracellular accumulation and cell sensitivity; CTR2 down-regulation causes an increase (Blair *et al*., 2010). Furthermore, ATP7A (Samimi *et al*., 2004) and ATP7B (Yoshizawa *et al*., 2007) up-regulation increase cisplatin efflux.
  The second mechanism depends on an increased sequestration of cisplatin by glutathione (GSH), metallothioneins and other cytoplasmic ”scavengers” with nucleophilic properties (Galluzzi *et al*., 2012). Cisplatin resistant cells show high levels of glutathione (Zhu *et al*., 2018), GSH-related enzymes (Sawers *et al*., 2014) and γ-glutamylcysteine synthetase (Lin *et al*., 2018). Furthermore, metallothioneins, a class of cysteine-rich proteins, exhibit high affinity for metal ions and are involved in detoxification processes binding and inactivating cisplatin (Theocharis *et al*., 2004).
- On-target resistance mechanisms. The ability of cancer cells to recognise and repair DNA damage results in on-target resistance effects (Galluzzi *et al*., 2012). Nucleotide Excision Repair (NER) is the main pathway for the repair of cisplatin-induced DNA damage (Neher *et al*., 2010a; Neher *et al*., 2010b; Nouspikel, 2009) and in cisplatin resistant cells there is an increase of NER activity (Siddik, 2003) and at the same time a decrease of Mismatch repair (MMR) activity (Sawant *et al*., 2015). In other cases, a class of DNA polymerases that mediates the translesion synthesis allows to tolerate cisplatin inter and intrastrand adducts (Srivastava *et al*., 2015).

- Post-target resistance mechanisms. These effects depend on *TP53* inactivation that alters apoptotic pathway. Several proteins, such as pro- and antiapoptotic members of the BCL-2 protein family, caspases, calpains, mitochondrial intermembrane proteins, take place in this pathway and modulate the cisplatin response (Galluzzi *et al*., 2012).
- Off-target resistance mechanisms. Finally, in cancer resistant cells, there are alterations in signaling pathways not directly connected to cisplatin response, including autophagy inhibition, EGFR/HER2 and PI3K/AKT1 pathways inhibition (Galluzzi *et al*., 2012).

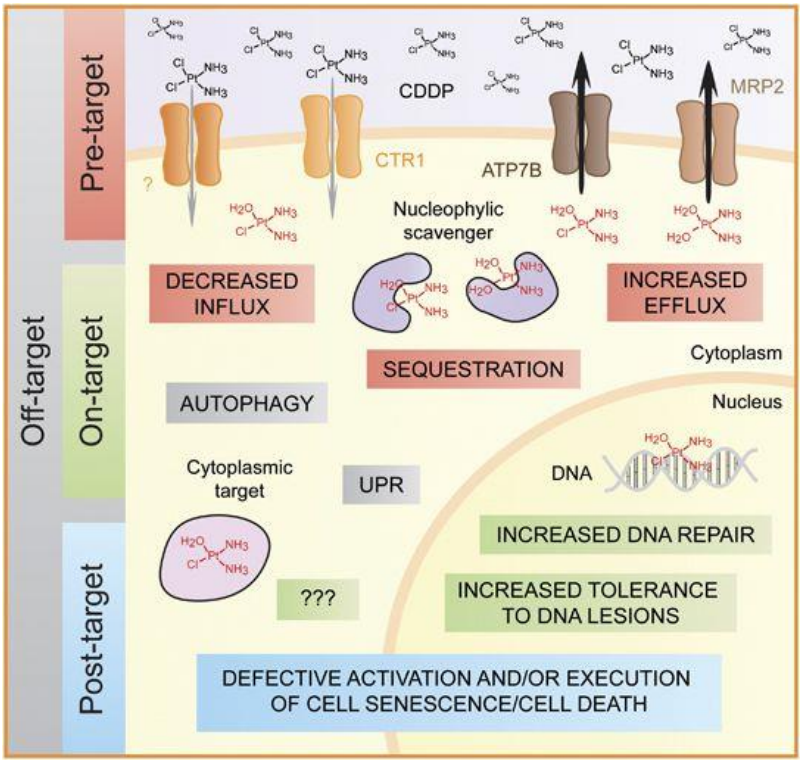

Figure 5. Cisplatin resistance mechanisms (Galluzzi *et al*., 2014).

Since cisplatin discovery, a lot of platinum coordination complexes have been synthetized. These compounds present the general formula PtA_2X_2, where A_2 are two monodentate or one bidentate amine ligand; X_2 are two monodentate or one bidentate anionic ligand (Cleare *et al*., 1973; Johnstone *et al*., 2015).

Platinum-based drugs can be divided into two classes: second and third generation drugs. Carboplatin [*cis*-diammine(1,1-cyclobutane dicarboxylato)platinum(II)] is a second generation Pt(II) drug that differs from cisplatin by the presence of a bidentate

dicarboxylate ligand instead of two chloride atoms (Fig. 6). It was developed in order to reduce cisplatin toxicity and it was approved by FDA in 1985 for the treatment of ovarian, endometrium, cervix, testes, breast, lung, bladder, head and neck cancers, retinoblastomas, neuroblastomas, nephroblastomas and brain tumors.

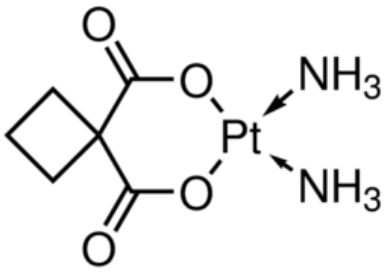

Figure 6. Carboplatin.

Carboplatin causes the same type of DNA adducts compared to cisplatin, but it shows reduced toxicity and activity given that its activation kinetics is slower than cisplatin (Lazarević *et al*., 2017).

Another second-generation platinum derivative is nedaplatin [*cis*-diammine-glycolatoplatinum] (Fig. 7). It is used in Japan for the treatment of head-neck, lung, oesophageal, bladder, testicular, ovarian and uterine cervical cancer, especially when cisplatin and carboplatin cannot be tolerated or show drug resistance. Nedaplatin causes the same DNA adducts than cisplatin but did not show significant advantage over cisplatin in response and survival (Hirakawa *et al*., 2017).

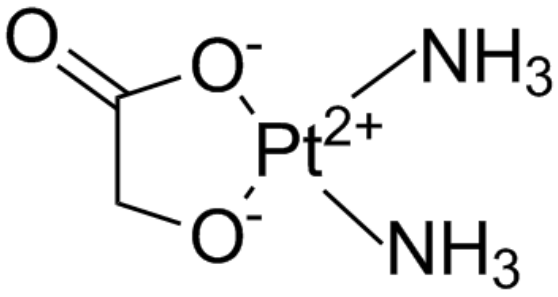

Figure 7. Nedaplatin.

Oxaliplatin [bidentate 1,2- diaminocyclohexane platinum(II)] is the first Pt(II) drug of third generation and was approved by FDA in 2002 in combination therapy with other

chemotherapeutic agents (5-fluorouracil and irinotecan) or targeted therapy for colorectal cancer treatment (Nielsen *et al*., 2014) (Fig. 8). It was developed to overcome resistance against cisplatin and carboplatin in colorectal cancer cells.

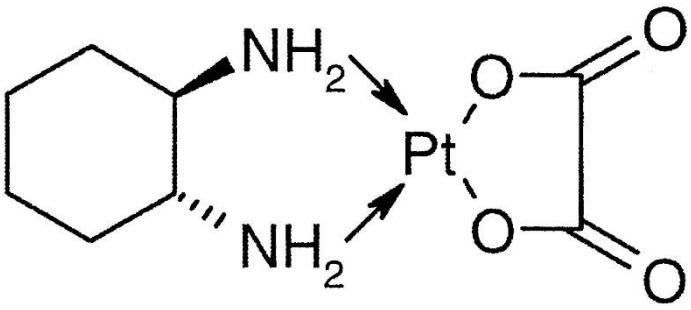

Figure 8. Oxaliplatin.

Other third-generation platinum drugs are heptaplatin and lobaplatin (Fig. 9). Heptaplatin [(*cis*-malonato [(4R,5R)-4,5–bis(aminomethyl)–2-isopropyl-1,3-dioxolane] platinum(II)] is synthetized and used in Korea for gastric cancer treatment. It shows lower toxicity than cisplatin and presents an important anticancer activity towards several cancer cell lines, including cisplatin resistant cell lines (Galanski *et al*., 2005; Galanski *et al*., 2006). Lobaplatin [1,2-diammino-methyl-cyclobutaneplatinum(II)-lactate] was approved only in China for the treatment of metastatic breast cancer, chronic myelogenous leukemia and small cell lung cancer (Li *et al*., 2016). Although it exhibits an interesting anticancer activity towards several cancer cell lines (Perabo *et al*., 2007; Wei *et al*., 2014), there is no strong evidence of the clinical activity of this compound.

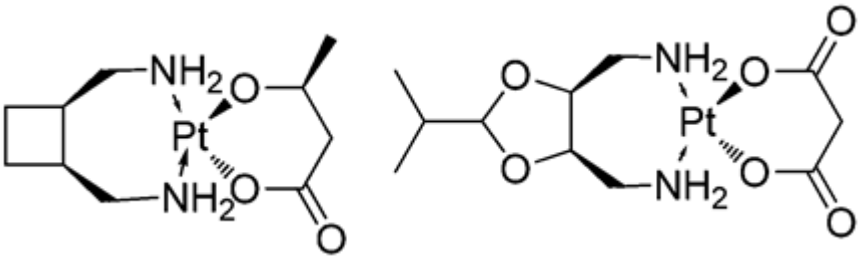

Figure 9. Lobaplatin and heptaplatin.

Only cisplatin, carboplatin and oxaliplatin have become clinical drugs globally, while nedaplatin, lobaplatin and heptaplatin received only regional approval (Bai *et al*., 2017).

In recent times, several new platinum compounds have been designed and synthetized and show a different mechanism of DNA interaction than cisplatin, carboplatin and oxaliplatin. Metal complexes can interact with DNA also by non-covalent interactions. The main ones are electrostatic interactions of positively charges of metal complexes with negatively charges of DNA phosphate groups, stacking interactions, groove bindings involving hydrogen bonds and Van der Waals interactions. These non-covalent interactions are due to a planar aromatic ligand, such as pyridine, bipyridine, terpyridine, phenanthroline, 8-hydroxyquinoline, naphthalene and thiosemicarbazones. The general formula of these agents is $[Pt(IL)(AL)]_2^+$, in which IL is an intercalating ligand and AL is a secondary ligand. The positive charge increases and improves solubility, cellular uptake and DNA affinity (Lazarević *et al*., 2017).

Another class of platinum complexes is Pt(IV) drugs, kinetically-inert octahedral prodrugs that can be reduced in cancer cells to active square planar Pt(II) species. The anticancer activity of Pt(IV) complexes is usually attributed to their reduction to Pt(II) products which bind to DNA. The reduction reaction involves intracellular or extracellular reductants such as glutathione, thiol groups of proteins, and ascorbic acid (Venkatesh *et al*., 2018). Kinetic inertness reduces the side-effects and allows the Pt(IV) drugs to be administered orally (Lazarević *et al*., 2017).

An example of Pt(IV) complexes is satraplatin [bis (acetato) amminedichlorido (cyclohexylamine) platinum (IV)] (Fig. 10). It exhibits activity through different pathways; it is believed to enter cells through passive diffusion and undergo activation by reduction to Pt(II), followed by binding to DNA (Venkatesh *et al*., 2018).

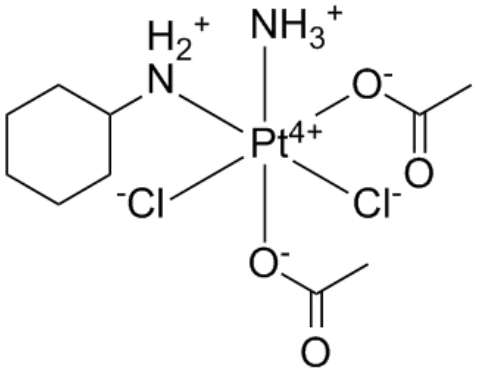

Figure 10. Satraplatin.

It is the first orally administered Pt(IV) drug and shows efficacy towards hormone-refractory prostate and small-cell lung cancers, but has not yet received the FDA approval given that it does not present a clear benefit in terms of survival.

An analogoue of satraplatin, LA-12 [(OC-6-43)-bis-(acetato)(1-adamantylamine) amminedichloroplatinum-(IV)] (Zak *et al*., 2004) demonstrated a high efficacy against a panel of cancer cell lines, including cisplatin-resistant cells (Zak *et al*., 2004; Kozubik *et al*., 2005; Svihalkova-Sindlerova *et al*., 2010), in p53-independent manner (Hrstka *et al*., 2008), but the action mechanism is unclear (Fig. 11). In mice, LA-12 is able to overcome resistance to cisplatin (Sova *et al*., 2006) and currently has undergone phase I clinical trials (Horváth *et al*., 2007).

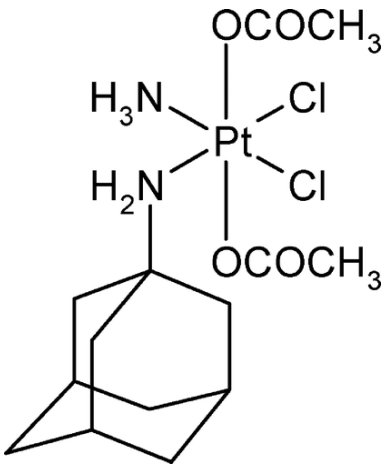

Figure 11. Platinum(IV) prodrug LA-12.

Multinuclear platinum agents with two or three platinum units are an alternative to Pt drugs (Brabec *et al*., 1999; Mangrum *et al*., 2011). These complexes induce different DNA adducts and are active at doses much lower than cisplatin and carboplatin, but are also much more toxic. The most important is BBR3464 that is a trinuclear platinum compound, where two terminal trans-$[PtCl(NH_3)_2]$ units are linked by a tetra amine [trans-$Pt(NH_3)_2\{H_2N(CH_2)_6NH_2\}_2]^{2+}$ unit (Kasparkova *et al*., 2002) (Fig. 12).

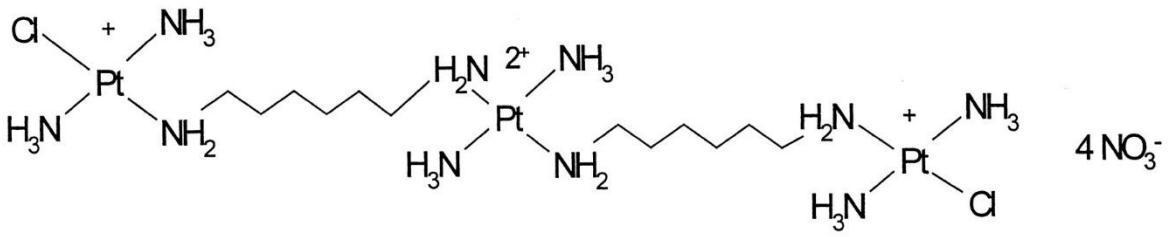

Figure 12. BBR3464: a novel triplatinum complex.

The two platinum units can form covalent bonds with the DNA bases, preferentially the guanine residues, and lead to various types of cross-links (Brabec *et al*., 1999). The central tetra amine platinum unit is positioned at the minor groove of DNA (Kasparkova *et al*., 2002). These events cause a DNA compaction that determines *in vitro* potent anticancer effects towards several cancer cell lines (Banerjee *et al*., 2010). Furthermore, BBR3464 is in phase II clinical trials for the treatment of refractory small cell lung cancer (Hensing *et al*., 2006).

The aim of the design of new platinum-based drug is to overcome both, intrinsic, and acquired resistance to conventional platinum treatment and to achieving the individualized therapy.

1.2.2 Copper-based anticancer agents

Copper (Cu) is the 29th element in the periodic table and belongs to the group 11 transition metals along with silver and gold. It is an essential micronutrient for all eukaryotic organisms and is involved in several biological processes, such as free radical detoxification, mitochondrial respiration, iron metabolism, and biosynthesis of neuroendocrine peptides (Grubman *et al*., 2014). Copper is also a cofactor in many enzymes: cytochrome-c oxidase, superoxide dismutase, glutathione peroxidase, metallothioneins and ceruloplasmin (Hordyjewska *et al*., 2014).

Although Cu is an essential element, Cu excess is toxic for cells and a complex system of proteins regulates its intracellular concentration. Copper uptake takes place through diet in the small intestine and in the stomach and then copper distribution is regulated by the liver into the bloodstream, where Cu binds two different proteins, ceruloplasmin and albumin (Linder *et al*., 1996; 2016). Several mechanisms control copper transport across cell membrane: in particular, copper transporter protein (CTR1) is responsible for import and copper ATP7A/B transporters for efflux. Other transporter proteins, such as antioxidant protein 1 (Atox1), Cu chaperone for superoxide dismutase (CCS) and cytochrome c oxidase assembly homolog (COX-17) are responsible for copper intracellular transport (Puig *et al*., 2002) (Fig. 13).

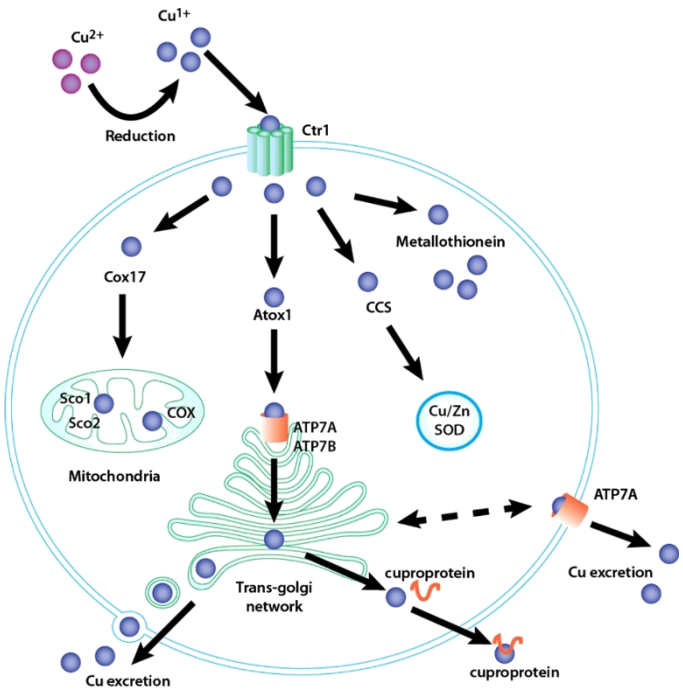

Figure 13. Model of cellular copper homoeostasis (Davies *et al*., 2016).

Dysregulation of cellular copper homeostasis leads to various diseases, like Menkes disease, a neurodegenerative disorder resulting from deficient activity of copper-dependent enzymes and caused by mutations in the *APT7A* gene (Smpokou *et al*., 2014), and Wilson disease, a copper storage disorder caused by mutations in the *ATP7B* gene (Ranucci *et al*., 2014). Additionally, copper has been strongly implicated in neurodegenerative diseases, such as Alzheimer (Ayton *et al*., 2012), Parkinson (Montes *et al*., 2014) and Creutzfeldt-Jakob (Brown, 2002), rheumatoid arthritis (Xin *et al*., 2015), epilepsy (Kheradmand *et al*., 2014), diabetes (Naka *et al*., 2013) and cancer. Frequently, cancer cells show an altered copper metabolism and many cancer types exhibit increased intratumoral copper concentration and/or altered systemic copper distribution (Denoyer *et al*., 2015).

Different response between normal and cancer cells to copper could explain the strong antiproliferative activity of copper-based compounds. Cu-complexes can participate in biological redox reactions, undergo ligand substitution and interact with biological molecules. Due to the physiological importance of Cu and its redox activity, many different Cu complexes have been investigated both *in vivo* and *in vitro* for their therapeutic potential in cancer therapy.

Copper can form coordination complexes especially with two different oxidation states Cu(I) and Cu(II), while there are few Cu(III) compounds biologically active (Tisato *et al*., 2010). Furthermore, Cu(II) complexes have been largely investigated for their anticancer potential because Cu(I) compounds are generally unstable towards oxidation to the Cu(II) form and so are less studied.

In copper-based compounds, the organic fragment (ligand, L) determines lipophilic/hydrophilic features, complex solubility in the extracellular fluid and the ability to permeate the plasmatic membrane. Furthermore, the ligand is responsible for biological properties of the complex: Cu(I) prefers ligands with soft donor atoms, such as phosphor, carbon, thioether sulphur, and aromatic amines; while nitrogen and oxygen donor ligands stabilize preferentially Cu(II). Copper complex stability depends on the strength of the Cu-L association.

Coordination competitors such as amino acids and proteins in the extracellular environment can dislocate the ligand from complexes that have low stability. The effects could be associated with an increase of the extracellular Cu concentration bound to

biomolecules. In contrast, a hypothetical complex characterized by a high stability will release copper in intra- and extra-cellular biological fluids and its activity can be ascribed to the chemical properties of the complex (Tardito *et al*., 2009).

Many copper complexes are now used for the treatment of various disorders (e.g., Alzheimer's disease and amyotrophic lateral sclerosis). In this way, "old copper complexes", such as clioquinol and tetrathiomolybdate, have been repurposed for cancer therapy and have demonstrated anticancer activity *in vitro* and *in vivo* studies (Denoyer *et al*., 2018).

The biological activity of copper complexes depends on the interaction with proteasome multiprotein complex, enzymes, and DNA (Santini *et al*., 2014). Furthermore, Cu(I) is the intracellular form of copper and its toxicity arises from that it can react with molecular oxygen or hydrogen peroxide to produce reactive oxygen species (ROS).

Cu-complexes can act as proteasome inhibitors. Ubiquitin-proteasome system (UPS) is a multiprotein complex located in the nucleus and cytoplasm of all eukaryotes and is involved in the regulation of protein concentration and in the degradation of unfolded proteins (Johnson, 2015). Several studies highlight that the high proteasome activity and high Cu concentration in cancer cells can be used as specific targets for cancer chemotherapy (Chen *et al*., 2008). In this way, Daniel and co-workers (2004) showed an approach that converts copper, which is essential for tumor cell proliferation and angiogenesis, into a cancer cell-killing agent. In this study, a copper complex deriving from the ligand 8-hydroxyquinoline (8-OHQ) and a copper(II) salt ($CuCl_2$) inhibits the proteasome *in vitro* and *in vivo* and also induces apoptosis in leukemia (Daniel *et al*., 2004) and breast cancer cells (Daniel *et al*., 2005). Furthermore, both 8-OHQ and other similar compounds coordinated with Cu, are preferentially cytotoxic to malignant cells over normal cells.

In other studies, Schiff bases Cu complex of quinoline 2 carboxaldehyde exhibits significant antiproliferative activity against prostate cancer cell lines by inhibiting the proteasome and leading to apoptosis. In particular, the antitumor activity is enhanced by the presence of thiocarbonyl group at the C2 position in the quinoline moiety upon Cu complexation (Adsule *et al*., 2006). The main mechanism by which copper complexes promote proteasome inhibition is not clear. Probably, in its Cu(I) state or during its reduction from Cu(II) to Cu(I), copper interacts with thiol and amino groups outside the active site of the proteasomal enzyme and thereby induces a conformational change in the protein structure causing inhibition of the proteasomal enzymes (Schimmer *et al*., 2012).

8-Hydroxyquinoline has attracted considerable interest as a privileged structure and its derivatives (HQs) have been explored for a broad range of biological applications. $[Cu(L)Cl_2]_2$, where L= 2-((2-(pyridin-2-yl)hydrazono)methyl)quinolin-8-ol, in MGC80-3 cells, causes the cell cycle block in the S phase, leading to the down-regulation of Cdc25 A, Cyclin B, Cyclin A, and CDK2, and the up-regulation of p27, p21, and p53 proteins. Indeed, it induces apoptosis via a mitochondrial dysfunction pathway, resulting to the significantly decreased level of bcl-2 protein, the increased levels of ROS, intracellular Ca(II), cytochrome c, apaf-1, caspase-3, and caspase-9 proteins (Yang *et al*., 2018).

Another approach in the design of Cu-based anticancer compounds provides for the use of copper ionophores that increases cellular copper levels and induces cytotoxicity via reactive oxygen species (ROS) formation. Indeed, copper is implicated in ROS generation and subsequent in cytotoxicity attributed to ROS generation (Schumacker, 2006). Cancer cells show higher level of intrinsic oxidative stress than normal cells and several copper complexes can increase the ROS generation via metal redox recycling and Fenton chemistry leading to the disruption of cellular redox homeostasis and the induction of cell death. Copper(II) complexes of 2-pyridyl ketone thiosemicarbazones are capable of eliminating cancer cells without concomitant increase in toxicity toward normal cells: in particular the combinations of azines and copper complexes induce cytotoxicity through the generation of ROS in breast cancer cell line MCF-7. This increase in ROS is insufficient to raise ROS level beyond the threshold for cell death in a normal cell line (Akladios *et al*., 2015).

Many studies suggest that DNA is the first intracellular target of platinum anticancer drugs because the interaction between small molecules and DNA can often cause DNA damage blocking cell division and resulting in cell death. *In vitro* studies of copper complex deriving from pyrazole show a strong cytotoxicity towards human leukemia HL-60, human gastric cancer BGC-823, and human mammary gland cancer MDA5 cell lines. Furthermore, the complex is able to bind to DNA by intercalation mode and to present a marked DNA-cleavage activity (Chen *et al*., 2007). Many Cu(II) complexes can effectively cleave DNA by the generated ROS, for example, singlet oxygen, superoxide anion radical and hydroxyl radical.

Recent studies show that binary copper(II) complexes containing intercalating ligands exhibit *in vitro* high cytotoxic effects toward A549, Caco-2 and MCF-7 cancer cell lines and are more potent than cisplatin. Probably, their hydrophobicity and their higher ability to

binding DNA are due to methyl groups on phenanthroline ligands that could be used in designing efficient anticancer agents (Inci *et al*., 2017)

Another copper(II) compound deriving from thioxotriazole exerts significant antiproliferative activity against human fibrosarcoma cell line HT1080 (Dallavalle *et al*., 2002). It induces non-apoptotic programmed cell death (Tardito *et al*., 2006) associated with copper accumulation and oxidative stress (Tardito *et al*., 2007).

Biochemical action of copper complexes with non-steroidal anti-inflammatory drugs (NSAIDs) has been recently studied. Some copper complex can interact with essential enzymes: Cu(II) chelates of salicylaldoxime and resoecylaldoxime are potent antiproliferative agents, exhibiting strong cytotoxic effects, by inducing cell arrest and apoptosis (Frezza *et al*. 2010). Their action may involve the inhibition of the topoisomerase II activity by preventing dimer formation of enzyme and its reaction with DNA (Hordyjewska *et al*., 2014).

Elesclomol (N'1,N'3-dimethyl-N'1,N'3-di(phenylcarbonothio-yl)malonohydrazide) is an anticancer drug and has just completed phase III clinical trials for patients with advanced melanoma (O'Day *et al*., 2013) and has also undergone phase II and III clinical trials for the treatment of several cancers (Yadav *et al.*, 2013). *In vitro* studies highlight that Elesclomol and Cu(II)- elesclomol display anticancer activity against a broad range of cancer cell lines yielding ROX via their chelation with copper(II) and redox cycling of copper(II) (Nagai *et al*., 2012; Vo *et al*., 2014). Probably, elesclomol cytotoxicity is due to induction of oxidative stress that is mediated through its Cu^{2+} complex (Hasinoff *et al*., 2014). It has also been shown that this agent can scavenge copper from the culture medium and selectively transport it to the mitochondria where it induces oxidative stress and then it was effluxed from the cell. Both the molecules cause a G1 block of cell cycle leading to induction of apoptosis. Furthermore, they induce DNA double strand breaks but the DNA-damaging mechanisms is still unclear (Hasinoff *et al*., 2015).

In medicinal chemistry, copper plays a key role in the design of metal based compounds, as an alternative to cisplatin and other platinum drugs. There are a lot of *in vitro* studies but the information for *in vivo* models is limited. In the future, it would be interesting to evaluate promising multi-target copper complexes, in human trials.

1.2.3 Nickel-based anticancer agents

Nickel (Ni) is the 28th element in the periodic table and belongs to the group 10 transition metals along with platinum and palladium.

Nickel is one of the essential trace elements. It is an essential cofactor in nickel-based enzymes, such as superoxide dismutase (Ryan *et al*., 2015), urease, hydrogenase (Volbeda *et al*., 1995), methyl-CoM reductase (Wongnate *et al*., 2015), carbon monoxide dehydrogenase (Wang *et al*., 2014) and acetyl-CoA synthase (Can *et al*., 2014). It helps in iron absorption, in addition to adrenaline and glucose metabolism, improves bone strength and may also aids in red blood cells production (Ragsdale, 1998; Kumar *et al*., 2016).

Chronic exposure to nickel can lead to cardiovascular, lung, skin and kidney diseases. Based on the high risk of lung cancer related to nickel exposure, metallic nickel has been listed as Group 2b possible human carcinogens, while nickel compounds as Group 1 carcinogenic to humans by the International Agency for Research on Cancer (IARC, 1973; Zhao *et al*., 2016). Nickel shows teratogenic potential and weakly mutagenic activity (Denkhaus *et al*., 2002).

On the other hand, nickel is considered as one of the compatible pharmacologically metals that can be suitable to develop novel anticancer agents. A lot of nickel complexes were designed for their biological potential. The main oxidation states of nickel are Ni(0) and Ni(II), while Ni(I) has been generally considered to be a relatively rare oxidation state because Ni(I) complexes were considered to be unstable (Lin *et al*., 2017).

The cytotoxic activity of nickel complexes is due to several mechanisms. First, Ni(II) complexes are able to interact with DNA and cause DNA damages. In this context, recently Cu(II) and Ni(II) complexes of aminonaphthoquinone showed *in vitro* anticancer activity against human breast (MCF7) and lung (A549) cancer cells. These complexes bind to DNA through intercalation mode and cleave the DNA. The biological activities may be due to the presence of bioactive quinone moiety and may enhance with coordination of metal ions to the ligand in the form of complexes (Kosiha *et al*., 2017).

Moreover, studies have shown that some nickel complexes can inhibit DNA repair by interfering with enzymes or proteins involved in DNA replication or repair. Furthermore, they can trigger apoptosis through intrinsic or extrinsic pathways.

Nickel compounds have been grouped according to starting ligand similarity. These ligands have been employed for the design of new complexes with structural and/or functional features that can enhance the biological potential of the starting molecule.

Among the different categories of ligands, the coordination of Schiff bases to transition metal ions has been extensively studied. The substituted heterocyclic moiety in combination with transition metal salts generate coordination compounds which possess enhanced physiochemical and pharmacological properties (Yu *et al*., 2017). An example is the nickel(II) diacetyl monoxime-2-pyridyl hydrazone complex that suppresses tumor growth in Ehrlich solid tumor mice model (Saad *et al*., 2017).

Gwaram and co-workers demonstrated that Schiff base compounds derived from morpholine are completely stable in biological systems. The nickel(II) is able to inhibit the growth of MCF-7 cells in a dose-dependent manner. The free ligand shows no significant inhibition activity at a concentration even higher than the complex which confirms that chelation of ligand with metal ion is significant for the activity of this complex (Gwaram *et al*., 2014).

Thiosemicarbazones are another class of ligands employed in the coordination process. Nickel(II) complexes containing 3-methoxy salicylaldehyde 4(N) substituted thiosemicarbazone exhibit significant degree of cytotoxicity against A549 cells. The cytotoxicity may be due to ROS-hypergeneration and lipid-peroxidation with subsequent depletion of cellular antioxidant pool resulting in the reduction of mitochondrial-membrane potential, caspase-3 activation, DNA fragmentation and apoptosis activation (Kalaivani *et al*., 2014).

In another study nickel(II) bis(isatin thiosemicarbazone) complexes were examined for their anticancer activity against a panel of human cancer cells. These molecules induce apoptosis through mitochondrial signaling pathway and G0/G1 cell cycle arrest in IM-9 cells. Experimental data reveal the downregulation of Bcl-2 (b-cell lymphoma-2), up-regulation of Bax (bcl-2 associated X protein), release of cytochrome c and activation of caspases-3. Furthermore, the complexes are not toxic to the normal Vero cells (*Cercopithecus aethiops* kidney normal cell line) (Balachandran *et al*., 2018).

Recently, the anticancer properties of metal complexes of Doxorubicin (DOX) have been studied. DOX belongs to the anthracycline group, a class of drugs that is commonly used for breast cancer chemotherapy, often in combination therapy with other compounds. It contains in its chemical structure a fragment of both hydrophilic and hydrophobic properties, which allows it to bind plasma proteins and cellular membranes. The nickel complex Ni-DOX significantly decreases cell viability and proliferation in MCF-7 cells after

24h treatment. An increased level of apoptosis, caspase-7 level and number of cells in G2/M phase were observed. These results suggest that doxorubicin complexed by nickel ions can be considered as a potential anti-breast cancer agent (Jabłońska-Trypuć *et al*., 2017).

1.3 Thiosemicarbazones

Thiosemicarbazones (TSC) derive from the reaction of a thiosemicarbazide and an aldehyde or ketone, and are a group of highly reactive compounds that form chelate complexes with metal ions (Chandra *et al*., 2014) (Fig. 14). Thiosemicarbazones have a broad spectrum of biological activities such as anticancer, antifungal, antibacterial and antiviral (Rogolino *et al*., 2017). The biological activities have been enhanced by complexation with metal ions and the biologically active compounds are planar molecules consisting of a pyridine ring or a N,N,S tridentate system (Pelosi, 2010).

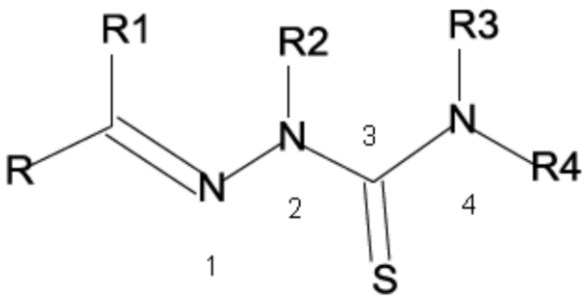

Figure 14. General scaffold of thiosemicarbazone. R, R1, R2, R3, R4 = H, alkyl, aryl.

The biological activity of the molecules is dependent on the parent aldehyde or ketone because the increased lipophilic character of starting molecules may be responsible for their enhanced biological potency. The lipophilicity promotes the crossing of the plasmatic membrane. The substitution on the C2 position can also vary the hydrophilic-lipophilic character of the compounds in order to increase the cell absorption. Furthermore, the presence of bulky groups at the N(4) position of the thiosemicarbazone moiety and the presence of additional binding site were found to greatly effect biological activity. In addition, the biological properties can be modify led by varying the nature and size of the carbonyl moiety; modifying the sulphur centre by alkylation; replacing the sulphur of the thiocarbonyl group by oxygen, selenium, imine or oxime and shifting the point of coordination of the thiosemicarbazone moiety by heterocyclic ring (Pahonţu *et al*., 2016). Nowadays, the majority of studies have focused on the structure-activity association of TSCs bearing six-member heterocycles, but also TSCs containing five-member heterocycles show antitumor effects (Zhu *et al*., 2017).

1.3.1 Molecular and cellular targets of thiosemicarbazones

1.3.1.1 Interaction of thiosemicarbazones with iron

It is well known that most of thiosemicarbazones have multiple molecular and cellular targets and interfere with several cell pathways.

α-N-heterocyclic derivates are potent iron chelators and they were developed to target the enhanced demand of cancer cells for iron. Under physiological conditions these chelators interact and bind iron in both Fe(II) and Fe(III) states and are able to redox cycle between these two oxidation states (Heffeter *et al*., 2018).

In this context, ribonucleotide reductase (RR) is the main target of α-N-heterocyclic thiosemicarbazones. It is an iron-containing enzyme and it is essential for DNA synthesis and repair because it catalyses the conversion of ribonucleoside diphosphates to the corresponding deoxyribonucleoside diphosphates. Usually, in cancer cells there is an overexpression of this enzyme making it an attractive target for cancer treatment (Aye *et al*., 2015).

RR consists of two large subunits and two small subunits. The carboxy terminal tails of the small subunits interact with the large subunits to form the enzymatic complex. In mammalian cells, each monomer of the large subunit (RRM1) contains an active site where substrate binding occurs, and two allosteric sites that control activity, substrate specificity and redox active disulfides that participate in substrate reduction. Each monomer of the small subunit contains an oxygen-linked, diferric iron center and a tyrosyl radical, essential for enzymatic activity (Shao *et al*., 2013).

RR regulation is controlled by RNA transcription and protein degradation in response to cell cycle and DNA repair signals. RRM1 protein levels are greater than those of small subunits and almost constant during cell cycle. Instead, there are two different small subunit subtypes: RRM2 and p53R2. RRM2 is a cell cycle-dependent protein, upregulated at the beginning of the S-phase and degraded via ubiquitination during the G2 phase of the cell cycle. In G2, cyclin-dependent kinase (CDK) phosphorylates Thr33 and promotes interaction and ubiquitylation of RRM2 by SCF cyclin F ubiquitin ligase. In G1, proteolysis of RRM2 is maintained by the APC/Cdh1 ubiquitin ligase and thus RRM2 levels remain low until APC/Cdh1 is inactivated near the start of S phase. The G1/S induction of RRM2 transcription is dependent on the transcription factor E2F1. If DNA damage occurs, cyclin F

is downregulated in an ataxia telangiectasia mutated (ATM) and Rad3-related (ATR)-dependent manner, thereby allowing RRM2 to accumulate (Guarino *et al*., 2014). p53R2 is a RRM2 homolog but is induced by DNA damage pathways. It is transcriptionally and post-translationally regulated by p53 and ATM, respectively. p53R2 expression level is lower than RRM2 but it remains constant during cell cycle (Wang *et al*., 2009) (Fig. 15).

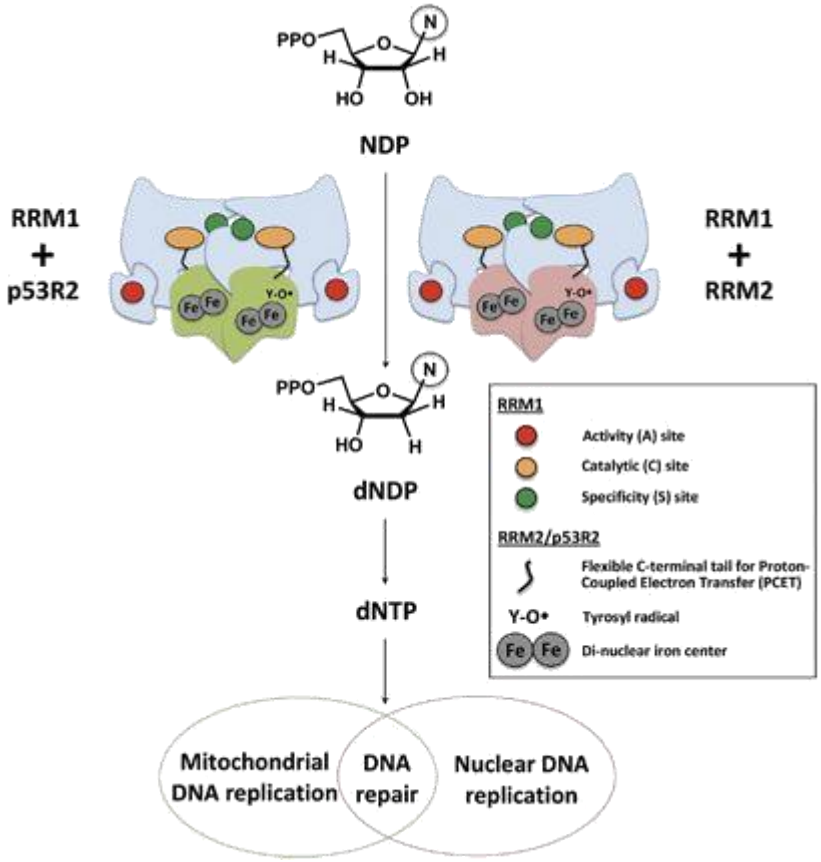

Figure 15. Ribonucleotide reductase and *de novo* dNTP biosynthesis (Aye *et al*., 2015).

Two different pathways supply dNTPs for DNA synthesis. The first uses the RRM2 activity, which maintains dNTPs for DNA replication during the S/G2 phases in a cell cycle-dependent manner. In the second one, p53R2 supplies dNTPs for DNA repair during G0/G1 phase in a p53-dependent manner (Nordlund *et al*., 2006). Besides its classical role in nuclear DNA replication, RR has different functions in other biological processes, including mitochondrial DNA replication, cell cycle regulation, DNA damage repair, and apoptosis (Kunos *et al*., 2017).

Many thiosemicarbazones target RR and act as RRM2 inhibitors, interfering with the essential di-iron tyrosyl radical center of the small subunit. Several studies demonstrate

that 3-aminopyridine-2-carboxaldehyde thiosemicarbazone, Triapine (Fig. 16), is a potent RRM2 inhibitor that works by quenching the tyrosyl radical and chelating iron in the catalytic site. Recently, *in vitro* studies suggested that Triapine seems to be an inefficient iron chelator (Chaston *et al*., 2003). It was suggested that the ability of Triapine to inhibit RRM2 is due to ROS generation, upon intracellular formation of the redox-active iron-Triapine complex.

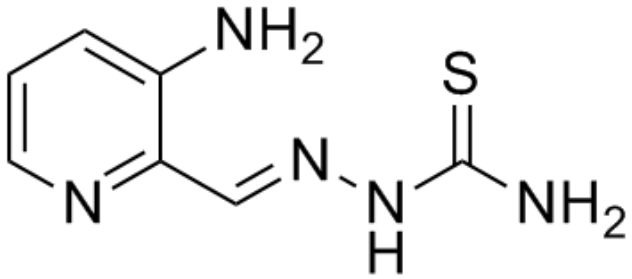

Figure 16. Triapine.

Other researches assumed that the iron(II) complex of Triapine could act as reductant, directly reducing the tyrosyl radical of the RRM2 subunit. Docking studies of mouse RR confirm these experimental data and reveal a possible Triapine-binding site with the pyridine ring of the thiosemicarbazone located in the pocket of the four amino acids Phe237, Phe241, Ser238 and Tyr324. Based on these results, it can be hypothesized that, following the binding of (metal-free) Triapine to the enzyme, an iron complex is formed locally, using the iron liberated during each catalytic cycle of the RR (Popović-Bijelić *et al*., 2011) (Fig.17).

The Fe(II)−Triapine complex may be formed by chelation of Fe from the differic cofactor in RRM2 *in vitro* (Popović-Bijelić *et al*., 2011) and/or from intracellular iron pools *in vivo* (Chaston *et al*., 2003). The potent inhibition of human and mouse RRM2 RR *in vitro* by catalytic amounts of Fe(II)−Triapine has been proposed to involve ROS. ROS had been detected in the aerobic reaction between human RRM2 RR and Fe(II)−Triapine, which had implicated that O_2 is important in tyrosyl radical destruction and that ROS may ultimately be responsible for the pharmacologic effects of Triapine in *vivo*. Several studies based on kinetic measurements of tyrosyl radical, and Fe loss, showed that the principle mechanism of human RRM2 RR inhibition by Triapine, is direct radical quenching, in an iron-loaded

protein. Furthermore, it implied that Fe(II)−Triapine can rapidly reduce the tyrosyl radical, while leaving the protein in the met-state (Aye *et al*., 2012; Ohui *et al*., 2018).

Triapine has been evaluated as a single agent in several phase I and phase II studies including advanced hematologic malignancies (Gojo *et al*., 2007), advanced solid tumors (Kunos *et al*., 2017), head and neck squamous cell carcinoma (Nutting *et al*., 2009) and renal cell carcinoma (Knox *et al*., 2007). There are also several clinical trials to evaluate this drug in combination therapy with other anticancer agents, such as cisplatin (Kunos *et al*., 2017), gemcitabine (Traynor *et al*., 2010), cytarabine (Odenike *et al*., 2008), doxorubicin (Schelman *et al*., 2009), irinotecan (Choi *et al*., 2010) or radiation (Kunos *et al*., 2013; Kunos *et al*., 2013; Kunos *et al*., 2014; Kunos *et al*., 2018).

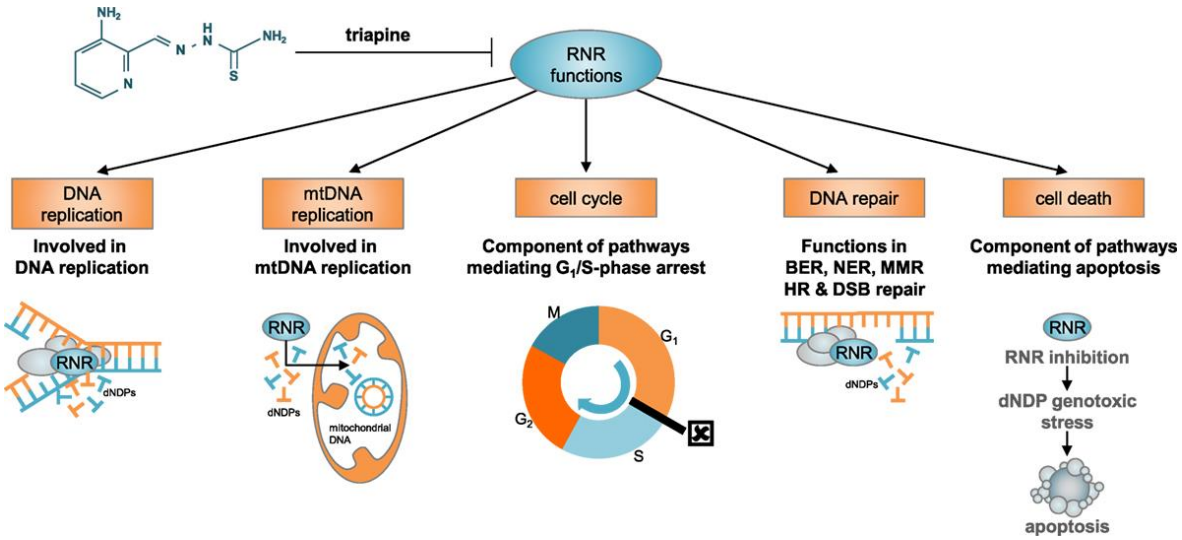

Figure 17. Ribonucleotide functions (Kunos *et al*., 2017).

Another series of ligands, the di-2-pyridyl thiosemicarbazones analogs (DpTs), exhibits pronounced antitumor activity acting as Fe chelators. The ability of DpT ligands to inhibit tumor cell growth was shown to correlate with their efficacy to induce Fe release and to prevent Fe uptake. Dp44mT (di-2-pyridylketone-4,4-dimethyl-3-thiosemicarbazone) is one of the most effective chelators developed in terms of its selective antitumor and antimetastatic activity both *in vitro* and *in vivo*. It is a dimethylated analog of Triapine, in which the addition of two methyl groups to the terminal position and the removal of the 3-amino group from the pyridine ring of Triapine, contribute to potentiation (Ishiguro *et al.,* 2014) (Fig. 18).

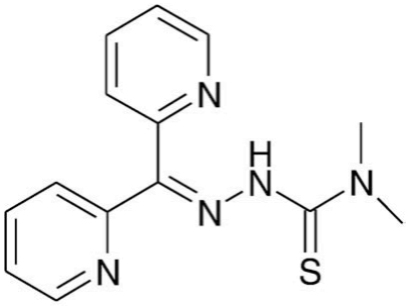

Figure 18. Chemical structure of Dp44mT.

This "super Triapine" induces apoptosis through the release of mitochondrial cyt c into the cytosol and the activation of caspase-3, -8, and -9. The release of cyt c could be mediated by the imbalance of Bcl-2 and Bax expression induced by incubation of cells with Dp44mT. Within lysosomes, Dp44mT forms cytotoxic iron or copper complexes that generate ROS resulting in lysosomal membrane permeabilization and cell death. Dp44mT has the ability to produce robust cell-killing within 1 h, while Triapine produces progressive cell-killing via inhibition of RR and arrest of DNA replication and this mechanism of action requires a long exposure time (≈16 h). In contrast to Triapine, Dp44mT does not appreciably inhibit DNA replication (Ishiguro *et al*., 2014).

1.3.1.2 Interaction of thiosemicarbazones with cell cycle progression

An altered iron homeostasis can also influence cell cycle regulation via cyclins and cyclin-dependent kinases (CDKs). Several thiosemicarbazones induce a modulation of cell cycle proteins, that includes kinases and cyclins involved in regulation and maintenance of the cell cycle in eukaryotic cells. Experimental data show mainly a downregulation of cyclin A and D as well as CDK2/4.

A second generation drug deriving from DpTs is the di-2-pyridylketone 4-cyclohexyl-4-methyl-3-thiosemicarbazone (DpC) which is under clinical phase I evaluation (NCT02688101). DpC induces CDKI and p21 upregulation and cyclin D1 down regulation, ribonucleotide reductase inhibition and strongly upregulates the metastasis suppressor, Ndrg1 (N-myc downstream-regulation gene 1), leading to the inhibition of ROCK1/MLC2 signalling that is important for cellular migration. All of these activities result in inhibiting

cell cycle progression (Lane *et al*., 2014). It has been demonstrate that the binding of CDK2 with iron ions could occur only to the phosphorylated form of the protein, indicating a direct regulation of CDK2 by the cellular metal homeostasis. In case of cyclin A, little is known about the mechanisms explaining how thiosemicarbazones could influence the expression levels of this protein.

In another study, the antitumor function of DpC may be mediated via the regulation of the expression of DNA damage signaling pathway-associated proteins: phospho-ATM, phospho-Chk1 (p-Chk-1), phospho-ATR, phospho-Chk2 (p-Chk-2), p-histone H2AX, breast cancer type 1 susceptibility protein and p53 increase with increasing concentration of DpC in Cal-27 cells (tongue cancer cell line) (Xu *et al*., 2018).

The expression of Ndrg1 is another important factor in the stress response. Alterations of the intracellular level of iron through chelation have been identified as one of the triggers of Ndrg1 up-regulation. Ndrg1, in fact, can be markedly increased in multiple cancer types *in vitro* and *in vivo* after treatment with Dp44mT and DpC. This gene is down-regulated in various cancers, which is often connected with p53 level (Kovacevic *et al*., 2006) but Ndrg1 upregulation is frequently reported in response to chemotherapy, leading to inhibition of growth and metastasis (Bae *et al*., 2013). The *Ndrg1* gene has also been reported to up-regulate p21 and activate WAF1/CIP1 expression as apoptotic triggers indicating a p53-independent pathway of apoptosis. Malarz and co-workers determined the influence of a series of thiosemicarbazones, containing the quinoline, 8-hydroxyquinoline, and di-2-pyridylketone moieties, on the expression of p53 and p21 proteins in human colon cancer cell line HCT116. Interestingly, none of the tested TSC induce the expression of the p53 protein. On the other hand, there is a considerable up-regulation of the p21 protein after treatment with all the compounds. All these experimental data indicate a p53-independent pathway of apoptosis (Malarz *et al*., 2018). Furthermore, different complexes tested in this study induce different effect on the expression of Cdc2 protein, which is involved in the transition from the G2 to M phase of cell cycle. The interaction between metal complexes and DNA could induce conformational changes, which could lead to DNA strand stress and damage.

A new α-N-heterocyclic thiosemicarbazone is COTI-2, a compound identified using a computational platform known as CHEMAS (Salim *et al*., 2016). This drug displays a strong anticancer activity against solid epithelial cancer and leukemia cell lines, especially in p53-mutant cell lines and is able to restores the wild-type function of the p53 protein. COTI-2 may act inhibiting the [phosphatidylinositol 3-kinase (PI3K)/Akt, a serinethreonine kinase /mammalian target of rapamycin (mTOR)] PI3K/AKT/mTOR pathway. In different models of tumor xenograft in mice, this drug induces significant tumor growth regression. Most importantly, COTI-2 is well-tolerated *in vivo* and shows a positive safety profile in mice with different genetic backgrounds. Although the precise mechanism of action of COTI-2 is still under investigation (Salim *et al*., 2016), it is undergoing a clinical phase I trial for treatment of advanced gynaecologic cancers (Duffy *et al*., 2017).

1.3.1.3 Interaction of thiosemicarbazones with topoisomerase

Topoisomerases are another important enzymatic target for the development of effective anticancer agents. These enzymes are able to control the topological state of DNA during replication, transcription, recombination and chromosomal segregation. There are two different types, type I and type II, which cleave transiently one or two strands of the DNA helix, respectively (De Oliveira *et al*., 2017).

Many topoisomerase inhibitors have been developed because cancer cells possess high levels of topoisomerase activity and show remarkable sensitivity to DNA-targeted drugs. Several square planar metal complexes of thiosemicarbazones inhibit topoisomerase, acting by stabilization of the cleavable products formed by topoisomerase-II and DNA (Pelosi, 2010). This ability increases significantly upon coordination with metal ions such as platinum(II), gold(III) and copper(II). Recently, the gold(III) complex of 3-(4-bromophenyl)-1-pyridin-2-ylprop2-en-1-one thiosemicarbazone resulted in high cytotoxic activity against a panel of cancer cell lines and inhibited topoisomerase Ib in a dose depended manner. Inhibition of the enzymatic activity is due to the presence of gold(III) but the thiosemicarbazone plays an important role, probably as a carrier of the metal (Sâmia *et al*., 2016).

A series of copper(II) complexes of quinoline-2-carboxaldehyde thiosemicarbazones resulted in inhibiting topoisomerase IIa *in vitro* in U937 cells. The positive charge of the dissociated form drives the metal complex to find its way in the enzyme structure and binds more favourably in negatively charged sites. The copper compounds, instead, strongly interact with the DNA phosphate group at the cut edge, likely preventing the relegation to the opposite strand (Bisceglie *et al*., 2015).

1.3.1.4 Interaction of thiosemicarbazones with multidrug resistance pathways

Certain thiosemicarbazones, mainly isatin derivatives such as Dp44mT, show increased toxicity against ABCB1-expressing MDR cells. ABCB1 is a member of multidrug resistance proteins (MDR), which are involved in the multidrug resistance (MDR) phenotype in tumours (Heffeter *et al*., 2018).

The "MDR-selective" toxicity is shared by several other compounds which are able to chelate metal ions including some 8-HQ or phen derivatives. Following the discovery of the lysosomal accumulation of the redox-active copper complex of Dp44mT, it was hypothesized that the increased toxicity against MDR cells is due to the function of lysosomal ABCB1. Whereas ABCB1 usually resides in the plasma membrane, glucose modulation was found to specifically increase the lysosomal accumulation of ABCB1 together with an increase of the sensitivity of MDR cells toward Dp44mT. A similar mechanism was assumed for related ligands including Ap44mT (the acetylpyridine analogue of PTSC) and DpC, as well as their zinc complexes (Heffeter *et al*., 2018).

Importantly, in cancer cells, the overexpression of ABC proteins and the phenomenon of MDR are associated with an elevated level of ROS and a modified antioxidative capacity. In particular, a high level of many antioxidant proteins plays a pivotal role in the development of multi-drug resistance (Malarz *et al*., 2018).

Taken together, the mechanisms responsible for MDR-selective toxicity of thiosemicarbazones are unknown but they represent a promising modality for the treatment of late stage patients after failure of therapy due to ABCB1 expression.

2. Aim of the research

The end goal of this project is the study of the biological activity of newly synthesized metal complexes, deriving from natural products, in order to identify their cellular targets and molecular action mechanisms. The exploitation of bioactive natural sources to obtain new agents with novel modes of action may represent an innovative and successful strategy in the field of medicinal chemistry. Many natural products and their chemical analogues have been proposed as starting molecules to synthetize compounds with increased biological potential. The tested molecules belong to the class of thiosemicarbazones, very attractive metal-chelating ligands, that show coordinating versatility and the possibility to easily modify the molecular backbone, tuning their physical and chemical properties.

This thesis can be divided into three sections.

- Aim 1.

The first section is part of "Aflatox project" focused on the design and the synthesis of new types of inhibitors of proliferation and aflatoxins production of *Aspergillus flavus*. In this context, we developed a new approach to assess toxicity and genotoxicity of the new compounds in order to identify their harmless effects to the environment and to the human health. All these results have contributed to the creation of a database correlating chemical structures and biological/toxicological activities.

- Aim 2.

In this section, we investigated the antiproliferative potential of different thiosemicarbazone metal complexes.

In our laboratory, citronellal, vanillin, morpholin, cinnamaldehyde and cuminaldehyde have been chosen as starting aldehydes to prepare different thiosemicarbazones and their corresponding metal complexes with the aim to study how substituent groups could influence their biological activity.

In previous studies, the free ligands did not show any significant cytotoxic effect, independently from the presence or the absence of a substituent on the terminal aminic nitrogen. On the contrary, metal complexes showed marked biological activity: for example, copper complexes with the morpholine ligand presented a highest inhibition of proliferation on central nervous system cell line SN-K-MC, cervical cancer cells HeLa and leukemia cells Jurkat and K562 (Bisceglie *et al*., 2018). Furthermore, the nickel(II) and the

copper(II) complexes of cinnamaldehyde and cuminaldehyde thiosemicarbazones showed antileukemic activity on U937 human cell line. Metal complexes of cuminaldehyde thiosemicarbazone cause G2/M phase cell cycle arrest suggesting a possible action on topoisomerase II. All of these molecules activate caspase-9 and caspase-3, while caspase-8 activity is significantly induced by both cinnamaldehyde metal complexes (Bisceglie *et al*., 2014).

In other studies, citronellal was used to synthetize the nickel ($[Ni(tcitr)_2]$) (Buschini *et al*., 2009) and the copper ($[Cu(tcitr)_2]$) (Bisceglie *et al*., 2012) complexes, where tcitr = citronellalthiosemicarbazonate. Both the complexes demonstrated a strong cytotoxic activity against a panel of cancer cells. In particular, many analyses were carried out employing a leukemia cell line (U937). $[Ni(tcitr)_2]$ is not active on G0 cells (fresh leukocytes) but is able to induce perturbation of the cell cycle on stimulated lymphocytes and U937 cells, in which a G2/M block was detected. The nickel complex causes p53 independent-intrinsic-apoptosis via down-regulation of Bcl-2, mitochondrial membrane potential loss, caspases-3 and -9 activation (Buschini *et al*., 2009). $[Ni(tcitr)_2]$ also caused DNA damage but neither mutagenicity nor recovery were detected. It interacted with DNA and altered DNA conformation creating knot-like structures and hairpins but it did not induce gene mutation or chromosomal damage (Buschini *et al*., 2014). The action mechanism is still unclear but this nickel complex is a promising candidate for the synthesis of new metal thiosemicarbazones with potential biological activity.

In this research, all these experimental data were used to better understand the action mechanism of $[Ni(tcitr)_2]$, $[Cu(tcitr)_2]$ and a new platinum complex $[Pt(tcitr)_2]$. Starting from these metal complexes, we detected the antiproliferative activity of their corresponding dimethylated derivatives. All compounds were screened for their cytotoxic effect on a panel of human cancer cell lines selected from the National Cancer Institute "60 Human Tumor Cell Line Anticancer Drug Screen". We performed also *in vitro* studies to detect genotoxic and mutagenic activities and to identity an interaction of metal complexes with DNA.

Human leukemic U937 cell line was used as an *in vitro* model for mRNA expression studies. First, we examined the modulation of the transcription of the enzyme ribonucleotide

reductase (RR) as possible target of the metal complexes. Indeed, many thiosemicarbazones target RR, interfering with the essential di-iron tyrosyl radical center of its small subunit.

Subsequently, DNA damage induced by metal complexes treatment has been related to mRNA levels of several proteins that regulate DNA damage response and genome integrity. In particular, we focused on the DNA damage sensors, Chk1 and Chk2, that participate in G2/M checkpoint control through the ataxia telangiectasia mutated (ATM)/ATM RAD3 related (ATR) pathway. To determine the correlation between proliferation inhibition and cell cycle blockage, we analysed the expression levels of cyclin A/Cdk2 complex, that are known to participate in the initiation of mitosis in human cancer cells, and of cyclin B, a key component involved in G2 to M phase transition. Furthermore, in order to understand metal complexes transport into U937 cells, we studied hCTR1, a transmembrane protein that is involved in the uptake of platinum anticancer drugs.

- Aim 3

The last section of this project was carried out at the International Agency for Research on Cancer (IARC). Cytotoxic activity of metal complexes was investigated using different cell lines resulting from primary tumour samples and collected as part of a multicenter case-control study coordinated by IARC. Cells were selected for a different pattern of *TP53* mutations. p53 is a tumor suppressor protein and its mutation leading to loss of wild-type p53 activity has been frequently detected in multiple cancer types. Furthermore, perturbations in p53 signaling pathways were required to cancer development and progression. Cells sensitivity was correlated with *TP53* status in order to understand if the cytotoxic mechanisms of the compounds could occur through a p53-dependent pathway. In this study, the copper complex exhibits the strong antiproliferative activity against tumour samples.

Subsequently, through western blot analysis we determined different post translational modifications of p53 protein induced by the treatment with copper complex. We studied several p53 post-translational modifications, such as acetylation and phosphorylation in specific sites, induced when cells were exposed to genotoxic stimuli.

In conclusion, these results highlight that the treatment with metal complexes could trigger specific cellular pathways leading to apoptosis. Furthermore, thiosemicarbazone scaffold represents a good starting point for the development of new anticancer agents.

3. Materials and methods

3.1 General procedure for the synthesis of thiosemicarbazones

Thiosemicarbazones are a class of versatile molecules which can be easily synthesized through a condensation between an equimolar amount of a thiosemicarbazide and an aldehyde or ketone (Fig. 19).

The reaction is usually performed using ethanol as solvent to create a mixture of reagents which is refluxed and stirred from 8 up to 24 hours. The reaction time depends on the reactivity of the carbonyl group of the aldehyde/ketone and can be accelerated using a mild acid catalysis. The reaction is monitored through TLC (thin layer chromatography) and once the reagents are consumed the mixture is cooled to room temperature and left at -4°C until the product precipitation. The product is then collected through filtration, washed many times with a volatile solvent and dried under vacuum. The obtained thiosemicarbazone is characterised using different techniques: FT-IR (Fourier transform infrared) spectrophotometry, ^{1}H-NMR (proton nuclear magnetic resonance spectroscopy), UV-visible spectroscopy, ESI-MS (ElectroSpray Ionization Mass Spectrometry) and single crystal XRD (X-Ray diffraction).

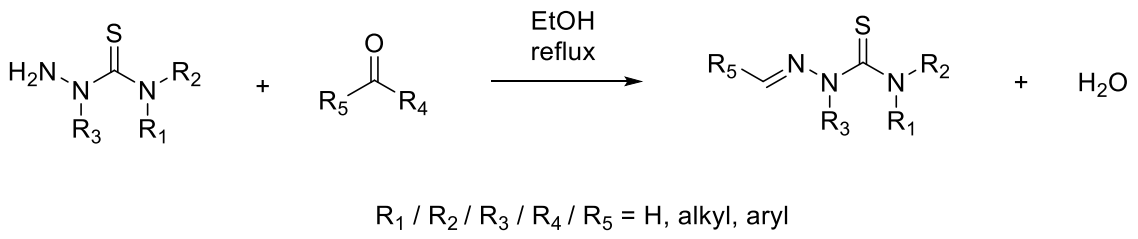

Figure 19. Chemical reaction to synthesize thiosemicarbazones.

3.2 General procedure for the synthesis of thiosemicarbazone metal complexes

The desired thiosemicarbazone ligand is mixed with the appropriate metal salt (Zinc(II) / Copper(II) / Nickel(II) / Platinum(II) acetate) in ethanol using a metal to ligand ratio of 1 : 2. The reagent mixture is left under stirring at room temperature for 2 hours and it usually changes colour during the reaction. Finally, the solvent is removed under reduced pressure and the product is washed twice with diethylether and dried under vacuum. The complex obtained is then characterised by infrared spectroscopy, UV-visible spectroscopy, ESI-MS and single crystal XRD. The ^{1}H-NMR can be used only when the metal centre is diamagnetic (nickel or zinc) and not for paramagnetic elements like copper and platinum (Fig. 20).

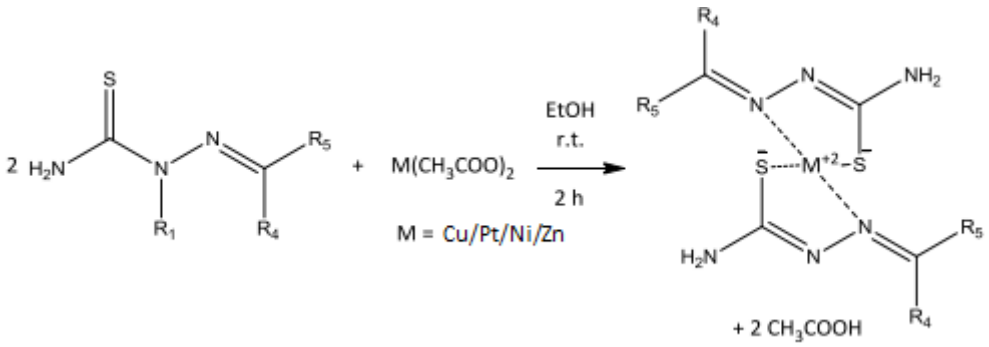

Figure 20. Chemical reaction to synthesize metal complexes of thiosemicarbazones.

The tested molecules are detailed in Appendix.

3.3 Cell lines

The biological activity of the new active molecules with antifungal and antimicotozigen potential was assessed on normal cells: human fibroblast cell line Hs27 (ATCC, CRL1634), human lung epithelial cell line HFL1 (ATCC, CCL-153), human colon epithelial cell line Crl1790 (ATCC, CCD 841 CoN). These cell lines represent the human districts related to possible xenobiotic ways of interaction with the human body, to investigate the exposition risks (Zani *et al*., 2015). We also performed toxicological assays on human histiocytic lymphoma cell line U937 (ATCC, CRL-3253). *In vitro* cytotoxic effects of antiproliferative molecules were investigated on a panel of human cancer cell lines selected from the National Cancer Institute "60 Human Tumor Cell Line Anticancer Drug Screen" (Table 1).

Table 1. Cell lines used for *in vitro* studies.

Cell line	Desease	Culture Properties
U937 (ATCC, CRL-3253)	Histiocytic lymphoma	Suspension
HT29 (ATCC, HTB-38)	Colorectal adenocarcinoma	Adherent
Jurkat (ATCC, TIB-152)	Acute T cell leukemia	Suspension
MCF7 (ATCC HTB-22)	Breast adenocarcinoma	Adherent
A549 (ATCC, CCL-185)	Lung carcinoma	Adherent
HeLa (ATCC, CCL-2)	Cervix adenocarcinoma	Adherent
HL-60 (ATCC, CCL-240)	Acute promyelocytic leukemia	Suspension
K-562 (ATCC, CCL-243)	Chronic myelogenous leukemia	Suspension
T-47D (ATCC, HTB-133)	Breast ductal carcinoma	Adherent
SK-N-MC (ATCC, HTB-10)	Neuroepithelioma	Adherent
U266 (ATCC, TIB-196)	Myeloma	Suspension
THP-1 (ATCC, TIB-202)	Acute monocytic leukemia	Suspension
CCRF-CEM (ATCC, CCL-119)	Acute lymphoblastic leukemia	Suspension
PC-3 (ATCC, CRL-1435)	Prostate adenocarcinoma	Adherent
HT-1080 (ATCC, CCL-121)	Fibrosarcoma	Adherent
A375 (ATCC, CRL-1619)	Melanoma	Adherent
SH-SY5Y (ATCC, CRL-2266)	Neuroblastoma	Mixed

The last part of this project was carried out at the International Agency for Research on Cancer (IARC). *In vitro* studies were performed on four different solid cancer cell lines obtained from primary tumours samples, embedded surgical materials in paraffin (Table 2) (Saulnier *et al*., 2012).

Table 2. Cell lines used for *in vitro* studies at IARC.

Cell line	Desease	Culture Properties
HNC-212	Oral cavity cancer	Adherent
HNC-211	Tonsil cancer	Adherent
HNC-41	Tonsil cancer	Adherent
PNS-136	Paranasal sinus cancer	Adherent

Cells were selected for a different pattern of *TP53* mutations. Since in more than 50% of tumors p53 is mutated, in a previous study the state of p53 in tumor samples were analysed. Cells were collected and DNA extraction was performed. The DNA was sequenced and screened for *TP53* mutations. Furthermore, in order to evaluate the expression of p53 protein, cellular pellets from each cell line were lisate and analyse by Immunoblot for the level of p53. The results are listed in table 3.

Table 3. p53 status and protein level in primary tumours samples.

Cell line	Exon	Codon base	AA change	p53 levels
HNC-41	WT (4-9)	-	-	+
PNS-136	WT (4-9)	-	-	+++
HNC-211	6	177-183	In frame	+
HNC-212	6 9	196 CGA-CCA 331 CAG-AG	Arg-Pro Frameshift	++

+ = basal expression; ++/+++= overexpression

3.4 Culture conditions

A549, HeLa, Jurkat, K-562, U937, U266, THP-1, CCRF-CEM cells were cultured in Roswell Park Memorial Institute Medium (RPMI-1640); A375, HL-60, HNC-41, HNC-211, HNC212, Hs27, HT29, MCF7, PNS-136, SK-N-MC and T-47D cells in Dulbecco's Modified Eagle Medium (DMEM); HFL-1 and PC3 cells in Kaighn's Modification of Ham's F-12 Medium (F-12K) and CRL1790, HT-1080 and SH-SY5Y cells in Eagle's Minimum Essential Medium (EMEM). All media were supplemented with 10% (v/v) fetal bovine serum (FBS), 1% penicillin (100 U/ml)/streptomycin (100 µg/ml) and 1% L-Glutamine (2 mM). Adherent cells were grown as a subconfluent monolayer. Flasks and plates were maintained at 37°C and 5% CO_2 in a humidified atmosphere. Culture medium was refreshed every two or three days during sub-culturing and determination of cell numbers and viabilities was performed with the trypan blue exclusion method (see below).

Most of cell lines were obtained from the American Type Culture Collection (ATCC); U937 cells were obtained from the American Tissue Culture Collection (Rockville, MD); HNC-41, HNC-211, HNC-212 and PNS-136 were collected as part of a multicenter case–control study coordinated by IARC as described by Saulnier and co-workers (Saulnier *et al*., 2012).

3.5 Trypan blue exclusion method

The percentage of live cells was assessed by Trypan blue exclusion method. After treatment with the newly synthesized molecules, cells were resuspended in complete medium and Trypan blue was added. 100 cells for each concentration were counted manually using a hemocytometer.

3.6 Cell proliferation assay

The antiproliferative activity was evaluated by CellTiter 96® AQueous One Solution Cell Proliferation Assay (Promega Corporation, Madison WI, USA), a colorimetric assay that allows us to determine the number of viable cells in proliferation.

The CellTiter 96® AQueous One Solution Reagent contains a tetrazolium compound [3-(4,5-dimethylthiazol-2-yl)-5-(3-carboxymethoxyphenyl)-2-(4-sulfophenyl)-2H-tetrazolium, inner salt; MTS] and an electron coupling reagent (phenazine ethosulfate; PES). PES has

enhanced chemical stability, which allows it to be combined with MTS to form a stable solution. The MTS tetrazolium compound is reduced by cells into a coloured formazan product that is soluble in the culture medium. This conversion is accomplished by NADPH or NADH produced by dehydrogenase enzyme in metabolically active cells.

Briefly, 100 µL of a suspension of cells in exponential growth (5 $\times 10^4$/mL in complete medium without phenol red supplemented with 5% FBS) were added into 96-well plates (FALCON®, Becton Dickinson, Meylan Cedex, France) 24h before treatment. Plates were incubated at 37 °C in a humidified 5% CO_2 incubator. After this recover period, increasing concentrations of compounds (0.5-1.0-5.0-10.0-50.0-100.0 µM) were added to the medium and cells were left exposed for 24-48-72h. Negative control was represented by 100 µM DMSO. After treatment period, MTS reagent was added to each well. At the end of exposure time, the absorbance of the formazan product was measured at 485 nm by a microwell plate reader (TECAN SpectraFluor Plus, Männedorf, Switzerland).

The percent growth was obtained by the formula:

Percent growth = $[1 - (OD_{485}$ treated/OD_{485} control$)] \times 100$

The cytotoxicity response parameters GI_{50}, drug concentration inducing a 50% reduction of the cell number in comparison to untreated control cells cultured in parallel, were extrapolated from concentration-response curves.

3.7 Alkaline Comet Assay

The Alkaline Comet Assay is an approach for assessing DNA damage evaluating the presence, after electrophoresis, of fragmented DNA outside the core of the nucleus. Relaxed and/or broken DNA fragments, negatively charged, migrate toward the anode and the resulting image has the appearance of a comet. The amount of DNA migrated from the head of the comet indicates the extent of the DNA damage. This quantity is dependent on the size of DNA fragments and the number of broken ends in the strands. The comet assay is usually performed at pH>13 to detect single and double breaks, alkali-labile sites (adducts, apurinic and apirimidinic sites, oxidation of the nitrogenous bases).

U937 cells were seeded 24h before treatment at a concentration of 1 x 10^5 cell/mL in 1 mL wells. Cells were treated with increased concentrations of the compounds for 1h and 24h. Positive and negative controls were represented by ethylmethanesulfonate (EMS) [2 mM], and DMSO [100 µM], respectively. After treatment period at 37 °C, determination of cell numbers and viabilities was performed with the trypan blue exclusion method (see above). Only the treatments that had a viability higher than 70% have been processed in the assay. Cells were transferred onto degreased microscope slides previously dipped in 1% normal melting agarose (NMA) for the first layer. The agarose was allowed to set for 20 min at 4 °C before addition of a final layer of low melting agarose (LMA). Cell lysis was carried out at 4 °C overnight by exposing the cells to a buffer containing 2.5 M NaCl, 10 mM Na_2EDTA, 10 mM Tris–HCl, 1% Triton X-100 and 10% DMSO, pH 10. The electrophoretic migration was performed in an alkaline buffer (1 mM Na_2EDTA, 300 mM NaOH, 0 °C) at pH > 13 (DNA unwinding: 20 min; electrophoresis: 20 min, 0.78 Vcm^{-1} 300 mA), to detect single and double DNA strand breaks and alkali-labile sites. Slides were then washed with a neutralisation solution (0.4 M Tris–HCl, pH 7.5).

DNA was stained with 75 µl ethidium bromide (10 µg/mL) before the examination at 400 X magnification under a Leica DMLS fluorescence microscope (excitation filter BP 515–560 nm, barrier filter LP 580 nm), using an automatic image analysis system (Comet Assay IV – Perceptive Instruments Ltd) (Fig. 21). Percentage of DNA in the tail region of the comet (TI, tail intensity) provided representative data on genotoxic effects. For each sample, coded and evaluated blind, 100 cells were analysed.

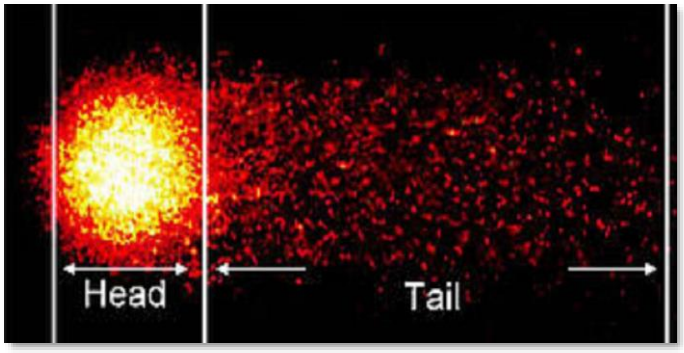

Figure 21. Typical damaged DNA in Alkaline Comet Assay.

The cells showing completely fragmented chromatin (i.e. hedgehogs cells) were assessed as a further indicator of cytotoxicity. These cells were not evaluated by image analysis but were recorded separately.

3.8 *Salmonella typhimurium* reversion test

The *Salmonella typhimurium* reversion test (Ames test) was employed for the assessment of the gene mutation activity of compounds. The experiment was performed using *Salmonella typhimurium* strains TA98 and TA100 in the plate incorporation method, with and without rat liver S9 mix (exogenous metabolic activation system). Five doses (2.5–5.0-10.0-50.0-100.0 mg per plate) of the metal complexes were tested in both strains and the colonies that appeared were counted. Positive controls were 2-nitrofluorene [20.0 mg per plate] for TA98 -S9 strain, sodium azide [15.0 mg per plate] for TA100 -S9 strain, and 2-aminoanthracene [10.0 mg per plate] for both strains with S9. DMSO was tested as negative control.

The data of Ames test are reported as mean and standard deviation of revertant plate. In accordance with the guidelines (OECD, No 471), the results of the Ames test were considered positive if two consecutive dose levels or the highest non-toxic dose level produced a response at least twice that of the solvent control (DMSO), and at least two of these consecutive doses showed a dose-response relationship.

3.9 Cytofluorimetric analysis of cell cycle

Cell phase distribution was assayed by determining the DNA content of nuclei labelled with propidium iodide (PI) using flow cytometry.

U937 cells were seeded 24h before treatment at a concentration of 5 x 10^5 cell/mL in 1 mL of complete medium. Plates were incubated at 37 °C in a humidified 5% CO_2 incubator. After this recover period, cells were treated with the platinum and the copper complexes of citronellal thiosemicarbazone using the GI_{50} concentrations (7.0 µM and 33.0 µM, respectively) and incubated for 4 and 24h. Cells were collected, washed in PBS w/o Ca^{2+} and Mg^{2+} and fixed with 1 mL of 70% ethanol at 4 °C for 2h. After fixation, cells were washed once in PBS. Cellular pellets were resuspended in 0.5 mL PBS added with 2.5 µL of 1 mg/mL propidium iodide and 2 µl of RNAse (1mg/ml) and were incubated at 37 C in a water bath for 30 minutes. For each sample, 12000 events were analysed using NovoCyte ™ flow cytometry.

3.10 Real time PCR

Real Time PCR was performed on cDNA obtained from U937, HNC-41, PNS-136, HNC-211 and HNC-212 cells.

3.10.1 RNA extraction

$2x10^6$ cells were seeded in flasks with complete medium. After 24h, cells were treated with two different concentrations of metal complexes: one toxic, corresponding to GI_{50} value, and a subtoxic one, 10 times lower than GI_{50} (Table 4).

Table 4. Different concentrations of metal complexes used for RNA extraction.

Cell line	Metal complex	Concentration
U937	$[Ni(tcitr)_2]$	1.0 µM 10.0 µM
	$[Pt(tcitr)_2]$	0.7 µM 7.0 µM
	$[Cu(tcitr)_2]$	3.3 µM 33.0 µM
HNC-41	$[Cu(tcitr)_2]$	0.72 µM 7.2 µM
PNS-136	$[Cu(tcitr)_2]$	1.85 µM 18.5 µM
HNC-211	$[Cu(tcitr)_2]$	0.65 µM 6.5 µM
HNC-212	$[Cu(tcitr)_2]$	0.85 µM 8.5 µM

Cells were treated for 1-4-24 h. After treatment period, cells were collected. Total RNA was extracted using GeneJET RNA Purification Kit (Thermo Fisher Scientific) according to manufacturer's protocol.

The concentration and purity of the extracted RNA was determined with a Nanodrop 2000 spectrophotometer (Thermo Fisher Scientific). We evaluated the 260/230 and 260/280

ratios as an indirect measure of RNA purity. The ratio of absorbance at 260 nm and 280 nm is used to determine the presence of proteins, phenol or other contaminants that absorb strongly at or near 280 nm, while RNA absorbs at 260 nm. A ratio of ≈2.0 is generally accepted as "pure" for RNA samples. The ratio of absorbance at 260 nm and 230 nm is used to determine the presence of contaminants which absorb at 230 nm. Expected 260/230 values are commonly in the range of 2.0-2.2.

3.10.2 cDNA synthesis

For each cell line, total RNA (1 μg) was reverse-transcribed using QuantiTect® Reverse Transcription Kit (Qiagen) according to manufacturer's protocol.

The genomic DNA elimination reaction was prepared on ice according to table 5, was incubated for 2 min at 42 °C and then was placed immediately on ice:

Table 5. Genomic DNA elimination reaction components.

Component	Volume/reaction
gDNA Wipeout Buffer, 7X	2 μl
Template RNA	1 μg
RNase-free water	Variable
Total reaction volume	14 μl

The reverse-transcription master mix was prepared on ice as shown in table 6:

Table 6. Reverse-transcription reaction components.

Component	Volume/reaction
Reverse-transcription master mix Quantiscript Reverse Transcriptase	1 μl
Quantiscript RT Buffer 5X	4 μl
RT Primer mix	1 μl
Template RNA	14 μl
Total reaction volume	20 μl

The mix was incubated for 15 min at 42 °C, for 3 min at 95 °C to inactivate Quantiscript Reverse Transcriptase and then stored at -20 °C.

3.10.3 Real time PCR

After cDNA synthesis, RT-PCR was carried out using the QuantiNova™ SYBR® Green PCR Kit (Qiagen). During PCR, SYBR Green intercalates into the dsDNA helix and the increase in SYBR Green fluorescence is directly proportional to the amount of dsDNA generated. In solution, the unbound dye exhibits very little fluorescence; however, fluorescence (measured at 530 nm) is greatly enhanced (100-fold) upon binding to DNA due to conformational changes.

The primers used in the RT-PCR analysis were obtained from Eurofins Genomics and are presented in Table 7.

Table 7. Primer sequences used for real time polymerase chain reaction (RT-PCR).

Gene	Primer forward (5'-3')	Primer reverse (5'-3')
GAPDH	ATGACATCAAGAAGGTGGTG	CATACCAGGAAATGAGCTTG
RRM1	AAGAGCAGCGTGCCAGAGAT	ACACATCAAAGACCAGTCCTGATTAG
RRM2	ACCAACTAGCCACACACCATGA	GGACTGTTTAATCCCGCTGT
p53R2	CCTTGCGATGGATAGCAGATAGA	GCCAGAATATAGCAGCAAAAGATC
hCTR1	TCACCATCACCCAACCACTT	TCTTAAAGCCAAAGTAGAAGGTCA
Cyclin A1	GTCAGAGAGGGGATGGCAT	CCAGTCCACCAGAATCGTG
Cyclin B1	CGGGAAGTCACTGGAAACAT	AAACATGGCAGTGACACCAA
Chk1	GGTGCCTATGGAGAAGTTCAA	TCTACGGCACGCTTCATATC
Chk2	CGGATGTTGAGGCTCACGA	TATGCCCTGGGACTGTGAGG
ATM	CAGCAGCTGTTACCTGTTTG	TAGATAGGCCAGCATTGGAT
ATR	TGTCTGTACTCTTCACGGCATGTT	AAGAGGTCCACATGTCCGTGTT
Cdk2	GAAACTCTGAAGCCGACCAG	GCCCTCTCAGTGTCCAGAAG
Cdc2	GGTTCCTAGTACTGCAATTCG	TTTGCCAGAAATTCGTTTGG

The reaction mix was prepared on ice according to table 8:

Table 8. Real time PCR Reaction Setup.

Component	Volume/reaction
2X SYBR Green PCR Master Mix	10 µl
QN ROX Reference Dye	2 µl
Primer forward	0.7 µM
Primer reverse	0.7 µM
Total reaction volume	20 µl

We added template cDNA (2 µl) to the individual PCR tubes and the we programmed the real time PCR cycler (StepOnePlus Real-TimePCR System) following the protocol directions reported in table 9:

Table 9. Cycling conditions.

Step	Time	Temperature
PCR initial heat inactivation	2 min	95 °C
Denaturation	5 s	95 °C
Combined annealing/extension	10 s	60 °C
Number of cycles	35-40	
Melting curve analysis		

The comparative Ct method was used for relative mRNA quantification; glyceraldehyde 3-phosphate dehydrogenase gene (*GAPDH*) was used for the normalization of the expression level. Each experimental condition was performed in triplicate.

3.11 Western Blot

3.11.1 Protein extraction from cell cultures

Protein extraction was performed on HNC-41, PNS-136, HNC-211 and HNC-212 cell lines. $8x10^5$ cells were seeded in 6-well plates with complete medium. After 24h, cells were treated for 1-4-24 h with two different concentrations of copper complex $[Cu(tcitr)_2]$ using the protocol previously described. After treatment period, cells were collected as following: first the cells had been washed twice with ice-cold PBS, 500µL/well of fresh PBS + 3% FBS was added to scrape and collect the cells into a new tube. Then cells were centrifugated at 5000 g for 3 minutes; supernatants were discarded and the remaining pellets were washed with PBS and centrifuged again. The pellets thus obtained were resuspended in 70 µL of ice-cold RIPA buffer (50mM TrisHCl (pH 7.5), 150mM NaCl, 10mM $MgCl_2$, some detergents (0.5% Na- deoxycholate, 1% Nonidet P-40) and protease inhibitor cocktail (Roche)), a lysis buffer that enables efficient cell lysis and protein solubilization. Cells were then incubated on ice for 30 minutes vortexing every 10 minutes, sonicated with biorupt 15'' ON 60'' OFF and then centrifuged for 10 minutes at 13000 rpm at 4 °C. The supernatants containing the protein were transferred into new tubes and stored at -80 °C.

3.11.2 Determination of protein concentration

The protein content of lysates was quantified by spectrophotometry, using the Bradford method, a spectroscopic analytical procedure used to measure the concentration of protein in a solution. The assay is based on the observation that the absorbance maximum for an acidic solution of Coomassie Brilliant Blue G-250 shifts from 465 nm to 595 nm when binding to protein occurs. Both hydrophobic and ionic interactions stabilize the anionic form of the dye, causing a visible colour change from red to blue form. The protein concentration of a test sample is determined by comparison to that of a series of protein standards known to reproducibly exhibit a linear absorbance profile in this assay. Although different protein standards can be used, we have chosen the most widely used protein as our standard - Bovine Serum Albumin (BSA).

Standard curve has been prepared using a serial dilution of BSA (scalar volume 1 µg/µL to 10 µg/µL of BSA in 500 µL of Bradford). Bradford reagent was used initially as blank and then to dilute the samples to quantify (3µl of samples in 500 µL of Bradford reagent). Protein samples were assayed in duplicate. Then, the absorbance at 595 nm obtained from samples was evaluated by comparing it to the calibration curve. For the analysis we used a linear regression system. The measurement was performed by Biophotometer Eppendorf Spectophotometer. The protein lysates were then stored at-20 °C until use.

3.11.3 Electrophoresis

Samples were resolved by sodium dodecyl sulfate polyacrylamide gel electrophoresis (SDS-PAGE), used to separate proteins according to their electrophoretic mobility, a function of length of polypeptide chain or molecular weight, and according to their size. SDS is a detergent that disrupts hydrophobic areas and coats proteins with many negative charges which overwhelms any positive charges the protein had, due to positively charged R-groups. The resulting protein has been denatured by SDS that reduced to its primary structure-amino acid sequence and as a result has been linearized.

We used 20 µg of protein cell lysate for each sample, solubilized in 5X SDS-PAGE loading buffer (250mM Tris-HCl, pH 6.8, 2.5% SDS; 35% Glycerol, 0.025% (w/v) Bromophenol blue, 125 mM DTT). Samples were denatured for 2 minutes at 100 °C before loading. A range of molecular weight markers enabled the determination of the protein size and also to monitor the progress of the electrophoretic run.

The system is set up with a stacking gel at pH 6.8, buffered by Tris-HCl, a running gel buffered to pH 8.8 by Tris-HCl. The stacking gel has a low concentration of acrylamide (4%) and the running gel a higher concentration (12%) capable of retarding the movement of the proteins used. Samples were loaded into a vertical electrophoresis apparatus and the electrophoresis was conducted at a constant current of 30 mA.

3.11.4 Blotting and blocking

Trans-Blot® Turbo™ semidry electrophoretic transfer cell (Bio-Rad) (130 mA, 1 h 30 min) was used for the protein transfer from gel to Polyscreen polyvinylidene difluoride (PVDF) membrane (NEN Life Sciences).

Polyacrylamide gel was put in direct contact with the nitrocellulose membrane, between two filter paper layers, soaked with transfer buffer. The sandwich thus assembled was inserted in the appropriate cassette of the instrument.

The complete protein transfer was ensured by staining the membrane with Ponceau and polyacrylamide gel with Coomassie Brilliant Blue (0.2% Coomassie powder, 50% methanol, 10% acetic acid): membranes and gels were incubated on a shaker. After having ensured the complete transfer, membranes were impermeabilized with TBS-Tween 0.1% (Tris-buffered saline with addiction of 0.1% Tween 20 SIGMA). Blocking of non-specific binding is achieved by placing the nitrocellulose membrane with a blocking solution (5% skim milk powder and/or BSA in TBS-Tween 0.1%) at 4 °C overnight on a shaker. Proteins contained in blocking solution attaches to the membrane in all places where the target proteins have not attached. This reduces "noise" in the final product of the western blot, leading to clearer results, and eliminates false positives.

3.11.5 Hybridization with antibodies

For the dilution and the condition of incubation of primary and secondary antibodies were followed the relative datasheets.

Antibodies against the following proteins were used: GAPDH (2118; Cell Signaling Technology); p53 (DO-1) (sc-126; Santa Cruz Biotechnology); phospho-p53 (Ser15) (9284; Cell Signaling Technology); phospho-p53 (Ser33) (2526; Cell Signaling Technology); phospho-p53 (Ser392) (9281; Cell Signaling Technology); Acetyl-p53 (Lys382) (2525; Cell Signaling Technology); mTOR (2972; Cell Signaling Technology).

Images were produced using the ChemiDoc XRS imaging system (Bio-Rad) and data were analysed by densitometry with the ImageLab software.

3.12 Statistical analysis

The “IBM SPSS Statistics 24” software was used to analyse statistical differences between samples. The mean values from the repeated experiments were used in a one-way analysis of variance (ANOVA). If significant F-values ($p < 0.05$) were obtained, Student's t-test (Bonferroni's version) was performed.

4. Results

4.1. "Aflatox project": cytotoxicity and genotoxicity of antifungal and antiaflatoxigenic molecules

Nowadays, one of the major causes of food spoilage is the presence of fungal pathogens, that produce mycotoxins.

Mycotoxins are toxic secondary metabolites, produced by many filamentous fungi belonging to the *phylum Ascomycota*. They can contaminate cereals, nuts, dried fruit, coffee, cocoa, spices, oil seeds, and some derived products, such as beer, wine, and fruit juices, and can also enter the human food chain. Among the different type of mycotoxins, the most important are aflatoxins (AFs), which are produced mainly by *Aspergillus flavus* and *Aspergillus parasiticus* (Marroquín-Cardona *et al*., 2014). Several studies in human and in animal models demonstrated that AFs have carcinogenic, teratogenic, hepatotoxic, mutagenic, and immunosuppressive effects, with the liver the main organ affected (Alshannaq *et al*., 2017). The International Agency for Research on Cancer (IARC) has classified both B- and G-type aflatoxins as Group 1 mutagens, whereas AF-M1 is classified in Group 2B (IARC, 2015; Ostry *et al*., 2017).

Mycotoxin contamination is considered a global problem and represents a challenge to food safety. They can accumulate in food during agricultural, storage, and processing practices; furthermore, many mycotoxins are not easily eliminated during food processing because of their stability against heat, physical, and chemical treatments. Several strategies have been proposed to prevent the toxic effects of mycotoxins in general, and of aflatoxins in particular; however, no clear-cut solutions exist (Sarma *et al*., 2017).

In this context, "Aflatox project" aims to develop a biotechnological approach to identify new typologies of inhibitors of *Aspergillus flavus* proliferation and/or aflatoxins production (Zani *et al*., 2015). Our research group has set up a screening procedure to design, synthesize and identify new compounds to reduce the risk of food contamination by aflatoxins.

A number of studies highlighted that natural products are important sources for the development of new drugs, featuring unique modes of action, low mammalian toxicity, easy decomposition, environmental friendliness, desirable biological activities, and specificity to target species. In particular, several researches proposed natural products and

their chemical analogues as crop-protective agents. In addition, inorganic substances, like copper salts, have been long used for their capacity of inhibiting the development of fungi and bacteria and can have effects on growth of *A. flavus* and aflatoxins production.

In our study, natural molecules represent the starting point to obtain the corresponding thiosemicarbazones, introducing the thio- group and yielding more active compounds than the parental ones. Furthermore, thiosemicarbazones were coordinated with metal ions, in particular copper, nickel and zinc, to synergistically improve the capability of the free ligands to inhibit toxin production (Rogolino *et al*., 2017). The most active compounds have been modified in their structure and in their physicochemical properties (hydrophilicity and electronegativity modifications, acidity suppression, redox potential, etc.) in order to study the mechanism of action and to improve the biological activity.

These molecules once synthesized and characterized, were initially tested to determine antifungal and antiaflatoxigenic properties. We evaluated effects on *A. flavus* growth and aflatoxin biosynthesis and accumulation. Subsequently, we selected the most active antifungal or antimycotoxigenic compounds and we performed cytotoxic and genotoxic *in vitro* assays on different cells (plant, bacterial and human cells) to assess their impact on the environment and on human health. In fact, the identification of the toxicological properties of new chemical substances is a fundamental step in protecting human and environmental health. Furthermore, all these experimental data were used to create a Q-SAR (Quantitative structure-activity relationship) database correlating chemical structures and biological/toxicological activities (Zani *et al*., 2015).

In this research, we reported the study of the safety profile of a series of functionalized thiosemicarbazones and their metal complexes in order to assess the potential toxic and genotoxic risks for human health. In particular, in our laboratory a screening of the direct toxicity were performed through MTS assay to identify cytotoxic effects of the new molecules. The test was carried out against three different normal cell lines: Hs27 cells representing epidermal contact, HFL-1 cells representing inhalation and CRL1790 cells representing ingestion. In addition, we also used a leukocytes cancer cell line (U937), that is a good cell model to identify cytotoxicity of drugs (Rogolino *et al*., 2017).

All cell lines were treated with increasing concentration of compounds in the range from 0.5 to 100.0 µM for 24h in order to identify a dose-response curve. The cytotoxicity response parameter GI_{50} (50% reduction of cell growth) was extrapolated from each dose-response curve. We selected the compounds with the lowest antiproliferative effect on cells to be further analysed for their genotoxic effects. Cytotoxic compounds were excluded from the study.

Alkaline Comet Assay were performed on U937 cells to identify the genotoxic potential of not cytotoxic molecules. The test is able to measure DNA damage and is usually carried out at pH>13 to detect, in addition to single and double strand breaks, alkali-labile sites such as adducts, a purinic and apyrimidinic sites, oxidation of the nitrogenous bases, etc. The percentage of DNA in the tail of the comet (TI%) provided a representative data on genotoxic effects of the molecules. Cells were treated with 25.0-50.0-75.0-100.0 µM of the molecules for 1 and 24h (Zani *et al*., 2015).

4.1.1. Cuminaldehyde derivates

Cuminaldehyde is one of the major components of cumin essential oil, known for its natural mycostatic properties (Naveed *et al*., 2013; Oroojalian *et al*., 2010). First, we synthesized Htcum, a thiosemicarbazone containing aromatic fragment deriving from cuminaldehyde. To identify the possible factors that endow cuminaldehyde of its properties, we have started by modifying the two constituting moieties: the thiosemicarbazone and the cuminaldehyde fragments (Degola *et al*., 2015).

As a first comparison, we synthesized the semicarbazone, an analogue of cuminaldehyde thiosemicarbazone with the sulfur replaced by an oxygen (Hscum). This modification was investigated in order to focus on the role played by sulfur and oxygen to form weak/strong hydrogen bonds and also to identify their redox potentials. In general, sulfur forms weaker hydrogen bonds than oxygen due to a lower electronegativity and is more subject to oxidation, through the formation of disulfide bridges. In fact, thiosemicarbazones, owing to their thione-thiol tautomerism, in their thiolic form can behave as reducers and therefore also as ROS generators or radical scavengers.

As a second step, we modified the cuminaldehyde thiosemicarbazone by synthesizing its meta- and ortho-isomers. The choice of the ortho- (oHtcum) and meta- (mHtcum) isopropyl derivatives of Htcum is based on the fact that these analogues possess a hydrophobicity very similar to cuminaldehyde, but present different shapes. This comparison aims at understanding if the position of the isopropyl group plays a generic role as a hydrophobic fragment that allows the molecule to enter the cell or if its location is part of a specific molecular mechanism (Degola *et al*., 2017).

Htcum and mHtcum were effective in decreasing toxin accumulation, while oHtcum, Hscum, and cuminaldehyde only slightly reduced aflatoxins content of the culture medium and did not interfere with conidium germination and hyphal elongation. Interestingly, mHtcum, at difference with Htcum, did not affect fungal growth significantly (Degola *et al*., 2017).

The cytotoxic effect of each substance was analysed. The ligand cuminaldehyde induced a mild cytotoxic effect on colon (CRL1790) and skin cells (Hs27). Hscum and Htcum caused a growth inhibition of Hs27 and HFL1 cells, respectively. The GI_{50} values highlighted that mHtcum and oHtcum did not show antiproliferative activity against human healthy cell lines up to 100µM.

Interestingly, Htcum and mHtcum induced a mild growth inhibition in U937 cells (Table 10).

Table 10. GI_{50} value (µM), concentration of drug that causes a 50% reduction of cell growth, obtained in human healthy cell lines (CRL1790; Hs27; HFL1) and U937 cancer cell line.

	CRL1790	**Hs27**	**HFL1**	**U937**
Cuminaldehyde	77.5	91.0	>100.0	>100.0
Hscum	>100.0	96.0	>100.0	>100.0
Htcum	100.0	100.0	85.0	53.0
mHtcum	>100.0	>100.0	>100.0	73.0
oHtcum	>100.0	>100.0	>100.0	>100.0

Starting from the different cuminaldehyde thiosemicarbazones, the corresponding zinc and copper complexes were synthesized and tested for their antimycotoxigenic activity. Only

the copper complex of Htcum showed any effects on fungal growth and aflatoxin production. In the other cases, metal plays a pivotal role in biological potency of the molecule. In fact, these metal complexes displayed potent *in vitro* cytotoxic effects against human cells (Table 11).

Table 11. GI_{50} value (μM), concentration of drug that causes a 50% reduction of cell growth, obtained in human healthy cell lines (CRL1790; Hs27; HFL1) and U937 cancer cell line.

	CRL1790	Hs27	HFL1	U937
X	33.5	21.0	27.0	36.0
Y + Zn	54.0	41.5	42.0	>100.0
Z + Zn	30.0	36.0	33.0	32.0
F24	31.5	26.0	32.5	20.0
F23	28.5	18.0	32.0	24.0

The importance of methyl groups in modulating biological activity, selectivity, solubility, metabolism and pharmacokinetic/pharmacodynamic properties of biologically active molecules is highlighted in literature. Structural modification, such as substituent replacements at different parts of the molecules, could optimize the activity of promising compounds. The methyl group was introduced in order to modify the cuminaldehyde thiosemicarbazone moiety, obtaining the 3 isopropylbenzaldehyde-2-methyl-3-thiosemicarbazone (F30). It induced a mild antiproliferative activity, especially on CRL1790 and U937 cells, and did not show effects on HFL1 cells proliferation (Table 12).

In the second case, the methyl group was used to modify the bis(2-isopropylbenzaldehydethiosemicarbazonate)copper(II) complex, yielding methyl bis-(2-isopropylbenzaldehydethiosemicarbazonate) Cu(II) complex (F40). The treatment with this compound caused a strong inhibition of cell proliferation, in particular against colon cells (Table 12).

Table 12. GI_{50} value (µM), concentration of drug that causes a 50% reduction of cell growth, obtained in human healthy cell lines (CRL1790; Hs27; HFL1) and U937 cancer cell line.

	CRL1790	Hs27	HFL1	U937
F30	60.5	97.0	>100.0	66.0
F40	9.5	31.0	17.5	20.0

Among cuminaldehyde derivates, mHtcum was the best candidate in term of inhibition of aflatoxin production and safety against human cells. We performed Alkaline Comet Assay to identify its genotoxic potential: mHtcum did not show genotoxic potential against U937 cells, after 24h treatment, as expected, it displayed a strong toxic activity, especially at the highest concentrations (Fig. 22).

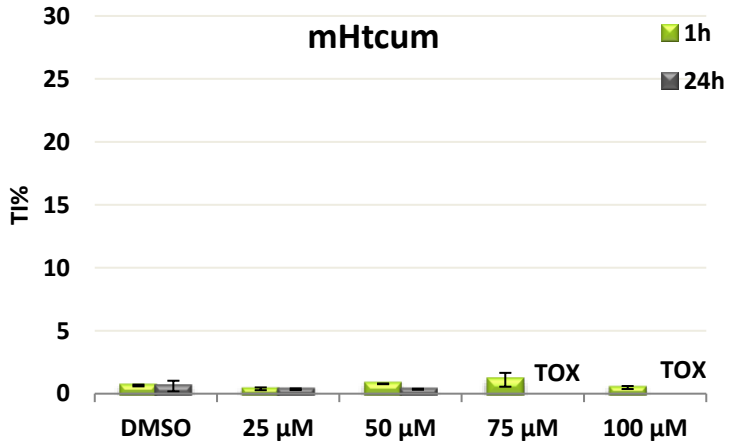

Figure 22. Genotoxic activity of mHtcum using Alkaline Comet assay on U937 cells treated for 1 h and 24 h. TI%: percentage of tail intensity. TOX: viability <70%.

4.1.2. Perillaldehyde derivates

Perillaldehyde is a natural compound found in the herb perilla and in the peel of citrus fruits (Maronpot *et al*., 2018). Two different derivates of perillaldehyde were synthesized: V, the parent thiosemicarbazone ligand, and T, the corresponding nickel complex. Molecule T is a good inhibitor of aflatoxin production, but unexpectedly it is less effective than the parent organic molecule in inhibiting mycelium growth. Both molecules induced a stronger antiproliferative activity on normal cells (Hs27 and Crl1790) compared to tumor cells (U937). Hs27 cells showed the major sensitivity to the tested molecules. The GI_{50} induced

by V resulted 34.0 µM for Hs27 and 71.0 µM for Crl1790 (Table 13). It is noteworthy that the proliferative activity of Hs27 cells was strongly reduced starting from the dose 5.0 µM (Zani *et al*., 2017) (Fig. 23).

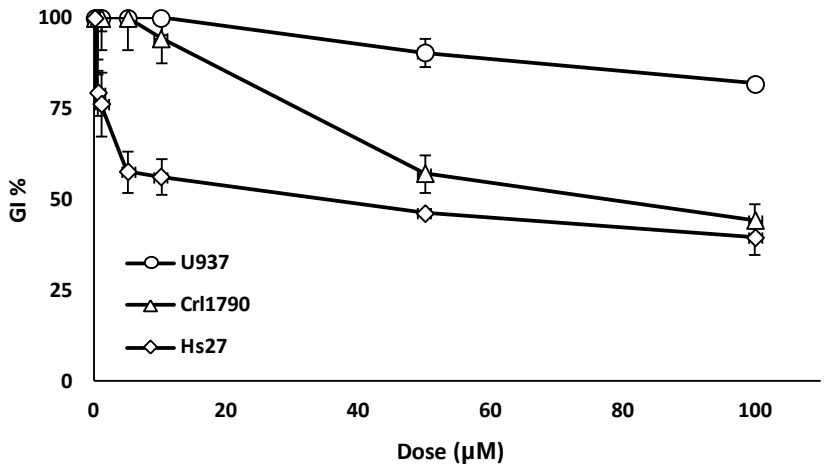

Figure 23. Antiproliferative activity detected by MTS assay on human cell lines (Hs27, Crl1790, U937) treated for 24 h with V. GI%: percent of growth inhibition (Zani *et al*., 2017)

The GI_{50} induced by T resulted to be 35.0 µM for Hs27 and 49.0 µM for Crl1790 (Table 13); a mild antiproliferative activity was detected also on U937 cells, at the highest tested concentration (100.0 µM) the growth inhibition was around 55% (Zani *et al*., 2017) (Fig. 24).

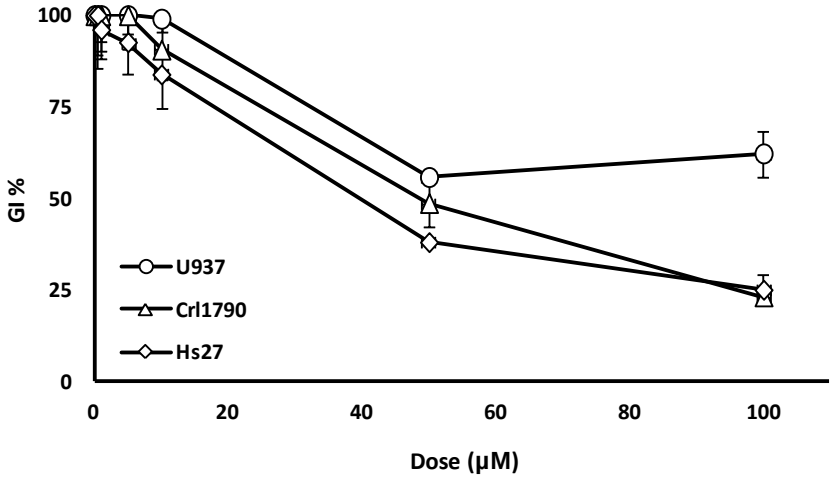

Figure 24. Antiproliferative activity detected by MTS assay on human cell lines (Hs27, Crl1790, U937) treated for 24 h with T. GI%: percent of growth inhibition (Zani *et al*., 2017).

Table 13. GI_{50} value (µM), concentration of drug that causes a 50% reduction of cell growth, obtained in human healthy cell lines (CRL1790; Hs27; HFL1) and U937 cancer cell line.

	CRL1790	Hs27	U937
V	71.0	34.0	>100.0
T	49.0	35.0	>100.0

DNA damaging activity was assessed at different time of exposure (1 h and 24 h) through the Comet Assay on U937 cells. This cell line showed to be less sensitive than normal cells to the toxic effects of the new molecules and for this reason was chosen to detect the subtoxic effects on DNA in human cells. No genotoxicity was detected on U937 cells treated with molecule V at both exposure times (Zani *et al*., 2017) (Fig. 25).

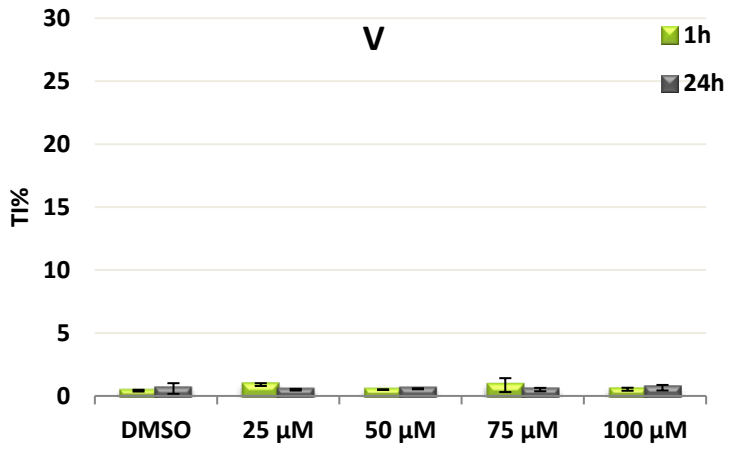

Figure 25. Genotoxic activity of V molecule using Alkaline Comet Assay on U937 cells treated for 1 h and 24 h. TI%: percentage of tail intensity (Zani *et al*., 2017).

Molecule T, after 1 h treatment, induced a significant dose dependent increase in the tail intensity percentage (TI%), without perturbing cell viability. After 24 h, no genotoxic activity was detected but the 100.0 µM dose induced a remarkable cytotoxic effect (Zani *et al*., 2017) (Fig. 26).

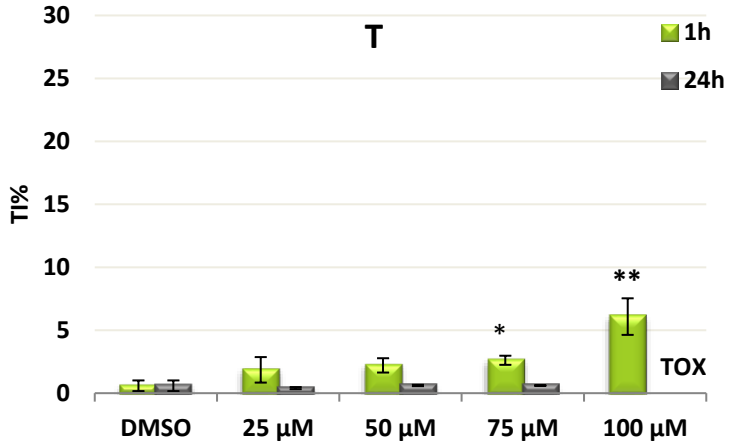

Figure 26. Genotoxic activity of T molecule using Alkaline Comet Assay on U937 cells treated for 1 h and 24 h. TOX: viability <70%. TI%: percentage of tail intensity. *p < 0.05; ** p < 0.01 (Zani *et al*., 2017).

The mutagenicity of V and T molecules was carried out through Ames test. Both molecules induced neither frameshift nor base-pair substitution point mutations in *Salmonella typhimurium* TA98 and TA100 strains, respectively, with and without metabolic activation (Zani *et al*., 2017).

4.1.3. Vanillin derivates

Vanillin (4-hydroxy-3-methoxybenzaldehyde) is a natural phenolic product, that has attracted the attention of biologists for several reasons. First, vanillin as a flavouring compound possesses general biosafety and has extensive uses in the food, beverage, and pharmaceutical industries. Second, vanillin presents a simple chemical structure, which may reduce the possibility of difficult synthesis to some extent. Third, vanillin derivates can present various biological activities, such as antitumor, antioxidant, antimicrobial, antifungal, anti-inflammatory, antimutagenic, and antiproliferative activities (Gupta *et al*., 2018). In this context, we functionalized vanillin and its derivates, synthesizing thiosemicarbazone ligands and their copper complexes.

We evaluated different ligands for their antifungal and antiaflatoxigenic ability. Among them, L5 halved the biomass increase of *A. flavus* at the maximum concentration used in the assay (100.0 µM). Furthermore, it reduced by 90% aflatoxins accumulation in amended cultures and displayed a moderate fungistatic activity. Also in this case, metal complexation

leads to species more active than the corresponding ligand in term of both fungistatic and aflatoxigenic profile. Generally, the copper complexes (2-3-5-6) showed a better activity profile then uncomplexed ligands (Rogolino *et al*., 2017).

The most promising compounds in term of activity (2, 3, 5, 6 and L5) were tested for their cytotoxicity against a panel of human cell lines. Unfortunately, all the copper complexes showed important cytotoxicity in the micromolar range, while L5 has not effect on cell proliferation (Rogolino *et al*., 2017) (Table 14).

Cell lines showed a different sensitivity after the treatment with D27: Hs27 did not present alteration in term of cell proliferation; while CRL1790, HFL1 and U937 cells showed a decrease of cell growth. D28 presented a cytotoxic effect mainly on lung cells (Table 14).

Table 14. GI_{50} value (µM), concentration of drug that causes a 50% reduction of cell growth, obtained in human healthy cell lines (CRL1790; Hs27; HFL1) and U937 cancer cell line.

	CRL1790	**Hs27**	**HFL1**	**U937**
L5	>100.0	>100.0	>100.0	>100.0
2	31.0	16.0	30.0	27.0
3	38.0	17.0	29.0	27.0
5	3.0	3.0	1.0	4.0
6	1.0	3.0	1.0	3.0
D27	46.0	>100.0	43.0	24.0
D28	>100.0	97.0	57.0	>100.0

Therefore, only L5 was chosen for further analysis of genotoxicity on U937 cells. After 1 h of exposure, L5 produced a dose-dependent DNA migration in the Comet Assay, starting from 25.0 µM, evidencing its genotoxic activity (Rogolino *et al*., 2017) (Fig. 27).

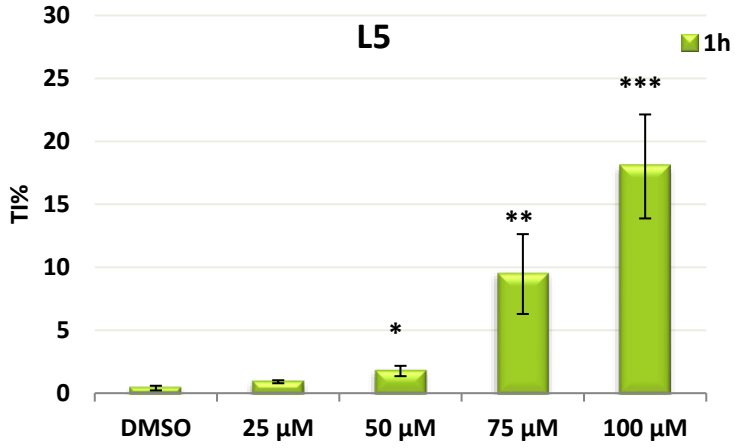

Figure 27. Genotoxic activity of L5 molecule using Alkaline Comet Assay on U937 cells treated for 1 h. TI%: percentage of tail intensity. *p < 0.05; **p < 0.01; ***p < 0.001.

L5 induced no mutagenicity in Ames test on *S. typhimurium* TA100 and TA98 strains with or without metabolic activation and no micronuclei increase was observed in micronuclei analysis. The chromosome aberration test in *Allium cepa* was carried out and statistically significant increase of aberrations was observed (Rogolino *et al*., 2017).

4.1.4. Jasmonic acid derivatives

Jasmonates display great potential in sustainable agriculture due to their various roles in natural mechanisms of plant defence, and because they are non-toxic, non-mutagenic, and easily metabolized. The first and the main compound in the group of jasmonates biosynthesized is jasmonic acid (Paprocka *et al*., 2018). It is among the most important signals of different stress responses in plants and is active in root growth, seed germination, stamen development or senescence. It and its derivatives originate from lipids of chloroplast membranes (Wasternack *et al*., 2018). Jasmonic acid was used to synthesise various derivates that were tested for their aflatoxigenic potential.

In this section, we evaluated the activity of a raw material, the cis jasmon (J) and of the most promising derivates: cis-jasmon thiosemicarbazone (F36), dihydrojasmon thiosemicarbazone (F31), and bis-(jasmonthiosemicarbazonate) Cu(II) complex (F44).

The introduction of thio-group in jasmon moiety did not cause changes in the biological activity of the ligand against healthy human cells. In fact, J, F31 and F36 did not cause

inhibition of cell proliferation. Interestingly, F36 induced a decrease of growth in cancer cells. After the coordination of cis-jasmon thiosemicarbazone with copper ion, the biological activity of the molecule was changed radically: the complex (F44) showed an important cytotoxic activity, in particular against lung cells (Table 15).

Table 15. GI_{50} value (µM), concentration of drug that causes a 50% reduction of cell growth, obtained in human healthy cell lines (CRL1790; Hs27; HFL1) and U937 cancer cell line.

	CRL1790	Hs27	HFL1	U937
J	>100.0	>100.0	>100.0	>100.0
F36	>100.0	>100.0	>100.0	40.0
F31	>100.0	>100.0	>100.0	>100.0
F44	38.0	28.0	5.0	18.0

In the Comet Assay, the compounds displayed a different genotoxic potential. The treatment of U937 cells with J for 1h resulted in a null genotoxic effect; on the contrary, J was able to cause DNA damage, in particular at 75.0 µM and 100.0 µM after 24h (Fig. 28).

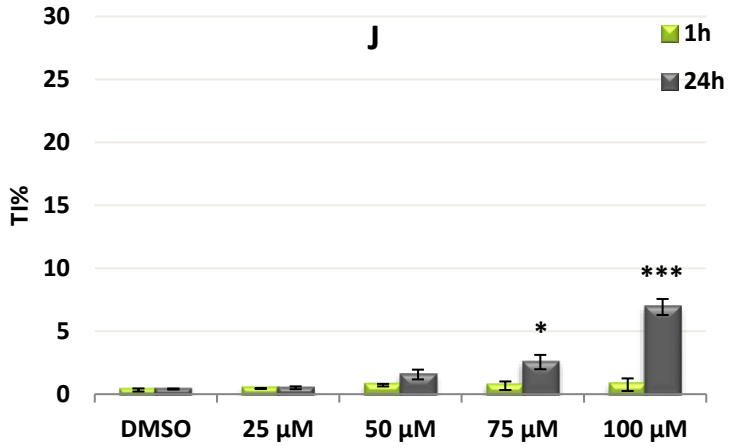

Figure 28. Genotoxic activity of J molecule using Alkaline Comet Assay on U937 cells treated for 1 h and 24 h. TI%: percentage of tail intensity. *p < 0.05; **p < 0.01; ***p < 0.001.

F36 was able to induce DNA damage in the concentration range of 25.0–100.0 µM at 1h treatment; while after 24h, F36 caused a genotoxic effect at the lowest concentration (25.0 µM) but in the other cases, as expected, it caused a decrease in cell viability % (Fig. 29).

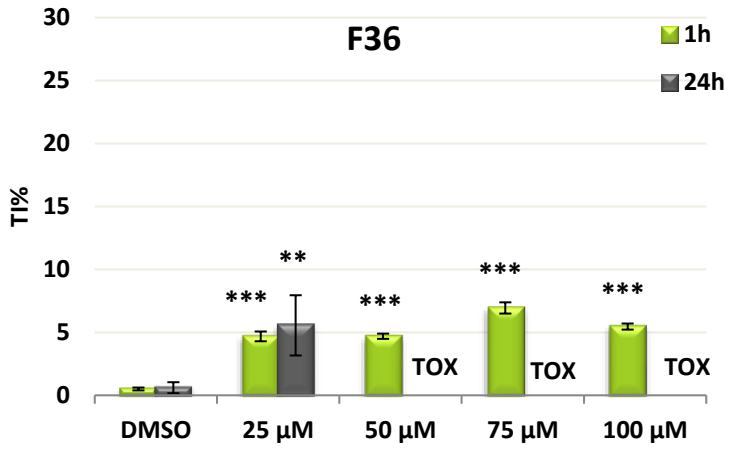

Figure 29. Genotoxic activity of F36 molecule using Alkaline Comet Assay on U937 cells treated for 1 h and 24 h. TI%: percentage of tail intensity. *p < 0.05; **p < 0.01; ***p < 0.001.

After the treatment with F31, DNA molecules were observed to be damaged in all the concentrations evaluated in the assay both after 1 and 24h. We observed a significant DNA migration already at the lowest concentration of compound (Fig. 30).

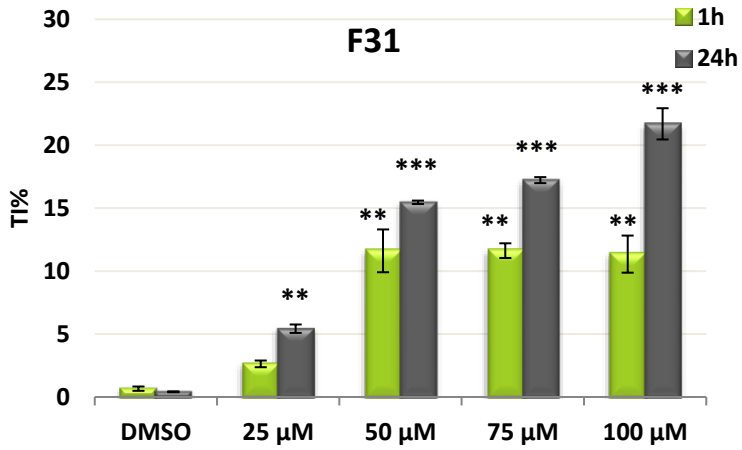

Figure 30. Genotoxic activity of F31 molecule using Alkaline Comet Assay on U937 cells treated for 1 h and 24 h. TI%: percentage of tail intensity. *p < 0.05; **p < 0.01; ***p < 0.001.

4.1.5. Anthraquinone derivatives

Quinones constitute a class of organic compounds characterized by the presence of a cyclic diketone structure. 9,10-Anthraquinones represent an important sub-group. Their structure is based on the rigid, planar three-ring aromatic system anthracene, which contains two keto functions at the 9- and 10-positions (Malik *et al*., 2016). Anthraquinones are extensively present in nature, found in plants, bacteria, fungi, and insects. They are widely used as pharmacological drugs and currently these compounds are used to treat a variety of conditions because of their wide ranging biological activities, including anti-inflammatory, antifungal, antibacterial, antiviral, and antiarthritic actions (Demarque *et al*., 2018).

Starting from anthraquinone moiety, we studied the cytotoxic activity of the 2-hydroxymethylanthraquinone (F47), that is essential for the synthesis of 2-formylanthraquinone (F57). Then, we designed and synthesized a series of functionalized thiosemicarbazones 2-formylanthraquinonethiosemicarbazone (F46) and 2-carboxylanthraquinone (F66).

The data obtained with MTS assay highlighted that F46 and F66 showed no antiproliferative effect against human cell lines. F47 was cytotoxic only on HFL1 cells, whereas F57 was slightly cytotoxic against both Hs27 and HFL1 cell lines (Table 16).

Table 16. GI_{50} value (µM), concentration of drug that causes a 50% reduction of cell growth, obtained in human healthy cell lines (CRL1790; Hs27; HFL1) and U937 cancer cell line.

	CRL1790	**Hs27**	**HFL1**	**U937**
F46	>100.0	>100.0	>100.0	>100.0
F47	>100.0	>100.0	58.0	>100.0
F57	>100.0	96.0	85.0	>100.0
F66	>100.0	>100.0	>100.0	>100.0

Among the anthraquinone derivates, the most promising compounds were F46 and F66. Interestingly, also in the Comet Assay, the compound F66 did not show genotoxic potential (Fig. 31).

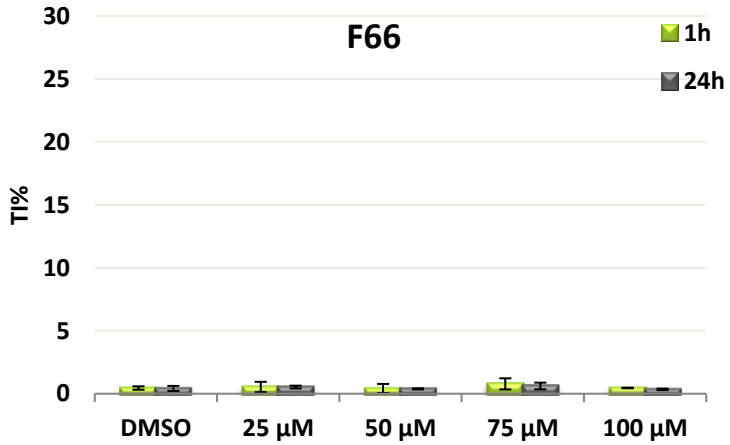

Figure 31. Genotoxic activity of F66 molecule using Alkaline Comet Assay on U937 cells treated for 1 h and 24 h. TI%: percentage of tail intensity. *p < 0.05; **p < 0.01; ***p < 0.001.

Unfortunately, in the Alkaline Comet Assay F46 produced crystals that interfered with the microscopic evaluation.

4.1.6. Cinnamaldehyde derivates

Cinnamaldehyde, an aldehydic component extracted from cinnamon bark, is known to provide antibacterial, antifungal, antiviral, bactericidal, antiparasitic, and larvicidal activities (Sawicki *et al*., 2018). In a previous study, we showed that trans-cinnamaldehyde thiosemicarbazone (Htcin) was very effective in inhibiting mycelium growth and aflatoxin accumulation. These results corroborate literature data, in which thiosemicarbazone showed greater activity than the ligand. Also, the cytotoxic activity on human cells (HFL-1 cell line) was performed: in the range of the tested doses, Htcin showed only a slight antiproliferative activity starting from 50.0 µM with an IC_{50} > 100.0 µM (Degola *et al*., 2015). In this case, the moiety of Htcin was modified with the introduction of methyl groups in N2 position, leading to cinnamaldehyde 4,4'-dimethyl thiosemicarbazone (F51). The GI_{50} data highlighted that F51 did not induce inhibition of cell growth. The corresponding zinc(II) complex (F53) showed an antiproliferative potential only against skin and lung cell lines,

with GI_{50} values equal to 41.0 µM and 39.5 µM, respectively; this cytotoxic effect was not observed against colon cells and leukocytes (Table 17). Other two cinnamaldehyde thiosemicarbazone derivates, cinnamaldehyde-N2-methylthiosemicarbazone (F61) and cinnamaldehyde-N2-methylthiosemicarbazone reduced form (F62), were analysed: healthy and cancer cells did not show inhibition of proliferation after the treatment with F61 and F62 (Table 17).

Table 17. GI_{50} value (µM), concentration of drug that causes a 50% reduction of cell growth, obtained in human healthy cell lines (CRL1790; Hs27; HFL1) and U937 cancer cell line.

	CRL1790	Hs27	HFL1	U937
F51	>100.0	>100.0	>100.0	>100.0
F53	>100.0	41.0	39.5	>100.0
F61	>100.0	>100.0	>100.0	>100.0
F62	>100.0	>100.0	>100.0	>100.0

Unfortunately, the Comet assay pointed out a strong genotoxic activity of F51 already at the lowest concentration employed in the test. This result increased after treatment of U937 cells for 24h: in this case, the compound induced DNA damage at 25.0 µM and 50.0 µM, while at the highest concentrations (75.0-100.0 µM) cell viability was less than 70% (Fig. 32).

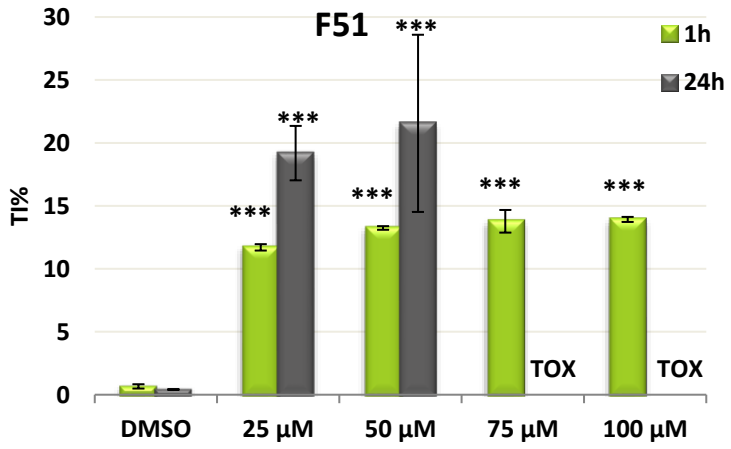

Figure 32. Genotoxic activity of F51 molecule using Alkaline Comet Assay on U937 cells treated for 1 h and 24 h. TI%: percentage of tail intensity. *p < 0.05; **p < 0.01; ***p < 0.001.

The Comet Assay demonstrated that F61 did not cause DNA damage after 1h treatment, but it was genotoxic after 24h, starting from 50.0 µM (Fig. 33).

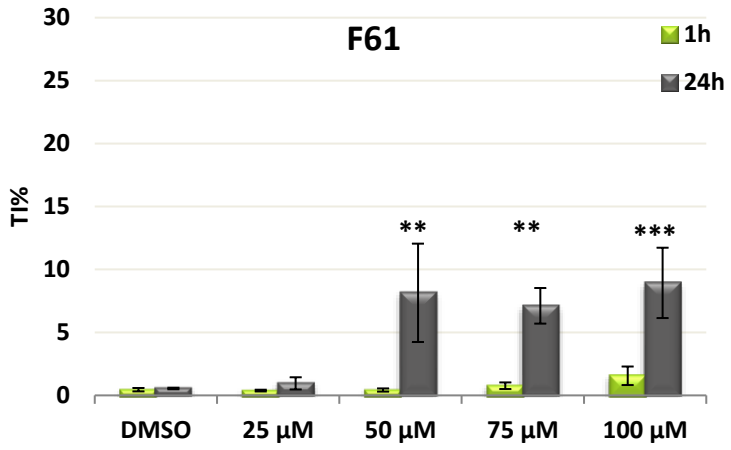

Figure 33. Genotoxic activity of F61 molecule using Alkaline Comet Assay on U937 cells treated for 1 h and 24 h. TI%: percentage of tail intensity. *p < 0.05; **p < 0.01; ***p < 0.001.

On the contrary, the reduced form (F62) had no genotoxic effects against human leukocytes (Fig. 34).

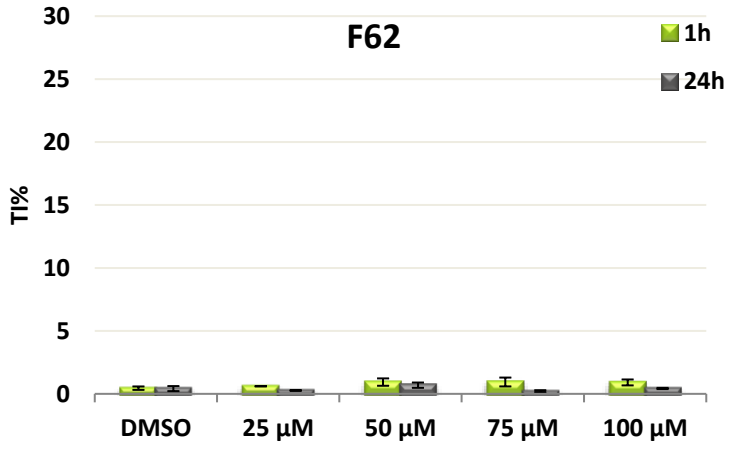

Figure 34. Genotoxic activity of F62 molecule using Alkaline Comet Assay on U937 cells treated for 1 h and 24 h. TI%: percentage of tail intensity. *p < 0.05; **p < 0.01; ***p < 0.001.

4.1.7. 2-acetylthiophene derivates

The thiophene ring is present in numerous pharmacologically important compounds and natural products (Mabkhot *et al.*, 2016). First, we synthesized 2-acetylthiophene thiosemicarbazone (F20), that did not induce antiproliferative activity against all cell lines used in this study.

On the contrary, a growth inhibition in healthy human cells was observed after the treatment with bis(2-acetylfuranthiosemicarbazonate)copper(II) complex (F25). No effects were observed after the treatment of the cancer cells (Table 18).

Table 18. GI_{50} value (µM), concentration of drug that causes a 50% reduction of cell growth, obtained in human healthy cell lines (CRL1790; Hs27; HFL1) and U937 cancer cell line.

	CRL1790	Hs27	HFL1	U937
F20	>100.0	>100.0	>100.0	>100.0
F25	10.0	33.5	25.0	>100.0

In the Alkaline Comet Assay, we observed in U937 cells a genotoxic activity induced by F20 in a dose-dependent manner. After 24h, cells were able to recover the DNA damage. In fact, we did not detect single and double DNA strand breaks and alkali-labile sites (Fig. 35).

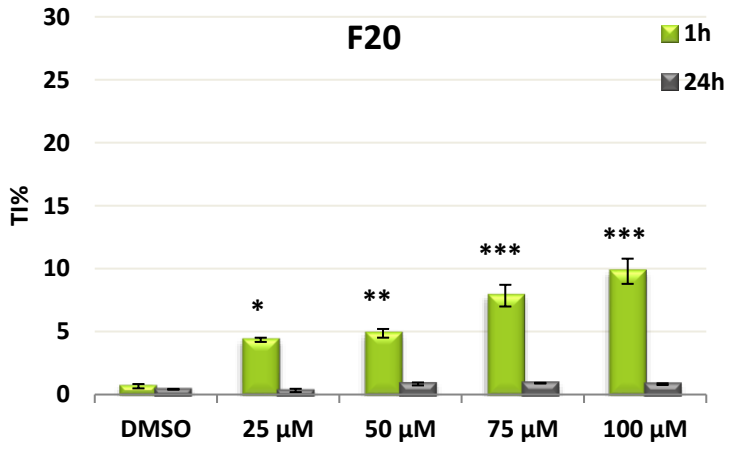

Figure 35. Genotoxic activity of F20 molecule using Alkaline Comet Assay on U937 cells treated for 1 h and 24 h. TI%: percentage of tail intensity. *p < 0.05; **p < 0.01; ***p < 0.001.

4.1.8. 1-(3-methoxyphenyl)-1-heptanone derivates

Two different derivates of 1-(3-methoxyphenyl)-1-heptanone were designed and synthesized: the (3-methoxyphenyl)-1-heptanone thiosemicarbazone (F22) and the corresponding copper complex (F26). Both the molecules induced an inhibition of cell proliferation against human healthy cell lines, but they did not affect the growth of cancer cells (Table 19).

Table 19. GI_{50} value (µM), concentration of drug that causes a 50% reduction of cell growth, obtained in human healthy cell lines (CRL1790; Hs27; HFL1) and U937 cancer cell line.

	CRL1790	Hs27	HFL1	U937
F22	34.0	27.0	42.5	>100.0
F26	36.5	1.0	34.0	>100.0

4.1.9. Long hydrophobic chain derivates

We synthesized three different thiosemicarbazone derivates, that contain a long alkyl chain: the heptanal thiosemicarbazone (F37), the nonanal thiosemicarbazone (F38) and the undecanal thiosemicarbazone (F39). F37 did not cause cellular growth inhibition; F38 and F39, with a longer alkyl chain than F37, exhibited obvious inhibitory activity in the MTS assay with low micromolar GI_{50} values (Table 20).

Table 20. GI_{50} value (µM), concentration of drug that causes a 50% reduction of cell growth, obtained in human healthy cell lines (CRL1790; Hs27; HFL1) and U937 cancer cell line.

	CRL1790	Hs27	HFL1	U937
F37	>100.0	>100.0	>100.0	>100.0
F38	32.0	63.0	80.0	41.0
F39	77.0	28.0	46.5	>100.0
F41	30.5	29.0	10.0	29.0
F42	44.0	30.5	35.0	>100.0

Also the copper complexes bis-(heptanal-thiosemicarbazonate) Cu(II) complex (F41) and bis-(nonanal-thiosemicarbazonate) Cu(II) complex (F42) showed antiproliferative activity against human cells (Table 20).

The evaluation of the genotoxic potential of F37 revealed that, after 1h, U937 cells did not present alterations in the DNA molecules. F37 caused a strong DNA damage at the highest concentrations after 24h treatment (Fig. 36).

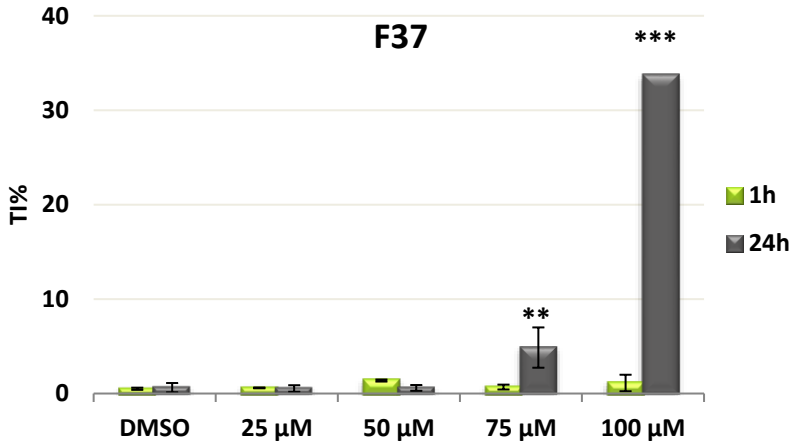

Figure 36. Genotoxic activity of F37 molecule using Alkaline Comet Assay on U937 cells treated for 1 h and 24 h. TI%: percentage of tail intensity. *p < 0.05; **p < 0.01; ***p < 0.001.

4.1.10. Benzophenone derivates

The benzophenones are a new class of agricultural fungicides. We used the benzophenone skeleton to synthesize the benzophenyl thiosemicarbazone (JB20). JB20 did not show antiproliferative activity against colon, skin and lung cell lines and presented a mild cytotoxic effect on cancer cells (Table 21).

Table 21. GI_{50} value (µM), concentration of drug that causes a 50% reduction of cell growth, obtained in human healthy cell lines (CRL1790; Hs27; HFL1) and U937 cancer cell line.

	CRL1790	Hs27	HFL1	U937
JB20	>100.0	>100.0	>100.0	73.0

Against U937 cells, JB20 induced DNA single and double strand breaks in a dose-dependent manner in both the treatment times (1 and 24h) (Fig. 37).

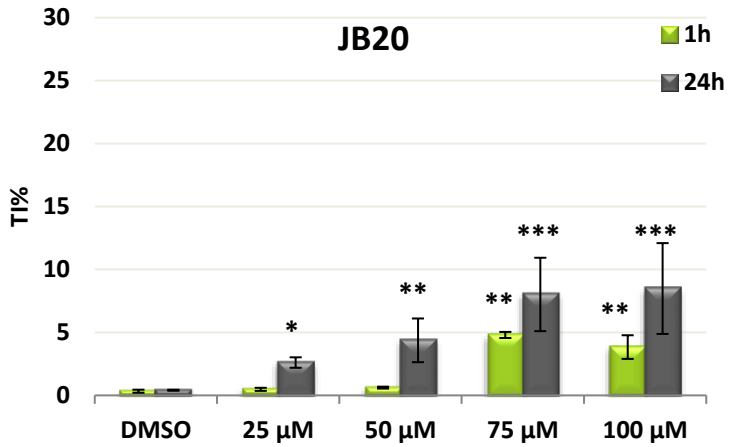

Figure 37. Genotoxic activity of JB20 molecule using Alkaline Comet Assay on U937 cells treated for 1 h and 24 h. TI%: percentage of tail intensity. *p < 0.05; **p < 0.01; ***p < 0.001.

4.1.11. Valerophenone derivates

Valerophenone is a representative of aromatic alkyl ketones and in this study was used to synthesize the corresponding thiosemicarbazone (JB24). In MTS assay, we observed a mild cytotoxic effect against skin fibroblasts and leukocytes (Table 22).

Table 22. GI_{50} value (µM), concentration of drug that causes a 50% reduction of cell growth, obtained in human healthy cell lines (CRL1790; Hs27; HFL1) and U937 cancer cell line.

	CRL1790	Hs27	HFL1	U937
JB24	100.0	79.5	>100.0	58.0

JB24 after 1h of treatment induced DNA damage at the highest concentrations (75.0 and 100.0 µM). After 24h it was genotoxic already at 25.0 µM; it caused, as expected, a reduction in cell viability and showed a toxic effect at the highest concentrations (Fig. 38).

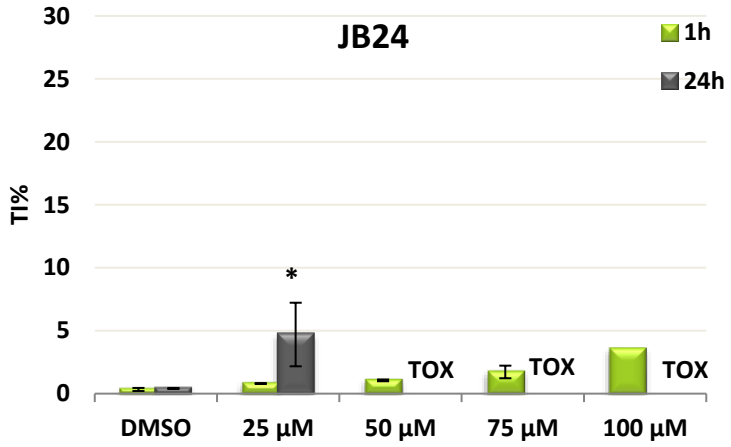

Figure 38. Genotoxic activity of JB24 molecule using Alkaline Comet Assay on U937 cells treated for 1 h and 24 h. TI%: percentage of tail intensity. *p < 0.05; **p < 0.01; ***p < 0.001.

4.2. Biological activity of citronellal thiosemicarbazone metal complexes on human cancer cell lines

For a long time, thiosemicarbazones and their derivates have been explored as backbone scaffolds for the design of novel antiproliferative agents, they showed marked and selective anti-tumour activity both *in vitro* and *in vivo*. Although the molecular mechanisms involved in the activity of TSCs have not been completely elucidated, a number of modes of action had been reported, such as the inhibition of cellular iron uptake from transferrin, the mobilization of iron from cells, the inhibition of the ribonucleotide reductase activity, the up-regulation of the metastasis suppressor protein, *N-myc downstream regulated gene 1*, and the formation redox active metal complexes that produce reactive oxygen species (ROS) (Serda *et al*., 2014).

Despite the parent aldehyde or ketone had been considered crucial for the anticancer activity of thiosemicarbazones, a lot of studies indicated that the antiproliferative potential increases with metal ion coordination. Thiosemicarbazone is a polar ligand and its interaction with a charged metal ion results in a structure in which hydrophobic part of the molecule is exposed to outside and this makes the entry of the complex inside a cell membrane feasible (Khan *et al*., 2015).

This research deals with the design, synthesis and biological evaluation of a series of thiosemicarbazone metal complexes. In this work, we have chosen citronellal, as starting aliphatic aldehyde to prepare the parent thiosemicarbazone (CitrTSC). In addition, to evaluate the influence of transition metals on the biological activity, nickel(II), platinum(II) and copper(II) have been chosen to prepare coordination compounds of citronellal thiosemicarbazone ([Ni(tcitr)$_2$], [Pt(tcitr)$_2$] and [Cu(tcitr)$_2$], respectively). First, we compared the cytotoxic effects against a panel of cancer cell lines; subsequently, we studied the possible interaction with the DNA molecule and the involvement of specific cellular pathways.

In previous studies, the antiproliferative properties of the nickel [Ni(tcitr)$_2$] (Buschini *et al*., 2009) and copper [Cu(tcitr)$_2$] complexes (Bisceglie *et al*., 2012) against cell line U937 after 24h of treatment were investigated. In particular, Buschini and co-workers focused on the comprehension of the action mechanism of [Ni(tcitr)$_2$]. The nickel complex entered the

U937 cells and exhibited a strong cytotoxic activity with GI_{50}=10.0 µM after 24h. Interestingly, no significant effects on viability were detected on fresh leukocytes after the treatment. In U937 cells [Ni(tcitr)$_2$] induced a G2M cell cycle arrest, p53 independent-intrinsic-apoptosis by down-regulation of Bcl-2, mitochondrial membrane potential loss and caspase activation (Buschini *et al*., 2009). A significant DNA damaging action was observed not due to DNA oxidation. Furthermore, [Ni(tcitr)$_2$] did not induce gene mutation or chromosomal damage, but altered the DNA conformation creating knot-like structures and hairpins. These results demonstrated that the nickel complex could be a promising candidate as a chemotherapeutic agent and a good model for the synthesis of new metal thiosemicarbazones with potential biological activity. However, its mechanism of action is still unclear.

4.2.1. Cytotoxic activity of metal complexes

In order to distinguish among the effects of the metal or of the ligand or their synergic activity, the ligand and the metal complexes were tested separately.

Citronellal was selected as the representative of aliphatic derivatives. Above of all citronellal thiosemicarbazone (CitrTSC) was tested for its antiproliferative activity against histiocytic lymphoma cells U937: CitrTSC did not show cytotoxic effect (Bisceglie *et al*., 2018).

In previous study the nickel [Ni(tcitr)$_2$] and the copper [Cu(tcitr)$_2$] complexes showed a strong inhibition of U937 cells proliferation: it is apparent that this activity is strongly influenced by metal complexation. Probably, the cytotoxic potential of the complex could depend on the presence of the metal ion, that could play an essential role.

According to the National Cancer Institute approach for the “60 human tumour cell line anticancer drug screen” (NCI60), we treated cells with various concentrations of [Ni(tcitr)$_2$] (0.5 - 100.0 µM). MTS assay was performed on cells deriving from 10 different districts in order to identity the selectivity of the compound. We determined dose-response curves and growth inhibiting concentrations at 50% (GI_{50}, 50% Growth Inhibition) was established. Data were expressed as mean of $\log_{10}$ of GI_{50}. Nickel complex was found to be most

selective toward leukemia and central nervous system (CNS) cancer subpanels. In particular, after 24h treatment, all the leukemia cell lines presented GI_{50}≤10.0 µM; also SK-N-MC and SH-SY5Y neuroblastoma cells showed a strong inhibition of cell proliferation with GI_{50}= 2.0 and 5.0 µM, respectively. On the contrary, colon, lung, prostate and breast cells showed less sensitivity against $[Ni(tcitr)_2]$ (Fig. 39).

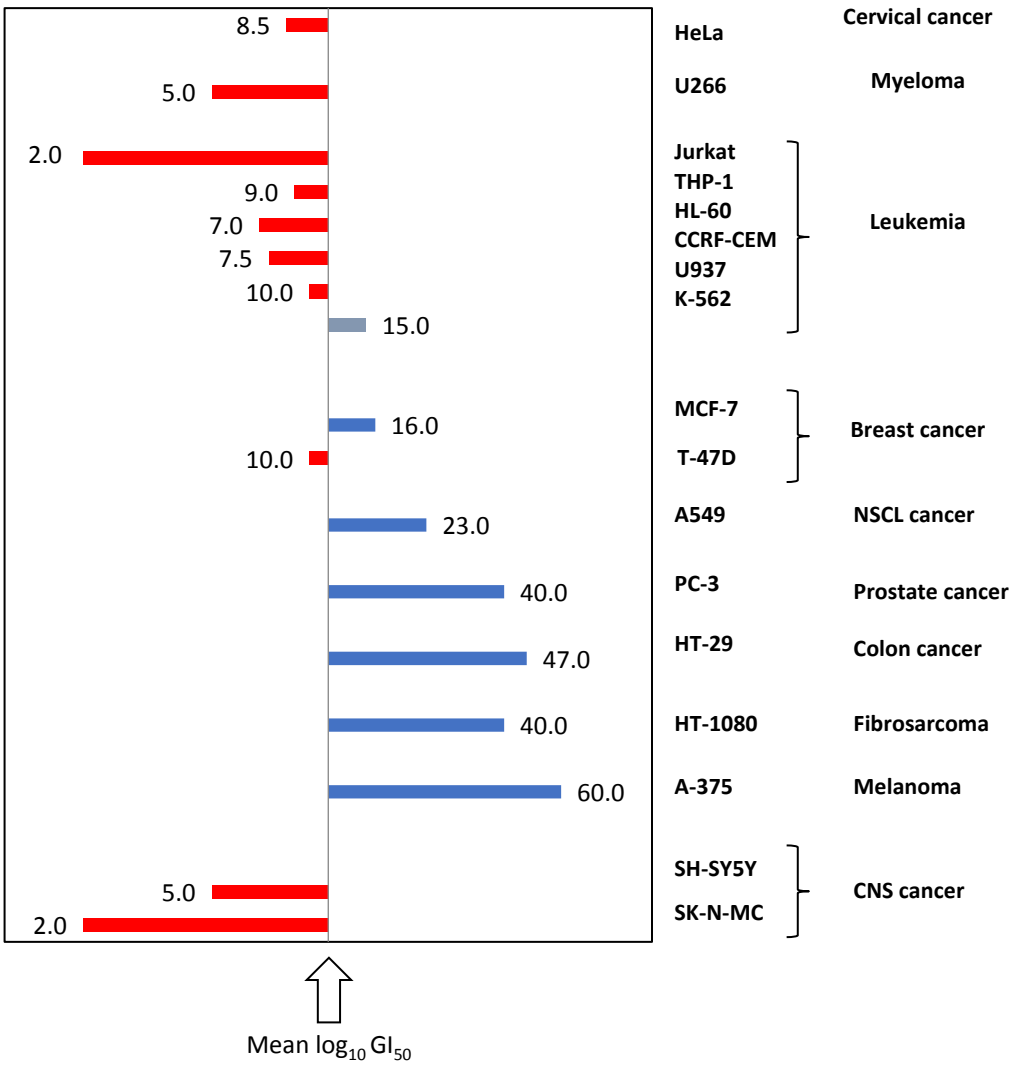

Figure 39. GI_{50} values (µM) were expressed as mean of log_{10} of GI_{50}. The red bars represent more sensitive cell lines, blue bars represent less sensitive cell lines.

In order to identify metal complexes selectivity, MTS assay was performed on a subpanel of four human cancer cell lines (U937, A549, HT-29 and SK-N-MC) to determine whether copper and platinum complexes could affect growth and proliferation of tumor cell. The

evaluation of their antiproliferative activity was carried out on a wide range of concentrations (0.5-100.0 µM) for different times of exposure (24-48-72h). Dose-response curves obtained after 24h treatment are displayed in Fig 40-41. Both the platinum and the copper complexes induced a dose-dependent inhibition of cell proliferation (Fig. 40-41).

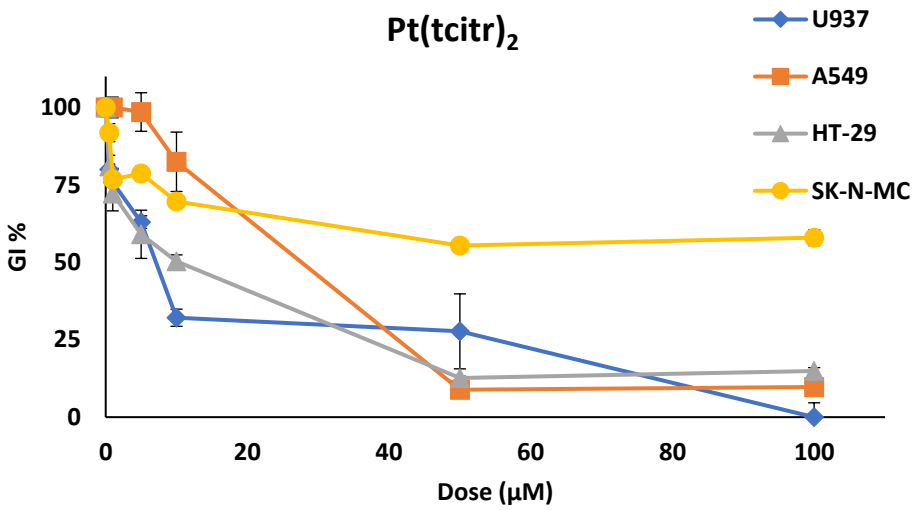

Figure 40. Dose-response curves obtained on U937, A549, HT-29 and SK-N-MC cells after 24h treatment with [Pt(tcitr)$_2$].

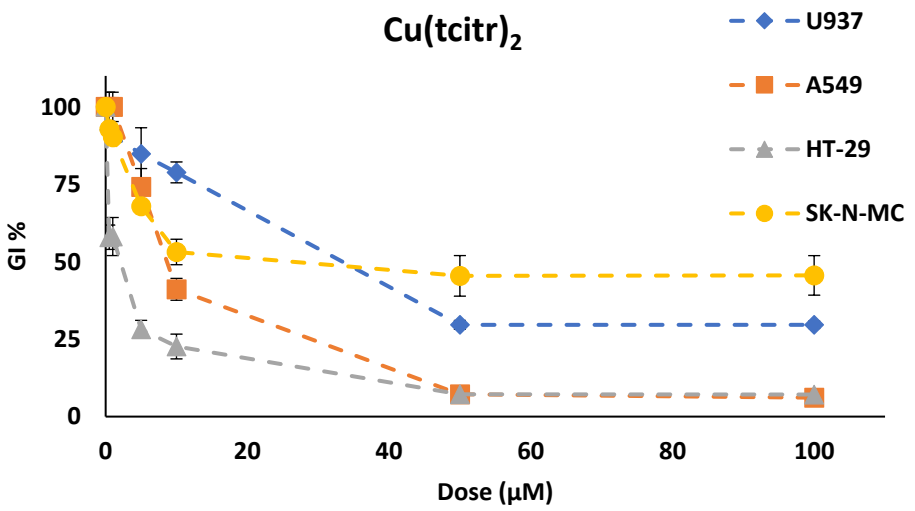

Figure 41. Dose-response curves obtained on U937, A549, HT-29 and SK-N-MC cells after 24h treatment with [Cu(tcitr)$_2$].

Furthermore, in the table 23 data were expressed as concentrations promoting 50% of cell growth inhibition (GI_{50}) after 24-48-72h treatment (Table 23). As mentioned above, [Ni(tcitr)$_2$)] inhibited mainly proliferation of U937 and SK-N-MC cells. Also after 48 and 72h treatment, leukemia and neuroblastoma cells were more sensitive than HT-29 and A549 cells.

After 24h, the platinum complex induced a considerable antiproliferative effect against U937 and HT29 cells and after 48h treatment adenocarcinoma cells was the most sensitive cell line. After 72h, also A549 cells presented an important inhibition of cell proliferation. Surprisingly, [Pt(tcitr)$_2$] did not alter growth of SK-N-MC cells.

Finally, the copper complex caused a strong cytotoxic effect on HT29 and A549 cell lines both after 24h and 48h treatment.

Table 23. GI_{50} (µM) values obtained after 24-48-72h treatment with metal complexes.

	Ni(tcitr)$_2$			**Pt(tcitr)$_2$**			**Cu(tcitr)$_2$**		
	24h	**48h**	**72h**	**24h**	**48h**	**72h**	**24h**	**48h**	**72h**
U937	10.0	2.1	8.0	7.0	25.8	13.0	33.0	12.0	30.0
HT-29	47.0	28.5	37.5	10.0	5.5	6.8	2.0	7.5	4.0
SK-N-MC	2.0	8.0	nd	>100.0	>100.0	nd	25.0	>100.0	nd
A549	23.0	47.5	57.0	25.5	27.0	6.0	8.0	6.5	24.0

4.2.2. Cytotoxic activity of dimethylated complexes

Starting from the nickel, platinum, and copper derivatives, we synthetized three different dimethylated compounds ([Ni(4dm-(tcitr)$_2$], [Pt(4dm-(tcitr)$_2$], and [Cu(4dm-(tcitr)$_2$]) introducing a methyl group in the original moiety. This modification could influence chemical properties of the molecules and consequently their biological activity.

Their cytotoxic effects were studied on leukemic cell line U937, already used as a model in our studies. Cells were treated for 24h and 48h with six different concentrations of compounds, ranging from 0.5 to 100.0 µM. Dose-response curve in U937 cells revealed that all the dimethylated complexes showed the same antiproliferative activity after 24h treatment (Fig. 42). GI$_{50}$ values were between 25.0 µM and 27.0 µM (Table 24).

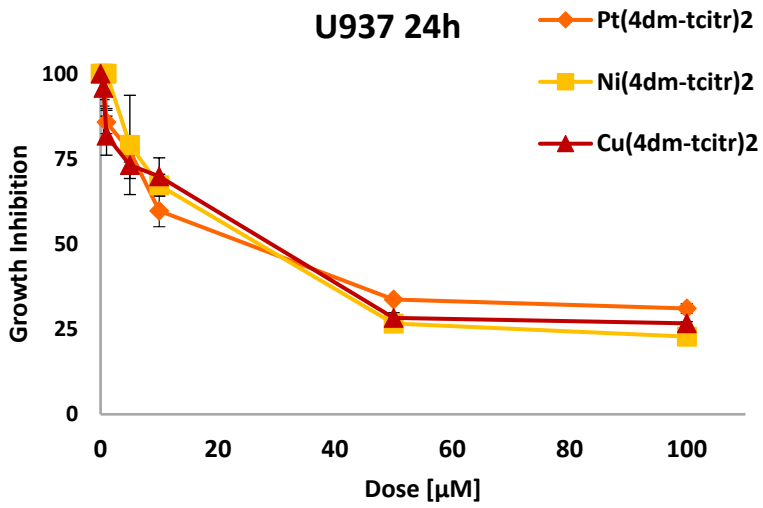

Figure 42. Dose-response curves obtained on U937 cells after 24h treatment with [Ni(4dm-tcitr)$_2$], [Pt(4dm-tcitr)$_2$] and [Cu(4dm-tcitr)$_2$].

After 48h treatment, nickel and copper dimethylated complexes were more cytotoxic than the [Pt(4dm-(tcitr)$_2$] in determining inhibition of cell proliferation (Fig. 43) (Table 24).

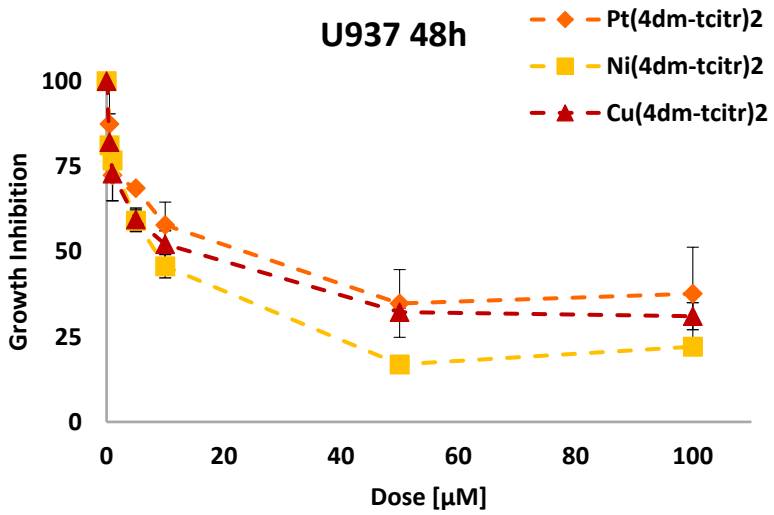

Figure 43. Dose-response curves obtained on U937 cells after 24h treatment with [Ni(4dm-tcitr)$_2$], [Pt(4dm-tcitr)$_2$] and [Cu(4dm-tcitr)$_2$].

All these results indicated that the introduction of a methyl group reduced the antiproliferative activity of the molecules (Table 24).

Table 24. GI$_{50}$ (µM) values obtained after 24-48h treatment with dimethylated metal complexes.

	Ni(4dm-tcitr)$_2$	**Pt(4dm-tcitr)$_2$**	**Cu(4dm-tcitr)$_2$**
24h	25.0	23.0	27.0
48h	8.0	23.0	11.0

4.2.3. Genotoxic activity of metal complexes

Many anticancer agents, particularly platinum(II) complexes, target the DNA through an intercalation process that causes DNA damage. In a previous study, $[Ni(tcitr)_2]$ caused a significant increase in DNA migration after 1h treatment, not due to oxidative stress (Fig. 44) (Buschini *et al*., 2009). Atomic Force Microscopy (AFM) revealed a deep conformational change in DNA molecule: the nickel complex altered DNA conformation creating knot-like structures and hairpins. Probably, heterochromatinization was a mechanism of nickel-mediated cytotoxicity (Buschini *et al*., 2014).

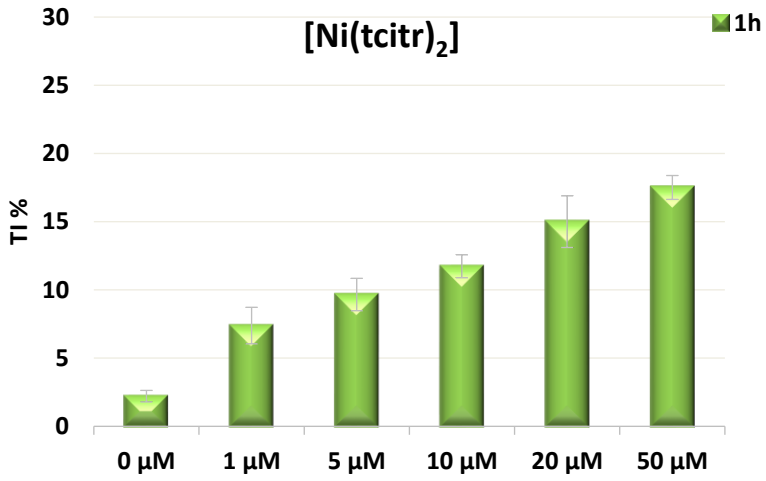

Figure 44. DNA damage detected by the Comet assay (pH > 13) in U937 cells treated with increasing dose of $[Ni(tcitr)_2]$ for 1h. DNA damage is expressed as tail intensity (TI%).

To understand if Cu and Pt metal complexes were able to induce alterations on the DNA molecule, we performed Alkaline Comet Assay on U937 cells that identifies different kinds of DNA damage, such as single and double strand breaks, incomplete excision repair sites and alkali-labile sites. Cells were treated for 1h and 24h with five increasing concentrations of copper and platinum complexes (1.0-5.0-10.0-20.0-50.0 µM).

The exposure of cells to metal complexes resulted in a considerable DNA damage, as revealed by a high DNA migration. Both the complexes showed a dose-dependent DNA migration, evidencing their genotoxic activity. As regards $[Pt(tcitr)_2]$, the lowest effective doses were 5.0 µM and 1.0 µM, respectively for 1h and 24h treatment (Fig. 45). $[Cu(tcitr)_2]$

was genotoxic at the highest concentrations (20.0-50.0 µM) after 1h treatment, while at 5.0 µM after 24h (Fig. 46).

Meanwhile, the induction of cell death after treatment with copper and platinum complexes was quantified by trypan blue exclusion method. $[Pt(tcitr)_2]$ and $[Cu(tcitr)_2]$ showed an increase in trypan blue-positive cells at the highest concentrations (20.0 and 50.0 µM) after 24h treatment (Fig. 45-46).

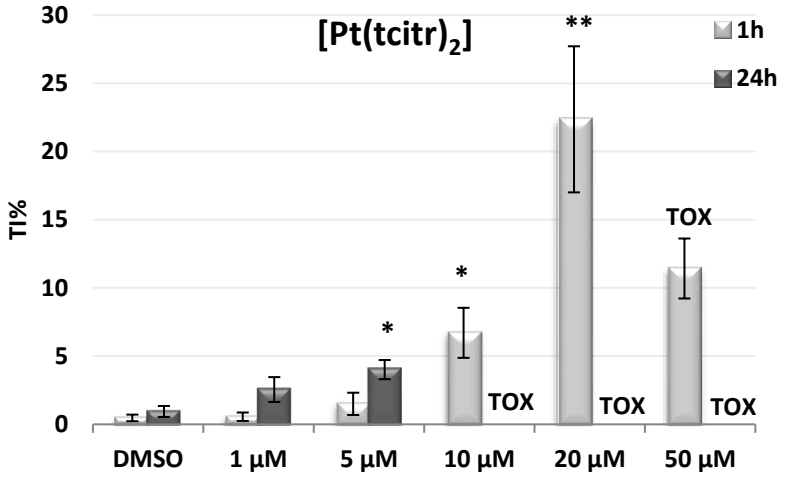

Figure 45. DNA damage detected by the Comet assay (pH > 13) in U937 cells treated with increasing dose of $[Pt(tcitr)_2]$ for 1h and 24h. DNA damage is expressed as tail intensity (TI%). TOX: viability <70%. *p < 0.05; **p < 0.01; ***p < 0.001.

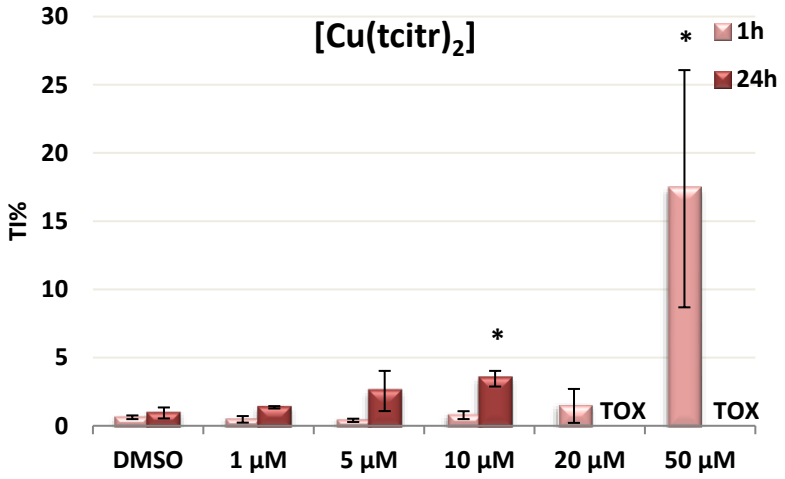

Figure 46. DNA damage detected by the Comet assay (pH > 13) in U937 cells treated with increasing dose of $[Cu(tcitr)_2]$ for 1h and 24h. DNA damage is expressed as tail intensity (TI%). TOX: viability <70%. *p < 0.05; **p < 0.01; ***p < 0.001.

In order to understand if the introduction of a methyl group could alter the genotoxic potential of the starting molecules, the Comet Assay was performed on the dimethylated complexes against U937 cells.

Also [Ni(4dm-(tcitr)$_2$], [Pt(4dm-(tcitr)$_2$], and [Cu(4dm-(tcitr)$_2$] induced DNA damage in leukocytes. All the results indicated that nickel, copper and platinum complexes are more genotoxic than their corresponding dimethylate compounds. In particular, [Ni(4dm-(tcitr)$_2$] induced DNA damage after 1h treatment at the highest concentrations (10.0-20.0-50.0 µM); after 24h, the DNA migration was reduced (Fig. 47).

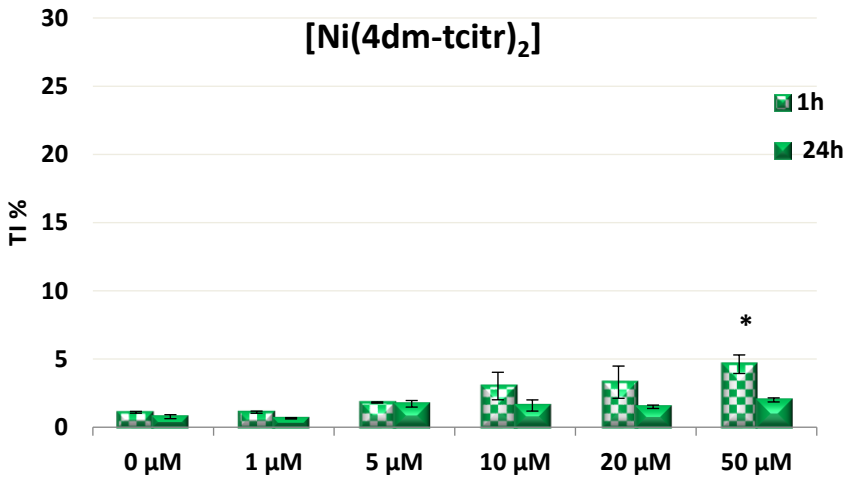

Figure 47. DNA damage detected by the Comet assay (pH > 13) in U937 cells treated with increasing dose of [Ni(4dm-tcitr)$_2$] for 1h and 24h. DNA damage is expressed as tail intensity (TI%). *p < 0.05; **p < 0.01; ***p < 0.001.

After 1h treatment, both platinum and copper dimethylated complexes were genotoxic at the highest concentrations (20.0-50.0 µM for [Pt(4dm-tcitr)$_2$]; 50.0 µM for [Cu(4dm-tcitr)$_2$]). After 24h, the lowest effective doses were 20.0 µM and 5.0 µM, respectively for [Pt(4dm-tcitr)$_2$] and [Cu(4dm-tcitr)$_2$]. A reduction of cell viability was detected through trypan blue staining at 50.0 µM after the treatment with both the complexes (Fig. 48-49).

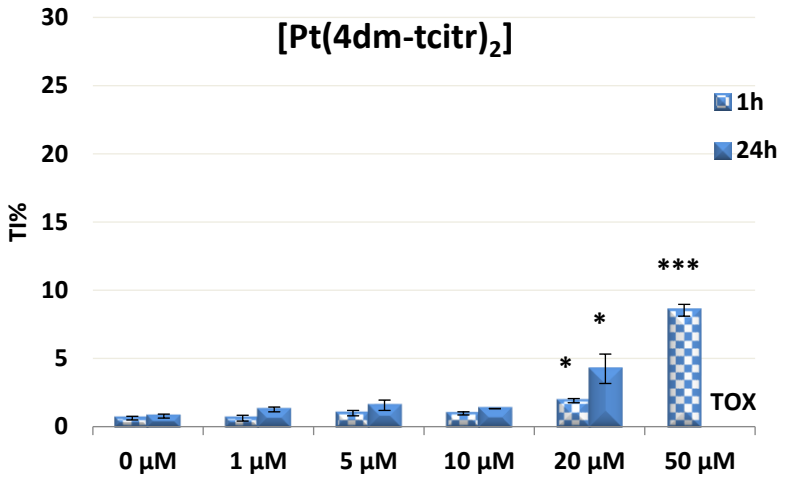

Figure 48. DNA damage detected by the Comet assay (pH > 13) in U937 cells treated with increasing dose of [Pt (4dm-tcitr)$_2$] for 1h and 24h. DNA damage is expressed as tail intensity (TI%). TOX: viability <70%. *p < 0.05; **p < 0.01; ***p < 0.001.

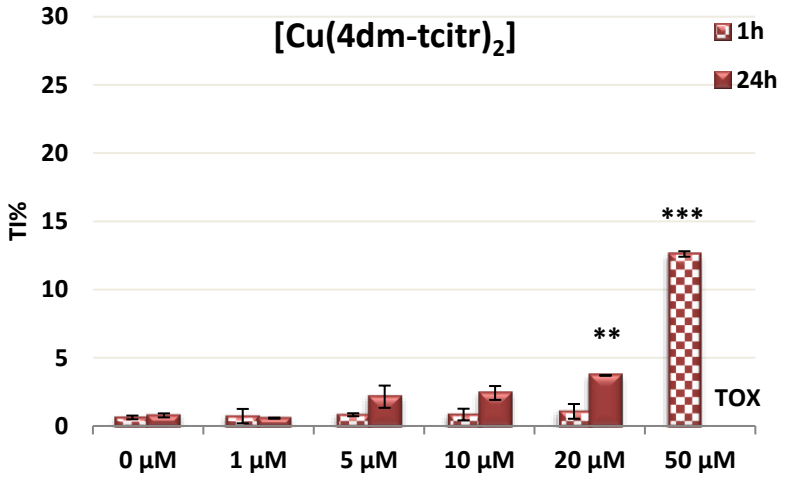

Figure 49. DNA damage detected by the Comet assay (pH > 13) in U937 cells treated with increasing dose of [Cu(4dm-tcitr)$_2$] for 1h and 24h. DNA damage is expressed as tail intensity (TI%). TOX: viability <70%. *p < 0.05; **p < 0.01; ***p < 0.001.

In conclusion, the dimethylated complexes presented less genotoxic activity than the parent compounds.

4.2.4. Mutagenic activity of metal complexes

In order to understand if the DNA damage caused by $[Ni(tcitr)_2]$ treatment at the subtoxic concentration (1 µM) could give rise to gene or chromosomal mutations, in a previous study Ames test and micronucleus assay were performed: $[Ni(tcitr)_2]$ did not induce gene mutation or micronuclei induction (Buschini *et al*., 2014).

In this work, we performed *Salmonella typhimurium* reversion test with TA98 (detecting frame-shifts) and in TA100 (detecting base substitutions) strains, with and without hexogen metabolic activation enzymatic mixture (S9). We used five different concentrations of $[Pt(tcitr)_2]$ and $[Cu(tcitr)_2]$: 2.5-5.0-10.0-50.0-100.0 µg/plate.

In accordance with the guidelines (OECD, No 471), the results of the Ames test were considered positive if mutagenicity ratio (MR) is >2. Both the complexes induced a promutagen activity in the test with TA98 + S9. In the other tests, we observed a low toxicity. Results are expressed as revertants/plate (mean ± standard deviation) and mutagenicity ratio (MR) in *S. typhimurium* TA98 and TA100 strains treated with $[Pt(tcitr)_2]$ (Table 25) and $[Cu(tcitr)_2]$ (Table 26), with and without S9 mix.

Table 25. Mutagenicity data in *S. typhimurium* TA98 and TA100 strains treated with $[Pt(tcitr)_2]$, with and without S9 activation. Results are expressed as revertants/plate (mean ± standard deviation) and mutagenicity ratio (MR). Positive controls: 2NF [20.0 µg per plate]:170±15 for TA98-S9. 2AA [10.0 µg per plate]: 86±3 for TA98+S9. SA [15.0 µg per plate]: 606±46 for TA100-S9. 2AA [10.0 µg per plate]: 413±44 for TA100+S9.

$[Pt(tcitr)_2]$	TA98 - S9		TA98 + S9		TA100 - S9		TA100 + S9	
µg/plate	Mean ± sd	MR	Mean ± sd	MR	Mean ± sd	MR	Mean ± sd	MR
DMSO	17±6	1.0	10±1	1.0	106±6	1.0	137±22	1.0
2.5	26±7	1.5	20±0	1.9	109±5	1.0	132±4	1.0
5.0	23±16	1.3	20±3	2.0	93±13	0.9	119±4	0.9
10.0	22±7	1.3	29±7	2.8	92±5	0.9	126±15	0.9
50.0	28±5	1.6	30±8	2.9	94±16	0.9	120±9	0.9
100.0	16±11	0.9	36±6	3.4	112±3	1.1	110±21	0.8

Table 26. Mutagenicity data in *S. typhimurium* TA98 and TA100 strains treated with [Cu(tcitr)$_2$], with and without S9 activation. Results are expressed as revertants/plate (mean ± standard deviation) and mutagenicity ratio (MR). Positive controls: 2NF [20.0 µg per plate]:170±15 for TA98-S9. 2AA [10.0 µg per plate]: 86±3 for TA98+S9. SA [15.0 µg per plate]: 606±46 for TA100-S9. 2AA [10.0 µg per plate]: 413±44 for TA100+S9.

[Cu(tcitr)$_2$]	TA98 - S9		TA98 + S9		TA100 - S9		TA100 + S9	
µg/plate	Mean ± sd	MR	Mean ± sd	MR	Mean ± sd	MR	Mean ± sd	MR
DMSO	17±6	1.0	10±1	1.0	106±6	1.0	138±23	1.0
2.5	38±11	2.2	17±4	1.6	127±16	1.2	127±0	0.9
5.0	31±11	1.8	21±0	2.0	109±2	1.0	117±16	0.8
10.0	32±17	1.9	22±4	2.1	107±20	1.0	119±15	0.9
50.0	30±15	1.7	22±8	2.1	107±7	1.0	116±11	0.8
100.0	31±11	1.8	14±1	1.3	99±2	0.9	100±6	0.7

4.2.5. Cell cycle analysis

In previous studies, we observed that the nickel complex was able to disrupt cell cycle progression in U937 cells inducing a G2/M cell cycle arrest (Buschini *et al*., 2009).

To determine the correlation between proliferation inhibition and cell cycle blockage, we analysed whether the citronellal derivatives affected cell cycle progression. Metal complexes action on cell cycle was assessed by determining the cell cycle phase distribution of U937 cells after treatment with GI_{50} concentrations of $[Cu(tcitr)_2]$ and $[Pt(tcitr)_2]$ for 4 and 24 h. Determinations were performed by measuring the DNA content of the cells by propidium iodide staining through flow cytometry. After 4h treatment with $[Pt(tcitr)_2]$ no significant difference was found between treated cells and control cells. After 24h treatment, the platinum complex caused an increase in S population from 40% to 69%, whereas G0-G1 phase cells decreased from 55% to 21% compared to control. These data suggested that $[Pt(tcitr)_2]$ could inhibit cell cycle progression, thus affecting U937 cell growth (Fig. 50). $[Cu(tcitr)_2]$ did not induce alterations in cell distribution during the cell cycle phases (Fig. 50). This results confirmed literature data (Bisceglie *et al*., 2012).

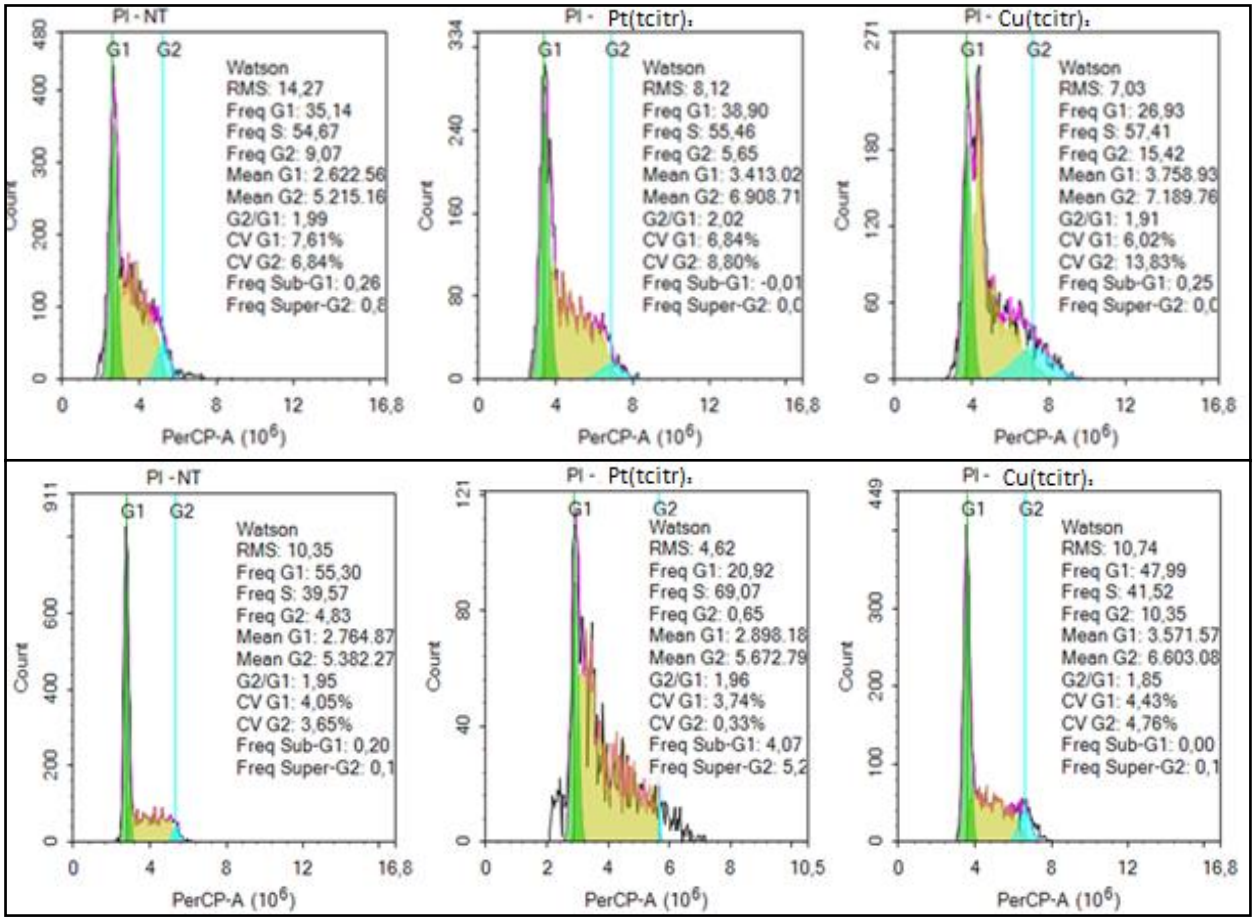

Figure 50. Effect of $[Pt(tcitr)_2]$ and $[Cu(tcitr)_2]$ on cell cycle distribution of U937 cells through flow cytometry analysis.

4.2.6. mRNA expression studies

Human leukemic U937 cell line was used as an *in vitro* model for mRNA expression studies. To analyse the effect of metal complexes on mRNA expression, U937 cells were treated with two concentrations of each compound: a toxic concentration, corresponding to the value of GI_{50} after 24h of treatment ([$Ni(tcitr)_2$]= 10.0 µM, [$Pt(tcitr)_2$] = 7.0 µM, [$Cu(tcitr)_2$] = 33.0 µM), and a subtoxic one with a value 10 times lower([$Ni(tcitr)_2$]= 1.0 µM, [$Pt(tcitr)_2$] = 0.7 µM[$Cu(tcitr)_2$] = 3.3 µM). The treatments were carried out for 1-4-24h.

Gene expression was normalized to the house keeping *GAPDH* gene. To evaluate the mRNA expression we used the Fold change value: if the fold change was >2, it means that the gene was upregulated; if the fold change was <0.5, it means that the gene was downregulated.

4.2.6.1. mRNA expression studies: the ribonucleotide reductase

First, we investigated the relationship between DNA damage, cell growth inhibition and ribonucleotide reductase enzyme expression levels to determine if the treatment with metal complexes could involve the intervention of this enzyme. The anticancer effects of some thiosemicarbazone derivatives are linked to the inhibition of ribonucleotide reductase (RR), an enzyme essential for *de novo* DNA synthesis. Furthermore, RR is involved in DNA repair after genotoxic stimuli. RR protein levels are highly expressed in tumour cells rendering this iron-dependent enzyme an excellent target for cancer chemotherapy (Graser-Loescher *et al*., 2015).

Human RR consists of two large RRM1 and two small RRM2 subunits forming an active tetramer. *p53R2* encodes an homologue R2 isoform. p53R2 protein expression is induced by DNA damage and contributes dNTPs for DNA repair in the G0/G1 cell cycle phase. The R2 subunit serves as a target for anticancer drugs inhibiting the non-heme iron subunit by either metal ion chelation or radical scavenging of the tyrosyl radical (Shao *et al*., 2013), a mechanism being also attributed to thiosemicarbazones.

Through Real Time PCR was possible to determine mRNA expression levels of RRM1 and RRM2. Only the treatment with [$Ni(tcitr)_2$] showed an interesting modulation of the expression of the subunits of RR. With regards to the large subunit, the treatment with 1.0 µM [$Ni(tcitr)_2$] leads to an up-regulation after 1h. In the other cases, there were no alterations in RRM1 expression. After 1.0 µM treatment we observed an increase of mRMA

level of RRM2, but after 24h the gene was down-regulated. On the contrary, the treatment with the toxic concentration of the nickel complex caused a very important up-regulation at all the exposure times (Fig. 51) (Table 27).

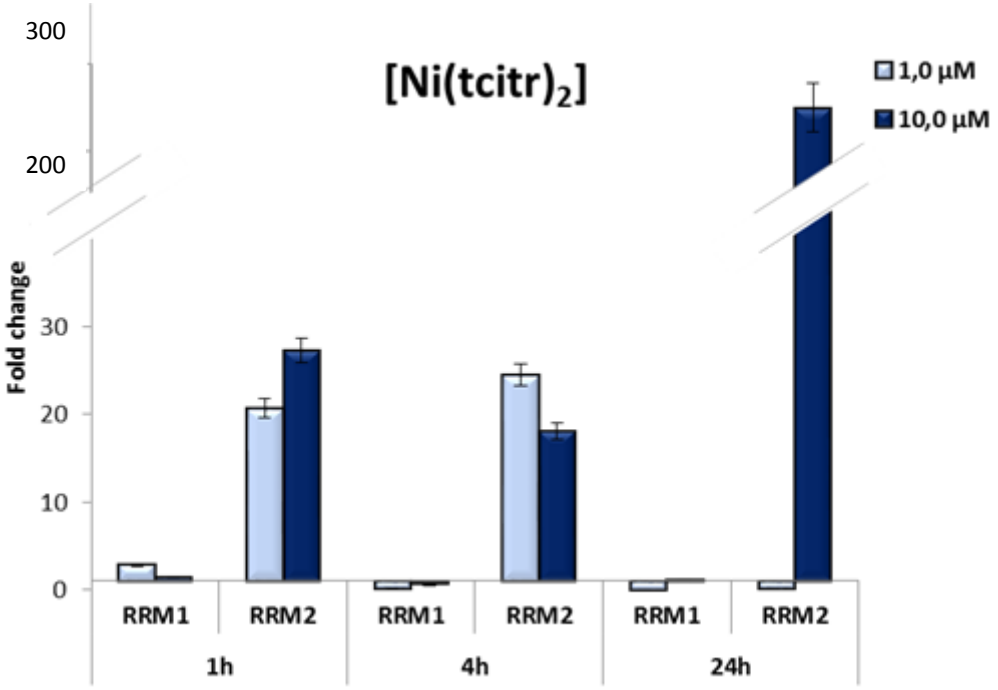

Figure 51. Effect of $[Ni(tcitr)_2]$ on the mRNA expression levels of RRM1 and RRM2. U937 cells were treated for 1-4-24 h with 1.0-10.0 µM of $[Ni(tcitr)_2]$, and the mRNA expression levels were measured by Real Time PCR.

Table 27. Fold change data (mean ± sd) related to mRNA expression of RRM1 and RRM2 in U937 cells treated for 1-4-24 h with 1.0-10.0 µM $[Ni(tcitr)_2]$.

	RRM1		RRM2	
	1.0 µM	**10.0 µM**	**1.0 µM**	**10.0 µM**
1h	2.82 ± 0.89	1.48 ± 0.02	20.74 ± 2.86	27.28 ± 2.45
4h	0.18 ± 0.02	0.65 ± 0.04	24.5 ± 3.35	18.07 ± 3.42
24h	0.01 ± 0.00	1.16 ± 0.39	0.07 ± 0.04	246.64 ± 12.27

The $[Cu(tcitr)_2]$ and the $[Pt(tcitr)_2]$ did not alter significantly the expression of both the subunits of the enzyme (Fig. 52-53) (Table 28-29).

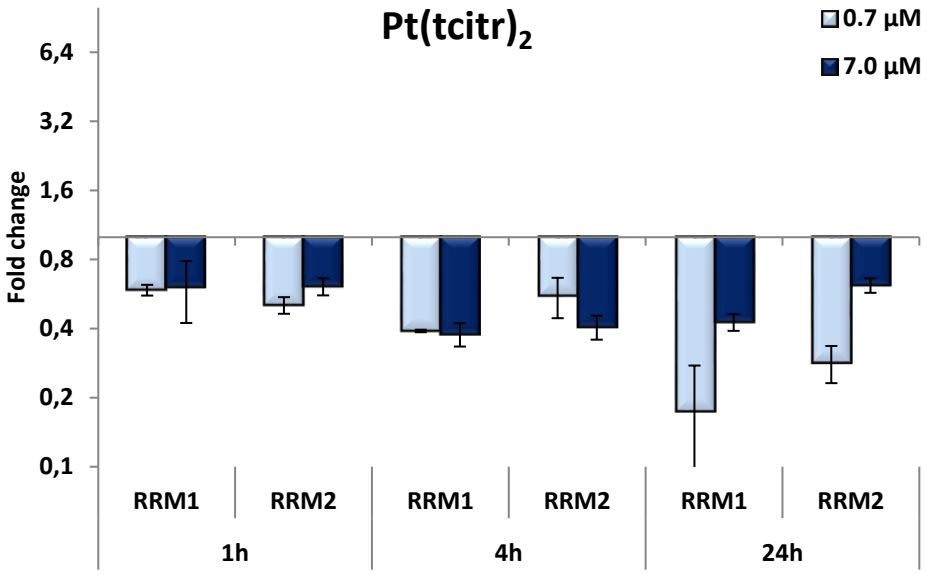

Figure 52. Effect of [Pt(tcitr)$_2$] on the mRNA expression levels of RRM1 and RRM2. U937 cells were treated for 1-4-24 h with 0.7-7.0 µM of [Pt(tcitr)$_2$], and the mRNA expression levels were measured by Real Time PCR.

Table 28. Fold change data (mean ± sd) related to mRNA expression of RRM1 and RRM2 in U937 cells treated for 1-4-24 h with 0.7-7.0 µM [Pt(tcitr)$_2$].

	RRM1		RRM2	
	0.7 µM	**7.0 µM**	**0.7 µM**	**7.0 µM**
1h	0.58 ± 0.03	0.61 ± 0.18	0.51 ± 0.11	0.61 ± 0.04
4h	0.39 ± 0.04	0.37 ± 0.05	0.55 ± 0.10	0.40 ± 0.03
24h	0.17 ± 0.00	0.42 ± 0.04	0.28 ± 0.05	0.62 ± 0.04

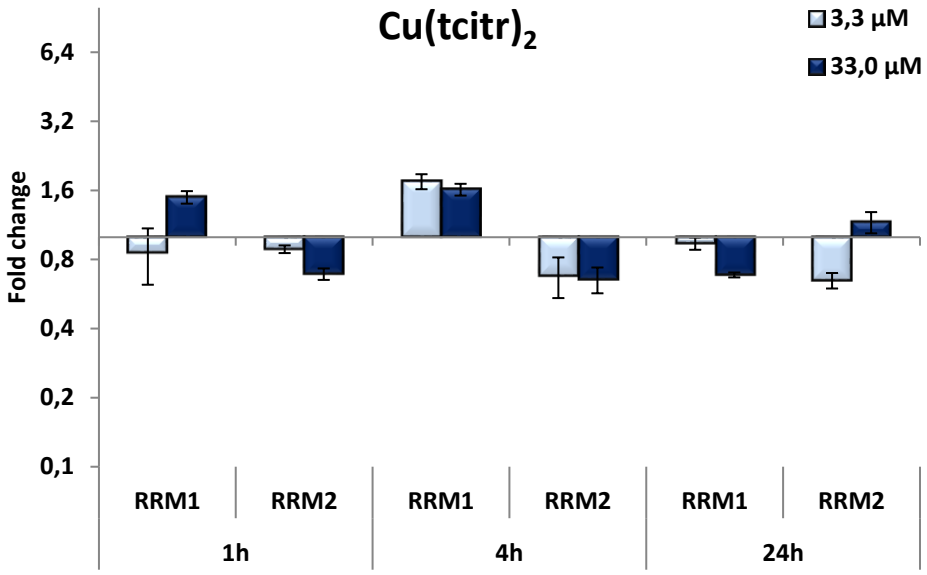

Figure 53. Effect of [Cu(tcitr)$_2$] on the mRNA expression levels of RRM1 and RRM2. U937 cells were treated for 1-4-24 h with 3.3-33.0 µM of [Cu(tcitr)$_2$], and the mRNA expression levels were measured by Real Time PCR.

Table 29. Fold change data (mean ± sd) related to mRNA expression of RRM1 and RRM2 in U937 cells treated for 1-4-24 h with 3.3-33.0 µM [Cu(tcitr)$_2$].

	RRM1		RRM2	
	3.3 µM	**33.0 µM**	**3.3 µM**	**33.0 µM**
1h	0.85 ± 0.23	1.49 ± 0.09	0.88 ± 0.13	0.69 ± 0.08
4h	1.75 ± 0.03	1.61 ± 0.03	0.67 ± 0.05	0.65 ± 0.01
24h	0.93 ± 0.13	0.68 ± 0.09	0.65 ± 0.05	1.16 ± 0.12

The Alkaline Comet Assay highlighted that the metal complexes generated an important DNA damage, that could be recognised by several DNA damage response pathways. After genotoxic stimulus, p53 induces cell-cycle arrest, expression and nuclear accumulation of p53R2, and subsequent activation of ribonucleotide reductase activity. We analysed the expression of the p53R2 subunit of the RR to understand if the cellular response to DNA damage induced by the metal complexes could involve p53.

The nickel complex affected the mRNA expression of p53R2: this subunit was down-regulated after 1h treatment with the subtoxic concentration and after 1 and 4h treatment with the toxic concentration. This result could indicate that [Ni(tcitr)$_2$] could act with a p53 independent mechanism. Also, the Pt and Cu complexes did not disrupt the basal level of

expression of p53R2 (Fig. 54) (Table 30): we may assume that the mechanism of action of the compounds could not involve p53.

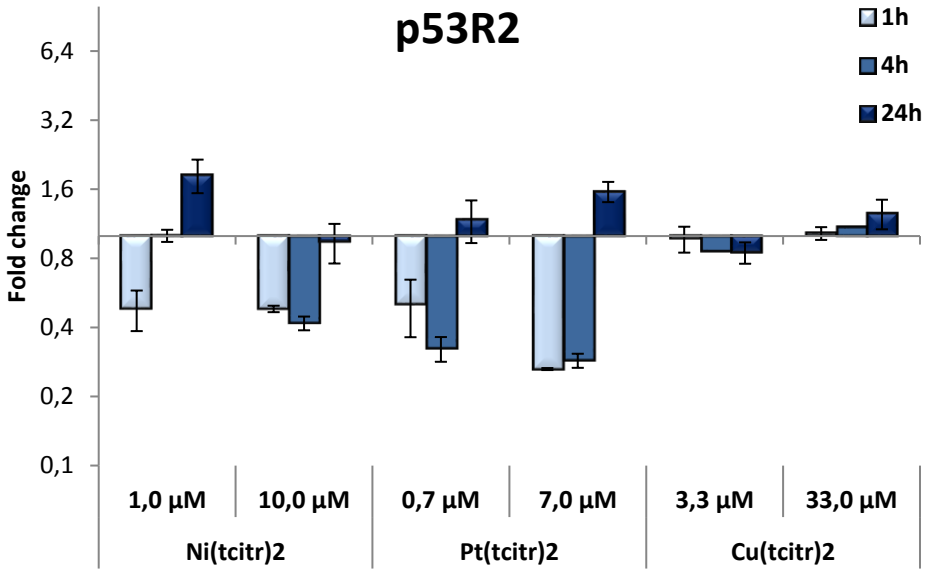

Figure 54. Effect of $[Ni(tcitr)_2]$, $[Pt(tcitr)_2]$ and $[Cu(tcitr)_2]$ on the mRNA expression levels of p53R2. U937 cells were treated for 1-4-24 h and the mRNA expression levels were measured by Real Time PCR.

Table 30. Fold change data (mean ± sd) related to mRNA expression of p53R2 in U937 cells treated for 1-4-24 h with metal complexes.

	$Ni(tcitr)_2$		$Pt(tcitr)_2$		$Cu(tcitr)_2$	
	1.0 µM	**10.0 µM**	**0.7 µM**	**7.0 µM**	**3.3 µM**	**33.0 µM**
1h	0.48 ± 0.09	0.48 ± 0.01	0.50 ± 0.14	0.26 ± 0.00	0.97 ± 0.12	1.02 ± 0.06
4h	1.00 ± 0.06	0.41 ± 0.02	0.32 ± 0.03	0.28 ± 0.02	0.85 ± 0.16	1.09 ± 0.01
24h	1.84 ± 0.03	0.94 ± 0.18	1.18 ± 0.25	1.56 ± 0.15	0.84 ± 0.09	1.25 ± 0.18

4.2.6.2. mRNA expression studies: DNA damage response pathway

Understanding the molecular basis of DNA-damage and DNA damage response pathways (DDR) is important in the development of effective anticancer drugs.

Ataxia-telangiectasia-mutated (ATM) and ataxia telangiectasia and Rad3-related (ATR) proteins are key regulators of DDR. ATM and ATR are kinases, that, in response to DNA breaks, undergo a rapid increase in their kinase activity. ATM is the kinase responsible for cellular responses to DSBs, which can include DNA repair, checkpoint activation and apoptosis induction. To achieve this, ATM phosphorylates several substrates in response to DNA damage. Instead, ATR is the DNA replication stress response kinase, phosphorylating many substrates in response to SSBs and alterations induced by agents such as UV. A key ATR function is to phosphorylate and activate the protein kinase Chk1. When activated, Chk1 promotes proteasomal degradation of CDC25A, a phosphatase that removes inhibitory modifications from cyclin-dependent kinases (CDKs).

First, we examined the changes in mRNA expression of ATM and ATR. The nickel complex induced a down-regulation of both the kinases after 1h of treatment with the toxic concentration (10.0 µM) (Fig. 55-56) (Table 31-32). [Pt(tcitr)$_2$] did not alter the mRNA levels, while the copper complex caused a strong reduction of ATR and ATM mRNA levels after 4h of toxic and subtoxic exposure. A normal level of transcription was restored after 24h (Fig. 55-56) (Table 31-32).

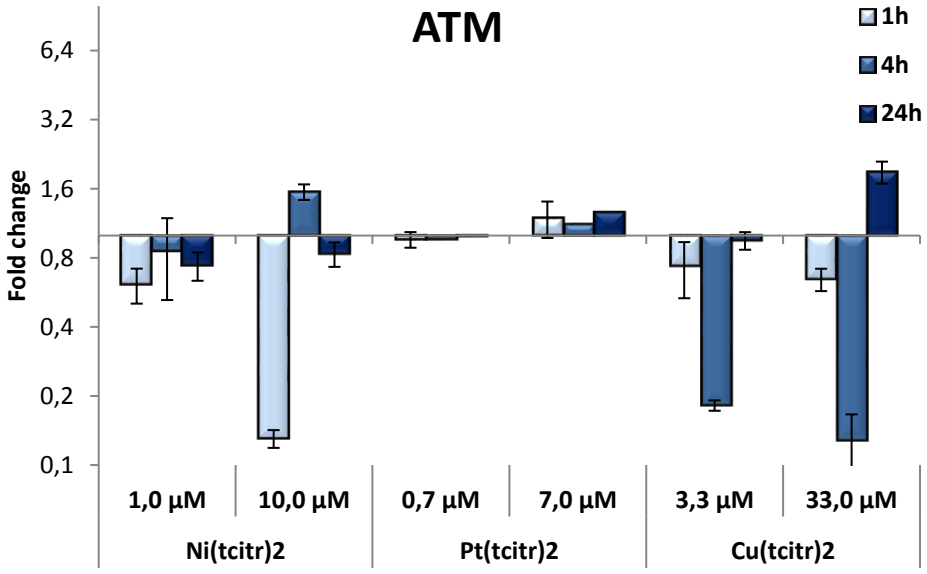

Figure 55. Effect of [Ni(tcitr)$_2$], [Pt(tcitr)$_2$] and [Cu(tcitr)$_2$] on the mRNA expression levels of ATM. U937 cells were treated for 1-4-24 h and the mRNA expression levels were measured by Real Time PCR.

Table 31. Fold change data (mean ± sd) related to mRNA expression of ATM in U937 cells treated for 1-4-24 h with metal complexes.

	$Ni(tcitr)_2$		$Pt(tcitr)_2$		$Cu(tcitr)_2$	
	1.0 µM	**10.0 µM**	**0.7 µM**	**7.0 µM**	**3.3 µM**	**33.0 µM**
1h	0.61 ± 0.11	0.13 ± 0.01	0.96 ± 0.07	1.19 ± 0.22	0.73 ± 0.20	0.64 ± 0.07
4h	0.85 ± 0.33	1.55 ± 0.12	0.96 ± 0.02	1.12 ± 0.36	0.18 ± 0.01	0.13 ± 0.04
24h	0.74 ± 0.10	0.83 ± 0.10	0.99 ± 0.06	1.26 ± 0.23	0.95 ± 0.08	1.89 ± 0.21

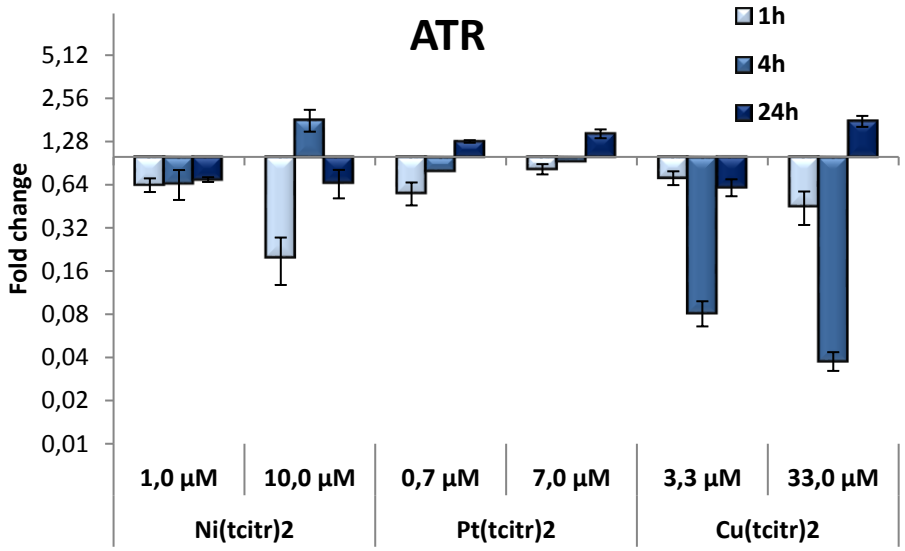

Figure 56. Effect of $[Ni(tcitr)_2]$, $[Pt(tcitr)_2]$ and $[Cu(tcitr)_2]$ on the mRNA expression levels of ATR. U937 cells were treated for 1-4-24 h and the mRNA expression levels were measured by Real Time PCR.

Table 32. Fold change data (mean ± sd) related to mRNA expression of ATR in U937 cells treated for 1-4-24 h with metal complexes.

	$Ni(tcitr)_2$		$Pt(tcitr)_2$		$Cu(tcitr)_2$	
	1.0 µM	**10.0 µM**	**0.7 µM**	**7.0 µM**	**3.3 µM**	**33.0 µM**
1h	0.64 ± 0.06	0.20 ± 0.07	0.56 ± 0.10	0.82 ± 0.07	0.71 ± 0.08	0.45 ± 0.11
4h	0.66 ± 0.15	1.81 ± 0.32	0.80 ± 0.11	0.94 ± 0.12	0.08 ± 0.01	0.04 ± 0.01
24h	0.70 ± 0.03	0.66 ± 0.15	1.28 ± 0.03	1.45 ± 0.10	0.62 ± 0.10	1.77 ± 0.15

Chk1 and Chk2 are crucial phosphorylation targets of ATM and ATR. In response to the DNA damage, ATM and ATR may phosphorylate Chk2 and Chk1, respectively. Both Chk2 and Chk1 also phosphorylate and stabilize p53 protein. However, p53 can be directly phosphorylated by ATM or ATR, resulting in the increase of its transcriptional activity.

We focused on the DNA damage sensors, Chk1 and Chk2, that participate in G2/M checkpoint control through the ATM/ATR pathway in order to identify if DNA damage induced by metal complexes could involve the DDR pathway.

[Ni(tcitr)$_2$] induced an important up-regulation of Chk1 gene after 4h of treatment with both the concentrations, while [Cu(tcitr)$_2$] induced an increase of mRNA level after 24h of treatment with the toxic concentration (Fig. 57) (Table 33). In the other cases, the compounds did not alter Chk1 expression.

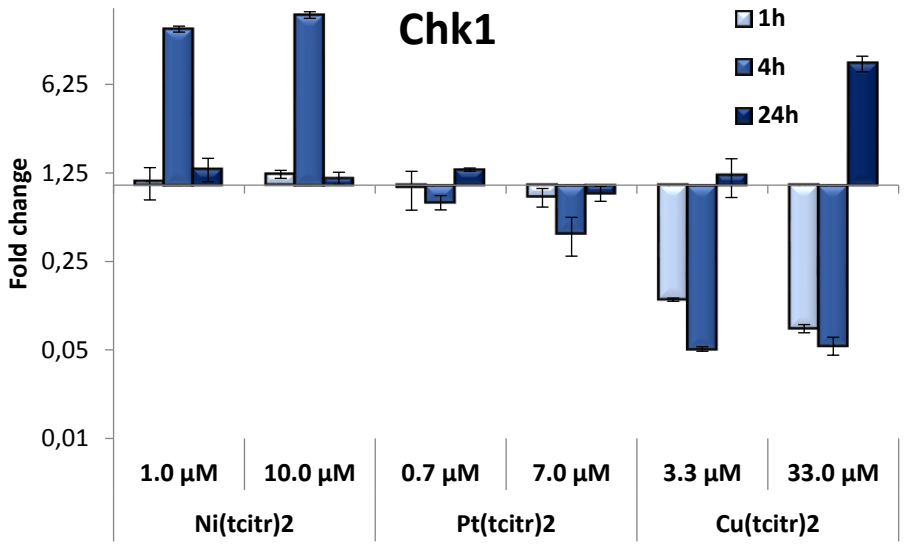

Figure 57. Effect of [Ni(tcitr)$_2$], [Pt(tcitr)$_2$] and [Cu(tcitr)$_2$] on the mRNA expression levels of ChK1. U937 cells were treated for 1-4-24 h and the mRNA expression levels were measured by Real Time PCR.

Table 33. Fold change data (mean ± sd) related to mRNA expression of Chk1 in U937 cells treated for 1-4-24 h with metal complexes.

	Ni(tcitr)$_2$		**Pt(tcitr)$_2$**		**Cu(tcitr)$_2$**	
	1.0 µM	**10.0 µM**	**0.7 µM**	**7.0 µM**	**3.3 µM**	**33.0 µM**
1h	1.06±0.31	1.22±0.08	0.96±0.32	0.80±0.13	0.12±0.01	0.07±0.01
4h	17.11±0.92	22.10±1.32	0.73±0.09	0.42±0.14	0.05±0.01	0.05±0.01
24h	1.34±0.28	1.14±0.13	1.32±0.03	0.86±0.11	1.21±0.4	9.14±1.29

With regards to Chk2, U937 cells showed an up-regulation after 1h of treatment with the nickel complex at both the concentrations; there was also an increase of mRNA level after 24h of treatment with 7.0 µM of platinum complex. Instead, the copper caused a relevant down regulation of Chk2 (Fig. 58) (Table 34).

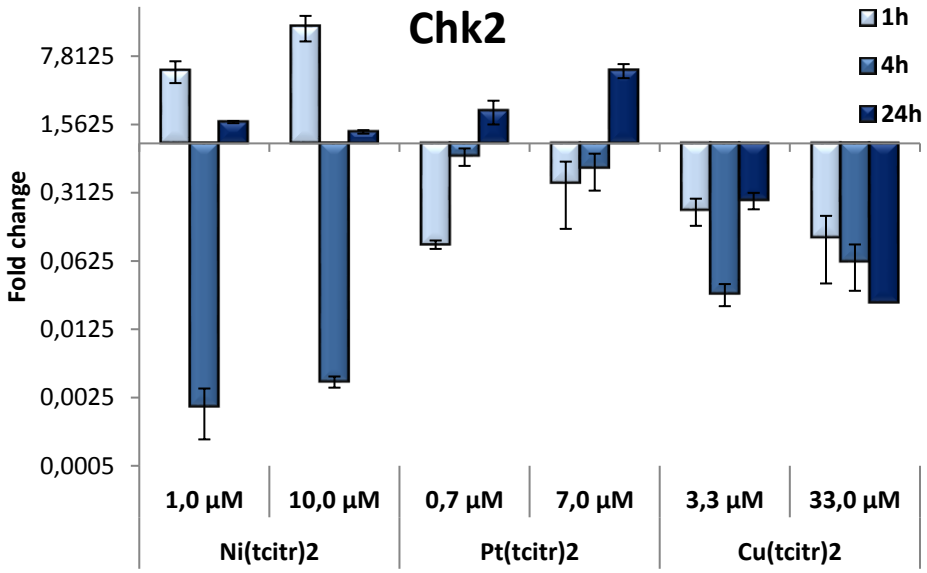

Figure 58. Effect of [Ni(tcitr)$_2$], [Pt(tcitr)$_2$] and [Cu(tcitr)$_2$] on the mRNA expression levels of ChK2. U937 cells were treated for 1-4-24 h and the mRNA expression levels were measured by Real Time PCR.

Table 34. Fold change data (mean ± sd) related to mRNA expression of Chk2 in U937 cells treated for 1-4-24 h with metal complexes.

	Ni(tcitr)$_2$		**Pt(tcitr)$_2$**		**Cu(tcitr)$_2$**	
	1.0 µM	**10.0 µM**	**0.7 µM**	**7.0 µM**	**3.3 µM**	**33.0 µM**
1h	5.53±1.39	15.62±4.56	0.09±0.00	0.39±0.25	0.21±0.06	0.11±0.07
4h	0.01±0.01	0.03±0.00	0.73±0.14	0.55±0.22	0.02±0.00	0.06±0.03
24h	1.65±0.04	1.31±0.05	2.15±0.58	5.5±0.91	0.26±.0.05	0.02±0.00

To determine the correlation between proliferation inhibition and cell cycle blockage, we analysed the expression levels of cyclin A/Cdk2 complex, that are known to participate in the initiation of mitosis in human cancer cells, and of cyclin B, a key component involved in G2 to M phase transition.

All the metal complexes induced a modulation of the expression of Cyclin A1. In particular, the subtoxic concentration of [Ni(tcitr)$_2$] up-regulated the gene after 24h; the toxic concentration of [Pt(tcitr)$_2$] caused an important increase of mRNA level after 24h. [Cu(tcitr)$_2$] induced an up-regulation after 1h but then the gene was down-regulated (Fig. 59) (Table 35).

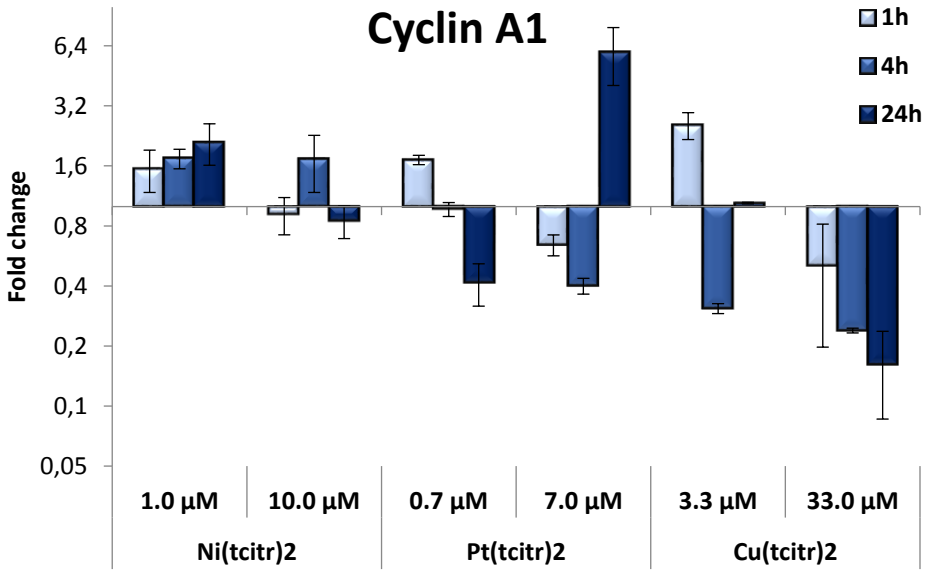

Figure 59. Effect of [Ni(tcitr)$_2$], [Pt(tcitr)$_2$] and [Cu(tcitr)$_2$] on the mRNA expression levels of Cyclin A1. U937 cells were treated for 1-4-24 h and the mRNA expression levels were measured by Real Time PCR.

Table 35. Fold change data (mean ± sd) related to mRNA expression of Cyclin A1 in U937 cells treated for 1-4-24 h with metal complexes.

	Ni(tcitr)$_2$		**Pt(tcitr)$_2$**		**Cu(tcitr)$_2$**	
	1.0 µM	**10.0 µM**	**0.7 µM**	**7.0 µM**	**3.3 µM**	**33.0 µM**
1h	1.54±0.37	0.91±0.19	1.71±0.09	0.64±0.07	5.56±0.39	0.50±0.03
4h	1.74±0.19	1.72±0.54	0.96±0.07	0.40±0.03	0.30±0.01	0.23±0.01
24h	2.11±0.49	0.85±0.16	0.41±0.09	5.97±1.92	1.04±0.01	0.16±0.07

The mRNA level of Cyclin B decreased mainly after the toxic treatment with the platinum and the copper complex (7.0 µM and 33.0 µM); while [Ni(tcitr)$_2$] caused an increase of Cyclin B expression after 4h with both the concentrations (Fig. 60) (Table 36).

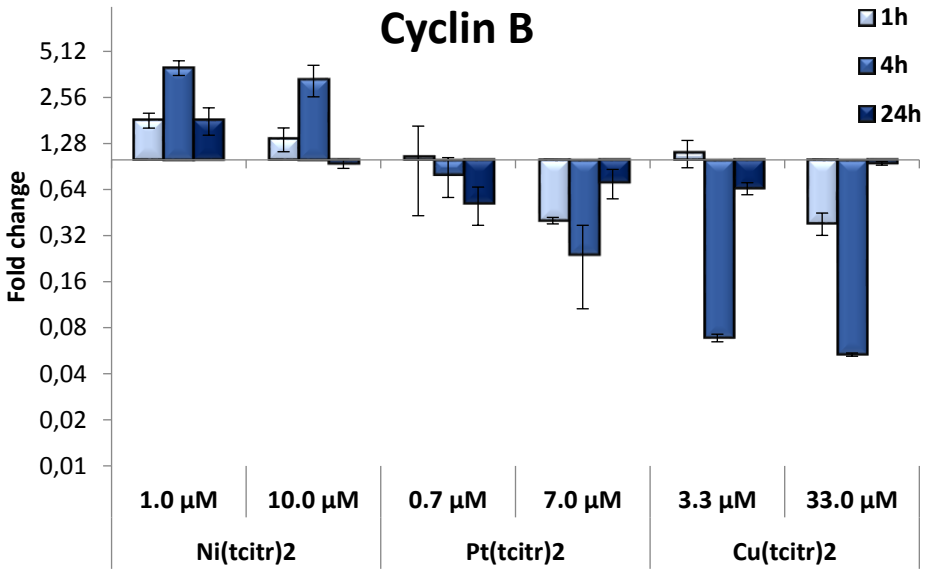

Figure 60. Effect of [Ni(tcitr)$_2$], [Pt(tcitr)$_2$] and [Cu(tcitr)$_2$] on the mRNA expression levels of Cyclin B. U937 cells were treated for 1-4-24 h and the mRNA expression levels were measured by Real Time PCR.

Table 36. Fold change data (mean ± sd) related to mRNA expression of Cyclin B in U937 cells treated for 1-4-24 h with metal complexes.

	Ni(tcitr)$_2$		**Pt(tcitr)$_2$**		**Cu(tcitr)$_2$**	
	1.0 µM	**10.0 µM**	**0.7 µM**	**7.0 µM**	**3.3 µM**	**33.0 µM**
1h	1.82 ± 0.20	1.37 ± 0.24	1.04 ± 0.61	0.40 ± 0.01	1.1 ± 0.22	0.38 ± 0.06
4h	4.00 ± 0.44	3.36 ± 0.78	0.80 ± 0.23	0.24 ± 0.13	0.06 ± 0.00	0.05 ± 0.00
24h	1.81 ± 0.37	0.94 ± 0.06	0.52 ± 0.14	0.71 ± 0.15	0.65 ± 0.05	0.95 ± 0.02

4.2.6.3. mRNA expression studies: cellular uptake

In order to understand metal complexes transport into U937 cells, we studied hCTR1, a transmembrane protein that is involved in the uptake of platinum anticancer drugs. The nickel complex did not alter its expression. [Ni(tcitr)$_2$] induced a decrease of mRNA level after the treatment with the toxic concentration; also [Cu(tcitr)$_2$] caused a down-regulation. hCTR1 was slightly up-regulated after the treatment with the toxic concentration (7.0 µM) of the platinum complex (Fig. 61) (Table 37).

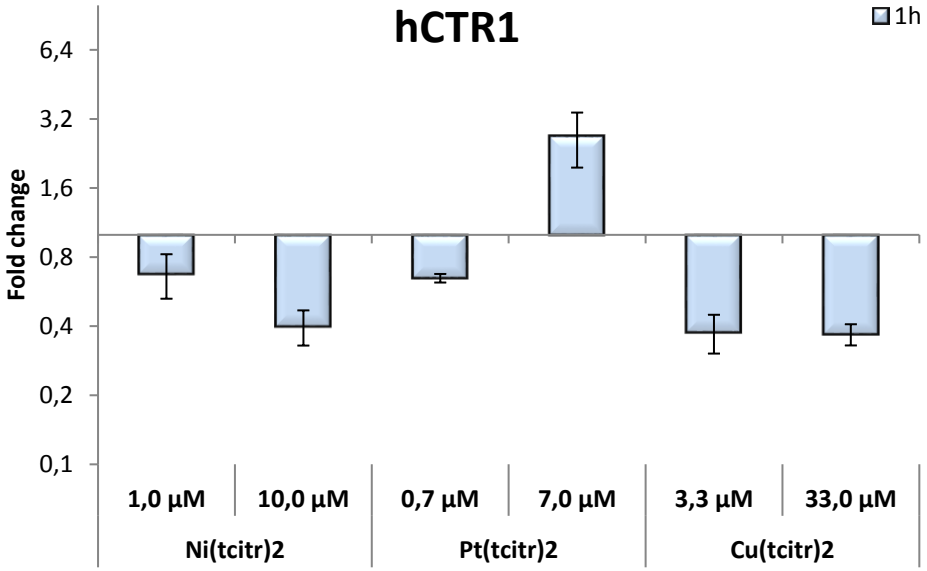

Figure 61. Effect of [Ni(tcitr)$_2$], [Pt(tcitr)$_2$] and [Cu(tcitr)$_2$] on the mRNA expression levels of hCTR1. U937 cells were treated for 1h and the mRNA expression levels were measured by Real Time PCR.

Table 37. Fold change data (mean ± sd) related to mRNA expression of hCTR1 in U937 cells treated for 1-4-24 h with metal complexes.

	Ni(tcitr)$_2$		Pt(tcitr)$_2$		Cu(tcitr)$_2$	
	1.0 µM	**10.0 µM**	**0.7 µM**	**7.0 µM**	**3.3 µM**	**33.0 µM**
1h	0.68 ± 0.14	0.4 ± 0.06	0.65 ± 0.02	2.68 ± 0.72	0.38 ± 0.07	0.37 ± 0.03

4.3. Biological activity of citronellal thiosemicarbazone metal complexes on primary tumour samples

Head and neck cancers (HNC) represent a heterogeneous cluster of aggressive malignancies, of which about 90% are squamous cell carcinomas (HNSCC). HNC arises in the oral cavity, salivary glands, larynx, pharynx, nasal cavity and paranasal sinuses, and is characterized by high morbidity and metastasis rates (Ward *et al*., 2018). A series of therapies has been applied in the treatment of HNSCC, including surgery, radiotherapy, neoadjuvant chemotherapy and a combination of these methods (Pang *et al*., 2018). Nevertheless, HNC are a collection of neoplasms that are difficult to treat.

Next-generation sequencing technologies contributed to understand the molecular and genetic pathogenesis of HNC. The major pathological pathways implicated in the tumorigenesis of HNC include dysregulation of four processes: cellular survival and proliferation, cell-cycle control, cellular differentiation and adhesion and invasion signalling. *TP53, CDKN2A, CASP8, FAT1, NOTCH1, HRAS, PIK3CA, MLL2, and FBXW7* represent the most frequently altered genes in HNC (Zhou *et al*., 2016).

The last part of this project was carried out at the International Agency for Research on Cancer (IARC) in the laboratory of the Infections and Cancer Biology Group led by Dr. M. Tommasino. Biological activity of nickel, platinum and copper complexes was investigated using different cancer cell lines, resulting from primary tumour samples and collected as part of a multicenter case-control study coordinated by IARC (Saulnier *et al*., 2012). Cells belong to the cluster of head and neck cancers: HNC-212 represents oral cavity cancer cells; HNC-211 and HNC-41 present tonsil cancer cells and PNS-136 represents paranasal sinus cancer cells.

Cells were selected for a different pattern of *TP53* mutations. p53, the “guardian of the genome”, is a tumour suppressor protein, that ensures genomic stability and thus prevents cancer onset. It regulates the transcription of numerous downstream target genes involved in cell-cycle arrest, apoptosis, senescence, and DNA repair (Lane *et al*., 2010). p53 mutation leads to loss of wild-type p53 activity and has been frequently detected in multiple cancer types, such as HNC. In these malignancies, disruption of p53 functions can be caused by mutation or HPV infection and can be requested for cancer development and progression.

HNC-41 and HNC-136 present *wt* p53 expression; while HNC-211 and HNC-212 show specific mutations in *TP53*.

4.3.1. Cytotoxic activity of metal complexes

In order to understand if the cytotoxic mechanisms of $[Ni(tcitr)_2]$, $[Pt(tcitr)_2]$, $[Cu(tcitr)_2]$ could occur through a p53-dependent pathway, we performed MTS assay. Cells were treated with the metal complexes for 24-48-72h and the dose-response curves were obtained. All the compounds were able to inhibit cell proliferation in a time-dependent manner. The copper complex exhibits the most cytotoxic effect against HNC cells, highlighted by GI_{50} values <20.0 µM (Table 27).

Table 27. GI_{50} (µM) values obtained after 24-48-72h treatment with metal complexes.

	$Ni(tcitr)_2$			**$Pt(tcitr)_2$**			**$Cu(tcitr)_2$**		
	24h	**48h**	**72h**	**24h**	**48h**	**72h**	**24h**	**48h**	**72h**
HNC-41	75.0	35.0	46.5	89.0	32.0	23.5	7.2	2.5	1.9
PNS-136	42.5	35.0	40.8	46.5	33.0	35.5	18.5	14.0	8.0
HNC-211	66.0	36.0	34.0	40.0	31.0	30.5	6.5	3.5	6.0
HNC-212	85.5	76.0	39.0	50.5	65.5	32.5	8.5	8.2	6.5

4.3.2. mRNA expression studies

Also in this case, to identify a possible target of $[Cu(tcitr)_2]$ we investigated the role of the ribonucleotide reductase enzyme (RR) in the response to the treatment with the copper complex. Several stimuli can activate RR, such as DNA damage, oxidative stress and alterations in cell cycle progression. On the other hand, the cytotoxic activity of many copper anticancer agents depends on ROS generation, that can lead to the activation of the apoptotic pathway. We performed mRNA expression studies of RR in order to identify a possible relationship between $[Cu(tcitr)_2]$ cytotoxic effect, ROS generation and RR expression. Each cell line was treated with the GI_{50} concentration of $[Cu(tcitr)_2]$, obtained after 24h treatment, and a subtoxic concentration 10 times lower than GI_{50}. The RNA extraction was performed after 1-4-24h treatment and the evaluation of RRM1 and RRM2 expression levels was carried out through Real Time PCR. Treated HNC-41 cells presented a modulation of the expression of RR subunits. In particular, the subtoxic concentration of $[Cu(tcitr)_2]$ (0.72 µM) was not able to alter the mRNA expression of RRM1 and RRM2 at 1 and 4h treatment, but after 24h $[Cu(tcitr)_2]$ induced a decrease of mRNA levels. The treatment with the toxic concentration (7.2 µM) caused a strong up-regulation of both the subunits already after 1h; after 4h the cells showed a reduction of the mRNA expression and at 24h RRM1 and RRM2 were down-regulated (Fig. 62).

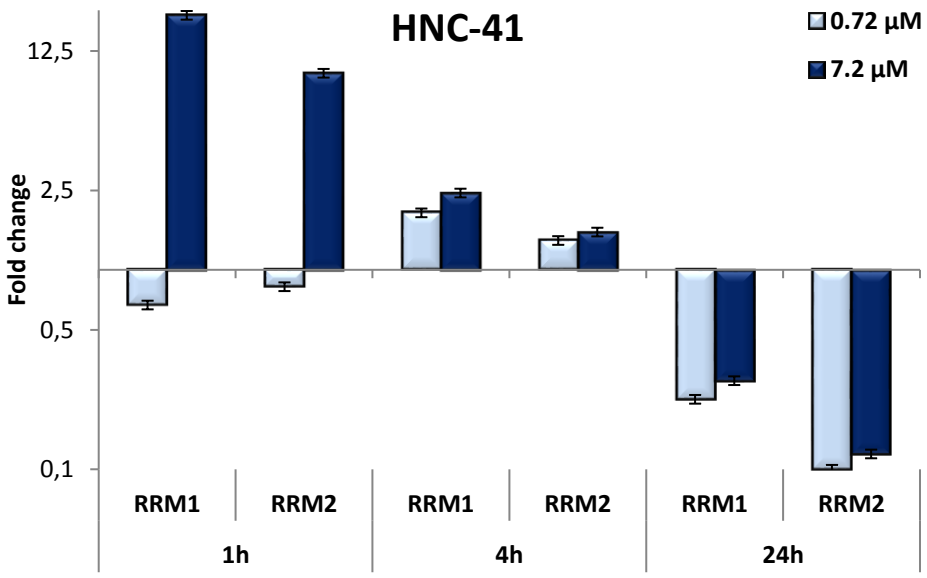

Figure 62. Effect of $[Cu(tcitr)_2]$ on the mRNA expression levels of RRM1 and RRM2. HNC-41 cells were treated for 1-4-24 h with 0.72-7.2 µM of $[Cu(tcitr)_2]$, and the mRNA expression levels were measured by Real Time PCR.

PNS-136 cells were treated with 1.85 µM and 18.5 µM of [Cu(tcitr)$_2$]. The treatment with 1.85 µM induced a RRM1 up-regulation after 4 and 24h. In subtoxic condition, RRM2 underwent an up-regulation after 1 and 4h, but its levels decreased after 24h, restoring the basal expression. The toxic concentration (18.5 µM) did not caused an expression modulation of RRM1 and RRM2: in fact, both the subunits showed a basal expression levels (Fig. 63).

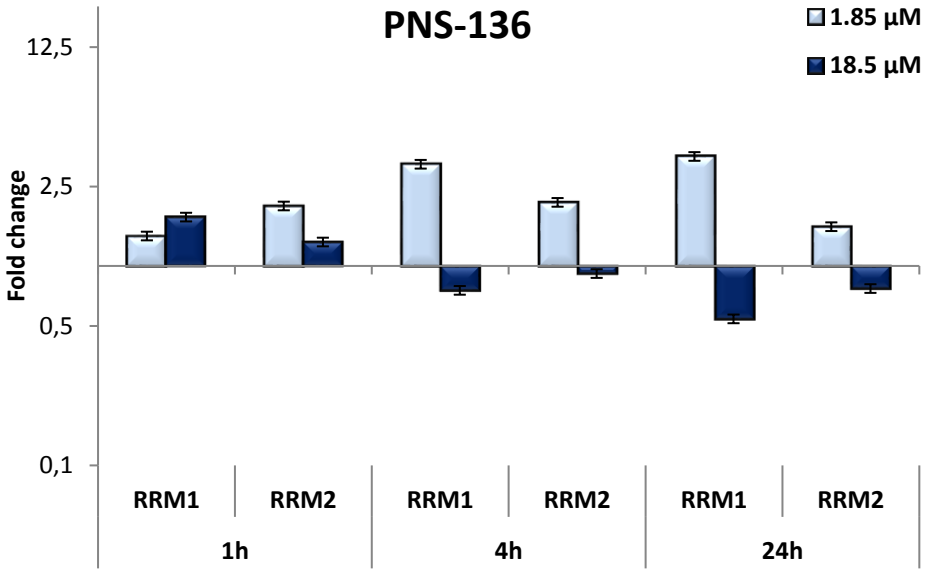

Figure 63. Effect of [Cu(tcitr)$_2$] on the mRNA expression levels of RRM1 and RRM2. PNS-136 cells were treated for 1-4-24 h with 1.85-18.5 µM of [Cu(tcitr)$_2$], and the mRNA expression levels were measured by Real Time PCR.

HNC-211 cells were treated with 0.65 µM and 6.5 µM of [Cu(tcitr)$_2$], while HNC-212 cells were treated with 0.85 µM and 8.5 µM [Cu(tcitr)$_2$]. Both these mutant p53 cell lines did not present any expression modulation of the subunits of the ribonucleotide reductase (Fig. 64-65).

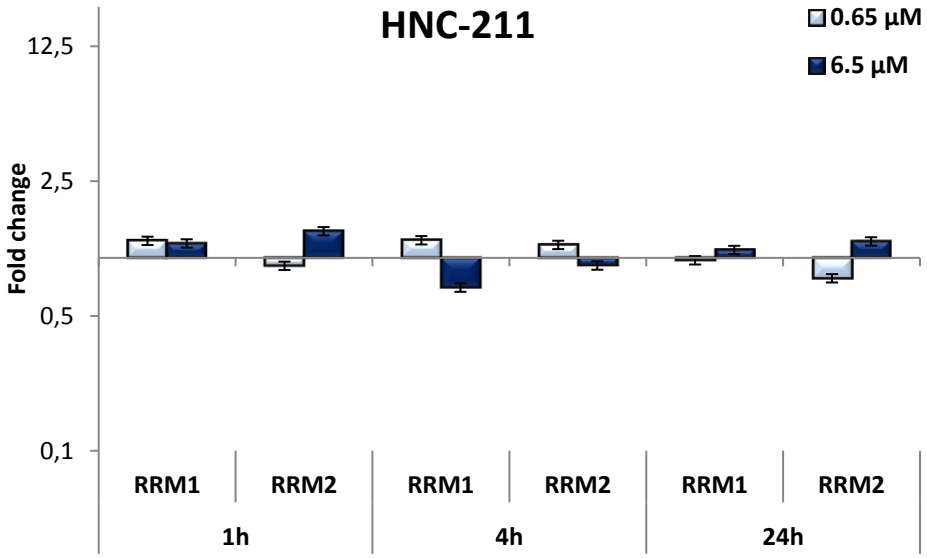

Figure 64. Effect of [Cu(tcitr)$_2$] on the mRNA expression levels of RRM1 and RRM2. HNC-211 cells were treated for 1-4-24 h with 0.65-6.5 µM of [Cu(tcitr)$_2$], and the mRNA expression levels were measured by Real Time PCR.

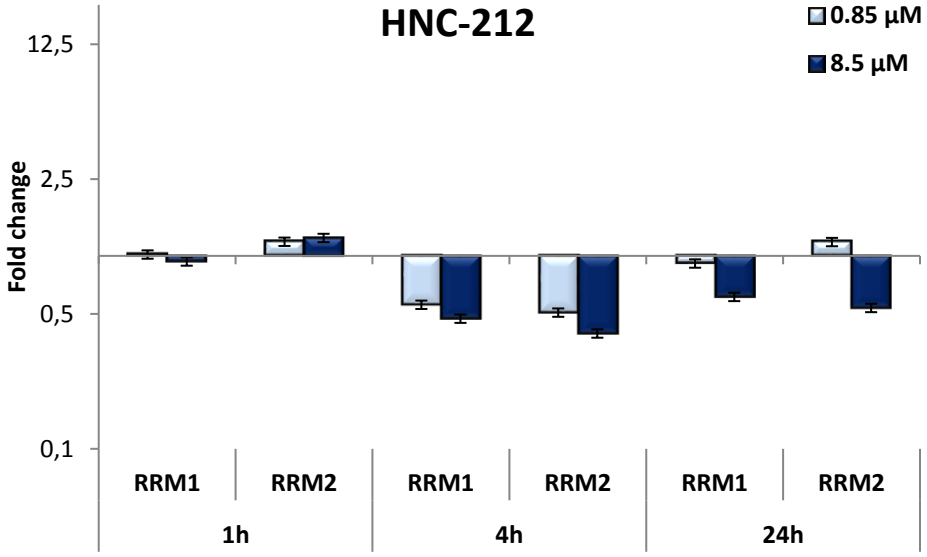

Figure 65. Effect of [Cu(tcitr)$_2$] on the mRNA expression levels of RRM1 and RRM2. HNC-212 cells were treated for 1-4-24 h with 0.85-8.5 µM of [Cu(tcitr)$_2$], and the mRNA expression levels were measured by Real Time PCR.

4.3.3. Protein expression studies

Cellular proteins extraction from HNC cell lines was performed after 1-4-24h treatment with toxic and subtoxic concentrations of [$Cu(tcitr)_2$]. Through western blot analysis we determined alterations in protein expression of p53 and mTOR induced by the treatment with copper complex in order to identify a possible correlation between [$Cu(tcitr)_2$] cytotoxic effect and a cellular response pathway, dependent on p53 or mTOR.

The *TP53* gene consists of 11 exons, the first of which is noncoding. p53 protein consists of 393 amino acids and comprises four regions with different functions: the N-terminal trans-activation domain (amino acids 20–42), the central DNA-binding domain (amino acids 103–292), the C-terminal tetramerization domain (amino acids 319–360), and the C-terminal regulatory domain (amino acids 364–393) (Lane *et al*., 2010).

In particular, we studied several p53 post-translational modifications, induced when cells were exposed to genotoxic stimuli. At least 20 sites in the p53 protein, located primarily in the N-terminal domains or in the C-terminal domain, are modified in response to the activation of different stress signalling pathways (Saito *et al*., 2003). p53 phosphorylation was examined at three sites (Ser15, Ser33, Ser392), p53 acetylation was examined at Lys382. Furthermore, we analysed the p53 total protein.

Serine 15 (Ser15) phosphorylation is a major focal point in the activation of p53: it is the primary target of the DNA damage response on the p53 protein and is phosphorylated by both the ATM and ATR protein kinases. Ser15 phosphorylation also triggers a sequential series of additional phosphorylation events in p53, including phosphorylation of Ser9 – 20 – 33 - 46 and Thr18, that contribute further to p53 induction and activation (Loughery *et al*., 2014). At the C terminus, phosphorylation of Ser392 was implicated in regulating the oligomerization state of p53 and its ability to bind DNA in a sequence-specific manner (Saito *et al*., 2003). The acetylation of the Lys382 site of p53 is thought to increase its sequence-specific DNA-binding activity and its protein stability (Ljungman *et al*., 2001).
Taken together, all these modifications are thought to be important for stimulating p53-mediated transactivation, cell cycle arrest and apoptosis.

The Western Blot analysis demonstrated that the phosphorylation of p53 on Ser15, Ser33 and Ser392, and acetylation of p53 on Lys379 were all decreased after treatment with the toxic concentration of [Cu(tcitr)$_2$]. In addition, the copper complex induced a very important reduction of p53 total protein (Fig. 66).

Surprisingly, we obtained the same results in all the cell lines (HNC-41 and PNS-136 wt p53 cells; HNC-211 and HNC-212 mutant p53 cells). Western blot analysis on PNS136 cells is presented as an example (Fig. 66).

The Western Blot quantification are detailed in Appendix.

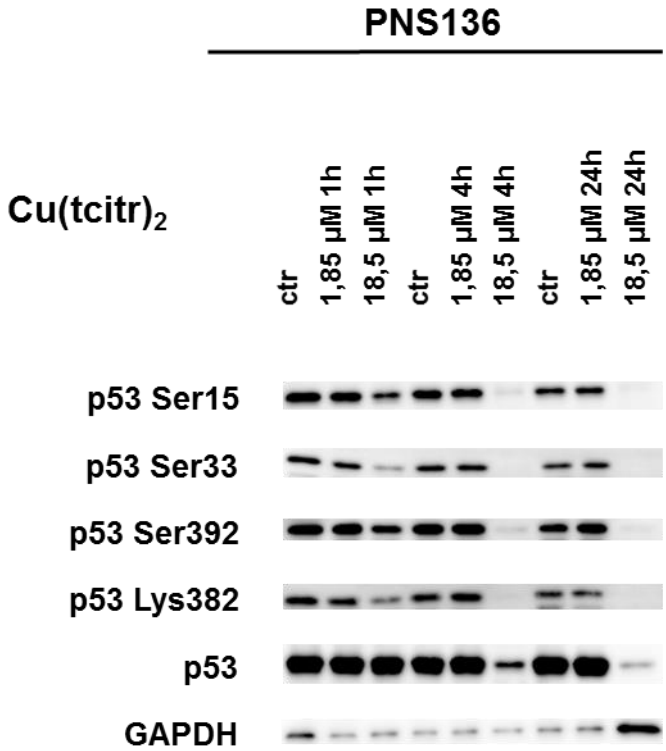

Figure 66. Effect of [Cu(tcitr)$_2$] on the expression levels of p53 protein in PNS-136 cells. Cells were treated with the indicated concentrations of [Cu(tcitr)$_2$] for 1-4-24 h. The expression levels of the proteins were analysed by western blot analysis.

Furthermore, we determined the modulation of mTOR protein after the treatment with [Cu(tcitr)$_2$]. In fact, after DNA damage, p53 regulates mTOR dependent pathway. Also in this case, we observed a reduction of mTOR expression protein compared to untreated cells mainly after 4 and 24h in all HNC cell lines (Fig. 67). Western blot analysis on PNS136 cells is presented as an example (Fig. 67).

The Western Blot quantification are detailed in Appendix.

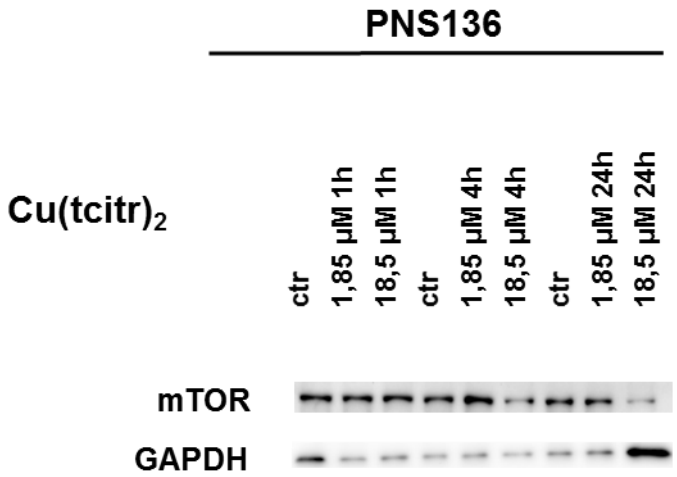

Figure 67. Effect of [Cu(tcitr)$_2$] on the expression levels of mTOR protein in PNS-136 cells. Cells were treated with the indicated concentrations of [Cu(tcitr)$_2$] for 1-4-24 h. The expression levels of the proteins were analysed by western blot analysis.

5. Discussion

Nature is a precious reservoir of novel bioactive compounds. Natural products play a key role in the discovery and development of new drugs and are essential to define scaffolds of molecule based on the activity of the parent molecule.

Our research group is working on thiosemicarbazones, a versatile class of Schiff bases ligands, having sulphur and nitrogen as donor atoms. They were prepared through condensation reactions between aldehydes or ketones with thiosemicarbazide (Khan *et al*., 2015). Thiosemicarbazide is an important structural motif that has the potential to display chemical functionality in bioactive molecules. Optimization of this structure can lead to the discovery of new active molecules.

TSCs represent a class of ligands that shows diverse range of biological activity, including antibacterial, antifungal, antiviral and anticancer effects. In this work, we focused mainly of TSCs with antifungal or anticancer activity.

5.1 Thiosemicarbazones as antifungal agents

Mycotoxin contamination in food represents a public health problem. Mycotoxins are secondary metabolites produced by fungi under specific conditions, such as high humidity, poor agricultural practices, or damaged and contaminated crops.

Among mycotoxins, aflatoxins are the most dangerous and are produced by fungal species from the genus *Aspergillus*, notably *A. flavus, A. parasiticus* and *A. nomius*, which develop naturally in food products. These fungi usually infect cereal crops and can lead to serious risks to human and animal health by causing hepatotoxicity, teratogenicity, and immunotoxicity (Kumar *et al*., 2017). There are more than 20 types of aflatoxin molecules, although the most prominent are aflatoxins B1, B2, G1, G2, M1, and M2. Aflatoxins are classified by the International Agency for Research on Cancer (IARC, 2012) as group 1 carcinogens. The most severe human health impact of aflatoxins is hepatocellular carcinoma, which is recognized as the 9th and 7th leading type of cancer in women and men, respectively (Ismail *et al*., 2018).

Aflatoxins exhibit great resistance to conventional treatments usually applied to food or feed processing, including pasteurization, sterilization and other thermal applications. Different approaches have been proposed to remove or degrade the aflatoxins in foods

and the most prominent can be categorized into physical, chemical, and biological methods.

In this context, the "Aflatox project" represents a new approach to develop new typologies of inhibitors of *Aspergillus* proliferation and particularly of aflatoxins production, harmless to the environment and to human health.

The first step of the project was the synthesis of a wide range of bioactive molecules, obtained starting from compounds of natural origin, which then were used as ligands for coordination with metal ions. We functionalized these compounds in order to modulate their main properties, such as solubility, complexing ability, and lipophilicity. Endogenous metal ions, mainly copper and zinc, were used to obtain the relative metal complexes (Zani *et al*., 2015). We set up a method to determine their effects on fungal germination and growth and aflatoxin biosynthesis. The new compounds were tested to detect mycelia growth inhibition and mycotoxin production against different strains of *A. flavus* (Zani *et al*., 2015).

Once the chemical-physical properties and the molecular structures of the new complexes have been elucidated and their antifungal and antimycotoxigenic activity determined, we developed an approach to assess toxicity and genotoxicity of the new compounds, before their diffusion in the environment. This approach was exploited for the design of new potential antifungal molecules without toxic side effects on humans.

To assess the potential toxic and genotoxic risks of the new molecules for the environment, a battery of tests with different genetic end-points was carried out: the Ames test to detect point mutations on bacteria and the micronucleus *Allium cepa* test to detect chromosomal damage (Zani *et al*., 2015).

The last step of the project was the toxicity and genotoxicity evaluation in human cells to determine the risk for human health. The biological activity of the new active molecules was assessed on normal cells deriving from human districts related to possible xenobiotic ways of interaction with the human body, to investigate the risks linked to specific exposition (Zani *et al*., 2015).

Starting from molecules of natural origin, we synthesized both semicarbazones (SCs) and thiosemicarbazones. SCs differ from TSCs only by replacing the sulfur atom with an oxygen atom. We observed that semicarbazones showed less activity in terms of inhibition of fungal growth and mycotoxin production than the corresponding TSCs. We can assume that

the sulfur atom could be essential for the biological activity of the compounds. We introduced the thio- group yielding the thiosemicarbazones to obtain more potent compounds with antifungal and antiaflatoxigenic ability.

In order to protect human health, one of the main goals of the project was to identify molecules without toxic effects against human cells. With regards to the cytotoxic potential, in this study semicarbazones and thiosemicarbazones did not present differences and generally they showed a very low antiproliferative activity.

To improve the capability of the free ligands to inhibit toxin production, copper and zinc complexes were then synthesized. Metal ions play a role in the aflatoxin biosynthesis. Unfortunately, the metal complexes displayed also a strong cytotoxic activity against human cell lines: in particular, the copper complexes were more cytotoxic than the zinc complexes.

Interestingly, different human cells showed different sensitivities against the complexes. The cytotoxicity of the compounds could depend on their ability to cross the phospholipid bilayer. The most of TSCs are molecules with a polar head, the thiosemicarbazide part, and an aromatic hydrophobic part. The metal coordination allows the ligand to hide the thiosemicarbazone polar part around the metal and the metal complex thus exposes the hydrophobic moiety to the solvent endowing it the features necessary to cross the cell membrane (Pelosi *et al*., 2010).

We do not yet know the mechanism involved in cellular uptake. Our molecules have molecular weight ranging from 150.0 g/mol to 1000.0 g/mol: therefore, the diffusion could be the main mechanism involved in cellular uptake. In addition, we can assume that cells utilize membrane transporters to facilitate the entry or export of molecules that are insufficiently permeable. The expression of these transporters may depend on cell type and consequently cellular sensitivity could depend on these mechanisms of active transport.

We did not exclude that the complex formation is a strategy by which a charged ion and a polar ligand molecule form a structure that exposes the hydrophobic part to the exterior and allows the two to enter the cell. This could explain the reason why complexes result to be more active than the parent ligands. Once inside, the metal ion and the thiosemicarbazone could act separately, the first altering the metal homeostasis within the cell and the other by interacting with enzymes or interfering with cellular pathways (Pelosi

et al., 2010). Indeed, several studies reported that TSCs could affect different cellular targets.

Alkaline Comet Assay was performed in order to identify the genotoxic load of molecules that showed any toxic activity. In general, our data indicate that both ligands and metal complexes could induce DNA damage at subtoxic concentration.

After the toxicological studies, the most promising compounds were F62 and F66, a cinnamaldehyde and an anthraquinone derivative, respectively.

All the results were registered in a database correlating chemical structures and biological/toxicological activities. Overall, we designed and synthesized a panel of 180 thiosemicarbazones: 76 ligands, 75 complexes and 29 starting materials. Among the ligands, we tested 5 semicarbazones and 71 thiosemicarbazones. The 75 metal complexes were synthesized using copper and zinc as main metal ions. The other complexes were obtained after complexation with nickel, manganese, iron and magnesium. The starting materials include 9 aldehydes, 6 ketones and 7 raw chemical materials.

The database reports the chemical and physical features including:

- Structure: chemical formula and molecular weight;
- Type: parent or derivative or raw material; ligand or metal complexes;
- Group: natural starting aldehyde;
- Chemical properties: LogP, H-bond acceptor and H-bond donator.

We also reported the ability to inhibit *A. flavus* growth and mycotoxin production and data related to cytotoxicity, genotoxicity and mutagenicity of the new molecules.

The preliminary analysis on the structure activity correlation did not identify single structural motifs responsible for the toxic activities of the compounds. Further analyses will be necessary to better understand these relationships.

5.2 Thiosemicarbazones as anticancer agents

In 1956, Brockman and co-workers reported the first study of the anticancer properties of thiosemicarbazones derived from 2-formylpyridine (Brockman *et al*., 1956). Since then, many researches were carried out to identify the regions of thiosemicarbazone molecules responsible for their biological activity. The anticancer effects of TSCs were closely related to the parent aldehyde or ketone group, the metal chelation ability and the terminal amino substitution. The parent aldehyde or ketone group is crucial for the anticancer activity of thiosemicarbazones: heterocyclic TSCs showed higher activity compared with aromatic compounds. The chemotherapeutic activity of nitro heterocycles is related to the nitro group attached to C-5 of the five membered heterocycles, containing appropriate substituents at C-2 (Arora *et al*., 2014). Furthermore, particular attention must be paid to metal thiosemicarbazone complexes, a class of experimental anticancer agents which shows inhibitory activities against cancer cells.

In this work, we focused on the mechanism of action of different metal complexes, derived from citronellal thiosemicarbazone, that showed antiproliferative activity on cancer cells: $[Ni(tcitr)_2]$, $[Pt(tcitr)_2]$ and $[Cu(tcitr)_2]$. All compounds were screened for antitumour effects using a selection of cell lines from the National Cancer Institute "60 Human Tumor Cell Line Anticancer Drug Screen". Cell lines showed different sensitivity to the compounds. In particular, the nickel complex showed an important antiproliferative effect toward leukemia and central nervous system cancer cell lines, while the platinum complex was able to inhibit mainly the proliferation of solid cancer cells, such as colon and lung adenocarcinoma. The copper complex displayed a peculiar anticancer activity in the micromolar range, against human primary tumour samples deriving from head and neck cancer.

In previous researches, $[Ni(tcitr)_2]$ showed interesting antiproliferative characteristics towards histiocytic lymphoma cell line U937. It induced G2/M cell cycle arrest and apoptosis by down-regulation of Bcl-2, mitochondrial membrane potential loss and caspase activation. $[Ni(tcitr)_2]$ displayed DNA damaging action but it was not due to DNA oxidation (Buschini *et al*., 2009). $[Ni(tcitr)_2]$ did not induce gene mutation or chromosomal damage,

but altered DNA conformation creating knot-like structures and hairpins (Buschini *et al*., 2014).

We have hypothesized previously that the DNA damage induced by the nickel complex could be due to a direct interaction between the complex and the DNA backbone and/or histones, giving rise to structural alterations of chromatin, such as heterochromatinization, that could interfere with a correct mitosis processes inducing apoptosis. To understand if the results obtained from the Alkaline Comet Assay, showing an important DNA migration starting from 1h treatment, could be related to a real DNA damage or to an altered DNA conformation that could produce alkali labile sites, we analysed the transcription profile of genes involved in DDR (such as ATM, ATR, Chk1, Chk2, Cyclin A1 and B). Identifying molecular pathways targeted by a compound is of paramount importance for the development of new drugs and the prediction of its mechanism of action has been attempted by using transcriptional expression profiles following drug treatment (Iorio *et al*., 2010).

Under genotoxic stress, the activation of ATM and/or ATR, DNA sensors for the initial response to single and double stranded DNA breaks, is a result of the formation their monomers or the induction of their transcription. After the treatment with the nickel complex, we did not observe an activation of the transcription of ATM and ATR. These results corroborate our hypothesis that $[Ni(tcitr)_2]$ did not induce SSB and/or DSB breaks, directly or indirectly. This data is in agreement with the lack of *in vitro* clastogen activity of $[Ni(tcitr)_2]$ on supercoiled DNA plasmid pBR322, previously reported (Buschini *et al*., 2014). We did not observe alterations in the mRNA levels of ATM and ATR, but in contrast we found a strong up-regulation of the DNA damage sensors, Chk1 and Chk2. Probably, the metal complex could activate alternative pathways that trigger the transcription of Chk1 and Chk2.

$[Ni(tcitr)_2]$ caused also an important up-regulation of Cyclin B, that together with Cdk1, is involved in the cell cycle progression. In stress condition, Cyclin B could interact with APC (anaphase promoting complex), which plays a central role in regulating mitosis and the G1 phase of the cell cycle. Furthermore, APC induces the degradation of cyclin B and inhibits cell cycle progression. This up-regulation could lead to the cell cycle block and could interfere with the normal transition from G2 phase to M phase, as reported for $[Ni(tcitr)_2]$.

These results could support a strong interference of [Ni(tcitr)$_2$] with the correct folding of chromosome during mitosis leading to apoptosis. Further analysis on proteins involved in the mitotic checkpoint could be important to better understand the relationship between DNA- [Ni(tcitr)$_2$] interactions and cellular toxicity.

Several thiosemicarbazones inhibit the small subunit of the ribonucleotide reductase, that represents probably the best described target of thiosemicarbazones. This metalloenzyme is crucial for DNA synthesis as well as DNA damage repair and is frequently overexpressed in cancer cells making it an attractive target for the treatment. Inhibition of the tyrosyl radical in the active center of the RRM2/p53R2 subunit was demonstrated for several thiosemicarbazones (including Triapine and Dp44mT). Furthermore, previous studies in *Saccharomyces cerevisiae* to clarify the action mechanism of [Ni(tcitr)$_2$] have shown, after analysis of collection of deletants, an enrichment in the classes of genes coding for components involved in nucleic acids metabolism such as ribonucleotide reductase (RR). To identify another possible target of the metal complex, U937 cells were treated with a toxic concentration and a subtoxic one of each compound. The nickel complex induced a very important modulation of the different subunits of RR. Probably, the strong RRM2 up-regulation could indicate that the compound could act targeting specifically this subunit of the enzyme. We analysed also the expression of p53R2 in order to determine if the cellular response induced by the metal complex could involve p53. We did not observe alteration in the transcription level of the p53R2 subunit: this result highlighted that the [Ni(tcitr)$_2$] could act with a p53-independent mechanism, as hypothesized before (Buschini *et al*., 2009).

We used the same approach to identify the molecular action mechanisms of the copper and the platinum complexes. Both induced a significant DNA damage highlighted through the Alkaline Comet Assay. DNA migration induced after 1h by [Cu(tcitr)$_2$] or [Pt(tcitr)$_2$] was less than the one induced by [Ni(tcitr)$_2$]. We presume that the DNA damage observed after the treatment with [Cu(tcitr)$_2$] could be due to an excessive production of ROS species, due to the fact that Cu could present different oxidation states in the cell. Oxidative stress due to ROS is known to cause DNA lesions of both SSB and DSB nature through the direct interaction of ROS with DNA (Rahal *et al*., 2016). We did not observe an activation of the

transcriptional profile of ATM and ATR but we showed an up-regulation of Chk1. Furthermore, [Cu(tcitr)$_2$] was not able to induce a cell cycle arrest (Bisceglie *et al*., 2012).

In HNC cells, the anticancer activity of [Cu(tcitr)$_2$] would not seem to be related to p53 mutational status (wt or mutant). Also in other studies regarding DpT analogs, p53 status did not affect the anticancer effect, indicating a p53-independent mechanism of antiproliferative activity (Heffeter *et al*., 2018). [Cu(tcitr)$_2$] treatment induced a WT-like expression in the p53 protein that restores p53 status: we hypothesize that this compound could restore the wild-type function of the p53 protein. This mechanism of action was proposed also for other thiosemicarbazones, such as COTI-2 (Heffeter *et al*., 2018).

It could be speculated that the down-regulation of both the ATM-ATR kinases, as we reported, could explain the decrease of p53 protein expression. p53 is regulated through phosphorylation of p53 protein at serine 15, mediated by ATM or ATR, to enhance its transactivating activity. Several studies highlighted that the down-regulation of ATM and ATR induced the degradation of p53 by MDM2 (Yang *et al*., 2004).

The platinum complex induced a strong DNA damage and acts as a promutagen agent. Most of the platinum anticancer agents target DNA. The connections between cell cycle and cell death were studied: we investigated if the treatment with the metal complexes could involve an alteration in the progression of cell cycle. Differently from [Ni(tcitr)$_2$], [Pt(tcitr)$_2$] induced a block in S phase as for cisplatin in several cancer cell lines (Mueller *et al*., 2006). Also for this molecule, no transcription of ATM and ATR was detected, while Chk2 was upregulated after 24h treatment. Chk2 is directly involved in G1-S cell cycle arrest. Cisplatin usually activates DDR through ATM involvement. It will be interesting to understand how [Pt(tcitr)$_2$] is able to modulate the cell cycle progression without modulating ATM transcription. It will be necessary to study the phosphorylation state of ATM protein after [Pt(tcitr)$_2$] treatment.

Methylation strategy plays an important role in drug design: a lot of studies highlighted the importance of methyl groups in modulating biological activity, selectivity, solubility, metabolism and pharmacokinetic/pharmacodynamic properties of biologically active molecules. The significant improvements in activity are usually the result of the methyl group's capacity to fill a hydrophobic pocket of the protein and/or to induce a conformational change of the molecule. Furthermore, addition of a methyl group to a specific molecule usually leads to an increase in lipophilicity and therefore a decrease in

water solubility (Sun *et al*., 2018). Starting from platinum, copper and nickel complexes, we measured the antiproliferative activity of dimethylated molecules against U937 cells. These dimethylated complexes displayed a mild anticancer effect compared to the parental compounds. The introduction of a methyl group in the skeleton of the starting molecules seems to be related to a decrease in their antitumor effects.

As for the parent molecules, the dimethylated complexes interacted with DNA and caused a DNA damage. The results indicate that the dimethylate compounds are less genotoxic than the starting molecules.

This study highlighted that the biological activity of our compounds depends on the metal ion used in the coordination process. Metals play a key role in the anticancer activity of thiosemicarbazones and the corresponding metal complexes represent an emerging class of experimental anticancer chemotherapeutic agents which shows *in vitro* antiproliferative activities.

The metal complexes could act as multitarget agents. The first target could be the DNA molecule and the second one could be the ribonucleotide reductase enzyme. Finally, the metal complexes are able to trigger several cellular pathways involved in DNA damage response and cell cycle progression.

In conclusion, these experimental data confirm that thiosemicarbazone scaffold represents a good starting point for the development of new anticancer agents.

6. References

Adsule S, Barve V, Chen D, Ahmed F, Dou QP, Padhye S, Sarkar FH. Novel Schiff base copper complexes of quinoline-2 carboxaldehyde as proteasome inhibitors in human prostate cancer cells. J Med Chem. 2006;49(24):7242-6.

Akladios FN, Andrew SD, Parkinson CJ. Selective induction of oxidative stress in cancer cells via synergistic combinations of agents targeting redox homeostasis. Bioorg Med Chem. 2015;23(13):3097-104.

Alshannaq A, Yu JH. Occurrence, Toxicity, and Analysis of Major Mycotoxins in Food. Int J Environ Res Public Health. 2017;14(6).

Arnott JA, Kumar R, Lobo Planey S. Lipophilicity Indices for Drug Development. Journal of Applied Biopharmaceutics and Pharmacokinetics, 2013, 1, 31-36.

Arora S, Agarwal S, Singhal S. Anticancer activities of thiosemicarbazides/ thiosemicarbazones: a review. Int J Pharm Pharm Sci, 2014. 6(9):34-41.

Aye Y, Long MJ, Stubbe J. Mechanistic studies of semicarbazone triapine targeting human ribonucleotide reductase in vitro and in mammalian cells: tyrosyl radical quenching not involving reactive oxygen species. J Biol Chem. 2012 Oct 12;287(42):35768-78.

Aye Y, Li M, Long MJ, Weiss RS. Ribonucleotide reductase and cancer: biological mechanisms and targeted therapies. Oncogene. 2015;34(16):2011-21.

Ayton S, Lei P, Bush AI. Metallostasis in Alzheimer's disease. Free Radic Biol Med. 2013;62:76-89.

Bae DH, Jansson PJ, Huang ML, Kovacevic Z, Kalinowski D, Lee CS, Sahni S, Richardson DR. The role of NDRG1 in the pathology and potential treatment of human cancers. J Clin Pathol. 2013;66(11):911-7.

Bai L, Gao C, Liu Q, Yu C, Zhang Z, Cai L, Yang B, Qian Y, Yang J, Liao X. Research progress in modern structure of platinum complexes. Eur J Med Chem. 2017;140:349-382.

Balachandran C, Haribabu J, Jeyalakshmi K, Bhuvanesh NSP, Karvembu R, Emi N, Awale S. Nickel(II) bis(isatin thiosemicarbazone) complexes induced apoptosis through

mitochondrial signaling pathway and G0/G1 cell cycle arrest in IM-9 cells. J Inorg Biochem. 2018;182:208-221.

Banerjee T, Dubey P, Mukhopadhyay R. Compacting effect of BBR3464, a new-generation trisplatinum anticancer agent, on DNA. Biochimie. 2010;92(7):846-51.

Bisceglie F, Tavone M, Mussi F, Azzoni S, Montalbano S, Franzoni S, Tarasconi P, Buschini A, Pelosi G. Effects of polar substituents on the biological activity of thiosemicarbazone metal complexes. J Inorg Biochem. 2018;179:60-70.

Bisceglie F, Musiari A, Pinelli S, Alinovi R, Menozzi I, Polverini E, Tarasconi P, Tavone M, Pelosi G. Quinoline-2-carboxaldehyde thiosemicarbazones and their Cu(II) and Ni(II) complexes as topoisomerase IIa inhibitors. J Inorg Biochem. 2015;152:10-9.

Bisceglie F, Pinelli S, Alinovi R, Goldoni M, Mutti A, Camerini A, Piola L, Tarasconi P, Pelosi G. Cinnamaldehyde and cuminaldehyde thiosemicarbazones and their copper(II) and nickel(II) complexes: a study to understand their biological activity. J Inorg Biochem. 2014;140:111-25.

Bisceglie F, Pinelli S, Alinovi R, Tarasconi P, Buschini A, Mussi F, Mutti A, Pelosi G. Copper(II) thiosemicarbazonate molecular modifications modulate apoptotic and oxidative effects on U937 cell line. J Inorg Biochem. 2012;116:195-203.

Blair BG, Larson CA, Adams PL, Abada PB, Safaei R, Howell SB. Regulation of copper transporter 2 expression by copper and cisplatin in human ovarian carcinoma cells. Mol Pharmacol. 2010;77(6):912-21.

Brabec V, Kaspárková J, Vrána O, Nováková O, Cox JW, Qu Y, Farrell N. DNA modifications by a novel bifunctional trinuclear platinum phase I anticancer agent. Biochemistry. 1999;38(21):6781-90.

Brockman RW, Thomson JR, Skipper HE. Observations on the antileukemic activity of pyridine-2-carboxaldehyde thiosemicarbazone and thiocarbohydrazone. Cancer Res. 1956;16(2):167-70.

Brown DR. Copper and prion diseases. Biochem Soc Trans. 2002;30(4):742-5.

Buschini A, Pinelli S, Alinovi R, Mussi F, Bisceglie F, Rivetti C, Doniselli N, Pelosi G. Unravelling mechanisms behind the biological activity of bis(S-citronellalthiosemicarbazonato)nickel(II). Metallomics. 2014;6(4):783-92.

Buschini A, Pinelli S, Pellacani C, Giordani F, Ferrari MB, Bisceglie F, Giannetto M, Pelosi G, Tarasconi P. Synthesis, characterization and deepening in the comprehension of the biological action mechanisms of a new nickel complex with antiproliferative activity. J Inorg Biochem. 2009;103(5):666-77.

Can M, Armstrong FA, Ragsdale SW. Structure, function, and mechanism of the nickel metalloenzymes, CO dehydrogenase, and acetyl-CoA synthase. Chem Rev. 2014;114(8):4149-74.

Chaston TB, Lovejoy DB, Watts RN, Richardson DR. Examination of the antiproliferative activity of iron chelators: multiple cellular targets and the different mechanism of action of triapine compared with desferrioxamine and the potent pyridoxal isonicotinoyl hydrazone analogue 311. Clin Cancer Res. 2003;9(1):402-14.

Chen D, Dou QP. New uses for old copper-binding drugs: converting the pro-angiogenic copper to a specific cancer cell death inducer. Expert Opin Ther Targets. 2008;12(6):739-48.

Chen R, Liu CS, Zhang H, Guo Y, Bu XH, Yang M. Three new Cu(II) and Cd(II) complexes with 3-(2-pyridyl)pyrazole-based ligand: syntheses, crystal structures, and evaluations for bioactivities. J Inorg Biochem. 2007;101(3):412-21.

Chandra S, Vandana. Synthesis, spectroscopic, anticancer and antibacterial studies of Ni(II) and Cu(II) complexes with 2-carboxybenzaldehyde thiosemicarbazone. Spectrochim Acta A Mol Biomol Spectrosc. 2014;129:333-8.

Choi BS, Alberti DB, Schelman WR, Kolesar JM, Thomas JP, Marnocha R, Eickhoff JC, Ivy SP, Wilding G, Holen KD. The maximum tolerated dose and biologic effects of 3-aminopyridine-2-carboxaldehyde thiosemicarbazone (3-AP) in combination with irinotecan for patients with refractory solid tumors. Cancer Chemother Pharmacol. 2010;66(5):973-80.

Cleare MJ, Hoeschele JD. Studies on the antitumor activity of group VIII transition metal complexes. Part I. Platinum(II) complexes. Bioinorg. Chem. 1973;2, 187–210.

(doi:10.1016/S0006-3061(00)80249-5).

Cragg GM, Newman DJ. Natural products: a continuing source of novel drug leads. Biochim Biophys Acta. 2013;1830(6):3670-95.

Dallavalle F, Gaccioli F, Franchi-Gazzola R, Lanfranchi M, Marchiò L, Pellinghelli MA, Tegoni M. Synthesis, molecular structure, solution equilibrium, and antiproliferative activity of thioxotriazoline and thioxotriazole complexes of copper II and palladium II. J Inorg Biochem. 2002;92(2):95-104.

Daniel KG, Gupta P, Harbach RH, Guida WC, Dou QP. Organic copper complexes as a new class of proteasome inhibitors and apoptosis inducers in human cancer cells. Biochem Pharmacol. 2004 Mar;67(6):1139-51.

Daniel KG, Chen D, Orlu S, Cui QC, Miller FR, Dou QP. Clioquinol and pyrrolidine dithiocarbamate complex with copper to form proteasome inhibitors and apoptosis inducers in human breast cancer cells. Breast Cancer Res. 2005;7(6):R897-908.

Dasari S, Tchounwou PB. Cisplatin in cancer therapy: molecular mechanisms of action. Eur J Pharmacol. 2014;740:364-78.

Davies KM, Mercer JF, Chen N, Double KL. Copper dyshomoeostasis in Parkinson's disease: implications for pathogenesis and indications for novel therapeutics. Clin Sci (Lond). 2016;130(8):565-74.

DeConti RC, Toftness BR, Lange RC, Creasey WA. Clinical and pharmacological studies with cis-diamminedichloroplatinum (II). Cancer Res. 1973;33(6):1310-5.

Degola F, Bisceglie F, Pioli M, Palmano S, Elviri L, Pelosi G, Lodi T, Restivo FM. Structural modification of cuminaldehyde thiosemicarbazone increases inhibition specificity toward aflatoxin biosynthesis and sclerotia development in Aspergillus flavus. Appl Microbiol Biotechnol. 2017;101(17):6683-6696.

Degola F, Morcia C, Bisceglie F, Mussi F, Tumino G, Ghizzoni R, Pelosi G, Terzi V, Buschini A, Restivo FM, Lodi T. *In vitro* evaluation of the activity of thiosemicarbazone derivatives against mycotoxigenic fungi affecting cereals. Int J Food Microbiol. 2015;200:104-11.

Demarque DP, Silva RMP, Santos LF, Leopoldino AM, Espreafico EM, Lopes NP. Cytotoxicity of Structurally Diverse Anthranoids and Correlation with Mechanism of Action and Side Effects. J Pharm Pharm Sci. 2018;21(1):347-353.

Denkhaus E, Salnikow K. Nickel essentiality, toxicity, and carcinogenicity. Crit Rev Oncol Hematol. 2002;42(1):35-56.

Denoyer D, Masaldan S, La Fontaine S, Cater MA. Targeting copper in cancer therapy: 'Copper That Cancer'. Metallomics. 2015;7(11):1459-76.

de Oliveira JF, Lima TS, Vendramini-Costa DB, de Lacerda Pedrosa SCB, Lafayette EA, da Silva RMF, de Almeida SMV, de Moura RO, Ruiz ALTG, de Carvalho JE, de Lima MDCA. Thiosemicarbazones and 4-thiazolidinones indole-based derivatives: Synthesis, evaluation of antiproliferative activity, cell death mechanisms and topoisomerase inhibition assay. Eur J Med Chem. 2017;136:305-314.

Dilruba S, Kalayda GV. Platinum-based drugs: past, present and future. Cancer Chemother Pharmacol. 2016;77(6):1103-24.

Duffy MJ, Synnott NC, Crown J. Mutant p53 as a target for cancer treatment. Eur J Cancer. 2017;83:258-265.

Duncan C, White AR. Copper complexes as therapeutic agents. Metallomics. 2012;4(2):127-38.

Ertl P, Rohde B, Selzer P. Fast calculation of molecular polar surface area as a sum of fragment-based contributions and its application to the prediction of drug transport properties. J Med Chem. 2000;43(20):3714-7.

Frezza M, Hindo S, Chen D, et al. Novel metals and metal complexes as platforms for cancer therapy. Curr Pharm Des. 2010;16(16):1813–1825.

Galanski M, Jakupec MA, Keppler BK. Update of the preclinical situation of anticancer platinum complexes: novel design strategies and innovative analytical approaches. Curr Med Chem. 2005;12(18):2075-94.

Galanski M. Recent developments in the field of anticancer platinum complexes. Recent Pat Anticancer Drug Discov. 2006;1(2):285-95.

Galluzzi L, Senovilla L, Vitale I, Michels J, Martins I, Kepp O, Castedo M, Kroemer G. Molecular mechanisms of cisplatin resistance. Oncogene. 2012;31(15):1869-83.

Galluzzi L, Vitale I, Michels J, Brenner C, Szabadkai G, Harel-Bellan A, Castedo M, Kroemer G. Systems biology of cisplatin resistance: past, present and future. Cell Death Dis. 2014;5:e1257.

Gojo I, Tidwell ML, Greer J, Takebe N, Seiter K, Pochron MF, Johnson B, Sznol M, Karp JE. Phase I and pharmacokinetic study of Triapine, a potent ribonucleotide reductase inhibitor, in adults with advanced hematologic malignancies. Leuk Res. 2007;31(9):1165-73.

Graf N, Lippard SJ. Redox activation of metal-based prodrugs as a strategy for drug delivery. Adv Drug Deliv Rev. 2012; 64(11): 993–1004.

Graser-Loescher G, Schoenhuber A, Ciglenec C, Eberl S, Krupitza G, Mader RM, Jadav SS, Jayaprakash V, Fritzer-Szekeres M, Szekeres T, Saiko P. Thiosemicarbazone derivatives, thiazolyl hydrazones, effectively inhibit leukemic tumor cell growth: Down-regulation of ribonucleotide reductase activity and synergism with arabinofuranosylcytosine. Food Chem Toxicol. 2017;108(Pt A):53-62.

Grubman A, White AR. Copper as a key regulator of cell signalling pathways. Expert Rev Mol Med. 2014 May;16:e11.

Guarino E, Salguero I2, Kearsey SE. Cellular regulation of ribonucleotide reductase in eukaryotes. Semin Cell Dev Biol. 2014;30:97-103.

Gupta VK, Karimi-Maleh H, Agarwal S, Karimi F, Bijad M, Farsi M, Shahidi SA. Fabrication of a Food Nano-Platform Sensor for Determination of Vanillin in Food Samples. Sensors (Basel). 2018 ;18(9).

Gwaram NS, Hassandarvish P. Synthesis, characterization and anticancer studies of some morpholine derived Schiff bases and their metal complexes. J App Pharm Sci. 2014; 4(10): 075-080.

Haas KL, Franz KJ. Application of Metal Coordination Chemistry to Explore and Manipulate Cell Biology. Chem Rev. 2009; 109(10): 4921–4960.

Hambley TW. Chemistry. Metal-based therapeutics. Science. 2007;318(5855):1392-3.

Harris TV, Szilagyi RK, McFarlane Holman KL. Electronic structural investigations of ruthenium compounds and anticancer prodrugs. J Biol Inorg Chem. 2009;14(6):891-8.

Hasinoff BB, Yadav AA, Patel D, Wu X. The cytotoxicity of the anticancer drug elesclomol is due to oxidative stress indirectly mediated through its complex with Cu(II). J Inorg Biochem. 2014 Aug;137:22-30.

Hasinoff BB, Wu X, Yadav AA, Patel D, Zhang H, Wang DS, Chen ZS, Yalowich JC. Cellular mechanisms of the cytotoxicity of the anticancer drug elesclomol and its complex with Cu(II). Biochem Pharmacol. 2015 Feb;93(3):266-76.

Heffeter P, Pape VFS, Enyedy ÉA, Keppler BK, Szakacs G, Kowol CR. Anticancer Thiosemicarbazones: Chemical Properties, Interaction with Iron Metabolism, and Resistance Development. Antioxid Redox Signal. 2018 Feb 26.

Hensing TA, Hanna NH, Gillenwater HH, Gabriella Camboni M, Allievi C, Socinski MA. Phase II study of BBR 3464 as treatment in patients with sensitive or refractory small cell lung cancer. Anticancer Drugs. 2006;17(6):697-704.

Hirakawa H, Kiba T, Saito Y, Watanabe Y, Suzuki T, Ota N. Nedaplatin as a Single-Agent Chemotherapy May Support Palliative Therapy for Patients with Adenoid Cystic Carcinoma: A Case Report. Case Rep Oncol. 2017;10(2):783-789.

Hordyjewska A, Popiołek Ł, Kocot J. The many "faces" of copper in medicine and treatment. Biometals. 2014;27(4):611-21.

Horváth V, Soucek K, Svihálková-Sindlerová L, Vondrácek J, Blanárová O, Hofmanová J, Sova P, Kozubík A. Different cell cycle modulation following treatment of human ovarian

carcinoma cells with a new platinum(IV) complex vs cisplatin. Invest New Drugs. 2007;25(5):435-43.

Hrstka R, Powell DJ, Kvardova V, Roubalova E, Bourougaa K, Candeias MM, Sova P, Zak F, Fåhraeus R, Vojtěsek B. The novel platinum(IV) complex LA-12 induces p53 and p53/47 responses that differ from the related drug, cisplatin. Anticancer Drugs. 2008;19(4):369-79.

IARC. International Agency for Research on Cancer (WHO); Lyon, France: 2015. Mycotoxin control in low- and middle income countries; pp. 31–42. Report No. 9.

IARC. International Agency for Research on Cancer (WHO); Lyon, France: 1973. Some inorganic and organometallic compounds. IARC Monogr Eval Carcinog Risk Chem Man. 1973; 2: 1–181.

Inci D, Aydın R, Vatan Ö, Zorlu Y, Çinkılıç N. New binary copper(II) complexes containing intercalating ligands: DNA interactions, an unusual static quenching mechanism of BSA and cytotoxic activities. J Biomol Struct Dyn. 2017:1-24.

Iorio F, Bosotti R, Scacheri E, Belcastro V, Mithbaokar P, Ferriero R, Murino L, Tagliaferri R, Brunetti-Pierri N, Isacchi A, di Bernardo D. Discovery of drug mode of action and drug repositioning from transcriptional responses. Proc Natl Acad Sci USA. 2010;107(33):14621-6.

Ishiguro K, Lin ZP, Penketh PG, Shyam K, Zhu R, Baumann RP, Zhu YL, Sartorelli AC, Rutherford TJ, Ratner ES. Distinct mechanisms of cell-kill by triapine and its terminally dimethylated derivative Dp44mT due to a loss or gain of activity of their copper(II) complexes. Biochem Pharmacol. 2014;91(3):312-22.

Ismail A, Gonçalves BL, de Neeff DV, Ponzilacqua B, Coppa CFSC, Hintzsche H, Sajid M, Cruz AG, Corassin CH, Oliveira CAF. Aflatoxin in foodstuffs: Occurrence and recent advances in decontamination. Food Res Int. 2018;113:74-85.

Jabłońska-Trypuć A, Świderski G, Krętowski R, Lewandowski W. Newly Synthesized Doxorubicin Complexes with Selected Metals-Synthesis, Structure and Anti-Breast Cancer Activity. Molecules. 2017;22(7).

Johnson DE. The ubiquitin-proteasome system: opportunities for therapeutic intervention in solid tumors. Endocr Relat Cancer. 2015 Feb;22(1):T1-17.

Johnstone TC, Suntharalingam K, Lippard SJ. Third row transition metals for the treatment of cancer. Philos Trans A Math Phys Eng Sci. 2015; 373(2037): 20140185.

Karasawa T, Steyger PS. An integrated view of cisplatin-induced nephrotoxicity and ototoxicity. Toxicol Lett. 2015;237(3):219-27.

Kasparkova J, Zehnulova J, Farrell N, Brabec V. DNA interstrand cross-links of the novel antitumor trinuclear platinum complex BBR3464. Conformation, recognition by high mobility group domain proteins, and nucleotide excision repair. J Biol Chem. 2002;277(50):48076-86.

Kalaivani P, Saranya S, Poornima P, Prabhakaran R, Dallemer F, Vijaya Padma V, Natarajan K. Biological evaluation of new nickel(II) metallates: Synthesis, DNA/protein binding and mitochondrial mediated apoptosis in human lung cancer cells (A549) via ROS hypergeneration and depletion of cellular antioxidant pool. Eur J Med Chem. 2014;82:584-99.

Kelland L. The resurgence of platinum-based cancer chemotherapy. Nat Rev Cancer. 2007;7(8):573-84.

Khan T, Ahmad R, Joshi S, Khan AR. Anticancer potential of metal thiosemicarbazone complexes: A review. Der Chemica Sinica, 2015, 6(12):1-11.

Kheradmand Z, Yarali B, Zare A, Pourpak Z, Shams S, Ashrafi MR. Comparison of Serum Zinc and Copper levels in Children and adolescents with Intractable and Controlled Epilepsy. Iran J Child Neurol. 2014;8(3):49-54.

Knox JJ, Hotte SJ, Kollmannsberger C, Winquist E, Fisher B, Eisenhauer EA. Phase II study of Triapine in patients with metastatic renal cell carcinoma: a trial of the National Cancer Institute of Canada Clinical Trials Group (NCIC IND.161). Invest New Drugs. 2007;25(5):471-7.

Kosiha A, Parthiban C, Elango KP. Synthesis, characterization and DNA binding/cleavage, protein binding and cytotoxicity studies of Co(II), Ni(II), Cu(II) and Zn(II) complexes of aminonaphthoquinone. J Photochem Photobiol B. 2017;168:165-174.

Kovacevic Z, Richardson DR. The metastasis suppressor, Ndrg-1: a new ally in the fight against cancer. Carcinogenesis. 2006;27(12):2355-66.

Kozubík A, Horváth V, Svihálková-Sindlerová L, Soucek K, Hofmanová J, Sova P, Kroutil A, Zák F, Mistr A, Turánek J. High effectiveness of platinum(IV) complex with adamantylamine in overcoming resistance to cisplatin and suppressing proliferation of ovarian cancer cells in vitro. Biochem Pharmacol. 2005;69(3):373-83.

Kumar P, Mahato DK, Kamle M, Mohanta TK, Kang SG. Aflatoxins: A Global Concern for Food Safety, Human Health and Their Management. Front Microbiol. 2017;7:2170.

Kumar S, Trivedi AV. A Review on Role of Nickel in the Biological System. Int J Curr Microbiol App Sci (2016) 5(3): 719-727.

Kunos CA, Ivy SP. Triapine Radiochemotherapy in Advanced Stage Cervical Cancer. Front Oncol. 2018;8:149.

Kunos CA, Chu E, Makower D, Kaubisch A, Sznol M, Ivy SP1. Phase I Trial of Triapine-Cisplatin-Paclitaxel Chemotherapy for Advanced Stage or Metastatic Solid Tumor Cancers. Front Oncol. 2017;7:62.

Kunos CA, Chu E, Beumer JH, Sznol M, Ivy SP. Phase I trial of daily triapine in combination with cisplatin chemotherapy for advanced-stage malignancies. Cancer Chemother Pharmacol. 2017;79(1):201-207.

Kunos CA, Sherertz TM. Long-Term Disease Control with Triapine-Based Radiochemotherapy for Patients with Stage IB2-IIIB Cervical Cancer. Front Oncol. 2014;4:184.

Kunos CA, Radivoyevitch T, Waggoner S, Debernardo R, Zanotti K, Resnick K, Fusco N, Adams R, Redline R, Faulhaber P, Dowlati A. Radiochemotherapy plus 3-aminopyridine-2-carboxaldehyde thiosemicarbazone (3-AP, NSC #663249) in advanced-stage cervical and vaginal cancers. Gynecol Oncol. 2013;130(1):75-80.

Kuo MT, Fu S, Savaraj N, Chen HH. Role of the human high-affinity copper transporter in copper homeostasis regulation and cisplatin sensitivity in cancer chemotherapy. Cancer Res. 2012;72(18):4616-21.

Lambert IH, Sørensen BH. Facilitating the Cellular Accumulation of Pt-Based Chemotherapeutic Drugs. Int J Mol Sci. 2018;19(8). pii: E2249.

Lane DJ, Mills TM, Shafie NH, Merlot AM, Saleh Moussa R, Kalinowski DS, Kovacevic Z, Richardson DR. Expanding horizons in iron chelation and the treatment of cancer: role of iron in the regulation of ER stress and the epithelial-mesenchymal transition. Biochim Biophys Acta. 2014;1845(2):166-81.

Lane D, Levine A. p53 Research: the past thirty years and the next thirty years. Cold Spring Harb Perspect Biol. 2010;2(12):a000893.

Lazarević T, Rilak A, Bugarčić ŽD. Platinum, palladium, gold and ruthenium complexes as anticancer agents: Current clinical uses, cytotoxicity studies and future perspectives. Eur J Med Chem. 2017;142:8-31.

Li L, Guo W, Wu K, Zhao Y, Luo Q, Zhang Q, Liu J, Xiong S, Wang F. Identification of binding sites of cisplatin to human copper chaperone protein Cox17 by high-resolution FT-ICR-MS. Rapid Commun Mass Spectrom. 2016;30 Suppl 1:168-72.

Li Y, Liu B, Yang F, Yu Y, Zeng A, Ye T, Yin W, Xie Y, Fu Z, Zhao C. Lobaplatin induces BGC-823 human gastric carcinoma cell apoptosis via ROS- mitochondrial apoptotic pathway and impairs cell migration and invasion. Biomed Pharmacother. 2016;83:1239-1246.

Lin LC, Chen CF, Ho CT, Liu JJ, Liu TZ, Chern CL. γ-Glutamylcysteine synthetase (γ-GCS) as a target for overcoming chemo- and radio-resistance of human hepatocellular carcinoma cells. Life Sci. 2018;198:25-31.

Lin CY, Power PP. Complexes of Ni(i): a "rare" oxidation state of growing importance. Chem Soc Rev. 2017;46(17):5347-5399.

Linder MC, Hazegh-Azam M. Copper biochemistry and molecular biology. Am J Clin Nutr. 1996 May;63(5):797S-811S.

Lipinski CA, Lombardo F, Dominy BW, Feeney PJ. Experimental and computational approaches to estimate solubility and permeability in drug discovery and development settings. Adv Drug Deliv Rev. 2001;46(1-3):3-26.

Lipinski CA. Lead- and drug-like compounds: the rule-of-five revolution. Drug Discov Today Technol. 2004;1(4):337-41.

Linder MC. Ceruloplasmin and other copper binding components of blood plasma and their functions: an update. Metallomics. 2016 Sep;8(9):887-905.

Mabkhot YN, Alatibi F, El-Sayed NN, Al-Showiman S, Kheder NA, Wadood A, Rauf A, Bawazeer S, Hadda TB. Antimicrobial Activity of Some Novel Armed Thiophene Derivatives and Petra/Osiris/Molinspiration (POM) Analyses. Molecules. 2016 Feb;21(2).

Malarz K, Mrozek-Wilczkiewicz A, Serda M, Rejmund M, Polanski J, Musiol R. The role of oxidative stress in activity of anticancer thiosemicarbazones. Oncotarget. 2018;9(25):17689-17710.

Malik EM, Müller CE. Anthraquinones As Pharmacological Tools and Drugs. Med Res Rev. 2016;36(4):705-48.

Mandic A, Viktorsson K, Strandberg L, Heiden T, Hansson J, Linder S, Shoshan MC. Calpain-mediated Bid cleavage and calpain-independent Bak modulation: two separate pathways in cisplatin-induced apoptosis. Mol Cell Biol. 2002;22(9):3003-13.

Mangrum JB, Farrell NP. Excursions in polynuclear platinum DNA binding. Chem Commun (Camb). 2010;46(36):6640-50.

Markowska A, Kasprzak B, Jaszczyńska-Nowinka K, Lubin J, Markowska J. Noble metals in oncology. Contemporary oncology. 2015; 19(4): 271–275.

Marloye M, Berger G, Gelbcke M, Dufrasne F. A survey of the mechanisms of action of anticancer transition metal complexes. Future Medical Chemistry. 2016; 8(18):2263-2286.

Marroquín-Cardona AG, Johnson NM, Phillips TD, Hayes AW. Mycotoxins in a changing global environment--a review. Food Chem Toxicol. 2014;69:220-30.

Maronpot RR, Hobbs CA, Hayashi S. Role of pathology peer review in interpretation of the comet assay. J Toxicol Pathol 2018; 31: 155–161

Montes S, Rivera-Mancia S, Diaz-Ruiz A, Tristan-Lopez L, Rios C. Copper and copper proteins in Parkinson's disease. Oxid Med Cell Longev. 2014;2014:147251.

Mueller S, Schittenhelm M, Honecker F, Malenke E, Lauber K, Wesselborg S, Hartmann JT, Bokemeyer C, Mayer F. Cell-cycle progression and response of germ cell tumors to cisplatin *in vitro*. Int J Oncol. 2006;29(2):471-9.

Muggia FM, Bonetti A, Hoeschele JD, Rozencweig M, Howell SB. Platinum Antitumor Complexes: 50 Years Since Barnett Rosenberg's Discovery. J Clin Oncol. 2015 ;33(35):4219-26.

Munteanu CR, Suntharalingam K. Advances in Cobalt Complexes as Anticancer Agents. Dalton Transactions. 2015,44, 13796-13808.

Nagai M, Vo NH, Shin Ogawa L, Chimmanamada D, Inoue T, Chu J, Beaudette-Zlatanova BC, Lu R, Blackman RK, Barsoum J, Koya K, Wada Y. The oncology drug elesclomol selectively transports copper to the mitochondria to induce oxidative stress in cancer cells. Free Radic Biol Med. 2012 May ;52(10):2142-50.

Naka T, Kaneto H, Katakami N, Matsuoka TA, Harada A, Yamasaki Y, Matsuhisa M, Shimomura I. Association of serum copper levels and glycemic control in patients with type 2 diabetes. Endocr J. 2013;60(3):393-6.

Nakayama K, Kanzaki A, Ogawa K, Miyazaki K, Neamati N, Takebayashi Y. Copper-transporting P-type adenosine triphosphatase (ATP7B) as a cisplatin based chemoresistance marker in ovarian carcinoma: comparative analysis with expression of MDR1, MRP1, MRP2, LRP and BCRP. Int J Cancer. 2002;101(5):488-95.

Naveed R, Hussain I, Tawab A, Tariq M, Rahman M, Hameed S, Mahmood MS, Siddique AB, Iqbal M. Antimicrobial activity of the bioactive components of essential oils from Pakistani spices against *Salmonella* and other multi-drug resistant bacteria. BMC Complement Altern Med. 2013;13:265.

Ndagi U, Mhlongo N, SolimanME. Metal complexes in cancer therapy – an update from drug design perspective. Drug Design, Development and Therapy. 2017:11 599–616.

Neher TM, Rechkunova NI, Lavrik OI, Turchi JJ. Photo-cross-linking of XPC-Rad23B to cisplatin-damaged DNA reveals contacts with both strands of the DNA duplex and spans the DNA adduct. Biochemistry. 2010(a);49(4):669-78.

Neher TM, Shuck SC, Liu JY, Zhang JT, Turchi JJ. Identification of novel small molecule inhibitors of the XPA protein using in silico based screening. ACS Chem Biol. 2010(b);5(10):953-65.

Nielsen DL, Palshof JA, Larsen FO, Jensen BV, Pfeiffer P. A systematic review of salvage therapy to patients with metastatic colorectal cancer previously treated with fluorouracil, oxaliplatin and irinotecan +/- targeted therapy. Cancer Treat Rev. 2014;40(6):701-15.

Nordlund P, Reichard P. Ribonucleotide reductases. Annu Rev Biochem. 2006;75:681-706.

Nouspikel T. DNA repair in mammalian cells : Nucleotide excision repair: variations on versatility. Cell Mol Life Sci. 2009;66(6):994-1009.

Nutting CM, van Herpen CM, Miah AB, Bhide SA, Machiels JP, Buter J, Kelly C, de Raucourt D, Harrington KJ. Phase II study of 3-AP Triapine in patients with recurrent or metastatic head and neck squamous cell carcinoma. Ann Oncol. 2009;20(7):1275-9.

O'Day SJ, Eggermont AM, Chiarion-Sileni V, Kefford R, Grob JJ, Mortier L, Robert C, Schachter J, Testori A, Mackiewicz J, Friedlander P, Garbe C, Ugurel S, Collichio F, Guo W, Lufkin J, Bahcall S, Vukovic V, Hauschild A. Final results of phase III SYMMETRY study: randomized, double-blind trial of elesclomol plus paclitaxel versus paclitaxel alone as treatment for chemotherapy-naive patients with advanced melanoma. J Clin Oncol. 2013 Mar;31(9):1211-8.

Odenike OM, Larson RA, Gajria D, Dolan ME, Delaney SM, Karrison TG, Ratain MJ, Stock W. Phase I study of the ribonucleotide reductase inhibitor 3-aminopyridine-2-carboxaldehyde-thiosemicarbazone (3-AP) in combination with high dose cytarabine in patients with advanced myeloid leukemia. Invest New Drugs. 2008;26(3):233-9.

OECD. Test No. 471: Bacterial Reverse Mutation Test. Paris, France: OECD Publishing; 1997.

Öhrvik H, Thiele DJ. The role of Ctr1 and Ctr2 in mammalian copper homeostasis and platinum-based chemotherapy. J Trace Elem Med Biol. 2015;31:178-82.

Ohui K, Afanasenko E, Bacher F, Ting RLX, Zafar A, Blanco-Cabra N, Torrents E, Dömötör O, May NV, Darvasiova D, Enyedy ÉA, Popović-Bijelić A, Reynisson J, Rapta P, Babak MV, Pastorin G, Arion VB. New Water-Soluble Copper(II) Complexes with Morpholine-Thiosemicarbazone Hybrids: Insights into the Anticancer and Antibacterial Mode of Action. J Med Chem. 2018 Dec 18.

Oroojalian F, Kasra-Kermanshahi R, Azizi M,. Bassami MR. Phytochemical composition of the essential oils from three Apiaceae species and their antibacterial effects on food-borne pathogens. Food Chemistry 120 (2010) 765–770.

Ostry V, Malir F, Toman J, Grosse Y. Mycotoxins as human carcinogens-the IARC Monographs classification. Mycotoxin Res. 2017 Feb;33(1):65-73.

Pahonțu E, Paraschivescu C, Ilieș DC, Poirier D, Oprean C, Păunescu V, Gulea A, Roșu T, Bratu O. Synthesis and Characterization of Novel Cu(II), Pd(II) and Pt(II) Complexes with 8-Ethyl-2-hydroxytricyclo(7.3.1.0(2,7))tridecan-13-one-thiosemicarbazone: Antimicrobial and in Vitro Antiproliferative Activity. Molecules. 2016;21(5).

Pang X, Tang YL, Liang XH. Transforming growth factor-β signaling in head and neck squamous cell carcinoma: Insights into cellular responses. Oncol Lett. 2018;16(4):4799-4806.

Paprocka M, Gliszczyńska A, Dancewicz K, Gabryś B. Novel Hydroxy- and Epoxy-cis-Jasmone and Dihydrojasmone Derivatives Affect the Foraging Activity of the Peach Potato Aphid Myzus persicae (Sulzer) (Homoptera: Aphididae). Molecules. 2018 Sep;23(9).

Pelosi G. Thiosemicarbazone Metal Complexes: From Structure to Activity. The Open Crystallography Journal, 2010, 3, 16-28.

Perabo FG, Muller SC. New agents for treatment of advanced transitional cell carcinoma. Ann Oncol. 2007;18:835–43.

Polêto MD, Rusu VH, Grisci BI, Dorn M, Lins RD, Verli H. Aromatic Rings Commonly Used in Medicinal Chemistry: Force Fields Comparison and Interactions With Water Toward the Design of New Chemical Entities. Front Pharmacol. 2018;9:395.

Popović-Bijelić A, Kowol CR, Lind ME, Luo J, Himo F, Enyedy EA, Arion VB, Gräslund A. Ribonucleotide reductase inhibition by metal complexes of Triapine (3-aminopyridine-2-carboxaldehyde thiosemicarbazone): a combined experimental and theoretical study. J Inorg Biochem. 2011;105(11):1422-31.

Puig S, Thiele DJ. Molecular mechanisms of copper uptake and distribution. Curr Opin Chem Biol. 2002 Apr;6(2):171-80.

Ragsdale SW. Nickel biochemistry. Curr Opin Chem Biol. 1998;2(2):208-15.

Rahal ON, Fatfat M, Hankache C, Osman B, Khalife H, Machaca K, Muhtasib HG. Chk1 and DNA-PK mediate TPEN-induced DNA damage in a ROS dependent manner in human colon cancer cells. Cancer Biol Ther. 2016;17(11):1139-1148.

Ranucci G, Socha P, Iorio R. Wilson disease: what is still unclear in pediatric patients? Clin Res Hepatol Gastroenterol. 2014;38(3):268-72.

Ryan KC, Guce AI, Johnson OE, Brunold TC, Cabelli DE, Garman SC, Maroney MJ. Nickel superoxide dismutase: structural and functional roles of His1 and its H-bonding network. Biochemistry. 2015;54(4):1016-27.

Rogolino D, Gatti A, Carcelli M, Pelosi G, Bisceglie F, Restivo FM, Degola F, Buschini A, Montalbano S, Feretti D, Zani C. Thiosemicarbazone scaffold for the design of antifungal and antiaflatoxigenic agents: evaluation of ligands and related copper complexes. Sci Rep. 2017;7(1):11214.

Rosenberg B, Vancamp L, Krigas T. Inhibition of cell division in *Escherichia coli* by electrolysis products from a platinum electrode. Nature. 1965; 205:698–699.

Rosenberg B, VanCamp L, Trosko JE, Mansour VH. Platinum compounds: a new class of potent antitumour agents. Nature. 1969; 222:385–386.

Saad EA, Hassanien MM, El-Lban FW. Nickel(II) diacetyl monoxime-2-pyridyl hydrazone complex can inhibit Ehrlich solid tumor growth in mice: A potential new antitumor drug. Biochem Biophys Res Commun. 2017;484(3):579-585.

Salim KY, Maleki Vareki S, Danter WR, Koropatnick J. COTI-2, a novel small molecule that is active against multiple human cancer cell lines *in vitro and in vivo*. Oncotarget. 2016;7(27):41363-41379. doi: 10.18632/oncotarget.9133.

Sâmia LB, Parrilha GL, Da Silva JG, Ramos JP, Souza-Fagundes EM, Castelli S, Vutey V, Desideri A, Beraldo H. Metal complexes of 3-(4-bromophenyl)-1-pyridin-2-ylprop-2-en-1-one thiosemicarbazone: cytotoxic activity and investigation on the mode of action of the gold(III) complex. Biometals. 2016;29(3):515-26.

Samimi G, Safaei R, Katano K, Holzer AK, Rochdi M, Tomioka M, Goodman M, Howell SB. Increased expression of the copper efflux transporter ATP7A mediates resistance to cisplatin, carboplatin, and oxaliplatin in ovarian cancer cells. Clin Cancer Res. 2004;10(14):4661-9.

Santini C, Pellei M, Gandin V, Porchia M, Tisato F, Marzano C. Advances in copper complexes as anticancer agents. Chem Rev. 2014 ;114(1):815-62.

Sarma UP, Bhetaria PJ, Devi P, Varma A. Aflatoxins: Implications on Health. Indian J Clin Biochem. 2017;32(2):124-133.

Saulnier A, Vaissière T, Yue J, Siouda M, Malfroy M, Accardi R, Creveaux M, Sebastian S, Shahzad N, Gheit T, Hussain I, Torrente M, Maffini FA, Calabrese L, Chiesa F, Cuenin C, Shukla R, Fathallah I, Matos E, Daudt A, Koifman S, Wünsch-Filho V, Menezes AM, Curado MP, Zaridze D, Boffetta P, Brennan P, Tommasino M, Herceg Z, Sylla BS. Inactivation of the putative suppressor gene DOK1 by promoter hypermethylation in primary human cancers. Int J Cancer. 2012;130(11):2484-94.

Sawant A, Kothandapani A, Zhitkovich A, Sobol RW, Patrick SM. Role of mismatch repair proteins in the processing of cisplatin interstrand cross-links. DNA Repair (Amst). 2015;35:126-36.

Sawers L, Ferguson MJ, Ihrig BR, Young HC, Chakravarty P, Wolf CR, Smith G. Glutathione S-transferase P1 (GSTP1) directly influences platinum drug chemosensitivity in ovarian tumour cell lines. Br J Cancer. 2014;111(6):1150-8.

Sawicki R, Golus J, Przekora A, Ludwiczuk A, Sieniawska E, Ginalska G. Antimycobacterial Activity of Cinnamaldehyde in a *Mycobacterium tuberculosis*(H37Ra) Model. Molecules. 2018 Sep;23(9).

Schimmer AD, Jitkova Y, Gronda M, Wang Z, Brandwein J, Chen C, Gupta V, Schuh A, Yee K, Chen J, Ackloo S, Booth T, Keays S, Minden MD. A phase I study of the metal ionophore clioquinol in patients with advanced hematologic malignancies. Clin Lymphoma Myeloma Leuk. 2012;12(5):330-6.

Schelman WR, Morgan-Meadows S, Marnocha R, Lee F, Eickhoff J, Huang W, Pomplun M, Jiang Z, Alberti D, Kolesar JM, Ivy P, Wilding G, Traynor AM. A phase I study of Triapine in combination with doxorubicin in patients with advanced solid tumors. Cancer Chemother Pharmacol. 2009;63(6):1147-56.

Schumacker PT. Reactive oxygen species in cancer cells: live by the sword, die by the sword. Cancer Cell. 2006 Sep;10(3):175-6.

Serda M, Kalinowski DS, Rasko N, Potůčková E, Mrozek-Wilczkiewicz A, Musiol R, Małecki JG, Sajewicz M, Ratuszna A, Muchowicz A, Gołąb J, Simůnek T, Richardson DR, Polanski J. Exploring the anti-cancer activity of novel thiosemicarbazones generated through the combination of retro-fragments: dissection of critical structure-activity relationships. PLoS One. 2014;9(10).

Shao J, Liu X, Zhu L, Yen Y. Targeting ribonucleotide reductase for cancer therapy. Expert Opin Ther Targets. 2013;17(12):1423-37.

Siddik ZH. Cisplatin: mode of cytotoxic action and molecular basis of resistance. Oncogene. 2003;22(47):7265-79.

Smpokou P, Samanta M, Berry GT, Hecht L, Engle EC, Lichter-Konecki U. Menkes disease in affected females: the clinical disease spectrum. Am J Med Genet A. 2015;167A(2):417-20.

Song IS, Savaraj N, Siddik ZH, Liu P, Wei Y, Wu CJ, Kuo MT. Role of human copper transporter Ctr1 in the transport of platinum-based antitumor agents in cisplatin-sensitive and cisplatin-resistant cells. Mol Cancer Ther. 2004;3(12):1543-9.

Sova P, Mistr A, Kroutil A, Zak F, Pouckova P, Zadinova M. Comparative anti-tumor efficacy of two orally administered platinum(IV) drugs in nude mice bearing human tumor xenografts. Anticancer Drugs. 2006;17(2):201-6.

Spreckelmeyer S, Orvig C, Casini A. Cellular transport mechanisms of cytotoxic metallodrugs: an overview beyond cisplatin. Molecules. 2014 Sep 29;19(10):15584-610.

Srivastava AK, Han C, Zhao R, Cui T, Dai Y, Mao C, Zhao W, Zhang X, Yu J, Wang QE. Enhanced expression of DNA polymerase eta contributes to cisplatin resistance of ovarian cancer stem cells. Proc Natl Acad Sci U S A. 2015;112(14):4411-6.

Svihálková-Sindlerová L, Foltinová V, Vaculová A, Horváth V, Soucek K, Sova P, Hofmanová J, Kozubík A. LA-12 overcomes confluence-dependent resistance of HT-29 colon cancer cells to Pt (II) compounds. Anticancer Res. 2010;30(4):1183-8.

Szczepański MA, Grzanka A, Litwiniec A, Gackowska L, Kubiszewska I, Grzanka D. Cytoskeletal changes during cellular response of the A549 lung cancer cells to continuous cisplatin treatment. Cell Biol Int. 2010;34(2):197-211.

Tadini-Buoninsegni F, Bartolommei G, Moncelli MR, Inesi G, Galliani A, Sinisi M, Losacco M, Natile G, Arnesano F. Translocation of platinum anticancer drugs by human copper ATPases ATP7A and ATP7B. Angew Chem Int Ed Engl. 2014;53(5):1297-301.

Tardito S, Marchiò L. Copper compounds in anticancer strategies. Curr Med Chem. 2009;16(11):1325-48.

Tardito S, Bussolati O, Maffini M, Tegoni M, Giannetto M, Dall'asta V, Franchi-Gazzola R, Lanfranchi M, Pellinghelli MA, Mucchino C, Mori G, Marchio L. Thioamido coordination in a thioxo-1,2,4-triazole copper(II) complex enhances nonapoptotic programmed cell death associated with copper accumulation and oxidative stress in human cancer cells. J Med Chem. 2007;50(8):1916-24.

Tardito S, Bussolati O, Gaccioli F, Gatti R, Guizzardi S, Uggeri J, Marchiò L, Lanfranchi M, Franchi-Gazzola R. Non-apoptotic programmed cell death induced by a copper(II) complex in human fibrosarcoma cells. Histochem Cell Biol. 2006;126(4):473-82.

Tisato F, Marzano C, Porchia M, Pellei M, Santini C. Copper in diseases and treatments, and copper-based anticancer strategies. Med Res Rev. 2010;30(4):708-49.

Theocharis SE, Margeli AP, Klijanienko JT, Kouraklis GP. Metallothionein expression in human neoplasia. Histopathology. 2004;45(2):103-18.

Thompson KH, Orvig C. Boon and Bane of Metal Ions in Medicine. Science. 2003; 300(5621):936-9.

Traynor AM, Lee JW, Bayer GK, Tate JM, Thomas SP, Mazurczak M, Graham DL, Kolesar JM, Schiller JH. A phase II trial of triapine (NSC# 663249) and gemcitabine as second line treatment of advanced non-small cell lung cancer: Eastern Cooperative Oncology Group Study 1503. Invest New Drugs. 2010 Feb;28(1):91-7.

Venkatesh V, Sadler PJ. Platinum(IV) Prodrugs. Met Ions Life Sci. 2018;18.

Visacri MB, Pincinato EC, Ferrari GB, Quintanilha JCF, Mazzola PG, Lima CSP, Moriel P. Adverse drug reactions and kinetics of cisplatin excretion in urine of patients undergoing cisplatin chemotherapy and radiotherapy for head and neck cancer: a prospective study. Daru. 2017;25(1):12.

Vo NH, Xia Z, Hanko J, Yun T, Bloom S, Shen J, Koya K, Sun L, Chen S. Synthesis, crystallographic characterization and electrochemical property of a copper(II) complex of the anticancer agent elesclomol. J Inorg Biochem. 2014 Jan;130:69-73.

Volbeda A, Charon MH, Piras C, Hatchikian EC, Frey M, Fontecilla-Camps JC. Crystal structure of the nickel-iron hydrogenase from Desulfovibrio gigas. Nature. 1995;373(6515):580-7.

Yadav AA, Patel D, Wu X, Hasinoff BB. Molecular mechanisms of the biological activity of the anticancer drug elesclomol and its complexes with Cu(II), Ni(II) and Pt(II). J Inorg Biochem. 2013 Sep;126:1-6.

Yang J, Xu ZP, Huang Y, Hamrick HE, Duerksen-Hughes PJ, Yu YN. ATM and ATR: sensing DNA damage. World J Gastroenterol. 2004;10(2):155-60.

Yang QY, Cao QQ, Qin QP, Deng CX, Liang H, Chen ZF. Syntheses, Crystal Structures, and Antitumor Activities of Copper(II) and Nickel(II) Complexes with 2-((2-(Pyridin-2-yl)hydrazono)methyl)quinolin-8-ol. Int J Mol Sci. 2018;19(7).

Yoshizawa K, Nozaki S, Kitahara H, Ohara T, Kato K, Kawashiri S, Yamamoto E. Copper efflux transporter (ATP7B) contributes to the acquisition of cisplatin-resistance in human oral squamous cell lines. Oncol Rep. 2007;18(4):987-91.

Yu H, Zhang W, Yu Q, Huang FP, Bian HD, Liang H. Ni(II) Complexes with Schiff Base Ligands: Preparation, Characterization, DNA/Protein Interaction and Cytotoxicity Studies. Molecules. 2017 Oct 24;22(10).

Xin L, Yang X, Cai G, Fan D, Xia Q, Liu L, Hu Y, Ding N, Xu S, Wang L, Li X, Zou Y, Pan F. Serum Levels of Copper and Zinc in Patients with Rheumatoid Arthritis: a Meta-analysis. Biol Trace Elem Res. 2015;168(1):1-10.

Xu YX, Zeng ML, Yu D, Ren J, Li F, Zheng A, Wang YP, Chen C, Tao ZZ. *In vitro* assessment of the role of DpC in the treatment of head and neck squamous cell carcinoma. Oncol Lett. 2018;15(5):7999-8004.

Wang X, Zhenchuk A, Wiman KG, Albertioni F. Regulation of p53R2 and its role as potential target for cancer therapy. Cancer Lett. 2009;276(1):1-7.

Wang D, Lippard SJ. Cellular processing of platinum anticancer drugs. Nat Rev Drug Discov. 2005;4(4):307-20.

Wang Y, Huang H, Zhang Q, Zhang P. Chirality in metal-based anticancer agents. Dalton Trans. 2018;47(12):4017-4026.

Wang VC, Ragsdale SW, Armstrong FA. Investigations of the efficient electrocatalytic interconversions of carbon dioxide and carbon monoxide by nickel-containing carbon monoxide dehydrogenases. Met Ions Life Sci. 2014;14:71-97.

Ward FJ, Dahal LN, Abu-Eid R. On the Road to Immunotherapy-Prospects for Treating Head and Neck Cancers With Checkpoint Inhibitor Antibodies. Front Immunol. 2018;9:2182.

Wasternack C, Strnad M. Jasmonates: News on Occurrence, Biosynthesis, Metabolism and Action of an Ancient Group of Signaling Compounds. Int J Mol Sci. 2018;19(9).

Wei W, Liu Z, Chen X, Bi F. Chemosensitivity of resistant colon cancer cell lines to lobaplatin, heptaplatin, and dicycloplatin. Int J Clin Pharmacol Ther. 2014;52(8):702-7.

Wongnate T, Ragsdale SW. The reaction mechanism of methyl-coenzyme M reductase: how an enzyme enforces strict binding order. J Biol Chem. 2015;290(15):9322-34.

Wu Y, Lai RY. Electrochemical Detection of Platinum (IV) Prodrug Satraplatin in Serum. Analytical Chemistry. 2015, 87 (21), 11092–11097.

Zani C, Bisceglie F, Restivo FM, Feretti D, Pioli M, Degola F, Montalbano S, Galati S, Pelosi G, Viola GVC, Carcelli M, Rogolino D, Ceretti E, Buschini A. A battery of assays as an integrated approach to evaluate fungal and mycotoxin inhibition properties and cytotoxic/genotoxic side-effects for the prioritization in the screening of thiosemicarbazone derivatives. Food Chem Toxicol. 2017;105:498-505.

Zani C, Restivo FM, Carcelli M, Feretti D, Pelosi G, Rogolino D, Degola F, Galati S, Bisceglie F, Buschini A. A Biotechnological Approach for the Development of New Antifungal Compounds to Protect the Environment and the Human Health. J Public Health Res. 2015;4(3):613.

Zák F, Turánek J, Kroutil A, Sova P, Mistr A, Poulová A, Mikolin P, Zák Z, Kasná A, Záluská D, Neca J, Sindlerová L, Kozubík A. Platinum(IV) complex with adamantylamine as nonleaving amine group: synthesis, characterization, and in vitro antitumor activity against a panel of cisplatin-resistant cancer cell lines. J Med Chem. 2004;47(3):761-3.

Zhao C, Chen X, Zang D, Lan X, Liao S, Yang C, Zhang P, Wu J, Li X, Liu N, Liao Y, Huang H, Shi X, Jiang L, Liu X, He Z, Dou QP, Wang X, Liu J. A novel nickel complex works as a proteasomal deubiquitinase inhibitor for cancer therapy. Oncogene. 2016;35(45):5916-5927.

Zhou G, Liu Z, Myers JN. TP53 Mutations in Head and Neck Squamous Cell Carcinoma and Their Impact on Disease Progression and Treatment Response. J Cell Biochem. 2016;117(12):2682-2692.

Zhu S, Shanbhag V, Wang Y, Lee J, Petris M. A Role for The ATP7A Copper Transporter in Tumorigenesis and Cisplatin Resistance. J Cancer. 2017;8(11):1952-1958.

Zhu Z, Du S, Du Y, Ren J, Ying G, Yan Z. Glutathione reductase mediates drug resistance in glioblastoma cells by regulating redox homeostasis. J Neurochem. 2018;144(1):93-104.

7. Appendix

7.1 The synthesized molecules and the acronyms used

Cuminaldehyde derivates	
Cuminaldehyde or 4-isopropylbenzaldehyde 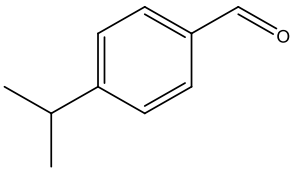 **Molecular Weight = 148.21 g/mol**	
4-isopropylbenzaldehyde-thiosemicarbazone 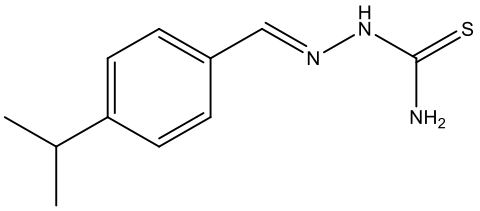 **Molecular Weight= 221.32 g/mol**	Htcum
4-isopropylbenzaldehyde-semicarbazone 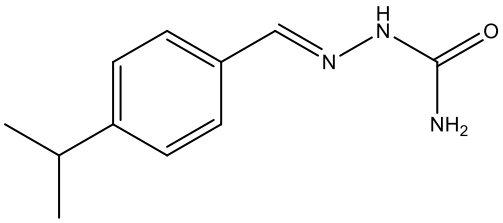 **Molecular Weight= 205.26 g/mol**	Hscum
3-isopropylbenzaldehyde-thiosemicarbazone 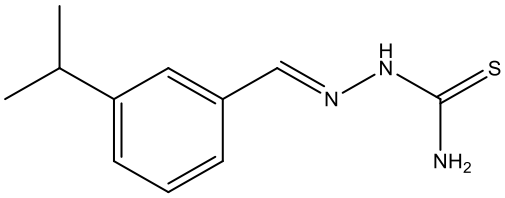 **Molecular Weight= 221.32 g/mol**	mHtcum
2-isopropylbenzaldehyde-thiosemicarbazone 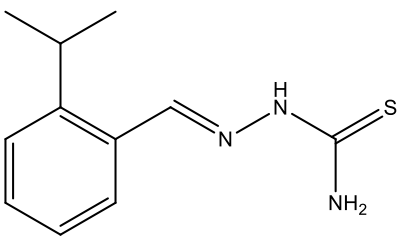 **Molecular Weight= 221.32 g/mol**	oHtcum

Cuminaldehyde derivates	
Bis(cuminaldehydethiosemicarbazonato)zinc(II) complex 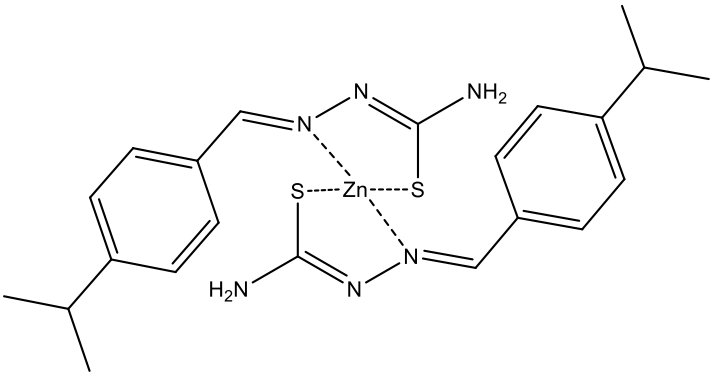 **Molecular Weight = 506.01 g/mol**	X
Bis(3-isopropylbenzaldehydethiosemicarbazonato)zinc (II) complex 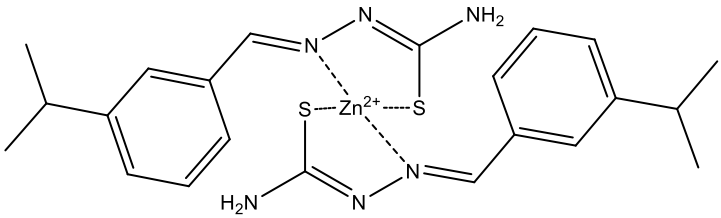 **Molecular Weight = 506.01 g/mol**	Y+Zn
Bis(2-isopropylbenzaldehydethiosemicarbazonato)zinc(II) complex 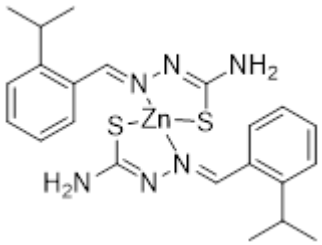 **Molecular Weight = 506.01 g/mol**	Z+Zn

Cuminaldehyde derivates	
Bis(3-isopropylbenzaldehydethiosemicarbazonato)copper(II) complex 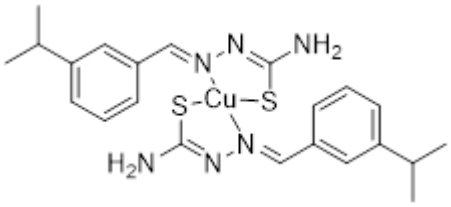 **Molecular Weight= 505.18 g/mol**	F24
Bis(2-isopropylbenzaldehydethiosemicarbazonato)copper(II) complex 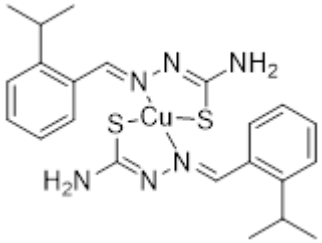 **Molecular Weight= 505.18 g/mol**	F23
3-isopropylbenzaldehyde-2-methyl-3-thiosemicarbazone 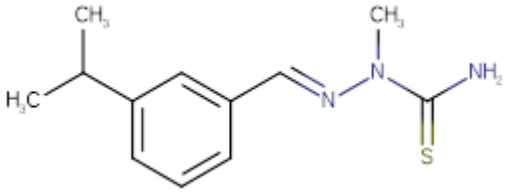 **Molecular Weight= 235.35 g/mol**	F30
Methyl bis(2-isopropylbenzaldehydethiosemicarbazonate) copper(II) complex 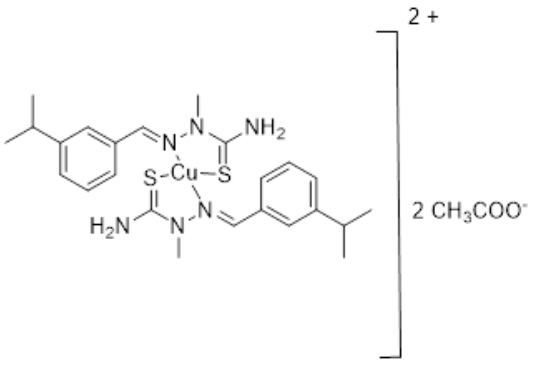 **Molecular Weight= 652.33 g/mol**	F40

Perillaldehyde derivates	
Perillaldehydethiosemicarbazone 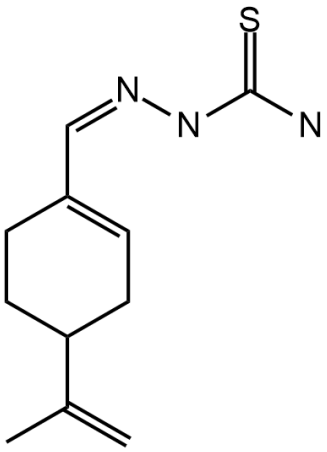 **Molecular Weight = 223.34 g/mol**	V
Bis(perillaldehydethiosemicarbazonato)nickel(II) complex 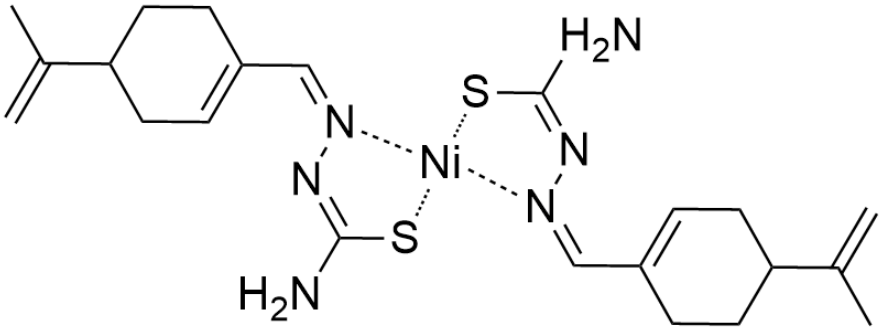 **Molecular Weight = 503.35 g/mol**	T

Vanillin derivates	
Cu_2[N'-(4-hydroxy-5-metoxyacetophenone) thiosemicarbazone] Cl_2 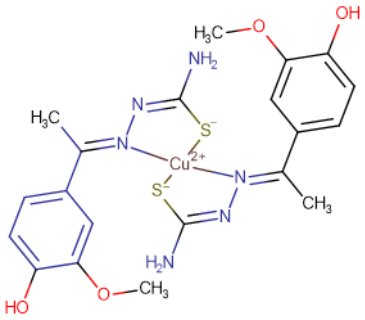 **Molecular Weight = 540.12 g/mol**	2
Cu_3[N'-(3 hydroxy-4-methoxybenzyliden) thiosemicarbazone]$_2$ Cl_2 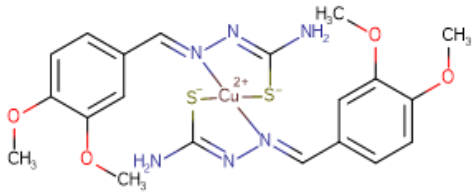 **Molecular Weight = 540.12 g/mol**	3
Copper bis-[5,5'-Bis-vanillin thiosemicarbazone] 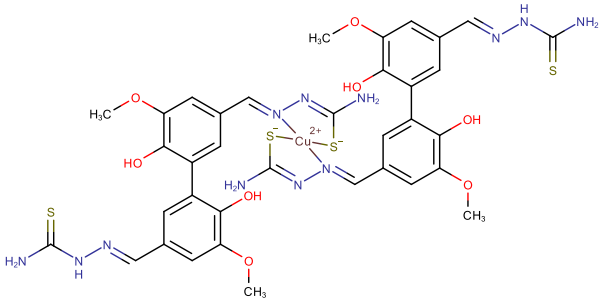 **Molecular Weight = 958.56 g/mol**	D27

Vanillin derivates	
1-(5-hydroxy-2-methyl-1-oxonaphthalen-4(1H)-ylidene) thiosemicarbazone 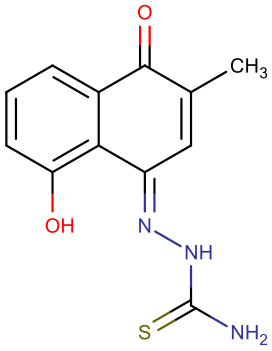 **Molecular Weight = 261.30g/mol**	D28
Cu[N'-(3,4-dimethoxybenzyliden)-3dimethylthiosemicarbazone]Cl 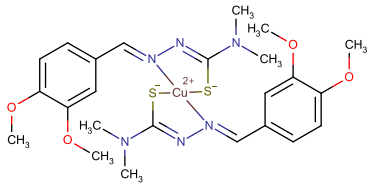 **Molecular Weight = 596.22 g/mol**	6
N'-(benzylden-3-dimethylthiosemicarbazone) 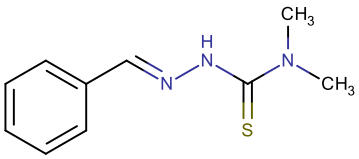 **Molecular Weight = 207.30 g/mol**	L5
Cu[N'-benzylden-3-dimethylthiosemicarbazone]Cl 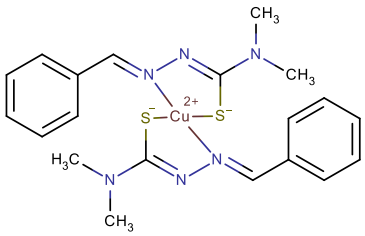 **Molecular Weight = 476.12 g/mol**	5

Jasmonic acid derivates	
Cis-jasmon 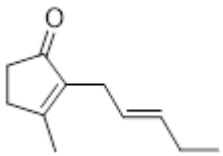 **Molecular Weight = 164.25 g/mol**	J
Cis-jasmon thiosemicarbazone 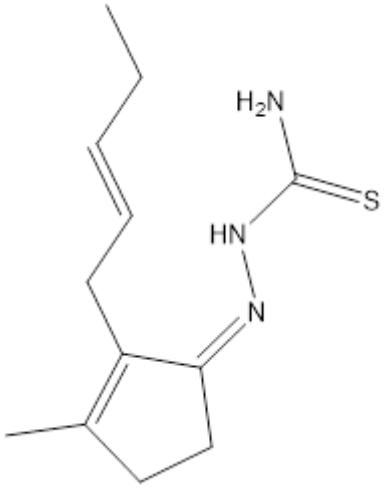 **Molecular Weight= 237.37g/mol**	F36
Dihydrojasmon thiosemicarbazone 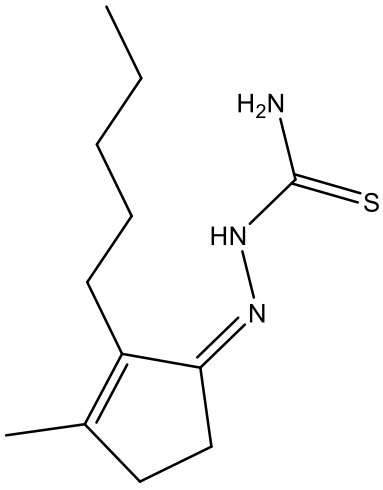 **Molecular Weight= 239.38 g/mol**	F31

Jasmonic acid derivates	
Bis-(jasmonthiosemicarbazonate) Cu(II) complex 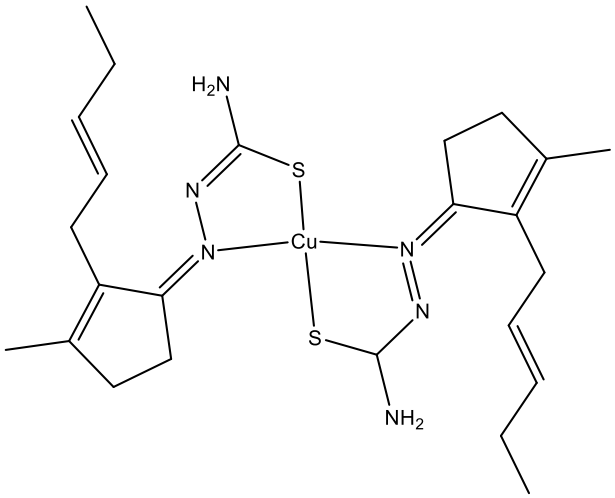 **Molecular Weight= 537.27/mol**	F44

Anthraquinone derivates	
2-hydroxymethylanthraquinone 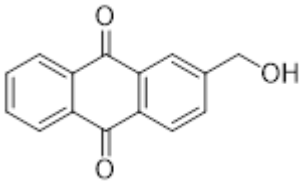 **Molecular Weight= 238.24 g/mol**	F47
2-formylanthraquinone 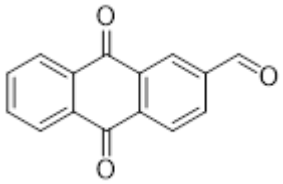 **Molecular Weight= 236.22 g/mol**	F57
2-formylanthraquinonethiosemicarbazone 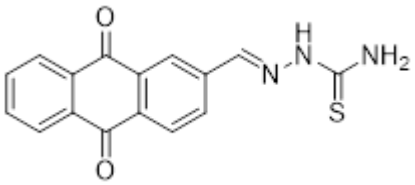 **Molecular Weight= 309.34 g/mol**	F46
2-carboxylic-acid anthraquinone 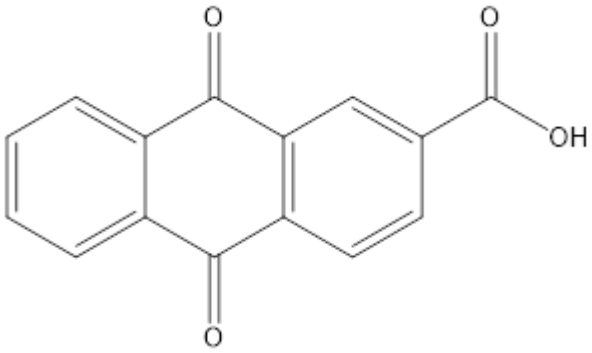 **Molecular Weight = 252.23**	F66

Cinnamaldehyde derivates	
Cinnamaldehyde 4,4'-dimethyl thiosemicarbazone 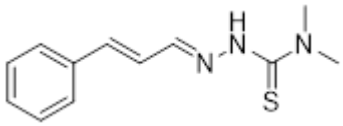 **Molecular Weight= 205.28 g/mol**	F51
Cinnamaldehyde 4,4'-dimethyl thiosemicarbazone zinc (II) complex 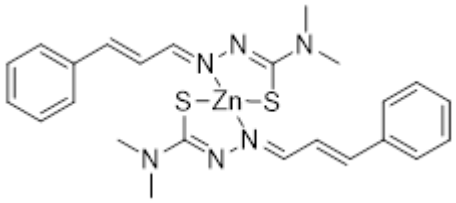 **Molecular Weight= 473.92 g/mol**	F53
Cinnamaldehyde-N2-methylthiosemicarbazone 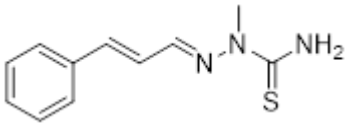 **Molecular weight = 219.31 g/mol**	F61
Cinnamaldehyde-N2-methylthiosemicarbazone (reduced form) 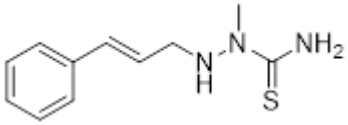 **Molecular Weight = 221.32 g/mol**	F62

2-acetylthiophene derivates	
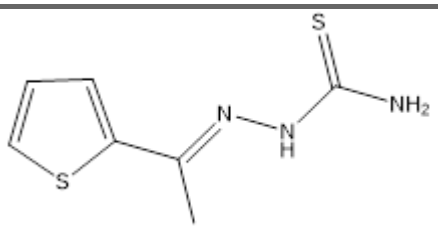 **2-acetylthiophenethiosemicarbazone** **Molecular Weight= 199.30 g/mol**	F20
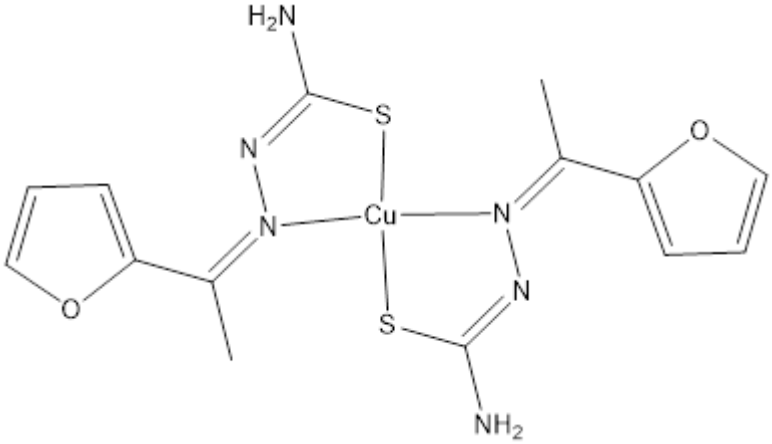 **bis(2-acetylfuranthiosemicarbazonate)copper(II) complex** **Molecular Weight= 428.01 g/mol**	F25

1-(3-methoxyphenyl)-1-heptanone derivates	
1-(3-methoxyphenyl)-1-heptanone thiosemicarbazone 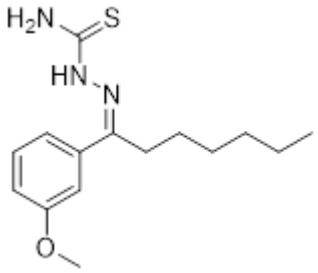 **Molecular Weight= 293.43 g/mol**	F22
Copper complex of 1-(3-methoxyphenyl)-1-heptanone thiosemicarbazone 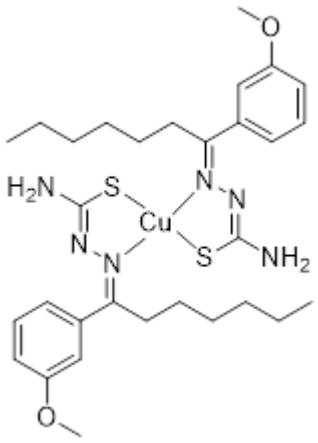 **Molecular Weight= 648.41 g/mol**	F26

Long hydrophobic chain derivates	
Heptanal thiosemicarbazone 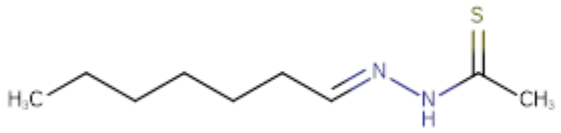 **Molecular Weight= 187.31 g/mol**	F37
Nonanal thiosemicarbazone 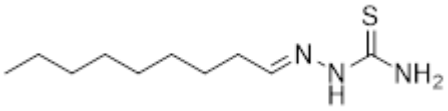 **Molecular Weight= 215.36 g/mol**	F38
Undecanal thiosemicarbazone 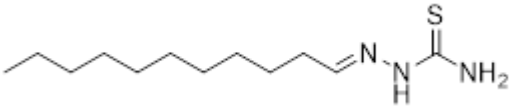 **Molecular Weight= 243.41 g/mol**	F39
Bis-(heptanal-thiosemicarbazonate) Cu(II) complex 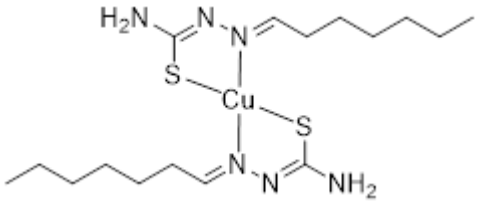 **Molecular Weight= 438.17 g/mol**	F41
Bis-(nonanal-thiosemicarbazonate) Cu(II) complex 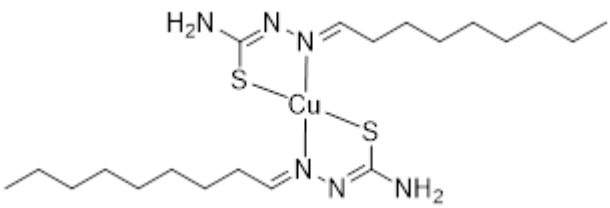 **Molecular Weight= 494.29 g/mol**	F42

Benzophenone derivates	
Benzophenone thiosemicarbazone 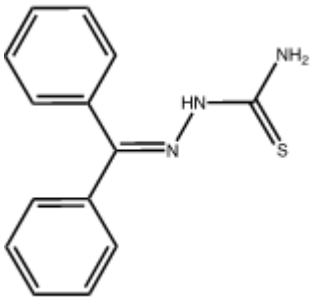 **Molecular Weight = 255.34 g/mol**	JB20

Valerophenone derivates	
Valerophenone thiosemicarbazone 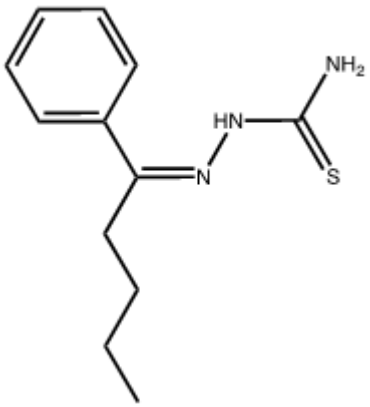 **Molecular Weight = 235.35 g/mol**	JB24

Citronellal derivates	
Nickel (II) complex of citronellal thiosemicarbazone 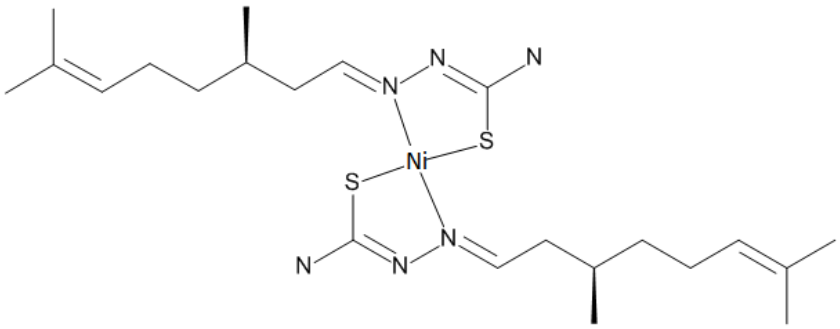 **Molecular Weight = 511.42 g/mol**	$Ni(tcitr)_2$
Platinum (II) complex of citronellal thiosemicarbazone 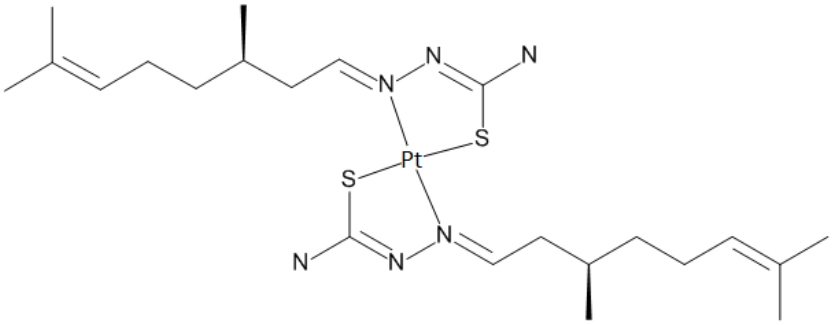 **Molecular Weight = 647.81 g/mol**	$Pt(tcitr)_2$
Copper (II) complex of citronellal thiosemicarbazone 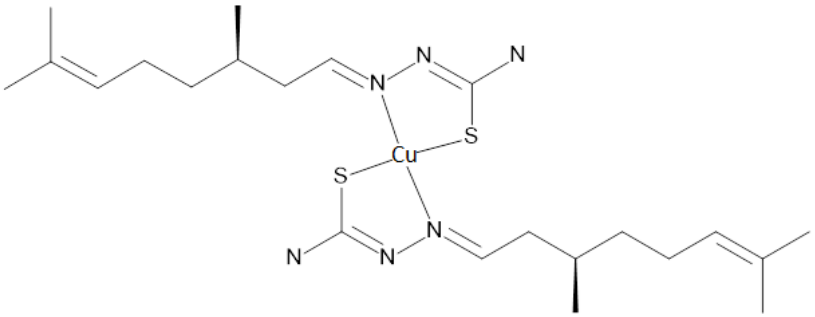 **Molecular Weight = 516.27 g/mol**	$Cu(tcitr)_2$

Citronellal derivates	
Nickel (II) complex of 4,4'-dimethyl-citronellal thiosemicarbazone 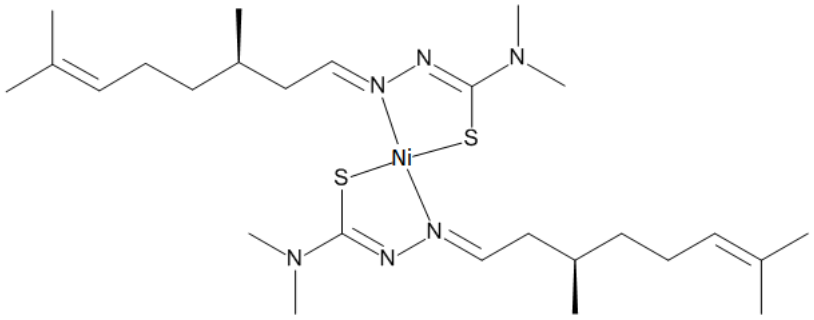 **Molecular Weight = 567.53 g/mol**	$Ni(4dm\text{-}tcitr)_2$
Platinum (II) complex of 4,4'-dimethyl-citronellal thiosemicarbazone 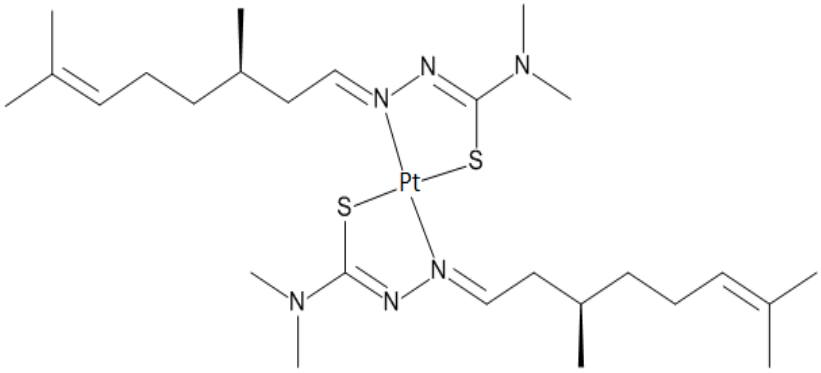 **Molecular Weight =703.92 g/mol**	$Pt(4dm\text{-}tcitr)_2$
Copper (II) complex of 4,4'-dimethyl-citronellal thiosemicarbazone 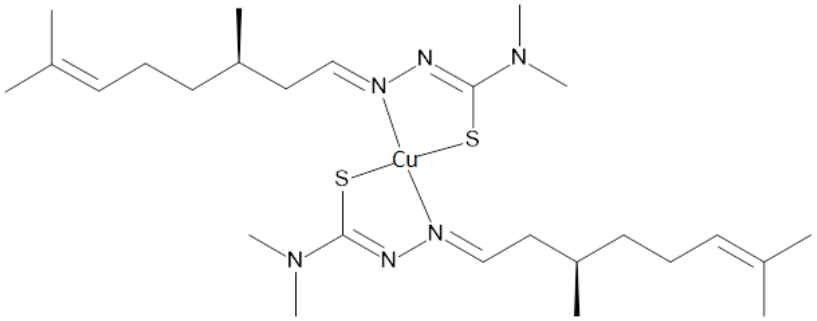 **Molecular Weight = 572.38 g/mol**	$Cu(4dm\text{-}tcitr)_2$

7.2 Western Blot quantification

PNS-136 cells were treated with the indicated concentrations of $[Cu(tcitr)_2]$ for 1-4-24 h. The expression levels of p53, p53 Ser15, p53 Lys382 and mTOR proteins were analysed by western blot analysis. The band intensities were quantified and normalized to GAPDH levels. Images were produced using the ChemiDoc XRS imaging system (Bio-Rad) and data were analysed by densitometry with the ImageLab software.

	GAPDH	p53	p53/GAPDH	Fold change
NT 1h	14642879.818	39912379.813	2.726	1.00
1.85 µM 1h	4768729.152	36254723.833	7.603	2.79
18.5 µM 1h	5597274.987	36078092.563	6.446	2.36
NT 4h	4337807.152	34269339.938	7.900	1.00
1.85 µM 4h	4730018.905	35911600.792	7.592	0.96
18.5 µM 4h	3591351.801	11179504.000	3.113	0.39
NT 24h	5782135.000	37949506.250	6.563	1.00
1.85 µM 24h	7413812.987	40484854.625	5.461	0.83
18.5 µM 24h	39611602.489	2257721.813	0.057	0.01

	GAPDH	p53 Ser15	p53 Ser15/GAPDH	Fold change
NT 1h	14642879.818	23271229.481	1.589	1.00
1.85 µM 1h	4768729.152	20567189.111	4.313	2.71
18.5 µM 1h	5597274.987	11502543.444	2.055	1.29
NT 4h	4337807.152	17670428.222	4.074	1.00
1.85 µM 4h	4730018.905	18490143.556	3.909	0.96
18.5 µM 4h	3591351.801	863513.778	0.240	0.06
NT 24h	5782135.000	12049668.333	2.084	1.00
1.85 µM 24h	7413812.987	12149754.667	1.639	0.79
18.5 µM 24h	39611602.489	146470.074	0.004	0.00

	GAPDH	p53 Lys382	p53 Lys382/GAPDH	Fold change
NT 1h	14642879.818	7188669.655	0.491	1.00
1.85 µM 1h	4768729.152	5386378.268	1.130	2.30
18.5 µM 1h	5597274.987	2808460.659	0.502	1.02
NT 4h	4337807.152	5226024.598	1.205	1.00
1.85 µM 4h	4730018.905	7331349.655	1.550	1.29
18.5 µM 4h	3591351.801	502857.5632	0.140	0.12
NT 24h	5782135.000	3898606.192	0.674	1.00
1.85 µM 24h	7413812.987	3553360.966	0.479	0.71
18.5 µM 24h	39611602.489	276695.7241	0.007	0.01

	GAPDH	mTOR	mTOR /GAPDH	Fold change
NT 1h	14642879.818	4452554.400	0.304	1.00
1.85 µM 1h	4768729.152	3688444.200	0.773	2.54
18.5 µM 1h	5597274.987	3935324.200	0.703	2.31
NT 4h	4337807.152	3405484.600	0.785	1.00
1.85 µM 4h	4730018.905	5774683.800	1.221	1.56
18.5 µM 4h	3591351.801	1534897.400	0.427	0.54
NT 24h	5782135.000	3437162.900	0.594	1.00
1.85 µM 24h	7413812.987	3147392.400	0.425	0.71
18.5 µM 24h	39611602.489	534024.600	0.013	0.02

	GAPDH	p53 Ser33	p53 Ser33/GAPDH	Fold change
NT 1h	8690068.667	9406517.564	1.082	1.00
1.85 µM 1h	4849976.000	5929823.455	1.223	1.13
18.5 µM 1h	5573226.667	1936433.382	0.347	0.32
NT 4h	2679140.000	6472937.555	2.416	1.00
1.85 µM 4h	2296000.000	6247525.491	2.721	1.13
18.5 µM 4h	2008575.111	490954.8727	0.244	0.10
NT 24h	3944860.000	4662145.927	1.182	1.00
1.85 µM 24h	3824272.889	4934401.945	1.290	1.09
18.5 µM 24h	19338469.778	442402.5455	0.023	0.02

	GAPDH	p53 Ser392	p53 Ser392/GAPDH	Fold change
NT 1h	8690068.667	24239240.400	2.789	1.00
1.85 µM 1h	4849976.000	19844817.920	4.092	1.47
18.5 µM 1h	5573226.667	14993760.320	2.690	0.96
NT 4h	2679140.000	21460649.480	8.010	1.00
1.85 µM 4h	2296000.000	23057835.920	10.043	1.25
18.5 µM 4h	2008575.111	1211506.880	0.603	0.08
NT 24h	3944860.000	14484542.960	3.672	1.00
1.85 µM 24h	3824272.889	19024841.680	4.975	1.35
18.5 µM 24h	19338469.778	83154.440	0.004	0.00

Food Control 73 (2017) 606–612

Contents lists available at ScienceDirect

Food Control

journal homepage: www.elsevier.com/locate/foodcont

Investigation of antibacterial activity of new classes of essential oils derivatives

Irene Bassanetti [a, *], Mauro Carcelli [a], Annamaria Buschini [b], Serena Montalbano [b], Giuliano Leonardi [c], Paolo Pelagatti [a], Giovanni Tosi [d], Paola Massi [d], Laura Fiorentini [d], Dominga Rogolino [a]

[a] Dipartimento di Chimica, Università di Parma, Parco Area delle Scienze 17/A, 43123, Parma, Italy
[b] Dipartimento di Biologia, Università di Parma, Parco Area delle Scienze 17/A, 43123, Parma, Italy
[c] Ordine Provinciale dei Chimici di Cremona, Via Palestro 66, 26100, Cremona, Italy
[d] Istituto Zooprofilattico Sperimentale della Lombardia e dell'Emilia Romagna, Sezione Diagnostica di Forlì, Via Don E. Servadei 3E/3F, 47122, Forlì, Italy

ARTICLE INFO

Article history:
Received 28 April 2016
Received in revised form
18 August 2016
Accepted 7 September 2016
Available online 9 September 2016

Keywords:
Essential oils derivatives
Antibacterial activity
Bioavailability
Food-borne pathogens

ABSTRACT

Essential oils (EOs) have deserved much attention in the past decades for their antimicrobial activity, since many of them have demonstrated efficacy against food-borne pathogenic and spoilage microorganisms. Moreover, they have potential application in animal nutrition as multifunctional feed supplements, avoiding or diminishing the use of antibiotics in livestock. However, low solubility and bioavailability as well as volatility and marked aromatic note are important limitations in food and feed applications. In this study we present the synthesis, characterization and evaluation of the antibacterial activity of new thymol, carvacrol and menthol derivatives. The new compounds have been designed to overcome the limitations of the precursors, such as poor water solubility and volatility, still maintaining a good antimicrobial profile. We evaluated the activity of the synthetized compounds against pathogens causing important foodborne diseases, *i.e. Clostridium perfringens*, *Salmonella typhimurium*, *Salmonella enteritidis* and *Escherichia coli*. The low MICs and MBCs values for some of the studied compounds, combined with water solubility and negligible cytotoxicity towards HT-29 human cells, confirmed the potential use for EOs derivatives in the food industry.

1. Introduction

Microorganisms causing food spoilage are a major concern for the food industry and the extension of shelf-life is an on-going demand for both retailers and consumers. Such extension is mainly achieved by technological improvements and addition of synthetic food preservatives. Natural products in general are an alternative to synthetic preservatives, and among them, essential oils (EOs) are typical antimicrobial agents without harmful residues. Since the 1990s, they have been widely studied for their antimicrobial activity and many EOs (e.g. thyme, oregano, cinnamon, horseradish) and their components have demonstrated antimicrobial efficacy against food-borne pathogenic and spoilage microorganisms (Arsi et al., 2014; Bakkali & Idaomar, 2008; Burt, 2004; Calo, Baker, Park, & Ricke, 2015; Kim & Rhee, 2016; Lang & Buchbauer, 2012; Pinheiro et al., 2015; Tajkarimi, Ibrahim, & Cliver, 2010). Another interesting area of application for EOs is animal nutrition. The prophylactic use of antibiotics in the livestock industry to obtain improvements in growth, feed consumption and decreased mortality caused by bacterial diseases has been a common practice for decades, especially for swine and poultry. However, the concern over the transmission and the proliferation of resistant bacteria via the food chain has led to the ban of the feed use of antibiotic growth promoters in livestock within the European Union since 2006. A wide range of EOs have the potential to act as multifunctional feed supplements for animals. Some EOs, in fact, are reported to have multiple actions in monogastric animals, including effects on performance, digestive systems, lipid metabolism, prevention of tissue oxidation and modulation of microbial

Abbreviations: EOs, essential oils; TGA, thermogravimetric analysis; HIA, heart infusion agar; BHI, brain heart infusion; MIC, minimal inhibitory concentration; MBC, minimal bactericidal concentration; GI%, growth inhibition percent.

* Corresponding author.
E-mail addresses: irene.bassanetti@unipr.it, irene.bassanetti@netbas.it (I. Bassanetti).

http://dx.doi.org/10.1016/j.foodcont.2016.09.010
0956-7135/

populations (Liang et al., 2013; Mitsch, Ko, Gabler, Losa, & Zimpernik, 2004; Zhaikai, Sai, Hongliang, & Xiangshu, 2015).

EOs antimicrobial activity has been attributed mainly to phenolic compounds (Pesavento et al., 2015), such as carvacrol and thymol (Cherallier, 1996; Lambert, Skandamis, Coote, & Nychas, 2001; Valero, 2006; Xu, Zhou, Ji, Pei, & Xu, 2008). They are additives generally recognized as safe and they are widely used as food preservatives (Goñi et al., 2009; Lv, Liang, Yuan, & Li, 2011). They can be directly incorporated into or coated onto packaging films, in order to enhance shelf-life (Calo, Crandall, O'Bryan, & Ricke, 2015). However, their low solubility and bioavailability limit the cytotoxic potential on bacteria, virus, fungi and parasites and their delivery is still a challenge (Kaur, Darokar, & Ahmad, 2014; Suntres, Coccimiglio, & Alipour, 2015). Additionally, the volatility and marked aromatic note of a lot of EOs, which are appreciable features in applications such as aromatherapy or perfume production, are conversely major limitations in food and feed applications. In fact, high concentrations are needed to ensure food safety, but effective concentrations usually result in negative flavour and in sensory changes, which discourages the consumption. The purpose of this study is the synthesis, characterization and evaluation of the antibacterial activity of new carvacrol, thymol and menthol derivatives (Fig. 1). The compounds have been designed with the aim of overcoming limitations, such as poor water solubility and volatility, still maintaining a good activity against pathogens. In this way, it would be possible to exploit the antibacterial properties of EOs active principles (i.e., menthol, carvacrol, thymol), but with more manageable compounds. Compounds **1**–**8** were synthetized and fully characterized and their activity against *Clostridium perfringens*, *Salmonella typhimurium*, *Salmonella enteritidis* and *Escherichia coli* is presented.

2. Materials and methods

2.1. Chemistry

All reagents and solvents were commercially available. NMR spectra were recorded on Bruker AVANCEIII (FT; 400 MHz, ^{1}H; 75 MHz, ^{13}C{^{1}H}). Chemical shifts (δ) for ^{1}H and ^{13}C{^{1}H} NMR spectra were referenced using internal solvent resonances and were reported relative to tetramethylsilane (TMS). FTIR spectra (4000–700 cm^{-1}) were recorded on a Nicolet Nexus spectrophotometer equipped with a Smart Orbit HATR accessory (diamond crystal). Melting points (mp) were determined using an Electrothermal melting point or a Köfler apparatus and are uncorrected (see Table 1). For **3**–**7** mass spectra were acquired in EI mode (positive ions) by mean of a DEP-probe (Direct Exposure Probe) mounting on the tip a Pt-filament with a DSQII Thermo Fisher apparatus equipped with a single quadrupole analyzer. The analyses were conducted in flash mode with an amperage gradient of 100 mA/s up to 1000 mA, correspondingly to an estimated temperature of 1000 °C. ESI mass of **8** was registered by using a Waters

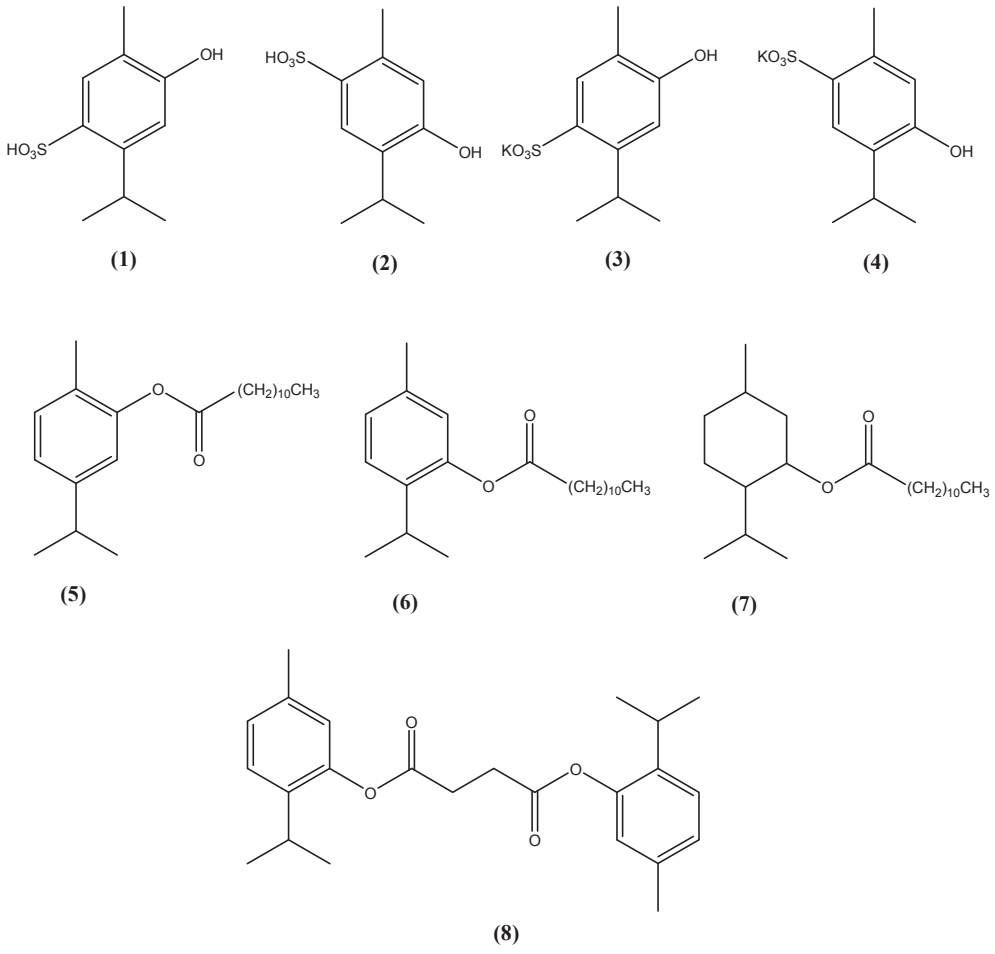

Fig. 1. Schematic representation of carvacrol, thymol and menthol derivatives **1**–**8**.

Table 1
Water solubility and melting point of **3** and **4** and their precursors.

	3	**4**	Carvacrol[a]	Thymol[b]
Solubility in water, t = 25 °C	~250 g/l	~190 g/l	~0.8 g/l	~0.9 g/l
Melting point	>270 °C	220 °C	3–4 °C	48–51 °C

[a] Lide, 1998.
[b] Yalkowsky, He, & Jain, 2010.

Acquity Ultraperformance spectrometer equipped with a Single Quadrupole Detector and UPLC Acquity Waters source. Working parameters were set as follows: source temperature 150 °C, desolvation temperature 300 °C, solvent flow 0.2 ml/min, capillary voltage 3 kV and cone voltage 60V. All mass spectra were recorded in full scan analysis mode in the range 0–1000 m/z. Thermogravimetric analysis (TGA) was performed on a TA Q50 ultramicro balance instrument (ramp rate = 5 °C min^{-1}) and under a N_2 flow rate of 90 mL min^{-1} at atmospheric pressure.

2.1.1. 4-Hydroxy-2-isopropyl-5-methyl benzene sulfonic acid (1)

Carvacrol (2.2 g, 0.013 mol) and sulfuric acid 96%w (2.1 ml, 0.038 mol) were mixed for 2 h under vacuum at 30 °C. The crude solid was recrystallized in water, yielding white crystals. IR (cm^{-1}): 3404br, 3221br, 2966w, 1734br, 1123m, 1164s, 1037s. ^{1}H NMR (400 MHz, DMSO-d_6, ppm, δ): 1.10 (d, 6H, CH_3(*i*-Pr)); 2.06 (s, 3H, CH_3); 4.01 (m, 1H, CH(*i*-Pr)); 6.67 (s, 1H, CH(Ph)); 7.43 (s, 1H, CH(Ph)). EI-MS (m/z): 230.0, $[C_{10}H_{14}O_4S]^+$; 215.0, $[C_9H_{11}O_4S]^+$.

2.1.2. 4-Hydroxy-5-isopropyl-2-methyl benzene sulfonic acid (2)

Thymol (2.2 g, 0.013 mol) and sulfuric acid 96%w (2.1 ml, 0.038 mol) were mixed for 2 h under vacuum at 40 °C. in water, yielding white crystals. IR (cm^{-1}): 3394br, 3285br, 2964w, 1701br, 1076m, 1011s.^{1}H NMR (400 MHz, DMSO-d_6, ppm, δ): 1.13 (d, 6H, CH_3(*i*-Pr)); 2.40 (s, 3H, CH_3); 3.14 (m, 1H, CH(*i*-Pr)); 6.56 (s, 1H, CH (Ph)); 7.51 (s, 1H, CH(Ph)). EI-MS (m/z): 230.0, $[C_{10}H_{14}O_4S]^+$; 215.0, $[C_9H_{11}O_4S]^+$.

2.1.3. Potassium 4-hydroxy-2-isopropyl-5-methyl benzene sulfonate (3)

1 (5 g) was dissolved in 5 ml of methanol and neutralized with a saturated solution of KOH in water (pH 7). The precipitate was removed by Büchner filtration and the filtrate was vacuum-dried yielding a white solid (3.3 g, 95%). IR (cm^{-1}): 3213br, 2966w, 1853w, 1492w, 1410m, 1301w, 1272m, 1164m, 1134m, 1088m, 1042s, 976w, 887w, 717w, 665m, 609m, 580s. ^{1}H NMR (400 MHz, DMSO-d_6, ppm, δ): 1.09 (d, 6H, CH_3(i-Pr)); 2.04 (s, 3H, CH_3); 4.02 (m, 1H, CH(i-Pr)); 6.72 (s, 1H, CH(Ph)); 7.43 (s, 1H, CH(Ph)); 9.22 (s, 1H, OH). ^{13}C{^{1}H}-NMR (75 MHz, DMSO-d_6, ppm, δ): 15.49 (CH_3), 24.09 (CH_3(i-Pr)), 27.71(CH(i-Pr)), 111.81 (CH(Ph)), 118.98 (CH(Ph)), 129.39 (CH(Ph)), 136.27 (CH(Ph)), 145.16 (CH(Ph)), 155.77 (CH(Ph)). EI-MS (m/z): 230.0, $[C_{10}H_{14}O_4S]^+$; 215.0, $[C_9H_{11}O_4S]^+$.

2.1.4. Potassium 4-hydroxy-5-isopropyl-2-methyl benzene sulfonate (4)

2 (5 g) was dissolved in 5 ml of methanol and neutralized (pH 7) with a saturated solution of KOH in water. The precipitate was removed by Büchner filtration and the filtrate was vacuum-dried yielding a white solid (3.2 g, 92%). IR (cm^{-1}): 3415wbr, 2996w, 2871vw, 1611w, 1578w, 1493w, 1459m, 1403w, 1339w, 1259w, 1203m, 1158s, 1130m, 1105w, 1079m, 1038s, 903w, 883w, 867w, 733m, 664s. ^{1}H NMR (400 MHz, DMSO-d_6, ppm, δ): 1.99 (d, 6H, CH_3(i-Pr)); 2.38 (s, 3H, CH_3); 3.16 (m, 1H, CH(i-Pr)); 6.51 (s, 1H, CH(Ph)); 7.50 (s, 1H, CH(Ph)); 9.19 (s, 1H, OH). ^{13}C{^{1}H}-NMR (75 MHz, DMSO-d_6, ppm, δ): 19.81 (CH_3), 22.63 (CH_3(i-Pr)), 25.91 (CH(i-Pr)), 117.26 (CH(Ph)), 124.71 (CH(Ph)), 129.70 (CH(Ph)), 133.47 (CH(Ph)), 136.02 (CH(Ph)), 155.63 (CH(Ph)). EI-MS (m/z): 230.0, $[C_{10}H_{14}O_4S]^+$; 215.0, $[C_9H_{11}O_4S]^+$.

2.1.5. 5-Isopropyl-2-methyl phenyl dodecanoate (5)

Carvacrol (2 g, 0.013 mol), lauric acid (2.6 g, 0.013 mol) and phosphoric acid (3 drops) were mixed under magnetic stirring at 150 °C under vacuum for 12 h. The crude product was poured in chloroform (4 ml) and purified by flash chromatography (gradient elution: hexane:dichloromethane 8:2 and then ethyl acetate 100%), yielding a colourless oil (2.2 g, 51%). IR (cm^{-1}): 2954m, 2916vs, 2848s, 1760m, 1701s, 1463m, 1428m, 1411m, 1302m, 1276m, 1247m, 1220m, 1193m, 1168m, 1141m, 1115m, 938m, 720m. ^{1}H NMR (400 MHz, $CDCl_3$, ppm, δ): 0.92 (t, 3H, CH_3); 1.26 (d, 6H, CH_3(i-Pr)); 1.30–1.47 (m, 14H, CH_2); 1.69 (m, 2H, CH_2); 1.80 (m, 2H, CH_2); 2.15 (s, 3H, CH_3); 2.59 (t, 2H, CH_2); 2.89 (m, 1H, CH(*i*-Pr)); 6.87 (d, 1H, CH (Ph)); 7.03 (dd, 1H, CH(Ph)); 7.16 (dd, 1H, CH(Ph)). EI-MS (m/z): 150, $[C_{10}H_{14}O]^+$; 135, $[C_{10}H_{14}]^+$; 332, $[C_{22}H_{36}O_2]^+$.

2.1.6. 2-Isopropyl-5-methyl phenyl dodecanoate (6)

Thymol (2 g, 0.013 mol), lauric acid (5.33 g, 0.026 mol) and phosphoric acid 85% (3 drops) are mixed under magnetic stirring at 150 °C in vacuum for 12 h. The crude product is poured in chloroform (4 ml) and purified by flash chromatography (silica, *n*-hexane 100%) yielding a colourless oil (1.2 g, 28%). IR (cm^{-1}): 2957m, 2923s, 2853m, 1709s, 1620w, 1584w, 1505w, 1456m, 1416m, 1378w, 1363w, 1290w, 1226m, 1150s, 1111m, 1087m, 1058w, 946m, 814m, 805m, 721w. ^{1}H NMR (400 MHz, $CDCl_3$, ppm, δ): 0.91 (t, 3H, CH_3); 1.22 (d, 6H, CH_3(*i*-Pr)); 1.30–1.46 (m, 16H, CH_2); 1.82 (m, 2H, CH_2); 2.34 (s, 3H, CH_3); 2.60 (t, 2H, CH_2); 2.98 (m, 1H, CH(*i*-Pr)); 6.82 (d, 1H, CH(Ph)); 7.04 (dd, 1H, CH(Ph)); 7.21 (dd, 1H, CH(Ph)). EI-MS (m/z): 150, $[C_{10}H_{14}O]^+$; 135, $[C_{10}H_{14}]^+$; 332, $[C_{22}H_{36}O_2]^+$.

2.1.7. 2-Isopropyl-5-methyl ciclohexyl dodecanoate (7)

Menthol (3 g, 0.019 mol), lauric acid (7 g, 0.35 mol) and phosphoric acid 85% (3 drops) are mixed under magnetic stirring at 100 °C under vacuum for 12 h. The crude was poured in chloroform (4 ml) and purified by flash chromatography (silica, *n*-hexane 100%) yielding a colourless oil (1.6 g, 36%). IR (cm^{-1}): 2956m, 2922s, 2853m, 1731s, 1683m, 1635m, 1558w, 1456m, 1369w, 1248w, 1175m, 1149m, 1107w, 1012m, 983m. ^{1}H NMR (400 MHz, $CDCl_3$, ppm, δ): 0.78 (d, 6H, CH_3(*i*-Pr)); 0.86–1.09 (m, 11H, CH); 1.28–1.31 (m, 18H, CH_2); 1.51 (m, 1H, CH); 1.61–1.72 (m, 4H, CH), 1.88 (m, 1H, CH(*i*-Pr)); 2.00 (m, 1H, CH(CHO)); 2.29 (t, 2H, CH_2), 4.70 (td, 1H,CHO). ESI-MS (m/z): 700, $[C_{44}H_{84}O_4Na]^+$; 361, $[C_{22}H_{42}O_2Na]^+$.

2.1.8. Bis(2-isopropyl-5-methyl phenyl) succinate (8)

Oxalyl chloride (1.7 ml, 0.02 mol) was added under nitrogen to a solution of succinic acid (1 g, 0.01 mol) in anhydrous THF (50 ml) in presence of DMF as catalyst (3 drops) and stirred at r.t for 1 h. Volatiles were removed under vacuum, then dry THF (50 ml) was added and thymol (2.85 g, 0.02 mol) was poured in the mixture; the solution was stirred for additional 4 h at r.t.. The volatiles were removed again and ethyl acetate (50 ml) was added. The organic phase was washed twice with water (50 ml) and with brine. Then it was dried with sodium sulphate, filtered and the filtrate was concentrated, giving rise to a pale yellow oil (1.8 g, 52%). IR (cm^{-1}): 3429br, 2961s, 2921m, 2871w, 1709s, 1619m, 1584m, 1518w, 1458m, 1419s, 1375m, 1336w, 1289s, 1259s, 1227s, 1152s, 1112w, 1087m, 1043m, 1005w, 945m, 855w, 807s, 738m. ^{1}H NMR (400 MHz, $CDCl_3$, ppm, δ): 1.26 (d, 12H, CH_3(*i*-Pr)); 2.07 (s, 2H, CH_2); 2.30 (s, 6H, CH_3); 3.19 (m, 2H, CH(*i*-Pr)); 6.60 (s, 2H, CH(Ph)); 6.75 (d, 2H, J = 7.6 Hz, CH(Ph)); 7.10 (d, 2H, J = 7.6 Hz, CH(Ph)). ^{13}C{^{1}H}-NMR (75 MHz, $CDCl_3$, ppm, δ): 20.87 (CH_3); 23.05 (CH_3(i-Pr)); 29.06 (CH_2); 116.03 (CH(Ph)); 121.59 (CH(Ph)); 126.23 (CH(Ph)); 131.48 (CH(Ph));

136.56 (CH(Ph)); 116.03 (CH(Ph)); 152.62 (CO). ESI-MS (m/z): 405, $[C_{24}H_{30}O_4Na]^+$; 363, $[C_{21}H_{24}O_4Na]^+$; 273, $[C_{14}H_{18}O_4Na]^+$.

2.2. Antimicrobial assays

2.2.1. Bacterial strains

The test microorganisms used in this study were isolated in poultry (at farm level). *Clostridium perfringens* (strain 191999/2014) was isolated from broiler chickens affected by necrotic enteritis. *Salmonella typhimurium* (strain 198306/2014) was isolated from viscera of egg-table layers. *Salmonella enteritidis* (strain 226620/20149) was isolated from faeces taken from an egg-table layer farm. *Escherichia coli* serotype O45 (strain 184049/2014) was isolated from broiler chickens affected by avian colibacillosis. The bacterial strains were isolated and identified using standard procedures adopted by IZSLER Forlì and maintained on slants with heart infusion agar (HIA) (Becton Dickinson GmbH, Germany) at +4 °C. To ensure culture purity, before the assays, a sample of culture of *Clostridium perfringens* was streaked on blood agar base (Oxoid Ltd., Basingstoke, UK) with 5% sheep blood and incubated overnight at 37 °C under anaerobic conditions (GENbag anaer, bioMérieux S.A., Marcy l'Etoile, France). For the same reason, samples of cultures of *Escherichia coli*, *Salmonella typhimurium* and *Salmonella enteritidis* were streaked on Hektoen Enteric Agar (Becton Dickinson GmbH, Germany) and incubated overnight at 37 °C. Then, one colony of each strain was grown in Brain Heart Infusion (BHI) broth (Becton Dickinson GmbH, Germany) and incubated overnight at 37 °C (under anaerobic conditions for *Clostridium perfringens*) and then titrated. For this purpose, serial 10-fold dilutions of each suspension were carried out in Buffered Peptone Water (Oxoid Ltd., Basingstoke, UK); each dilution was streaked on specific media and incubated overnight at 37 °C (under anaerobic conditions for *Clostridium perfringens*). Based on the results of the titration each bacterial suspension was diluted in BHI broth to a final concentration of 2 × 106 cfu/mL. Each bacterial suspension was stored at +4 °C until the use as inoculum in the antibacterial test described in the next paragraph. The following quality control strains were included with the tested microorganism: *Escherichia coli* ATCC 25922, *Clostridium perfringens* ATCC 13124, *Salmonella enteritidis* ATCC 49220 and *Salmonella typhimurium* ATCC 23564.

2.2.2. Minimal inhibitory concentration (MIC)

MICs were determined using a micro-broth dilution assay. Sterile 96-well microplates U-bottom were used (Cell Star, Greiner Bio-one, Germany) and 100 μl of fresh BHI broth was added to each well of the plate. Tested compounds were dissolved in distilled water and 5% DMSO (v/v, Merck) to obtain a 20% stock solution and 100 μl of this solution were added to each well of the first row. Then 100 μl were removed from the first row and mixed five times with the broth in the corresponding well of the next row. This doubling dilution was performed in column across the plate until the row "H" (100 μl removed from the row "H" were discharged). Then 100 μl of each bacterial suspension were added to each well. This procedure resulted in a final concentration of the bacterial inoculum of 1 × 106 cfu/mL and in a gradient of two fold dilutions of the tested product ranging from 10% to 0.09% (v/v). All experiments were performed in triplicate. The last three columns of each plate were used as control (growth of the bacterial suspension, absence of bacterial contamination of the BHI broth and of the stock solution of the test product). The microplates were sealed with parafilm and incubated at 37 °C for 24 h (under anaerobic conditions for *Clostridium perfringens*). MIC was defined as the lowest concentration of the test product that prevented visible bacterial growth in the triplicate wells. The determinations were repeated three times and results were expressed as average values.

2.2.3. Minimal bactericidal concentration (MBC)

MBC was determined inoculating the content of non-growth wells on plates of Brain Heart Infusion Agar (Becton Dickinson GmbH, Germany). All plates were incubated for 24 h at 37 °C (under anaerobic conditions for *Clostridium perfringens*). The MBC was recorded as the lowest concentration without bacterial growth.

2.3. Cytotoxicity assay

2.3.1. Human cell line

The HT29 human colorectal carcinoma cell line was obtained from the Northern Ireland Center for Food and Health. Cells were cultured in Dulbecco's Modified Eagle's medium (DMEM) supplemented with 10% fetal bovine serum, 1% L-glutamine and 1% penicillin–streptomycin in a humidified atmosphere at 5% CO_2 and 37 °C. The cultured cells were trypsinized with trypsin/EDTA for a maximum of 5 min and seeded with a subcoltivation ratio of 1:3. Determination of cell numbers and viabilities was performed with the trypan blue exclusion test.

2.3.2. MTS assay

The viability MTS assay (CellTiter96® AQ_{ueous}One Solution Cell Proliferation Assay, Promega Corporation, Madison, WI, USA) was performed to assess the cytotoxicity of the most antimicrobial drugs (carvacrol, thymol and compounds **1**–**4** and **8**) towards HT29 cell line. Tested compounds were dissolved in DMSO to obtain a 10 mM solution. 5×10^3 cells/well were seeded in 96-well plates in 100 μL of DMEM medium without phenol red, supplemented with 1% glutamine, 1% penicillin/streptomycin and 5% fetal bovine serum and then incubated at 37 °C in a humidified (95%) CO_2 (5%) incubator. After 24 h, cells were treated, in quadruplicate, with increasing concentrations of the compounds for further 24 h. The cytotoxicity assay was performed by adding 20 μL of the CellTiter96® AQ_{ueous}One Solution Cell Proliferation Assay directly to the culture wells, incubating for 4 h and then recording the absorbance at 485 nm with a 96-well plate reader (SPECTRAFlour, TECAN).

3. Results and discussion

3.1. Chemistry

The strategy used to overcome the problems of both solubility and volatility of thymol, carvacrol and menthol, is to properly functionalize the aromatic ring (compounds **1**–**4**) or the hydroxyl moiety (compounds **5**–**8**), developing two different classes of derivatives (Fig. 1). The sulfonic derivatives **1** and **2** have been obtained in a solvent free, one pot reaction by using an excess of sulfuric acid (96% in water). Both the products are white, hygroscopic solids and are water soluble. The corresponding potassium salts **3** and **4** were obtained through neutralization of a methanolic solution of the sulfonic acid, with an aqueous solution of KOH. It is worth of note that these syntheses, almost quantitative, do not require complex purification steps.

In the ^{1}H NMR spectra of **1**–**4**, the substitution at the para-position of the phenolic OH can be clearly evinced by the strong modification of the signal pattern in the aromatic region: the two doublets and the singlet of the parent compounds thymol and carvacrol in the range 6.7–7.2 ppm are substituted by two singlets at about 6.7 and 7.4 ppm. Moreover, the signals relative to the methyl and the *i*-propyl substituents are affected in different way by the presence of the sulfonate moiety in **1**, **3** and **2**, **4** respectively. In **1** and the corresponding potassium salt **3**, in fact, the presence of the SO_3 moiety in *orto* to the *i*-propyl implies a shift in the resonances of the CH of about 1 ppm (about 4 ppm vs 3.1 ppm of pure carvacrol), while the methyl signal is little influenced. For **2** and **4**,

on the contrary, the signal more influenced by the substitution is the methyl one (about 2.4 ppm vs 2.1 ppm of the parent compound). In the IR of **1**–**4** it is possible to observe the presence of two strong signals at about 1100 and 1000 cm^{-1}, ascribable to the SO_3 group. Mass data confirmed the proposed stoichiometry. The thermogravimetric analysis on **3** shows a weight loss of 4% at 90 °C attributable to a loss of water and a very sharp step at about 270 °C, corresponding to the decomposition of the product. Compounds **3** and **4** are white, crystalline solids stable at room temperature with a high water solubility (Table 1) and without the pungent odour typical of their precursor oils. These features are particularly attractive from a practical point of view, for potential applications as food and feed additives.

The higher melting points of **3** and **4**, compared with those of the pure EOs, ensure better handling. In fact, the volatility of EOs can involve a loss of the active ingredients during the production processes (dosing, mixing, hot pelleting, transporting and packaging), storage and administration, resulting in final amounts of EOs unavoidably and uncontrollably reduced. Furthermore, higher flash points (lower flammability) result in more safety working conditions.

Another convenient strategy to modify the physico-chemical properties of EOs is represented by the esterification of the phenolic moiety. The choice of the proper ester group could in principle allow to couple the biological properties of EOs with the activity of other types of molecules, such as caprylic acid (C8:0), capric acid (C10:0), and lauric acid (C12:0), medium chain fatty acids whose antimicrobial properties have been demonstrated against various pathogens (Arnfinnsson, Steingri, & Bergsson, 2001; Bergsson & Thormar, 2002; Desbois & Smith, 2010; Jang & Rhee, 2009; Nair, Kumar, Jennifer, & Venkitanarayan, 2004; Thormar, Hilmarsson, & Bergsson, 2006; Wang & Johnson, 1992). A synergic effect can be expected when such types of compounds are coupled with EOs, resulting in enhanced bactericidal effects and consequent reduced quantity of antimicrobials needed for food and feed treatment. With this strategy in mind, laurate esters of carvacrol, thymol and menthol were obtained (compounds **5**–**7**). The synthesis is an esterification between the hydroxyl group of the EO and the carboxyl group of the lauric acid. If in the classic Fisher esterification the alcohol is in excess, conversely in this synthesis the carboxylic acid is in excess over the alcohol. The solvent-free reaction is conducted in presence of an acid catalyst (H_3PO_4) under vacuum, in order to remove water and promote the reaction. For all the substrates the crude products were purified by flash chromatography on silica gel, yielding compounds **5**–**7** as colourless oils. The presence of the alkyl moiety can be inferred in the ^1H NMR spectra by the resonances in the range 1.0–2.6 ppm, while in the IR spectra the stretching of the C=O is evident at about 1700 cm^{-1}. Mass data confirmed the proposed stoichiometries. Contrary to compounds **1**–**4**, **5**–**7** are not water soluble, but their lipophilicity can be very useful, for example for encapsulation in solid lipid particles. The bioactive components dispersed throughout a solid lipid matrix can be applied in the delivery of therapeutic agents, include oral, parenteral, and topical drug delivery (Bondi et al., 2007; Liedtke, Wissing, Mu, & Ma, 2000; Mehnert & Mader, 2001; Radtke & Wissing, 2002).

The synthesis of the symmetric succinate ester of thymol **8** has been carried out by a multistep procedure (Fig. 2): first, the synthesis of the acyl chloride of succinic acid in dry THF was performed, and then, after addition of thymol, the pure product **8** was obtained as an odourless yellowish oil soluble in alcoholic solvents but not in water. Interestingly, esters **5**–**8** qualitatively present an attenuated odour respect to the parent compounds.

3.2. Antimicrobial activity

The *in vitro* antimicrobial activity of the EOs derivatives **1**–**8** has been tested and is presented in Table 2. Both the minimum inhibitory concentration (MIC) and minimum bactericidal concentration (MBC) are shown. MIC and MBC of the control strains showed only slight differences compared to those of the strains tested (Table 2). Compounds **1**–**4** revealed an interesting antimicrobial profile. In particular, the sulfonic acids **1** and **2** are characterized by MIC values in the range 0.37%–0.75% towards the four tested strains. Their potassium salts (**3** and **4**) show good antibacterial activities as well, although slightly lower with respect to their precursors **1** and **2**; against *Clostridium perfringens* compound **3** is active at the lowest concentration (0.37%, Table 2). Even if the antibacterial activities of **1**–**4** are lower to the ones shown by carvacrol and thymol, the remarkable solubility of these compounds in water, compared to the insolubility of the parent compounds, is a matter of great interest. It has to be taken into account, in fact, that the use of thymol and carvacrol as preservatives, directly added to the food or coated in active packaging, is hampered by their both water insolubility and marked odour, which can alter food taste (Calo et al., 2015). The use of derivatives like **1**–**4** could in principle overcome these problems, since they can directly be added to the food or used in coating packaging with better handling and diminished taste modifications. Another important point regards animal nutrition. There is a diffused need to find effective alternatives to the use of antibiotics as growth promoters, since in many countries they have been restricted or banned because of the emergence of resistance bacterial strains via the food chain. The use of EOs and their active principles have demonstrated promising results on animal performance (Liang et al., 2013; Mitsch et al., 2004; Zhaikai et al., 2015), and they represent a very attractive approach, but, again, as feed supplements they present serious limitations: they have stability problems during pelleting processing and their marked odour discourages animal consumption. Compounds **1**–**4**, characterized by low volatility and consequent

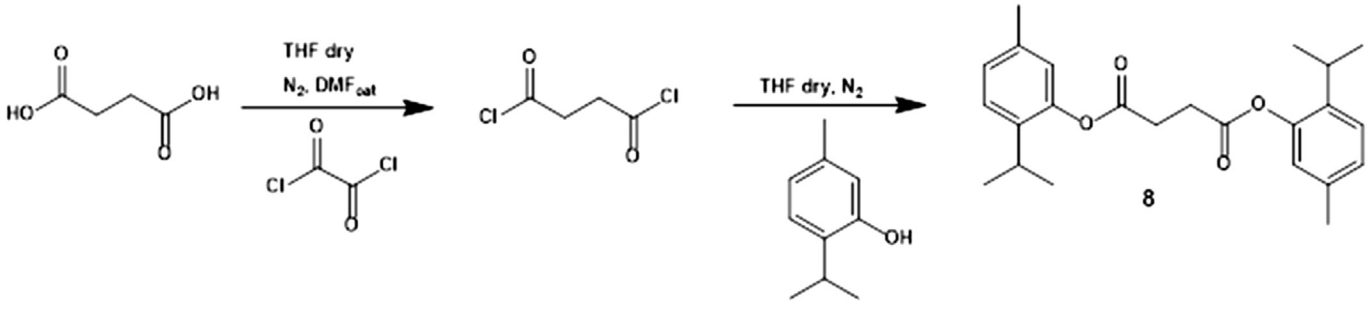

Fig. 2. Multistep synthesis of **8**.

Table 2
MIC and MBC (% v/v) of the essential oils derivatives **1**–**8**.

	Inhibitory activity (%v/v) against bacterial strains															
	Escherichia coli		*Escherichia coli* ATCC 25922		*Salmonella typhimurium*		*Salmonella typhimurium* ATCC 23564		*Salmonella enteritidis*		*Salmonella enteritidis* ATCC 49220		*Clostridium perfringens*		*Clostridium perfringens* ATCC 13124	
	MIC	MBC	MIC	MBC	MIC	MBC	MIC	MBC	MIC	MBC	MIC	MBC	MIC	MBC	MIC	MBC
1	0.75	0.75	0.75	0.75	0.75	0.75	0.75	0.75	0.37	0.37	0.37	0.37	0.37	0.37	0.37	0.37
2	0.75	0.75	0.75	0.75	0.37	0.37	0.37	0.37	0.37	0.37	0.75	0.75	0.37	0.37	0.37	0.37
3	5	5	5	5	1.25	1.25	1.25	1.25	1.25	1.25	1.25	1.25	0.37	0.37	0.37	0.37
4	2.5	2.5	5	5	5	5	5	5	5	5	2.5	2.5	1.25	1.25	1.25	1.25
5	>10	>10	>10	>10	>10	>10	>10	>10	>10	>10	>10	>10	>10	>10	>10	>10
6	>10	>10	>10	>10	>10	>10	>10	>10	>10	>10	>10	>10	>10	>10	>10	>10
7	>10	>10	>10	>10	>10	>10	>10	>10	>10	>10	>10	>10	>10	>10	>10	>10
8	≤0.09	≤0.09	≤0.09	≤0.09	≤0.09	≤0.09	≤0.09	≤0.09	≤0.09	≤0.09	≤0.09	≤0.09	≤0.09	≤0.09	≤0.09	≤0.09
Thymol	≤0.09	≤0.09	≤0.09	≤0.09	≤0.09	≤0.09	≤0.09	≤0.09	≤0.09	≤0.09	≤0.09	≤0.09	≤0.09	≤0.09	≤0.09	≤0.09
Carvacrol	≤0.09	≤0.09	≤0.09	≤0.09	0.37	0.37	0.75	0.75	≤0.09	≤0.09	≤0.09	≤0.09	≤0.09	≤0.09	≤0.09	≤0.09

much less marked odour, can be used instead of thymol and carvacrol as feed supplier and could in principle be better tolerated. Moreover, since they are water soluble, they can be directly used in animal drinking water.

Among all derivatives, the thymol succinate **8** was found to be the more active towards all tested strains, with antibacterial activities analogous to that of the parent compound (MIC and MBC values ≤ 0.09, Table 2). On the contrary, the mono-esters **5**, **6** and **7** did not show significant antimicrobial activity, with MIC ≥ 10%. It is worth noting again that compound **8** has a better organoleptic profile with respect to thymol.

Generally, the EOs possessing the strongest antibacterial properties contain a high percentage of phenolic compounds such as carvacrol and thymol. Both substances appear to make the cell membrane permeable (Lambert et al., 2001). The significance of the phenolic ring itself is demonstrated by the lack of activity of menthol compared to carvacrol (Ultee et al., 2002). This was confirmed in our study, since the MICs values of compound **7** were ≥10% (v/v). Interestingly, for all tested strains, MICs and MBCs are the same, indicating the bactericidal role of these compounds.

Most studies investigating the action of EOs against food spoilage organisms and food borne pathogens agree that, generally, EOs are slightly more active against gram-positive than gram-negative bacteria. In our study, the MICs and MBCs against the gram-positive *Clostridium perfringens* were equal to or less than those observed against the tested gram-negative bacteria. However, it has to be considered that previous *in vivo* studies indicated that the effects of the EOs on the proliferation of *Clostridium perfringens* in the intestines of broiler chickens are only partially due to a direct inhibition of the bacteria: digestive enzymes induced by EOs could also increase nutrient digestibility and improve the regulation and stabilization of the gut microbiota (Mitsch et al., 2004). Moreover, it is known that the chemical composition of EOs from a particular plant species can vary according to the geographical origin and harvesting period. It is therefore possible that variation in composition between batches of EOs is sufficient to cause variability in the degree of susceptibility of gram-negative and gram-positive bacteria (Dorman, Deans, Merr, & Myrtaceae, 2000).

3.3. Cytotoxicity

The good antimicrobial profile of compounds **1**–**4** and **8** allows to envisage the possibility to replace thymol, carvacrol or menthol, actually used as preservatives and in animal nutrition. In order to identify a possible risk for human health, we analyzed their cytotoxic profile on HT-29 human cells. Cytotoxic activity was detected through the MTS assay, a colorimetric method for determining the number of viable cells in proliferation and results are collected in Table 3. In the range of the doses used (1–100 μM), compounds **1**–**4** did not show any antiproliferative effects, with a profile even better of the parent compounds. Carvacrol and thymol, in fact, induced a mild cytotoxicity at the highest dose tested (100 μM). Compound **8** showed the highest antiproliferative effect on HT-29 human cells, inducing a reduction of viability of approximately 50% at 100 μM. Therefore, the sulfonic derivatives and their potassium salts (**1**–**4**) are very promising candidates as novel antimicrobial compounds to be used as food preservatives as well as feed supplement.

Table 3
Antiproliferative effects induced by increasing concentrations of **1**–**4** and **8** (24 h-treatment) on HT-29 human cells, detected by MTS assay. GI% (Growth Inhibition percent). Dose 0: DMSO at the highest concentration tested (1%).

Dose (μM)	GI%						
	Carvacrol	Thymol	1	2	3	4	8
0	100	100	100	100	100	100	100
1	92	100	100	100	100	100	100
5	100	100	97	100	100	100	93
10	88	100	100	100	100	100	100
50	92	100	95	100	100	100	83
100	72	79	100	100	100	100	56

4. Conclusions

The demand for natural alternatives to synthetic additives is rapidly increasing and the replacement, in foodstuffs, of synthetic antimicrobials by EOs and their active principles is getting considerable attention. Moreover, EOs have the potential to act as multifunctional feed supplements, avoiding or limiting the use of antibiotic growth promoters in livestock, with consequent important applications in the animal nutrition field. In the present work, we presented a series of carvacrol, menthol and thymol derivatives with promising MICs and MBCs values against some pathogens causing important foodborne diseases, *i.e. Clostridium perfringens*, *Salmonella typhimurium*, *Salmonella enteritidis* and *Escherichia coli*. In order to identify a possible risk for human health, the most active compounds (**1**–**4** and **8**) were tested for their cytotoxic activity on HT-29 human cells. While **8** showed a not negligible toxicity, **1**–**4** are not cytotoxic, with a profile even better than the parent compounds thymol and carvacrol.

Therefore, the low MICs and MBCs values of compounds **1**–**4**, combined with their water solubility, absence of toxicity towards human cells and improvement of the organoleptic properties

compared to the parent compounds, confirmed the potential use for these derivatives in the food industry for preservation of foodstuffs and increase of shelf life.

Further studies involving the incorporation of these compounds into foodstuffs are in progress. In the same way, further studies are in progress to elucidate the *in vivo* effects of the most active thymol and carvacrol derivatives in reducing the colonization of intestinal pathogenic bacteria and in modulating the microbiota of the gastrointestinal tract.

Notes

The compounds disclosed in this paper are the subject of the pending International Patent Application N. PCT/IB2015/053591.

Acknowledgements

This work was financially supported by Volare&Connecting LLC.

Centro Interdipartimentale di Misure “G. Casnati” of the University of Parma is thanked for instrument facilities.

References

Arnfinnsson, H., Steingri, L., & Bergsson, G. (2001). Killing of gram-positive cocci by fatty acids and monoglycerides. *APMIS, 109*, 670–678.

Arsi, K., Donoghue, A. M., Venkitanarayanan, K., Fanatico, A. C., Blore, P. J., & Donoghue, D. J. (2014). The efficacy of the natural plant extracts, thymol and carvacrol against Campylobacter colonization in broiler chickerns. *Journal of Food Safety, 34*, 321–325.

Bakkali, F., & Idaomar, M. (2008). Biological effects of essential oils – A review. *Food and Chemical Toxicology, 46*, 446–475.

Bergsson, G., & Thormar, H. (2002). Bactericidal effects of fatty acids and monoglycerides on Helicobacter pylori. *International Journal of Antimicrobial Agents, 20*, 258–262.

Bondi, L., Craparo, E., Giammona, G., Cervello, M., Azzolina, A., Diana, P., et al. (2007). Nanostructured lipid carriers-containing anticancer compounds: Preparation, characterization and cytotoxicity studies. *Drugs Delivery, 14*(2), 61–67.

Burt, S. (2004). Essential oils: Their antibacterial properties and potential applications in foods — a review. *International Journal of Food Microbiology, 94*, 223–253.

Calo, J. R., Baker, C. A., Park, S. H., & Ricke, S. C. (2015). Salmonella heidelberg strain responses to essential oil components. *Journal of Food Research, 4*(5), 73–80.

Calo, J. R., Crandall, P. G., O'Bryan, C. A., & Ricke, S. C. (2015). Essential oils as antimicrobials in food systems. A review. *Food Control, 54*, 111–119.

Cherallier, A. (1996). *The encyclopedia of medicinal plants*. London Daniel: Dorling Kindersley Limited.

Desbois, A. P., & Smith, V. J. (2010). Antibacterial free fatty acid: Activities, mechanisms of action and biotechnological potential. *Applied Microbiology Biotechnology, 85*, 1629–1642.

Dorman, H. J. D., Deans, S. G., Merr, L., & Myrtaceae, P. (2000). Antimicrobial agents from plant: Antibacterial activity of plant volatile oils. *Journal of Applied Microbiology, 88*, 308–316.

Goñi, P., López, P., Sánchez, C., Gómez-lus, R., Becerril, R., & Nerín, C. (2009). Antimicrobial activity in the vapour phase of a combination of cinnamon and clove essential oils. *Food Chemistry, 116*(4), 982–989.

Jang, H. I., & Rhee, M. S. (2009). Inhibitory effect of caprylic acid and mild heat on Cronobacter (Enterobacter sakazakii) in reconstituted infant formula and determination of injury by flow cytometry. *International Journal of Food Microbiology, 133*(1–2), 113–120.

Kaur, R., Darokar, M. P., & Ahmad, A. (2014). Synthesis of halogenated derivatives of thymol and their antimicrobial activities. *Medicinal Chemistry Research, 23*, 2212–2217.

Kim, S. A., & Rhee, M. S. (2016). Highly enhanced bactericidal effects of medium chain fatty acids (caprylic, capric and lauric acid) combined with edible plant essential thymol and vanillin against Escherichia coli. *Food Control, 60*, 447–454.

Lambert, R. J. W., Skandamis, P. N., Coote, P. J., & Nychas, G. J. E. (2001). A study of the minimum inhibitory concentration and mode of action of oregano essential oil, thymol and carvacrol. *Journal of Applied Microbiology, 91*, 453–462.

Lang, G., & Buchbauer, G. (2012). A review on recent research results (2008–2010) on essential oils as antimicrobials and antifungals. A review. *Flavour and Fragrance Journal, 27*, 13–39.

Liang, C., Xiaosong, W., Hongmei, J., Yu, H., Mingong, C., Jine, Y., et al. (2013). Review on QTL for milk production traits and application of non-antibiotic feed additives in dairy cattles. *Journal of Food, Agriculture & Environment, 11*(1), 511–515.

Lide, D. R. (1998). *Handbook of chemistry and physics* (87 ed., pp. 3–346). Boca Raton, FL: CRC Press.

Liedtke, S., Wissing, S., Mu, R. H., & Ma, K. (2000). Influence of high pressure homogenization equipment on nanodispersions characteristics. *International Journal of Pharmaceutics, 196*, 183–185.

Lv, F., Liang, H., Yuan, Q., & Li, C. (2011). In vitro antimicrobial effects and mechanism of action of selected plant essential oil combinations against four food-related microorganisms. *Food Research International, 44*(9), 3057–3064.

Mehnert, W., & Mader, K. (2001). Solid lipid nanoparticles production, characterization and applications. *Advanced Drug Delivery, 47*, 165–196.

Mitsch, P., Ko, B., Gabler, C., Losa, R., & Zimpernik, I. (2004). The effect of two different blends of essential oil components on the proliferation of Clostridium perfringens in the intestines of broiler chickens. *Poultry Science, 83*, 669–675.

Nair, M., Kumar, M., Jennifer, J., & Venkitanarayan, K. (2004). Inactivation of Enterobacter sakazakii in reconstituted infant formula by monocaprylin. *Journal of Food Protection, 12*, 2644–2857.

Pesavento, G., Calonico, C., Bilia, A. R., Barnabei, M., Calesini, F., Addona, R., et al. (2015). Antibacterial activity of Oregano, Rosmarinus and Thymus essential oils against Staphylococcus aureus and Listeria monocytogenes in beef meatballs. *Food Control, 54*, 188–199.

Pinheiro, P. F., Costa, A. V., Alves, T. A., Galter, I. N., Pinheiro, C. A., Pereira, A. F., et al. (2015). Phytotoxicity and cytotoxicity of essential oil from leaves of Plectranthus amboinicus, carvacrol, and thymol in plant bioassays. *Journal of Agricultural and Food Chemistry, 63*, 8981–8990.

Radtke, M., & Wissing, S. A. (2002). Solid lipid nanoparticles (SLN) and nanostructured lipid carriers (NLC) in cosmetic and dermatological preparations. *Advanced Drug Delivery, 1*, 131–155.

Suntres, Z. E., Coccimiglio, J., & Alipour, M. (2015). The bioactivity and toxicological actions of carvacrol. *Crit. Rev. Food Sci. Nutr., 55*, 304–318.

Tajkarimi, M. M., Ibrahim, S. A., & Cliver, D. O. (2010). Antimicrobial herb and spice compounds in food. *Food Control, 21*(9), 1199–1218.

Thormar, H., Hilmarsson, H., & Bergsson, G. (2006). Stable concentrated emulsions of the 1-Monoglyceride of capric acid (Monocaprin) with microbicidal activities against the food-borne bacteria Campylobacter, Salmonella, and Escherichia coli. *Applied Environmental Microbiology, 72*(1), 522–526.

Ultee, A., Bennik, M. H. J., Moezelaar, R., Ultee, A., Bennik, M. H. J., & Moezelaar, R. (2002). The phenolic hydroxyl group of carvacrol is essential for action against the food-borne pathogen Bacillus cereus. *Applied Environmental Microbiology, 68*(4), 1561–1568.

Valero, M. F. E. (2006). Synergistic bactericidal effect of carvacrol, cinnamaldehyde or thymol and refrigeration to inhibit Bacillus cereus in carrot broth. *Food Microbiology, 23*(1), 68–73.

Wang, L.-L., & Johnson, E. (1992). Inhibition of Listeria monocytogenes by fatty acids and monoglycerides. *Applied and Environmental Microbiology, 58*(2), 624–629.

Xu, J., Zhou, F., Ji, B., Pei, R., & Xu, N. (2008). The antibacterial mechanism of carvacrol and thymol against Escherichia coli. *Letters in Applied Microbiology, 47*, 174–179.

Yalkowsky, S. H., He, Y., & Jain, P. (2010). *Handbook of aqueous solubility data* (Second edition, p. 710). Boca Raton, FL: CRC Press.

Zhaikai, Z., Sai, Z., Hongliang, W., & Xiangshu, P. (2015). Essential oil and aromatic plants as feed additives in non-ruminant nutrition: A review. *Journal of Animal Science and Biotechnology, 6*, 1–10.

Food and Chemical Toxicology 105 (2017) 498–505

Contents lists available at ScienceDirect

Food and Chemical Toxicology

journal homepage: www.elsevier.com/locate/foodchemtox

A battery of assays as an integrated approach to evaluate fungal and mycotoxin inhibition properties and cytotoxic/genotoxic side-effects for the prioritization in the screening of thiosemicarbazone derivatives

Claudia Zani [a, *], Franco Bisceglie [b, c], Francesco Maria Restivo [b, c], Donatella Feretti [a], Marianna Pioli [b], Francesca Degola [b], Serena Montalbano [b], Serena Galati [b], Giorgio Pelosi [b, c], Gaia V.C. Viola [a], Mauro Carcelli [b, c], Dominga Rogolino [b, c], Elisabetta Ceretti [a], Annamaria Buschini [b, c]

[a] Department of Medical and Surgical Specialities, Radiological Sciences and Public Health, University of Brescia, Italy
[b] Department of Chemistry, Life Sciences and Environmental Sustainability, University of Parma, Italy
[c] Parma Unit, CIRCMSB (Consorzio Interuniversitario di Ricerca in Chimica dei Metalli nei Sistemi Biologici), Italy

ARTICLE INFO

Article history:
Received 14 November 2016
Received in revised form
2 May 2017
Accepted 4 May 2017
Available online 5 May 2017

Keywords:
Aflatoxins
Metal complexes
Antifungal activity
Toxicity
Genotoxicity

ABSTRACT

Aflatoxins represent a serious problem for a food economy based on cereal cultivations used to fodder animal and for human nutrition. The aims of our work are two-fold: first, to perform an evaluation of the activity of newly synthesized thiosemicarbazone compounds as antifungal and anti-mycotoxin agents and, second, to conduct studies on the toxic and genotoxic hazard potentials with a battery of tests with different endpoints. In this paper we report an initial study on two molecules: S-4-isopropenylcyclohexen-1-carbaldehydethiosemicarbazone and its metal complex, bis(S-4-isopropenylcyclohexen-1-carbaldehydethiosemicarbazonato)nickel (II). The outcome of the assays on fungi growth and aflatoxin production inhibition show that both molecules possess good antifungal activities, without inducing mutagenic effects on bacteria. From the assays to ascertain that the compounds have no adverse effects on human cells, we have found that they are cytotoxic and, in the case of the nickel compound, they also present genotoxic effects.

1. Introduction

Aflatoxins are a class of mycotoxins produced principally by two species of *Aspergillus*, namely *A. flavus* and *A. parasiticus*. In particular, depending on environmental conditions, such as hot and humid climates, these fungi proliferate and can produce aflatoxins (IARC, 2012). The proliferation of these molds has a dramatic influence on the bioeconomy since they grow on carbon-rich substrates like polysaccharides. Consequently, they are commonly found on starch-rich substrates, such as cereals, and their presence causes serious economic losses. Moreover, residues of aflatoxin and their metabolites can enter the food chain, since they can also be present in the meat, offals and eggs of animals fed with aflatoxin contaminated fodder (Richard, 2007). The presence of aflatoxins in food is known to be hazardous for human and animal health because it is at the origin of mutagenic and teratogenic effects, and consequently of tumorigenicity, and also of estrogenic, gastro-enteric, renal and hepatic disorders. In addition, it has been demonstrated that some mycotoxins induce immunodeficiency and reduce the resistance to infective diseases (Marin et al., 2013).

Among good agricultural practices, the use of synthetic fungicides is still the most effective way to intervene. A few molecules are known to inhibit, to a major or minor extent, aflatoxin biosynthesis, but their mechanism of action is still poorly understood (Holmes et al., 2008). It seems that the biosynthesis of mycotoxins is strictly connected to the redox equilibrium within the cell, and that the production of reactive oxygen species (ROS) by the

* Corresponding author. Department of Medical and Surgical Specialities, Radiological Sciences and Public Health, University of Brescia, Italy Viale Europa 11, 25123 Brescia, Italy.
E-mail address: claudia.zani@unibs.it (C. Zani).

http://dx.doi.org/10.1016/j.fct.2017.05.008
0278-6915/

mold and by the host, during the mold/plant interactions, is able to modulate the aflatoxin synthesis pathway (Holmes et al., 2008). Moreover, some studies highlight the importance of the role played by metal ions in the aflatoxin biosynthesis (Cuero and Ouellet, 2005).

The aim of our study is the evaluation of the antifungal activity of compounds possessing a thiosemicarbazone moiety. These substances are known to present significant inhibition activity on proliferating cells (Beraldo and Gambino, 2004; Bisceglie et al., 2014; Pervez et al., 2008) and also their metal complexes show an improved biological activity (Pelosi, 2010; Parrilha et al., 2011; Al-Amiery et al., 2012).

The new compounds we have been synthesizing must be not only efficient in their antifungal activity, but also harmless to the environment, to the ecosystems, and ultimately to human beings. The use of biocides has the undoubted advantage to preserve food, but may represent a risk to human health since consumers could be exposed to residues in food. Today, the use of chemical pesticides is strictly regulated and the removal of the most hazardous chemicals from the market is highly recommended and encouraged (Pal and Gardener, 2006). In recent years, the need to develop disease control measures has become a priority for scientists worldwide and, although restrictions have been imposed to protect food quality and the environment, chemicals are still our main resource to prevent food crop diseases.

The European Food Safety Authority (EFSA) reported that pesticide residues were detected in 46.7% of the food samples analyzed throughout the European Union in 2008. Residues of at least two pesticides were found in 27% of the samples analyzed, among which one-third contained residues of more than four pesticides (EFSA, 2010). Yet the risk assessment of pesticides for humans is based on the hazard characterization of individual active molecules, without taking into account possible combined effects of multiple residues in the diet. Today, more than 300 active substances are used to protect crops. A large number of studies have been published on the possible harmful effects of pesticides for human health especially among occupational exposed subjects (Bolognesi et al., 2011; Weichenthal et al., 2010), but only limited evidence exists regarding the risk for the general population through the consumption of contaminated food.

Pesticides residues which contaminate food vegetables could also present mutagenic/genotoxic effects on different cell types (Feretti et al., 2007; Altintop et al., 2012, 2016; Dos Santos et al., 2016), may act as endocrine disrupting chemicals and could affect reproductive activity in human (Chiu et al., 2015). Chronic exposure to low levels of pesticide residues may affect human health and in particular children can be exposed to pesticides residues by dietary ingestion because they eat more food per body mass than an adult and their diet is often rich in food contained high levels of pesticides residues, such as fruit juices or baby foods. For this reason, the second step of our research was to evaluate the harmlessness of these molecules and we assessed the toxic and genotoxic activities.

Until now, alternative methods to the use of chemicals have not given satisfactory results. It is in this perspective that our research is aimed at the identification of new compounds, based on natural molecules and functionalized so as to make them ligands for biometal ions, in the hope to obtain species highly active already at extremely low concentrations but harmless to the health of animals and to the environment. To this aim, we have created a new study approach and optimized a protocol that allows us to synthesize and rapidly evaluate the activity of newly synthesized molecules using a battery of assays, as described in Zani et al. (2015) and to prioritize molecules that deserve further studies. In this paper, we report the initial outcomes of our study on two molecules that have shown interesting results: S-4-isopropenylcyclohexen-1-carbaldehydethiosemicarbazone and its metal complex, bis(S-4-isopropenylcyclohexen-1-carbaldehydethiosemicarbazonato)nickel (II).

2. Materials and methods

2.1. Synthesis and characterization of S-4-isopropenylcyclohexen-1-carbaldehydethiosemicarbazone (molecule V)

Scheme 1 describes the synthesis of S-4-isopropenylcyclohexen-1-carbaldehydethiosemicarbazone that, from here on, will be referred to as molecule V.

Molecule V was synthesized following this procedure: 0.18 g of thiosemicarbazide (1.9 mmol) were dissolved in 20 mL of EtOH at reflux temperature. An equimolar amount of perillaldehyde (0.35 mL) was subsequently added dropwise. The resulting solution was left under magnetic stirring and refluxing for 14 h, and monitored by TLC (CH_3OH: CH_3CH_2OH = 2:1; Rf = 0.78). The pale yellow solution was then poured into a crystallizer, left evaporating at room temperature and a yellow product was isolated as crystals and characterized as reported below:

Yield: 85%.
M.P.: 147 °C.

Elemental Analysis % (theoretical): C 59.49 (59.10), H 7.46 (7.61), N 18.29 (18.80), S 14.49 (14.35), in agreement with a molecular weight of 223.35 corresponding to the anhydrous form of the ligand with formula $C_{11}H_{17}N_3S$.

IR (cm^{-1}): 3411 (vs) ν NH_2, 3159 (vs) ν NH, 2919 (w) ν CH_2, 1592 (vs) ν C=C, 1529 (vs) ν CN, 950 (m) ν C=S, 886 (s) ν C=S.
UV-Vis (CH_3OH, 10^{-5} M): ε_0 (294 nm) = 17381; 294 nm: $n \rightarrow \pi^*$; 243 nm: $n \rightarrow \sigma^*$.
MS m/z (rel. int.%): 246 ($M + Na^+$; 85), 224 (MH^+; 100), 198 (MH^+-C_2H_2; 20).
^1H NMR ($CDCl_3$; 300 MHz, ppm): 9.74 (1H, s, NHCS), 7.27 (1H, t, J = 6.0 Hz, CH=N), 7.08 and 6.36 (2H, 2 br s, 1H each, NH_2), 6.88 (1H, m), 2.6 (2H,m), 2.2 (2H, m), 1.90 (3H, s), 1.40 (1H, m).

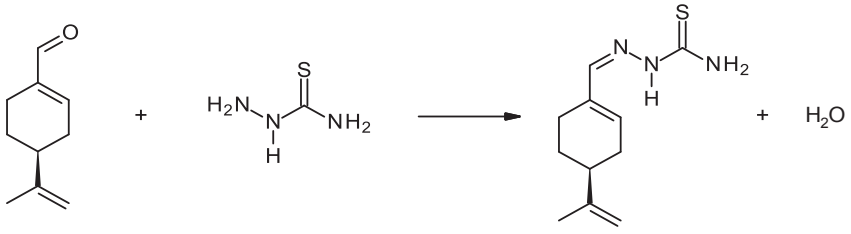

Scheme 1 Synthesis of S-4-isopropenylcyclohexen-1-carbaldehydethiosemicarbazone (molecule V)..

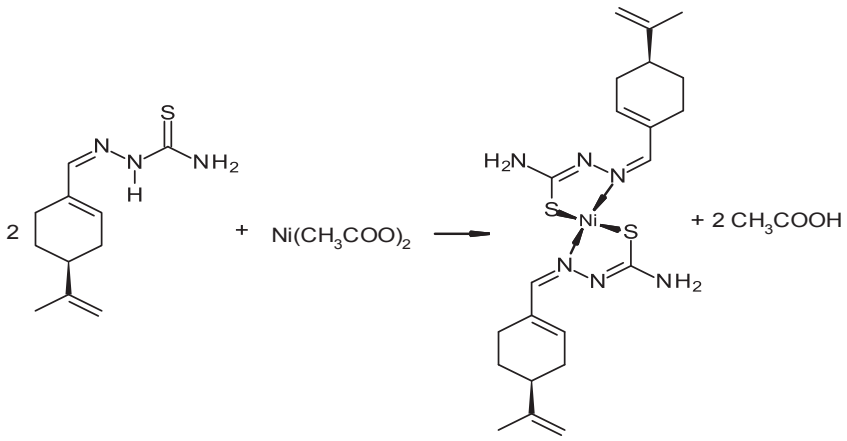

Scheme 2 Synthesis of bis(S-4-isopropenylcyclohexen-1-carbaldehydethiosemicarbazonato)nickel(II) (molecule T)..

2.2. Bis(S-4-isopropenylcyclohexen-1-carbaldehydethiosemicarbazonato)nickel(II) (molecule T)

Scheme 2 depicts the synthesis of the metal complex S-4-isopropenylcyclohexen-1-carbaldehydethiosemicarbazonate nickel (II) that will be quoted as molecule T.

Molecule T was synthesized using the following procedure: 0.57 g of molecule V (2.55 mmol) were dissolved in 50 mL of EtOH at reflux temperature. Then, 0.32 g of $Ni(CH_3COO)_2{\cdot}4H_2O$ (1.275 mmol) previously dissolved in 10 mL of water, were added to the ligand solution. The resulting mixture was left at reflux temperature under magnetic stirring for 4 h. The solution became dark brown and was poured into a crystallizer and left evaporating at room temperature. A homogeneous brown powder was isolated and characterized as reported below.

M.P.: 195 °C.

Elemental Analysis % (theoretical): C 52.68 (52.30), H 6.44 (6.81), N 16.51 (16.60), S 12.85 (12.72), in agreement with a molecular weight of 501.39 corresponding to the hypothesized stoichiometry.

IR (cm^{-1}): 3415 (vs) ν NH_2, 2920 (w) ν CH_2, 1592 (vs) ν C=C, 1515 (vs) ν CN, 946 (m) ν C=S, 871 (s) ν C=S.
MS m/z (rel. int.%): 554 ($M + Na^+$; 100).
^1H NMR ($CDCl_3$; 300 MHz, ppm), 7.05 (1H, t, CH=N), 7.05 and 6.34 (2H, 2 br s, 1H each, NH_2), 6.85 (1H, m), 2.62 (2H,m), 2.25 ppm (2H, m), 1.88 (3H, s), 1.40 (1H, m).

2.3. Evaluation of the effects of molecules V and T on in vitro mycelium growth

Strains of *A. flavus* used in this work were previously described in Degola et al. (2015). Conidia suspensions were obtained from 10-day YES-agar [2% (w/v) yeast extract (Difco, Detroit, MI), 5% (w/v) sucrose (Sigma, St Louis, MO), 2% (w/v) agar (Difco)] cultures incubated at 28 °C; conidia concentration (quantified by OD_{600}) and viability (>90%) were determined according to Degola et al. (2011). Conidial germination rate and post-germination hyphal outgrowth were assessed by analyzing changes in optical density of spore suspensions over time: in a 96 well microtiter plate (Sarstedt, Newton, NC, USA) 10^4 spores were inoculated in a final volume of 200 μL of YES liquid medium amended with 100 μM of V and T molecules and incubated at 28 °C. The optical density at 620 nm (OD_{620}) was recorded for each well between 38 and 46 h with a microplate reader (MULTISKAN EX, Thermo Electron Corporation, Vantaa, Finland) without shaking. Samples were inoculated in quadruplicate. The “Past 3.x” software was used to analyse statistical differences between samples. Analysis of variance was performed by Levene test. When p-values ($p < 0.05$) were obtained, Kruskal-Wallis test was performed.

2.4. Evaluation of the effect of molecules V and T on aflatoxin production

A high throughput procedure performed in a multiwell plate was used to assess aflatoxin accumulation in a coconut-milk derived medium (CCM) (Degola et al., 2011, 2012). The effect on aflatoxin biosynthesis was assessed by the above mentioned microplate fluorescence-based procedure as described in Degola et al. (2015). Briefly, suspensions of conidia were diluted to the appropriate concentrations and brought to the final concentration of 5×10^2 conidia/ well; cultures were set in a final volume of 200 μL/well of CCM medium added with V and T molecules. The plates were incubated in the dark under stationary conditions for up to 6 days at 25 °C. Aflatoxin accumulation was monitored by fluorescence emission determination: readings were performed directly from the bottom of wells of the culture plate with a microplate reader (TECAN SpectraFluor Plus, Männedorf, Switzerland) using the following parameters: $\lambda_{ex} = 360$ nm; $\lambda_{em} = 465$ nm; manual gain = 83; lag time = 0 μs; number of flashes = 3; and integration time = 200 μs?

The “Past 3.x” software was used to analyse statistical differences between samples. Analysis of variance was performed by Levene test. When p-values ($p < 0.05$) were obtained, Kruskal-Wallis test was performed.

2.5. Cytotoxicity of molecules V and T on human cells

The antiproliferative effects of the V and T molecules were evaluated by MTS assay (Cell Titer96® AQ_{ueous}One Solution Cell Proliferation Assay, Promega Corporation, Madison, WI, USA) towards different human cell lines: Hs27 foreskin fibroblasts, CRL1790 colon epithelial and U937 histiocytic lymphoma cells.

Hs27 (ATCC, CRL1634) and CRL 1790 (ATCC, CCD 841 CoN) were obtained from the American Type Culture Collection (ATCC). U937 cells were obtained from the American Tissue Culture Collection (Rockville, MD). Normal (Hs27 and CRL1790) and tumor (U937) cells were cultured in Dulbecco's Modified Eagle's medium (DMEM) and RPMI-1640 medium respectively, media were

supplemented with 10% (v/v) fetal bovine serum, 1% L-glutamine (2 mM) and 1% penicillin (100 units mL^{-1})/streptomycin (100 μg mL^{-1}). Hs27 and CRL1790 cells were used between passage numbers 5 and 20. Cells were maintained in a humidified atmosphere at 5% CO_2 and 37 °C and culture medium was refreshed every two or three days during sub-culturing.

The cytotoxicity was evaluated according to the following method: 5×10^3 cells/well were seeded in 96-well plates in 100 μL of medium without phenol red, supplemented with 1% glutamine, 1% penicillin/streptomycin and 5% fetal bovine serum and then incubated at 37 °C in a humidified (95%) CO_2 (5%) incubator. After 24 h, cells were treated, in quadruplicate, with increasing concentrations of the molecules in the range 0.5–100 μM for further 24 h. The assay was performed by adding 20 μL of the CellTiter96® AQ_{ueous}One Solution Cell Proliferation Assay directly to the culture wells, incubating for 4 h and then recording the absorbance at 485 nm with a 96-well plate reader (TECAN SpectraFluor Plus, Männedorf, Switzerland).

MTS assay was performed to identify GI_{50} value, that is the concentration of drug that causes a 50% reduction of cell growth.

2.6. Genotoxicity of molecules V and T on human cells

To assess primary DNA damage the alkaline version of Comet assay was performed with U937 cells as described in Buschini et al. (2009). Briefly, the cells were seeded at a concentration of 1×10^5 cell/mL in 24-well plates in 1 mL of medium, supplemented with 1% glutamine, 1% penicillin/streptomycin and 10% fetal bovine serum and then incubated at 37 °C in a humidified (95%) CO_2 (5%) incubator. After 24 h cells were treated, in duplicate, with increasing concentrations of the molecules in the range 25–100 μM for 1 and 24 h. After treatment, determination of cell numbers and viabilities were performed with the trypan blue exclusion method. Only the treatments that had a viability higher than 70% have been processed in the Comet assay. Positive and negative controls were represented by ethylmethanesulfonate (EMS), 2 mM, and DMSO, 100 μM, respectively. DNA was stained with 75 μL ethidium bromide (10 μg/mL) before the examination at 400 × magnification under a Leica DMLS fluorescence microscope (excitation filter BP 515–560 nm, barrier filter LP 580 nm), using an automatic image analysis system (Comet Assay IV – Perceptive Instruments Ltd, UK).

The "IBM SPSS Statistics 24" software was used to analyse statistical differences between samples. The mean values from the repeated experiments were used in a one-way analysis of variance (ANOVA). If significant F-values ($p < 0.05$) were obtained, Student's *t*-test (Bonferroni's version) was performed.

2.7. Mutagenicity of molecules V and T

The V and T molecules were dissolved in a compatible solvent (DMSO) and assayed with the Salmonella/microsome test (Ames test) at increasing doses (0.1, 1, 10, 50, 100 μM/plate), with *S. typhimurium* TA98 and TA100 strains, with and without metabolic activation (S9 mix) to highlight the presence of indirect and direct mutagenic activity. The experimental procedure was the standard plate incorporation method (Maron and Ames, 1983). Salmonella TA98 strain detects frame-shift mutagens and TA100 strain responds to base-pair substitution. According to what has been reported in the review of Mortelmans and Zeiger (2000) we tested the molecules only with strains TA98 and TA100 because it was considered as a first tier approach to be sufficient to identify approximately 90% of the mutagens. Moreover these strains are the most widely used for environmental studies (APHA, 2012).

Positive controls were 2-nitrofluorene (10 μg/plate) and sodium azide (10 μg/plate) for TA98 without S9 and TA100 without S9, respectively, and 2-aminofluorene (20 μg/plate) for both strains with S9. DMSO was tested as the negative controls. The data obtained are presented as revertants per plates computed by means of two replicates with their relative standard deviation. Moreover, the results were expressed as mutagenicity ratio (RM) dividing the revertants/plate by spontaneous mutation rate. Minimum significant ratio was used as a statistical parameter to characterise the fold-change between different doses tested of molecules. The results of the test were considered positive if two consecutive dose levels or the highest non-toxic dose level produced a response at least twice that of the solvent control and at least two of these consecutive doses showed a dose-response relationship (APHA, 2012; Mortelmans and Zeiger, 2000).

3. Results

3.1. Antifungal and antimycotoxigenic activities of molecules V and T

The data reported in Table 1 show that molecule V possesses a good growth inhibitory activity. In fact, we recorded a decrease of 48.7% in mycelial growth compared to the control at the concentration of 50 μM and contextually, a decrease of mycotoxin accumulation of about 78% (compared to control). Increasing the concentration of molecule V up to 100 μM, both antifungal and antimycotoxigenic activities increased.

Differently from V, its nickel complex T showed a very limited activity on mycelia growth: 4.6% and 12.8% inhibition, at 50 μM and 100 μM, respectively, compared to control. Surprisingly, T displayed a comparable or even higher efficacy on preventing toxin accumulation (85% and 90% inhibition at 50 μM and 100 μM, respectively) when compared to V. Concentrations of thiosemicarbazone molecules over 100 μM were not taken into account for fungi treatments, since an inhibitory effect of the solvent (DMSO) was observed on both mycelium growth and aflatoxin production.

3.2. Cytotoxicity of molecules V and T on human cells

To test cytotoxic effects of the new molecules we selected normal cell lines that represent the different routes of exposure by which this kind of chemicals can come in contact with, and/or enter human bodies by epidermal contact (Hs27) and ingestion (CRL1790). In addition, we have also used a tumoral cell line (U937), because it represents a good cell model used worldwide to identify cytotoxicity of drugs.

Both molecules, V and its nickel complex T, induced a stronger antiproliferative activity on normal cells (Hs27 and Crl1790) compared to tumor cells (U937) (Fig. 1). Hs27 cells, human foreskin fibroblasts, showed the major sensitivity to the tested molecules. The IC_{50} induced by V resulted 34 μM for Hs27 and 71 μM for Crl1790; it is noteworthy that the proliferative activity of Hs27 cells was strongly reduced starting from the dose 5 μM. The IC_{50} induced by T resulted to be 35 μM for Hs27 and 49 for Crl1790; a mild

Table 1
Antifungal and anti-aflatoxigenic activities of V and T molecules expressed respectively as mean percentage inhibition of growth and of aflatoxin production (in comparison with non-treated controls; mean ± SD). Statistical differences between V and T were reported.

	Inhibition of mycelium growth (%)		Inhibition of aflatoxin production (%)	
	50 μM	100 μM	50 μM	100 μM
V	48.3 ± 7.2*	75.5 ± 4.7*	71.3 ± 3.5*	86.7 ± 1.6
T	4.5 ± 1.9	11.8 ± 2.8	84.5 ± 1.8	89.6 ± 6.8

*$p < 0.05$.

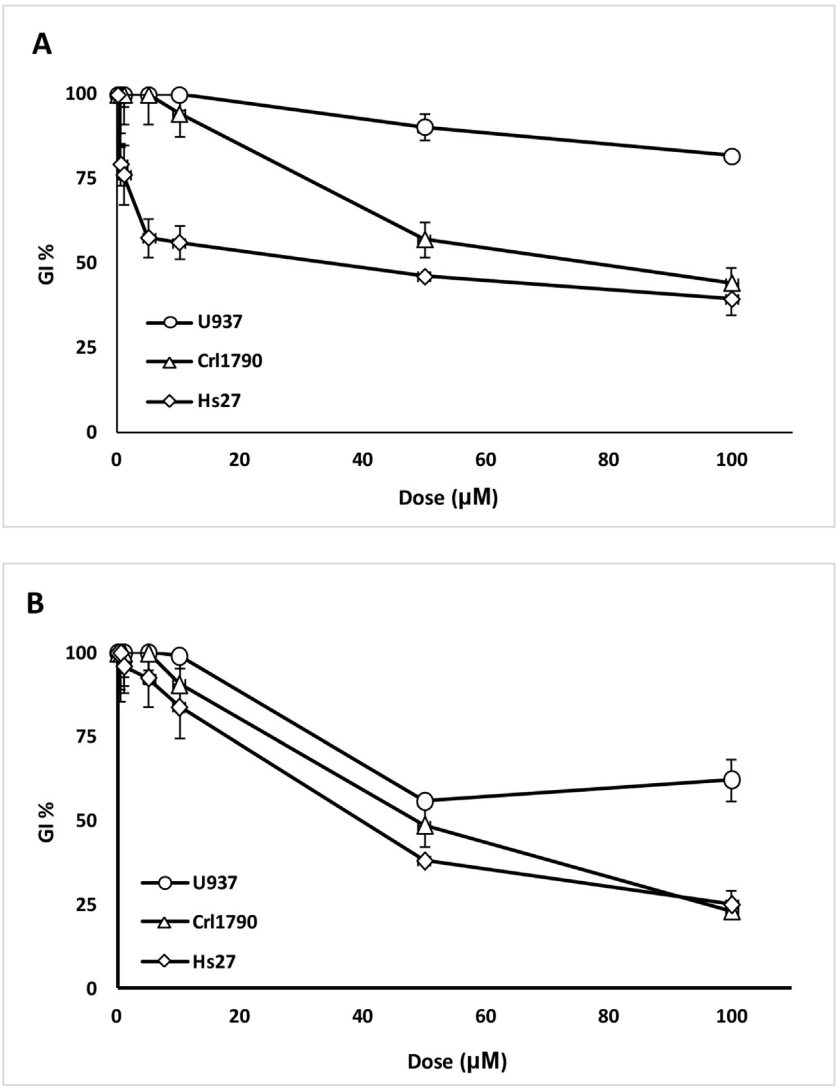

Fig. 1. Antiproliferative activity detected by MTS assay on human cell lines (Hs27, Crl1790, U937) treated for 24 h with V (A) or T (B). GI%: percent of growth inhibition.

antiproliferative activity was detected also on U937 cells, at the highest tested concentration (100 μM) the growth inhibition was around 55%.

3.3. Genotoxicity of molecules V and T on human cells

To identify if the newly synthesized molecules were able to induce subtoxic DNA alterations, their DNA damaging activity was assessed at different time of exposure (1 h and 24 h) through the Comet assay. We performed the alkaline version of Comet Assay on U937 cells, a good cell model used worldwide to identify genotoxic activity of drugs. This cell line showed to be less sensitive than normal cells to the toxic effects of the new molecules and for this reason was chosen to detect the subtoxic effects on DNA in human cells. No genotoxicity was detected on U937 cells treated with molecule V at both exposure times (Fig. 2). Molecule T, after 1 h treatment, induced a significant dose dependent increase in the tail intensity percentage (TI%) (ANOVA, $p < 0.001$), without perturbing cell viability. After 24 h, no genotoxic activity was detected but the 100 μM dose induced a remarkable cytotoxic effect (Fig. 2). A severe DNA damage and/or an incomplete or altered repair could produce cytotoxic effects leading to cell death.

3.4. Mutagenicity of molecules V and T

In Table 2, the results of mutagenicity test carried out on V and T molecule are reported using TA98 and TA100 Salmonella strains expressed as number of revertants for plate (mean values ± SD) and mutagenicity ratio (RM). The results were negative at all doses tested and did not show any mutagenic activity. In detail, both molecules induced neither frameshift nor base-pair substitution point mutations in *S. typhimurium* TA98 and TA100 strains, respectively, with and without metabolic activation (±S9).

4. Discussion

Thiosemicarbazones are molecules known to present a significant inhibition activity on proliferating cells (Beraldo and Gambino, 2004; Pervez et al., 2008; Bisceglie et al., 2014) and their metal complexes systematically show improved biological activity (Parrilha et al., 2011; Pelosi, 2010; Al-Amiery et al., 2012; Kljun et al., 2014). Their antifungal properties have also been reported in the literature (Beraldo and Gambino, 2004), but their effects on mycotoxin production is still a poorly investigated aspect (Degola et al., 2015). On this basis, we have envisaged the synthesis of

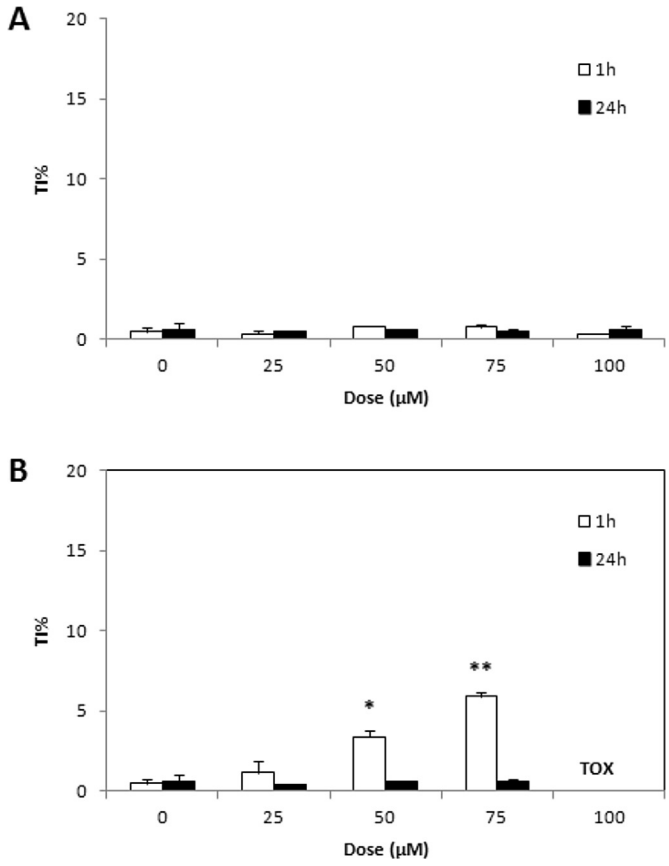

Fig. 2. Genotoxicity activity of V (A) and T (B) molecules using alkaline Comet assay on U937 cells treated for 1 h and 24 h. As positive control was used EMS (2 mM): TI $\%_{1h} = 4.26 \pm 1.32$; $TI\%_{24h} = 45.14 \pm 2.00$. TOX: viability ≤70% TI%: percentage of tail intensity. *$p < 0.05$; ** $p < 0.01$.

new molecules obtained from natural substances with mild antifungal properties, by functionalization with the thiosemicarbazide moiety in order to make them able to bind metal ions.

In this work, two molecules, namely V, which is the parent thiosemicarbazone ligand, and T, the corresponding nickel complex, were synthesized and tested for their antifungal and anti-mycotoxigenic activities, and subsequently for their cytotoxic and genotoxic/mutagenic effects.

Our study has shown that the nickel complex (molecule T) is a good aflatoxin production inhibitor, but quite unexpectedly it is less effective than the parent organic molecule (Table 2) in inhibiting mycelium growth. As far as these two properties are concerned, both molecules could in principle be used as antifungal products, but candidate hits must be not only efficient, but also harmless to the environment, the ecosystems, and ultimately to human beings. To this aim, we tested the antiproliferative activity of molecules V and T on three human cell lines (Hs27, CRL1790, U937) representative of tissues with which the compounds could come in contact. The results for both molecules showed a high cytotoxicity on normal cell lines (Hs27, CRL1790). Molecule V showed no genotoxic activity in the Comet assay on human cell lines and no mutagenic activity in Ames test on bacteria. The nickel complex (T), already at the dose of 50 μM (the first dose tested for antifungal activity), induced a 50% cell growth inhibition in normal cell lines. Molecule T did not induce gene mutation on bacteria, but it was able to produce DNA damaging effects on U937 cells. This behavior is quite similar to the toxicological activity of other nickel tiosemicarbazones already found by the authors (Buschini et al., 2009).

Table 3 qualitatively summarizes all results obtained in tests with different end-points. Based on these results, we can conclude that even though molecules V and T present a remarkable effectiveness as regards their antifungal activity, they cannot be considered "safe" and therefore, as such, must be discarded. Nevertheless, these findings open up the way to the design of similar molecules equally effective, but without side-effects on biological processes and/or organisms. In addition, these molecules could also be modified to study the effects of the molecular shape on the mechanisms of toxin biosynthesis, and this could allow to find more specific inhibitors or new strategies to fight mycotoxin contamination of food and feed commodities.

Thiosemicarbazones derivates represent very attractive molecules for a great variety of biological applications not only in the agronomic field, but also in medicine for their pharmacological activities (Altintop et al., 2012, 2015; Dos Santos et al., 2016). To our knowledge, many studies showed good anti-mycotic activity of thiosemicarbazones derivates for human pathogens, but only a few studies examined their mutagenicity and citotoxicity (Altıntop et al., 2016) and their potential use for agronomic applications (Degola et al., 2015).

The direct control of mycotoxin-producing fungi by using synthetic fungicides is still the most effective way to intervene, but the extensive use of fungicides generates long term residues in food and in the environment. To date the consumption of vegetables is the major source of non-occupational pesticide exposure for humans. Many studies have shown that low levels of pesticide exposure is associated with an increased risk of cancer and other chronic diseases (Fortes et al., 2013). On the other hands, aflatoxin

Table 2
Mutagenicity of V and T molecules evaluated with TA98 and TA100 (±S9) strains in Ames test expressed as number of revertants/plate (mean ± SD) and mutagenicity ratio (MR).

Samples	DOSE (μM/plate)	TA 98-S9		TA98 + S9		TA100-S9		TA100 + S9	
		mean ± SD	MR	mean ± SD	MR	mean ± SD	MR	mean ± SD	MR
V	0.1	19.5 ± 2.1	0.9	37.5 ± 6.4	1.2	117.5 ± 10.6	1.2	93.0 ± 0.0	0.9
	1	24.0 ± 4.2	1.1	42.0 ± 14.1	1.3	89.0 ± 2.8	0.9	115.0 ± 4.2	1.1
	10	19.5 ± 3.5	0.9	40.0 ± 5.7	1.3	105.0 ± 5.7	1.0	113.0 ± 18.4	1.1
	50	15.0 ± 0.0	0.7	35.0 ± 7.1	1.1	99.5 ± 3.5	1.0	104.5 ± 17.7	1.0
	100	20.5 ± 6.4	1.0	35.5 ± 0.7	1.1	103.5 ± 3.5	1.0	112.5 ± 3.5	1.1
T	0.1	20.0 ± 1.4	0.9	24.5 ± 0.7	0.8	100.5 ± 14.8	1.0	113.0 ± 24.0	1.1
	1	18.0 ± 1.4	0.8	33.5 ± 2.1	1.1	109.0 ± 18.1	1.1	118.5 ± 3.5	1.2
	10	16.5 ± 6.4	0.8	33.5 ± 0.7	1.1	92.0 ± 2.8	0.9	99.0 ± 9.9	1.0
	50	30.5 ± 10.6	1.4	31.0 ± 9.9	1.0	110.5 ± 0.7	1.1	110.5 ± 10.6	1.1
	100	23.0 ± 4.2	1.1	25.0 ± 5.7	0.8	97.5 ± 3.5	1.0	123.5 ± 9.2	1.2
Negative Control		21.4 ± 7.5		32.0 ± 8.5		102.0 ± 13.1		102.0 ± 8.8	

Positive controls for TA98 (±S9) and TA100 (±S9): >1000.

Table 3
Summary of the results obtained in tests with different end-points.

Molecules	Inhibition of mycelium growth	Inhibition of aflatoxin production	Cytotoxicity#		Genotoxicity	Mutagenicity
			Normal cells	Tumour cells		
V	+	+	+	-	-	-
T	-	+	+	-	+	-

+ = positive results in test; - = negative results in test.
# a positive results was identified when GI_{50} was <100 μM.

contamination of crops is a significant health problem and efficacy and safety aspects have to be reconciled. Molecules more effective but less toxic for health and environment are continuously studied to control mycelium growth and aflatoxin production (Yang et al., 2016). The use of natural molecules and their chemical analogues is desirable as crop protective agents to promote food quality and reduce the health risks to consumers.

To sum up, this research utilized a new approach for the evaluation of the antifungal activity and aflatoxin inhibition properties of new molecules and for the study of their toxicity (Zani et al., 2015) by means of a battery of tests on human and bacterial cells with different genetic end-points. It allowed us also to assess the potential risks related to the use of these new molecules. It must also be stressed that this approach was in line with the requirements of European Directive 2010/63/EU on the use of alternative methods to animals models in toxicological studies.

Competing interests

The authors declare that they have no competing interests.

Authors' contributions

The authors contributed equally to this work. All authors have taken part in the academic discussions of the manuscript's content. All authors have approved the final version.

Acknowledgements

We are grateful to Cariplo Foundation for funding this study, Grant N. 2014-0555.

Transparency document

Transparency document related to this article can be found online at http://dx.doi.org/10.1016/j.fct.2017.05.008

References

Al-Amiery, A.A., Kadhum, A.A., Mohamad, A.B., 2012. Antifungal and antioxidant activities of pyrrolidonethiosemicarbazone complexes. Bioinorg. Chem. Appl. 2012, 795812. http://dx.doi.org/10.1155/2012/795812.

Altıntop, M.D., Atlı, Ö., Ilgın, S., Demirel, R., Özdemir, A., Kaplancıklı, Z.A., 2016. Synthesis and biological evaluation of new naphthalene substituted thiosemicarbazone derivatives as potent antifungal and anticancer agents. Eur. J. Med. Chem. 108, 406–414. http://dx.doi.org/10.1016/j.ejmech.2015.11.041.

Altıntop, M.D., Özdemir, A., Turan-Zitouni, G., Ilgın, S., Atlı, Ö., Demirel, R., Kaplancikli, Z.A., 2015. A novel series of thiazolyl-pyrazoline derivatives: synthesis and evaluation of antifungal activity, cytotoxicity and genotoxicity. Eur. J. Med. Chem. 92, 342–352. http://dx.doi.org/10.1016/j.ejmech.2014.12.055.

Altıntop, M.D., Özdemir, A., Turan-Zitouni, G., Ilgın, S., Atlı, Ö., İşcan, G., Kaplancıklı, Z.A., 2012. Synthesis and biological evaluation of some hydrazone derivatives as new anticandidal and anticancer agents. Eur. J. Med. Chem. 58, 299–307. http://dx.doi.org/10.1016/j.ejmech.2012.10.011.

APHA, 2012. Standard Method for the Examination of Water and Wastewater, 1360 pp. ISBN 978-087553-013-0, twenty-second ed. American Public Health Association, American Water Works Association, Water Environment Federation, Washington DC, USA.

Beraldo, H., Gambino, D., 2004. The wide pharmacological versatility of semicarbazones, thiosemicarbazones and their metal complexes. Mini-Rev. Med. Chem. 4, 31–39.

Bisceglie, F., Pinelli, S., Alinovi, R., Goldoni, M., Mutti, A., Camerini, A., Piola, L., Tarasconi, P., Pelosi, G., 2014. Cinnamaldehyde and cuminaldehyde thiosemicarbazones and their copper(II) and nickel(II) complexes: a study to understand their biological activity. J. Inorg. Biochem. 140, 111–125.

Bolognesi, C., Creus, A., Ostrosky-Wegman, P., Marcos, R., 2011. Micronuclei and pesticide exposure. Mutagenesis 26, 19–26. http://dx.doi.org/10.1093/mutage/geq070.

Buschini, A., Ferrarini, L., Franzoni, S., Galati, S., Lazzaretti, M., Mussi, F., Northfleet de Albuquerque, C., Araújo Domingues, M., Zucchi, T., Poli, P., 2009. Genotoxicity revaluation of three commercial nitroheterocyclic drugs: nifurtimox, benznidazole, and metronidazole. J. Parasitol. Res. 2009, 463575. http://dx.doi.org/10.1155/2009/463575.

Chiu, Y.H., Afeiche, M.C., Gaskins, A.J., Williams, P.L., Petrozza, J.C., Tanrikut, C., Hauser, R., Chavarro, J.E., 2015. Fruit and vegetable intake and their pesticide residues in relation to semen quality among men from a fertility clinic. Hum. Reprod. 30, 1342–1351. http://dx.doi.org/10.1093/humrep/dev064.

Cuero, R., Ouellet, T., 2005. Metal ions modulate gene expression and accumulation of the mycotoxins aflatoxin and zearalenone. J. Appl. Microbiol. 98, 598–605.

Degola, F., Berni, E., Restivo, F.M., 2011. Laboratory tests for assessing efficacy of atoxigenic Aspergillus flavus strains as biocontrol agents. Int. J. Food Microbiol. 146, 235–243. http://dx.doi.org/10.1016/j.ijfoodmicro.2011.02.020.

Degola, F., Dall'Asta, C., Restivo, F.M., 2012. Development of a simple and high-throughput method for detecting aflatoxins production in culture media. Lett. Appl.Microbiol. 55, 82–89. http://dx.doi.org/10.1111/j.1472-765X.2012.03264.x.

Degola, F., Morcia, C., Bisceglie, F., Mussi, F., Tumino, G., Ghizzoni, R., Pelosi, G., Terzi, V., Buschini, A., Restivo, F.M., Lodi, T., 2015. In vitro evaluation of the activity of thiosemicarbazone derivatives against mycotoxigenic fungi affecting cereals. Int. J. Food Microbiol. 200, 104–111. http://dx.doi.org/10.1016/j.ijfoodmicro.2015.02.009.

Dos Santos, T.A., da Silva, A.C., Silva, E.B., Gomes, P.A., Espíndola, J.W., Cardoso, M.V., Moreira, D.R., Leite, A.C., Pereira, V.R., 2016. Antitumor and immunomodulatory activities of thiosemicarbazones and 1,3-thiazoles in Jurkat and HT-29 cells. Biomed. Pharmacother. 82, 555–560. http://dx.doi.org/10.1016/j.biopha.2016.05.038.

EFSA, 2010. Management of left-censored data in dietary exposure assessment of chemical substances. EFSA J. 446, 1–127.

Feretti, D., Zerbini, I., Zani, C., Ceretti, E., Moretti, M., Monarca, S., 2007. Allium cepa chromosome aberration and micronucleus tests applied to study genotoxicity of extracts from pesticide-treated vegetables and grapes. Food Addit. Contam 24, 561–572.

Fortes, C., Mastroeni, S., Pilla, M.A., Antonelli, G., Lunghini, L., Aprea, C., 2013. The relation between dietary habits and urinary levels of 3-phenoxybenzoic acid, a pyrethroid metabolite. Food Chem. Toxicol. 52, 91–96.

Holmes, R.A., Boston, R.S., Payne, G.A., 2008. Diverse inhibitors of aflatoxin biosynthesis. Appl. Microbiol. Biotechnol. 78, 559–572. http://dx.doi.org/10.1007/s00253-008-1362-0.

IARC, 2012. Risk assessment and risk management of mycotoxins. IARC Sci. Publ. 158, 105–117.

Kljun, J., Scott, A.J., LanišnikRižner, T., Keiser, J., Turel, I., 2014. Synthesis and biological evaluation of organoruthenium complexes with azole antifungal agents. First crystal structure of a tioconazole metal complex. Organometallics 33, 1594–1601.

Marin, S., Ramos, A.J., Cano-Sancho, G., Sanchis, V., 2013. Mycotoxins: occurrence, toxicology, and exposure assessment. Food Chem. Toxicol. 60, 218–237. http://dx.doi.org/10.1016/j.fct.2013.07.047.

Maron, D.M., Ames, B.N., 1983. Revised methods for the Salmonella mutagenicity test. Mut. Res. 113, 173–215.

Mortelmans, K., Zeiger, E., 2000. The Ames Salmonella/microsome mutagenicity assay. Mutat. Res. 455, 29–60.

Pal, K.K., Gardener, B.M., 2006. Biological control of plant pathogens. plant health Instr. 2, 1117–1142.

Parrilha, G.L., da Silva, J.G., Gouveia, L.F., Gasparoto, A.K., Dias, R.P., Rocha, W.R., Santos, D.A., Speziali, N.L., Beraldo, H., 2011. Pyridine-derived thiosemicarbazones and their tin(IV) complexes with antifungal activity against Candida spp. Eur. J. Med. Chem. 46, 1473–1482.

Pelosi, G., 2010. Thiosemicarbazone metal complexes: from structure to activity. Open Crystallogr. J. 3, 16–28.

Pervez, H., Iqbal, M.S., Tahir, M.Y., Nasim, F.U., Choudhary, M.I., Khan, K.M., 2008. In vitro cytotoxic, antibacterial, antifungal and urease inhibitory activities of

some N4-substituted isatin-3-thiosemicarbazones. J. Enzyme Inhib. Med. Chem. 23, 848–854. http://dx.doi.org/10.1080/14756360701746179.
Richard, J.L., 2007. Some major mycotoxins and their mycotoxicoses- an overview. Int. J. Food Microbiol. 119, 3–10.
Weichenthal, S., Moase, C., Chan, P., 2010. A review of pesticide exposure and cancerincidence in the Agricultural Health Study cohort. Environ Health Perspect. 118, 1117–1125. http://dx.doi.org/10.1289/ehp.0901731.
Yang, X., Lv, Y., Huang, K., Luo, Y., Xu, W., 2016. Zinc inhibits aflatoxin B1-induced cytotoxicity and genotoxicity in human hepatocytes (HepG2 cells). Food Chem. Toxicol. 92, 17–25.
Zani, C., Restivo, F.M., Carcelli, M., Feretti, D., Pelosi, G., Rogolino, D., Degola, F., Galati, S., Bisceglie, F., Buschini, A., 2015. A Biotechnological approach for the development of new antifungal compounds to protect the environment and the human health. J. Public Health Res. 4, 613. http://dx.doi.org/10.4081/jphr.2015.613.

SCIENTIFIC REPORTS

OPEN

Received: 26 June 2017
Accepted: 29 August 2017
Published online: 11 September 2017

Thiosemicarbazone scaffold for the design of antifungal and antiaflatoxigenic agents: evaluation of ligands and related copper complexes

Dominga Rogolino[1], Anna Gatti[1], Mauro Carcelli[1], Giorgio Pelosi[1], Franco Bisceglie[1], Francesco Maria Restivo[1], Francesca Degola[1], Annamaria Buschini[1], Serena Montalbano[1], Donatella Feretti[2] & Claudia Zani[2]

The issue of food contamination by aflatoxins presently constitutes a social emergency, since they represent a severe risk for human and animal health. On the other hand, the use of pesticides has to be contained, since this generates long term residues in food and in the environment. Here we present the synthesis of a series of chelating ligands based on the thiosemicarbazone scaffold, to be evaluated for their antifungal and antiaflatoxigenic effects. Starting from molecules of natural origin of known antifungal properties, we introduced the thio- group and then the corresponding copper complexes were synthesised. Some molecules highlighted aflatoxin inhibition in the range 67–92% at 100 μM. The most active compounds were evaluated for their cytotoxic effects on human cells. While all the copper complexes showed high cytotoxicity in the micromolar range, one of the ligand has no effect on cell proliferation. This hit was chosen for further analysis of mutagenicity and genotoxicity on bacteria, plants and human cells. Analysis of the data underlined the importance of the safety profile evaluation for hit compounds to be developed as crop-protective agents and at the same time that the thiosemicarbazone scaffold represents a good starting point for the development of aflatoxigenic inhibitors.

Food security and preservation is an ongoing major concern: it is in fact estimated that about 40% of the food produced worldwide is lost or spoiled. This not only reduces its availability, but, by forcing agricultural productivity, also has an impact on global climate change[1]. One of the most important cause of food spoilage is related to the presence of fungi, in particular of *Aspergillus*, *Penicillium*, *Fusarium* and *Alternaria* genera[2]. These fungi, in fact, are the principal producers of mycotoxins, and aflatoxins (AF) in particular, secondary metabolites with a severe toxic and carcinogenic potential. AF can lead to the induction of teratogenic, carcinogenic, oestrogenic, neurotoxic and immunosuppressive effects in humans and animals. They persist also in processed products, like milk or cheese, and represent therefore a great risk for human health[3]. AF can contaminate a wide variety of important agricultural products, causing important economic losses, and strict values are imposed for food consumption[4].

The direct control of mycotoxin-producing fungi by using synthetic fungicides is still the most effective way to intervene, but it is well known that the extensive use of fungicides generates long term residues in food and in the environment[5]. Concerns on food safety and environmental health, combined with the global issue of emerging resistant pest strains, make urgent to develop novel crop-protective agents[6]. In this scenario, the exploitation of bioactive natural sources to obtain new agents with novel modes of actions may represent an innovative, successful strategy to minimize at the same time mycotoxin production and the use of harmful pesticides. Many

[1]Department of Chemistry, Life Sciences and Environmental Sustainability and CIRCMSB (Consorzio Interuniversitario di Ricerca in Chimica dei Metalli nei Sistemi Biologici), Università di Parma, Parco Area delle Scienze, 43124, Parma, Italy. [2]Department of Medical and Surgical Specialities, Radiological Sciences and Public Health, University of Brescia, Viale Europa 11, 25123, Brescia, Italy. Correspondence and requests for materials should be addressed to D.R. (email: dominga.rogolino@unipr.it)

natural products and their chemical analogues have been proposed as crop-protective agents[7]. Phenolic compounds with antioxidant activity, including eugenol, ferulic acid, vanillin and vanillylacetone, have been reported as AF inhibitors[8]. Moreover, recent studies have demonstrated the antifungal activities of some naturally occurring acetophenone derivatives[9]. On the other hand, inorganic substances, like copper salts, have been long used for their capacity of inhibiting the development of moulds and bacteria and can have effect on growth of *A. parasiticus* and aflatoxin production[10]. Some studies suggested that metal ions can influence the growth and the mycotoxin production of the toxigenic fungi *A. flavus* and *F. graminearum* and that this effect can be related to the ability of metal ions to intervene on the pattern of gene expressions of *A. flavus*[9,11]. The lipidic membrane that surrounds the cell constitutes a barrier to metal ions diffusion, but small hydrophobic molecules can easily diffuse through this barrier. Metal chelation could improve lipophilicity, facilitating the penetration of the complexes into lipid membranes, and, in this way, metal complexes should restrict proliferation of the microorganisms. Thiosemicarbazones represent a very attractive class of metal-chelating ligands for their coordinating versatility and the possibility to easily modify the molecular backbone and tuning their physical and chemical properties. They have a great variety of biological properties both as free ligands and as metal complexes[12]. Recently, we have disclosed the potential of some thiosemicarbazones for crop protection and food spoilage control, with a particular focus on the activity of these compounds against the two major genera of cereal mycotoxigenic fungi, i.e. *Fusarium* and *Aspergillus*[13,14]. Here we present the evaluation of other thiosemicarbazone ligands (**L1–L6**) for their antifungal and anti-aflatoxin activity towards *A. flavus*. Starting from molecules of natural origin, like vanillin and its derivatives, we introduced the thio- group in the perspective to obtain more potent compounds; copper complexes were then synthesised, with the aim to synergistically improve the capability of the free ligands to inhibit toxin production. The effects of **L1–L6** and of their copper complexes on fungal growth and aflatoxin biosynthesis were determined. With a view to use these compounds in field, an assessment of the cyto- and geno-toxic effects on healthy human cells, particularly on human cell lines deriving from the districts that can be exposed to chemicals (gastrointestinal tract, pulmonary epithelium and epidermis) was performed on the most active compounds. Finally, best hits were evaluated for their toxic and genotoxic activities on bacteria and plants cells.

Materials and Methods

Chemicals were purchased from Sigma-Aldrich Srl (Milano, Italy). Dulbecco's Modified Eagle's medium (DMEM) and RPMI-1640 medium were purchased from Lonza Group Ltd (Basel, Switzerland); Ham's Nutrient Mixture F-12 and Fetal bovine serum (FBS) were purchased from EuroClone S.p.a. (Milano, Italy). Hs27 (ATCC, CRL1634), CRL 1790 (ATCC, CCD 841 CoN) and HFL1(ATCC, CCL-153) were obtained from the American Type Culture Collection (ATCC). U937 cells were obtained from the American Tissue Culture Collection (Rockville, MD). CellTiter96® AQ_{ueous}One Solution Cell Proliferation Assay was purchased from Promega Corporation, Madison, WI, USA.

Chemistry. The purity of the compounds was determined by elemental analysis and verified to be ≥95%. ^{1}H-NMR spectra were obtained in a 5 mm NMR precision tube at 298 K on a Bruker Avance 400 FT spectrophotometer. The ATR-IR spectra were recorded by means of a Nicolet-Nexus (Thermo Fisher) spectrophotometer by using a diamond crystal plate in the range of 4000–400 cm^{-1}. Elemental analyses were performed by using a FlashEA 1112 series CHNS/O analyzer (Thermo Fisher) with gas-chromatographic separation. Electrospray mass spectral analyses (ESI-MS) were performed with an electrospray ionization (ESI) time-of-flight Micromass 4LCZ spectrometer. Samples were prepared in methanol. The MS spectra were recorded in methanol and acquired in positive EI mode by means of a DEP-probe (Direct Exposure Probe) mounting on the tip of a Re-filament with a DSQII Thermo Fisher apparatus, equipped with a single quadrupole analyzer. ICP data were obtained by mean of an emission spectrometer JY 2501 with coupled plasma induction in radial configuration HORIBA Jobin Yvon (Kyoto, Japan), ULTIMA2 model. Instrumental features: monochromator Model JY 2501; focal length 1 m; resolution 5 pm; nitrogen flow 2 l/min.

ICP source: nebulizer Meinhard, cyclonic spraying chamber; argon flow 12 l/min; wavelengths range 160–785 nm; optical bench temperature 32 °C. The wavelength used for quantitative analysis was chosen by examining the emission line with greater relative intensity, ensuring that there were no spectral interference with the Argon emission lines. Acquisition parameters: wavelength Cu (nm): 224.700; Voltage (V): 580; gain: 100. The quantitative analysis was performed after the acquisition of a calibration line using standard solutions in HNO_3 at 2%, to simulate the final acidity of the samples; the concentration range of the standards varied from 1 mg/L to 100 mg/L. Compounds were dissolved in 10 mL of CH_3OH (2% HNO_3). Data acquisition and processing were performed using the ICP JY v 5.2 software (Jobin Yvon).

The synthesis of **L1–L6** (Fig. 1) was performed by using a procedure previously reported[15]. The aldehyde was dissolved in a hot ethanol solution containing few drops of glacial acetic acid. An equimolar amount of the appropriate thiosemicarbazide was added to the solution and the reaction was heated under reflux for 24 h. The solution was cooled r.t. and the ligands were obtained as precipitates. After filtration the solid was washed several times with cold ethanol and ether and then dried under vacuum.

*N'-(3,4-dihydroxybenzyliden)thiosemicarbazone **L1***. Brown solid. Yield: 81%. ^{1}H-NMR (DMSO-d_6, 25 °C), δ: 11.20 (s, 1 H, NNH); 9.47, 9.01 (2 s, 1 H + 1 H, OH); 8.04, 7.71 (2 s, 1 H + 1 H, NH_2); 7.89 (s, 1 H, CH = N); 7.17 (s, 1 H, CH_{Ar}); 7.00 (d, 1 H, J = 8 Hz, CH_{Ar}); 6.74 (d, 1 H, J = 8 Hz, CH_{Ar}). EI-MS: m/z = 211.0 $[M + H]^+$.

*N'-(3-metoxy-4-hydroxy-acetophenone)thiosemicarbazone **L2***. Yellow solid. Yield: 87%. ^{1}H-NMR (DMSO-d_6, 25 °C), δ: 10.03 (s, 1 H, NNH); 9.34 (s, 1 H, OH); 8.22, 7.87 (2 s, 1 H + 1 H, NH_2); 7.49 (d, 1 H, J = 2 Hz, CH_{Ar}); 7.26

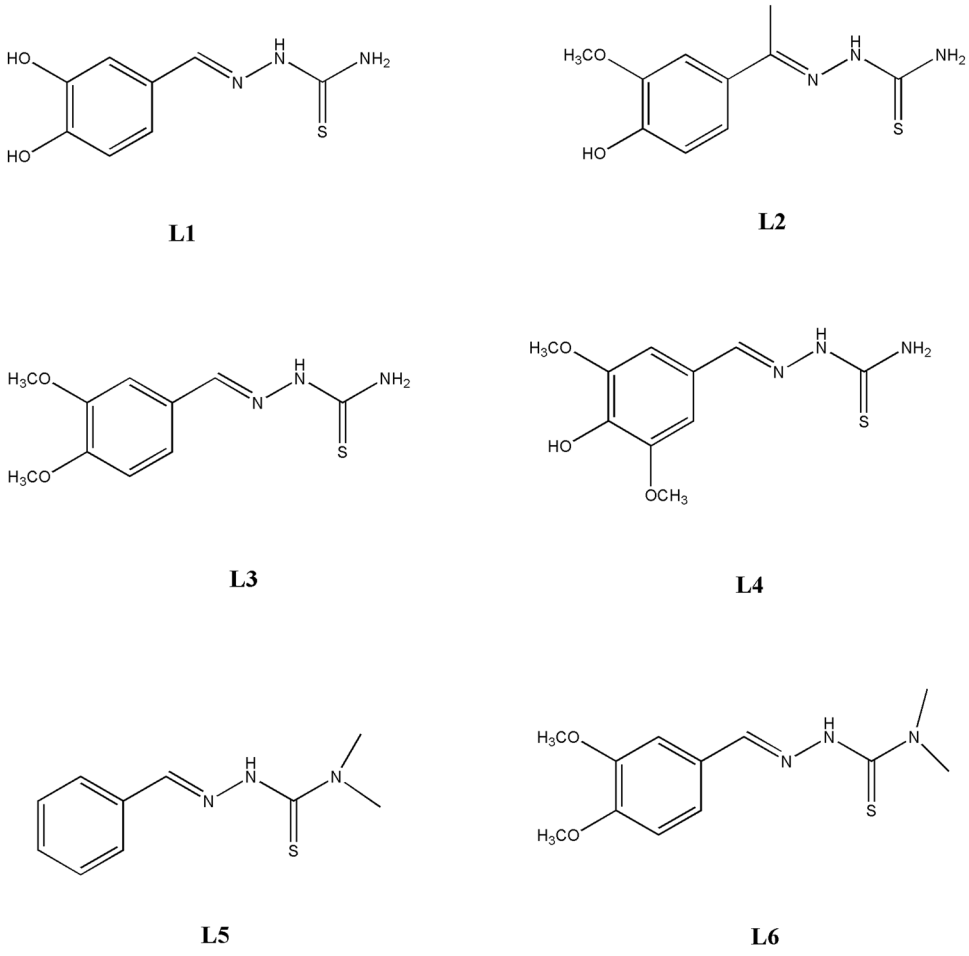

Figure 1. Thiosemicarbazone ligands **L1–L6**.

(dd, 1 H, J = 8 Hz, J' = 2 Hz, CH_{Ar}); 6.76 (d, 1 H, J = 8 Hz, CH_{Ar}); 3.84 (s, 3 H, OCH_3); 2.25 (s, 3 H, CH_3). EI-MS: m/z = 240.0 $[M+H]^+$.

*N'-(3,4-dimetoxybenzyliden)thiosemicarbazone **L3***. Pink solid. Yield: 64%. ^{1}H-NMR (DMSO-d_6, 25 °C), δ: 11.18 (s, 1 H, NNH); 9.48, 8.99 (2 s, 1 H + 1 H, OH); 8.30 (t_{broad}, 1 H, NH_{Et}); 7.89 (s, 1 H, CH = N); 7.21 (d, 1 H, J = 2 Hz, CH_{Ar}); 6.99 (dd, 1 H, J = 8 Hz, J' = 2 Hz, CH_{Ar}); 6.75 (d, 1 H, J = 8 Hz, CH_{Ar}); 3.55 (m, 2 H, J = 7 Hz, CH_2); 1.12 (t, 3 H, J = 7 Hz, CH_3). EI-MS: m/z = 240.0 $[M+H]^+$.

*N'-(3,5-dimetoxy-4-hydroxybenzyliden)thiosemicarbazone **L4***. Brown solid. Yield: 90%. ^{1}H-NMR (DMSO-d_6, 25 °C), δ: 11.32 (s, 1 H, NNH); 8.80 (s, 1 H, OH); 8.13, 7.99 (s + s, 1 H + 1 H, NH_2); 7.92 (s, 1 H, CH = N); 7.05 (s, 1 H, CH_{Ar}); 3.81 (s, 6 H, OCH_3). EI-MS: m/z = 255.0 $[M+H]^+$.

*N'-(benzyliden)-4,4-dimethylthiosemicarbazone **L5***. Yellow solid. Yield: 57%. ^{1}H-NMR (DMSO-d_6, 25 °C), δ: 10.95 (s, 1 H, NNH); 8.20 (s, 1 H, CH = N); 7.64 (d, 2 H, J = 7 Hz, CH_{Ar}); 7.38 (m, 3 H, CH_{Ar}); 3.30 (s, 6 H, NCH_3). EI-MS ($C_{10}H_{13}N_3S$, CH_3OH): m/z = 207.0 $[M+H]^+$.

*N'-(3,4-dimetoxybenzyliden)-4,4-dimethylthiosemicarbazone **L6***. Red solid. Yield: 61%. ^{1}H-NMR (DMSO-d_6, 25 °C), δ: 10.84 (s, 1 H, NNH); 8.10 (s, 1 H, CH = N); 7.25 (s, 1 H, CH_{Ar}); 7.12 (d, 1 H, J = 8.4 Hz, CH_{Ar}); 6.99 (d, 1 H, J = 8.4 Hz, CH_{Ar}); 3.79 (s, 6 H, NCH_3). EI-MS ($C_{12}H_{17}N_3SO_2$, CH_3OH): m/z = 268.0 $[M+H]^+$.

*General method for the synthesis of copper complexes **1–6***. 100 mg (2 eq.) of the thiosemicarbazone ligand were dissolved in 10 ml of degassed methanol. 1 eq. of $CuCl_2 \cdot 2H_2O$ was dissolved in 5 mL of degassed methanol and this solution was added to the previous one. The mixture was stirred at room temperature for 4 hours under N_2. Then, it was cooled overnight; the precipitate was filtered off and washed with ether.

*Cu_3(**L1**)(**L1**-H)Cl_2 (**1**)*. Orange powder. Yield = 25%. ^{1}H-NMR (DMSO-d_6, 25 °C), δ: 11.68 (s, 1 H, NNH); 9.62, 9.04 (2 s, 1 H + 1 H, OH); 8.57, 8.37 (2 s, 1 H + 1 H, NH_2); 7.97 (s, 1 H, CH = N); 7.24 (s, 1 H, CH_{Ar}); 7.07 (d, 1 H, J = 9 Hz, CH_{Ar}); 6.74 (d, 1 H, J = 8.5 Hz, CH_{Ar}). ESI-MS (CH_3OH): m/z = 485 (100, $[ML_2]^+$), (50, 332

[MLCl + Na]$^+$). Anal. calcd. for $C_{16}H_{17}N_6S_2O_4Cu_3Cl_2$: C 28.14, H 2.51, N 12.30. Found: C 28.19, H 2.37, N 12.32. ICP: Cu found 28.9%, calcd. 27.9%.

*Cu_2(**L2**)$Cl_2.H_2O$ (**2**).* Green powder. Yield = 28%. ^{1}H-NMR (DMSO-d_6, 25 °C) δ: 10.48 (s, 1 H, NNH); 9.43 (s, 1 H, OH); 8.79, 8.42 (2 s, 1 H + 1 H, NH_2); 7.55 (s, 1 H, CH_{Ar}); 7.33 (d, 1 H, J = 8.5 Hz, CH_{Ar}); 6.78 (d, 1 H, J = 8.5 Hz, CH_{Ar}); 3.85 (s, 3 H, OCH_3); 2.37 (s, 3 H, CH_3). ESI-MS (CH_3OH): m/z = 541 (100, [ML_2]$^+$), 302 (40, [ML]$^+$). Anal. calcd. for $C_{10}H_{13}N_3SO_2Cu_2Cl_2 + H_2O$: C 26.39, H 3.32, N 9.23. Found: C 25.81, H 2.87, N 8.93. ICP: Cu found 29.5%, calcd. 27.9%.

*Cu_3(**L3**)(**L3**-H)Cl_2 (**3**).* Yellow powder. Yield = 28%. ^{1}H-NMR (DMSO-d_6, 25 °C) δ: 11.76 (s, 1 H, NNH); 8.65, 8.58 (2 s, 1 H + 1 H, NH_2); 7.55 (s, 1 H, CH_{Ar}); 8.05 (s, 1 H, CH = N); 7.58 (s, 1 H, CH_{Ar}); 7.21(d, 1 H, J = 8.5 Hz, CH_{Ar}); 6.98 (d, 1 H, J = 8.5 Hz, CH_{Ar}); 3.83, 3.80 (2 s, 3 H + 3 H, OCH_3). ESI-MS (CH_3OH): m/z = 541 (90, [ML_2]$^+$), 302 (100, [ML]$^+$). Anal. calcd. for $C_{20}H_{25}N_6S_2O_4Cu_3Cl_2$: C 32.51, H 3.41, N 11.37. Found: C 32.71, H 3.55, N 11.44. ICP: Cu found 26.1%, calcd. 25.8%.

*Cu_3(**L4**)(**L4**-H)Cl_2 $2H_2O$(**4**).* Yellow powder. Yield = 37%. ^{1}H-NMR (DMSO-d_6, 25 °C) δ: 11.81 (s, 1 H, NNH); 8.95 (s, 1 H, OH); 8.70, 8.66 (2 s, 1 H + 1 H, NH_2); 8.01 (s, 1 H, CH = N); 7.13 (s, 1 H, CH_{Ar}). ESI-MS (CH_3OH): m/z = 573 (100, [ML_2]$^+$). Anal. calcd. for $C_{20}H_{25}N_6S_2O_6Cu_3Cl_2 + 2H_2O$: C 29.77, H 3.62, N 10.41. Found: C 29.45, H 3.49, N 10.47. ICP: Cu found 21.8%, calcd. 23.6%.

*Cu(**L5′**)Cl (**5**).* Yellow powder. Yield = 33%. ^{1}H-NMR (DMSO-d_6, 25 °C) δ: 7.78 (m, 2 H, CH_{Ar}); 7.48 (m, 3 H, CH_{Ar}) 3.84, 3.81 (2 s, 3 H + 3 H, $N(CH_3)_2$). ESI-MS (CH_3OH): m/z = 476 (40, [ML_2 + H]$^+$), 270 (100, [ML + H]$^+$).

Crystals of **L5′**, a cyclized form of **L5**, suitable for X-ray diffraction analysis were obtained during some attempts to recrystallize **5**; crystals of **5′** suitable for X-ray diffraction analysis were obtained by vapour diffusion of ether in a saturated DMF solution of **5**.

*Cu(**L6′**)Cl (**6**).* Yellow powder. Yield = 37%. ^{1}H-NMR (DMSO-d_6, 25 °C) δ: 7.29 (d, 1 H, J = 8 Hz, CH_{Ar}); 7.06 (d, 1 H, J = 8 Hz, CH_{Ar}); 7.00 (s, 1 H, CH_{Ar}); 4.16, 4.09 (2 s, 3 H + 3 H, OCH_3); 3.83, 3.80 (2 s, 3 H + 3 H, $N(CH_3)_2$). ESI-MS (CH_3OH): m/z = 596 (50, [ML_2]$^+$), 330 (100, [ML]$^+$). ICP: Cu found 18.7%, calcd. for $C_{12}H_{15}N_3O_2SCuCl$: 19.3%. Crystals of **6′** suitable for X-ray diffraction analysis were obtained by vapour diffusion of ether in a saturated DMF solution of **6**.

X-ray structures. **L5′** and **6′** were collected at 100 K under nitrogen flux at Elettra Sincrotrone (Trieste, Italy) on beamline XRD1 with a wavelength of 0.7 Å (NdBFe Multipole Wiggler, Hybrid linear, 4.27 keV with a power of 8.6 kW, source size full width half maximum (fwhm) beam size at sample of 2.0 × 0.37 mm, 0.7 × 0.2 mm, and photon flux 1012–1013 ph/s), Dectris Pilatus 2 M detector. Data were reduced with CrysalisPro software[16]. For **5′**, single crystal X-ray diffraction analysis was performed on a SMART APEX2 diffractometer using Mo Kα radiation (λ = 0.71073 Å, Lorentz polarization and absorption correction applied) at room temperature (293 K). The SAINT[17] software was used for integration of reflection intensity and scaling, SADABS[18] for absorption correction. A semi-empirical absorption correction, based on multiple scanned equivalent reflections, has been carried out and gave 0.3658 < T < 0.7459). Structures were solved by direct methods using SIR97[19] and refined by full-matrix least-squares on all F2 using SHELXL97[20] implemented in the WinGX package[21]. For all the structures, anisotropic displacement parameters were refined except for hydrogen atoms. Hydrogen atoms were introduced in calculated positions riding on their carrier atoms.

L5′. The crystal system is orthorhombic, space group $Pna2_1$, cell parameters $a = 15.4877(2)$, $b = 5.8132(1)$, $c = 11.1034(1)$ Å, $V = 999.67(2)$ Å^3. The asymmetric unit is formed by a single molecule of formula $C_{10}H_{12}Cl_2N_3S$, $M = 206.29$ Da, $Z = 4$, $D_c = 1.37$ g cm^{-3}, $\mu = 2.85$ mm^{-1}, $F(000) = 436$. A total of 17969 reflections were collected up to a θ range of 33.10° (±22 h, ±8 k, ±15 l), 3388 unique reflections ($R_{int} = 0.038$).

5′. The crystal system is triclinic, space group *P-1*, cell parameters $a = 8.124(3)$, $b = 8.477(3)$, $c = 9.761(4)$ Å, $\alpha = 100.121(6)$, $\beta = 114.531(5)$, $\gamma = 98.713(6)$°, $V = 582.8(4)$ Å^3. The asymmetric unit is formed by half a molecule of formula $C_{10}H_{11}ClCu_{0.5}N_3S$, $M = 272.50$ Da, $Z = 2$, $D_c = 1.55$ g cm^{-3}, $\mu = 13.66$ mm^{-1}, $F(000) = 279$. A total of 7598 reflections were collected up to a θ range of 27.39° (±10 h, ±10 k, ±12 l), 2632 unique reflections ($R_{int} = 0.044$).

6′. The crystal system is monoclinic, space group $P2_1/n$, cell parameters $a = 9.0147(2)$, $b = 13.5881(3)$, $c = 11.5443(2)$ Å, $\beta = 105.418(2)$°, $V = 582.8(4)$ Å^3. The asymmetric unit is formed by half a molecule of formula $C_{12}H_{15}ClCu_{0.5}N_3O_2S$, $M = 332.55$ Da, $Z = 4$, $D_c = 1.62$ g cm^{-3}, $\mu = 11.92$ mm^{-1}, $F(000) = 686$. A total of 12038 reflections were collected up to a θ range of 29.99° (±12 h, ±17 k, ±16 l), 2632 unique reflections ($R_{int} = 0.043$).

All the non-hydrogen atoms in the molecules were refined anisotropically. The hydrogen atoms were partly found and partly placed in the ideal positions using riding models.

CCDC 1556287, 1556288 and 1556289 contain the supplementary crystallographic data (see also the attached CIF file). These data can be obtained free of charge from The Cambridge Crystallographic Data Centre via http://www.ccdc.cam.ac.uk/data_request/cif.

***A. flavus* strains.** A toxigenic and an atoxigenic strain of *A. flavus* were used[14].

Effect on *A. flavus* growth. Conidia of *A. flavus* strains obtained from 10-day YES-agar [2% (w/v) yeast extract (Difco, Detroit, MI), 5% (w/v) sucrose (Sigma, St Louis, MO), 2% (w/v) agar (Difco)] cultures were quantified by OD_{600}, and viability (>90%) was determined according to previously disclosed methods[22]. Conidial germination rate and post-germination hyphal outgrowth were assessed by analyzing changes in optical density

of spore suspensions after 38–46 h: in a 96 well microtiter plate (Sarstedt, Newton, NC, USA) 5×10^3 spores were inoculated in a final volume of 200 μL of YES liquid medium amended with molecules (50 or 100 μM), and incubated statically at 28 °C. DMSO (0.5% and 1% respectively) was used as control. The optical density at 620 nm was recorded for each well with a microplate reader (MULTISKAN EX, Thermo Electron Corporation, Vantaa, Finland) without shaking. Samples were inoculated in quadruplicate.

Effect on aflatoxin accumulation. The high throughput procedure described in our previous works[22,23] was used to assess aflatoxin accumulation in a coconut-milk derived medium (CCM). Briefly, suspensions of conidia were diluted and brought to the final concentration of 5×10^2 conidia/well; cultures were set in a final volume of 200 μL/well of CCM medium added with molecules at 50 or 100 μM. DMSO (0.5% and 1% respectively) was used as control. The plates were incubated in the dark under stationary conditions for 6 days at 25 °C. Aflatoxin accumulation was monitored by fluorescence emission determination: readings were performed directly from the bottom of wells of the culture plate with a microplate reader (TECAN SpectraFluor Plus, Männedorf, Switzerland) using the following parameters: $\lambda_{ex} = 360$ nm; $\lambda_{em} = 465$ nm; manual gain = 83; lag time = 0 μs; number of flashes = 3; and integration time = 200 μs. Samples were inoculated in quadruplicate.

Statistical analysis. For statistical analyses one-way analysis of variance (ANOVA) was used in the Past 3.x software. Results of mycelial growth and aflatoxin accumulation were analyzed by Tukey's test; differences were considered significant at $p < 0.001$.

Cytotoxicity. The antiproliferative effect of the compounds was evaluated by MTS assay (CellTiter96® AQ_{ueous} One Solution Cell Proliferation Assay) towards different human cell lines: Hs27 foreskin fibroblasts, CRL1790 colon epithelial, HFL1 lung fibroblasts and U937 histiocytic lymphoma cells. Hs27 and CRL1790 were cultured in DMEM supplemented with 10% (v/v) fetal bovine serum, 1% L-glutamine (2 mM) and 1% penicillin (100 units mL^{-1})/streptomycin (100 μg mL^{-1}). HFL1were cultured in Ham's Nutrient Mixture F-12 with L-Glutamine supplemented with 10% (v/v) fetal bovine serum and 1% penicillin (100 units mL^{-1})/streptomycin (100 μg mL^{-1}). U937 cells were cultured in RPMI-1640 medium supplemented with 10% (v/v) fetal bovine serum, 1% L-glutamine (2 mM) and 1% penicillin (100 units mL^{-1})/streptomycin (100 μg mL^{-1}). Hs27, CRL1790 and HFL1cells were used between passage numbers 5 and 20. Cells were maintained in a humidified atmosphere at 5% CO_2 and 37 °C and culture medium was refreshed every two or three days during sub-culturing.

The cytotoxicity was evaluated according to the following method: 5×10^3 cells/well were seeded in 96-well plates in 100 μL of medium without phenol red with 5% fetal bovine serum and then incubated at 37 °C in a humidified (95%) CO_2 (5%) incubator. After 24 h, cells were treated, in quadruplicate, with increasing concentrations of the molecules in the range 0.5 to 100 μM for further 24 h. The assay was performed by adding 20 μL of the CellTiter96® AQ_{ueous} One Solution Cell Proliferation Assay directly to the culture wells, incubating for 4 h and then recording the absorbance at 485 nm with a 96-well plate reader (TECAN SpectraFluor Plus, Männedorf, Switzerland). MTS assay was performed to identify GI_{50} value, that is the concentration of drug that causes a 50% reduction of cell growth[24].

Genotoxicity on human cells. To assess primary DNA damage the alkaline version of Comet assay was performed with U937 cells as described in a previously published work[25]. Briefly, the cells were seeded at a concentration of 1×10^5 cell/mL in 24-well plates in 1 mL of medium, supplemented with 1% glutamine, 1% penicillin/streptomycin and 10% fetal bovine serum and then incubated at 37 °C in a humidified (95%) CO_2 (5%) incubator. After 24 h cells were treated, in duplicate, with increasing concentrations of the molecules in the range 25 to 100 μM for 1 h. After treatment, determinations of cell numbers and viabilities were performed with the trypan blue exclusion method. Only the treatments that had a viability higher than 70% have been processed in the Comet assay. Positive and negative controls were represented by ethylmethanesulfonate (EMS), 2 mM, and DMSO, 100 μM, respectively. DNA was stained with 75 μL ethidium bromide (10 μg/mL) before the examination at 400 × magnification under a Leica DMLS fluorescence microscope (excitation filter BP 515–560 nm, barrier filter LP 580 nm), using an automatic image analysis system (Comet Assay IV – Perceptive Instruments Ltd, UK). The "IBM SPSS Statistics 24" software was used to analyze statistical differences between samples. The mean values from the repeated experiments were used in a one-way analysis of variance (ANOVA). If significant F-values ($P < 0.05$) were obtained, Student's t test (Bonferroni's version) was performed.

Mutagenicity assessment of L5 on bacteria and plants cells. The samples in DMSO underwent the *Salmonella*/microsome test (Ames test) at increasing doses, with *S. typhimurium* TA98 and TA100 strains, with and without metabolic activation (S9 mix) to highlight the presence of indirect and direct mutagenic substances. A range of doses from 0.1 to 100 μM/plate was applied. TA98 strain detects frame-shift mutagens and TA100 strain responds to base-pair substitution mutations[26]. For positive control, 2-nitrofluorene for TA98 without S9 (10 μg/plate), sodium azide for TA100 without S9 (10 μg/plate), and 2-aminofluorene for both strains with S9 mix (20 μg/plate) were used, respectively. DMSO was used as negative control. The results were expressed as number of revertants/plate. All experiments were conducted in duplicate. The data obtained were the average of duplicate plates and were expressed as mutagenicity ratio, dividing the revertants/plate by the spontaneous mutation rate. Results were considered positive if two consecutive dose levels or the highest non-toxic dose level produced a response at least twice that of the solvent control, and at least two of these consecutive doses showed a dose-response relationship[27,28].

A. cepa test: in a preliminary toxicity assay, equal-sized young bulbs of onion were exposed for 72 hours in the dark to different concentrations (from 0.1 to 100 μM) of each molecules. Root length was used to calculate the EC_{50} value of the compound[29,30] and to identify the concentrations to be used in the *A. cepa* genotoxicity assay. Other macroscopic parameters (turgescence, consistency, change in colour, root tip shape) were used as toxicity indexes[29,30].

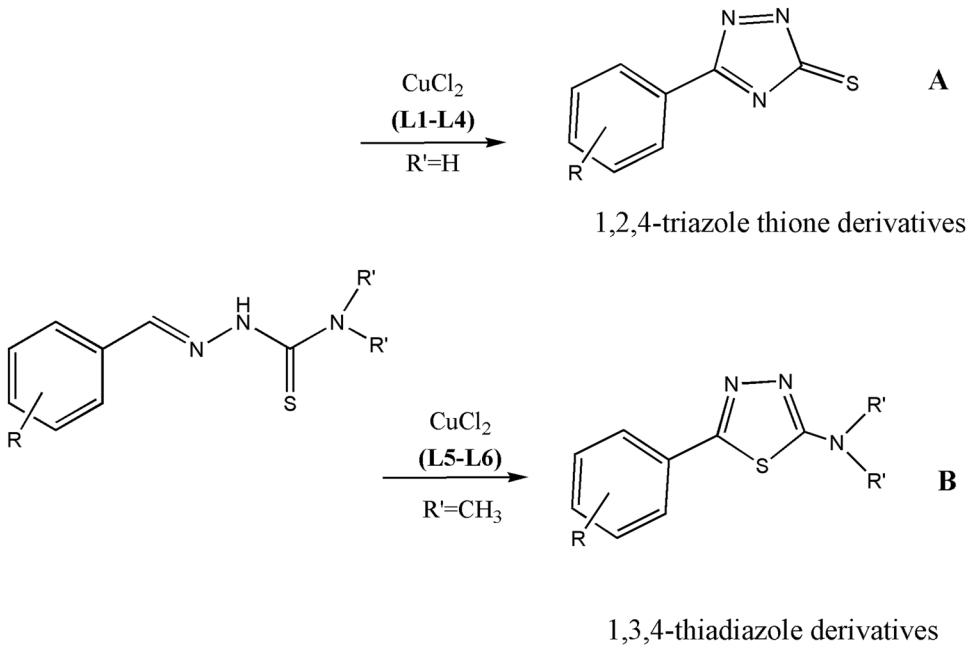

Figure 2. Possible cyclisation products for thiosemicarbazones **L1–L6**.

The *A. cepa* micronucleus test was performed using equal-sized young bulbs per sample[31]. After 72-hour pre-germination in Rank solution, the bulbs were exposed to 4 doses of compounds (10–100 µM) for 24 hours. Negative (Rank solution + DMSO, 24 h) and positive (maleic hydrazide 10 mg/l, 6 h) controls were performed. After exposure, the roots remained in recovery time for 44 hours and were then fixed in Carnoy's solution. For microscopic analysis 5000 cells/sample were scored for mitotic index (as a measure of cellular division and therefore of sample toxicity) and 10000 cells/sample were scored for micronucleus frequency. The results were reported as number of micronuclei per 100 cells and the data were analysed by using χ^2 and Dunnett's tests. *A. cepa* aberration test was carried out according to Cabaradvic[32], based on Fiskesjo method with minor modifications[29,30]. After 72-hour pre-germination in Rank solution, the bulbs were exposed to 4 doses of compounds (10–100 µM) for 24 h. After treatment, roots were fixed in Carnoy's solution. 5 slides for sample were prepared by using Feulgen technique for analyse mitotic index (MI), mitosis distribution and type and frequency of chromosomal aberrations (structural and numerical ones) in different mitosis phases. For mitotic index evaluation 5000 cells for samples were scored; for chromosomal aberration 1000 cells in division cycle for sample (metaphase, anaphase and telophase) were scored. Statistical analysis was performed using analysis of variance (ANOVA) for mitotic index and Mann-Whitney test for chromosomal aberration. All *A. cepa* experiments were performed in duplicate (two independent assays).

Results

Chemistry. Ligands **L1–L6** (Fig. 1) were synthesised by condensation between an aldehyde and thiosemicarbazide or 4,4-dimethyl-3-thiosemicarbazide[15]. All ligands were characterised by the usual spectroscopic techniques and data are reported in the Experimental Section. Although for these ligands it is possible *E/Z* isomerisation around the C = N double bond, the ^{1}H-NMR spectra of **L1–L6** registered in d_6-DMSO showed just one set of signals, that can be related to the *E* isomer. **L1–L4** are reacted with $CuCl_2$ leading to the isolation of the copper(I) complexes **1–4**: ^{1}H-NMR, IR, mass, ICP and elemental analysis data are reported in the Experimental Section. All the isolated copper compounds are stable at room temperature, non-hygroscopic and insoluble in water, as well as in the common organic solvents, but readily soluble in DMF and DMSO. The ^{1}H-NMR spectra of **1–4** present sharp signal, relative to diamagnetic Cu(I) complexes (Fig. S1). In the protonic spectra of **1–4**, both the signal relative to the NH, the NH_2 and the iminic proton are shifted to lower fields, as can be seen in Figure S1. In order to better clarify the redox process involving the metal centre, the mother liqueur, obtained after filtration of complex **3**, was completely evaporated and the ^{1}H-NMR of the corresponding crude product is reported in Figure S2. In this case, the protonic spectrum lacks of the signals relative to both the iminic and the NH_2 proton and data are in accord with the presence of a cyclized form of the ligand, as a result of an intramolecular oxidative cyclisation of the thiosemicarbazone ligand (Fig. 2), as discussed in the following paragraph. In the IR spectra of **1–4** there is a strong band between 3500 and 3000 cm^{-1}, relative to the symmetric and asymmetric stretching mode of NH_2. ESI-mass spectra of **1–4** are reported in Figures S3–S6.

A different behaviour is observed when **L5** and **L6** are reacted with copper(II). Again, ^{1}H-NMR spectra of the corresponding complexes **5** and **6** reveal sharp signal, indicating the presence of diamagnetic Cu(I) coordination compounds. The absence of signals relative to the iminic and the NH protons in the 8–10 ppm range is in accord with the presence of a cyclized form of the ligand coordinated to the metal centre.

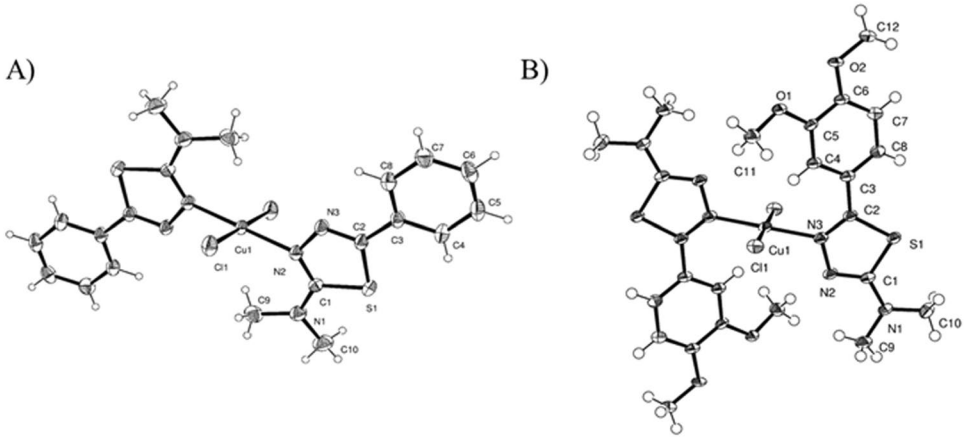

Figure 3. ORTEP representation of **5′** (**A**) and **6′** (**B**) with ellipsoids at 50% probability.

	Growth Inhibition (%)		Aflatoxin Inhibition (%)	
Compound	50 μm	100 μm	50 μm	100 μm
L1	0.6 ± 0.3	0.5 ± 0.6	6.1 ± 0.8	1.1 ± 0.3
L2	47.5 ± 2.5*	51.7 ± 2.3*	26.7 ± 2.4*	17.7 ± 9.5*
L3	25.9 ± 1.6*	25.6 ± 2.3*	24.8 ± 3.0*	25.7 ± 4.7*
L4	0.4 ± 0.4	0.7 ± 0.6	13.8 ± 1.8*	20.7 ± 1.4*
L5	23.8 ± 1.5*	43.9 ± 1.9*	78.0 ± 6.9 *	92.3 ± 4.2*
L6	5.8 ± 0.8*	21.8 ± 1.7*	41.8 ± 2.7*	48.6 ± 1.4*
1	—	—	0.6 ± 0.7	6.6 ± 0.4
2	59.7 ± 1.4*	73.6 ± 3.0*	52.0 ± 3.3*	72.7 ± 3.9*
3	40.5 ± 1.3*	51.0 ± 1.9*	61.1 ± 2.4*	79.0 ± 2.2*
4	28.0 ± 0.6*	62.7 ± 2.4*	48.8 ± 2.2*	62.1 ± 1.4*
5	0.6 ± 0.3	1.1 ± 0.4	36.6 ± 2.0*	67.3 ± 2.1*
6	1.0 ± 0.3	6.2 ± 0.9*	60.7 ± 1.2*	67.8 ± 3.4*

Table 1. Antifungal and anti-aflatoxigenic activities for **L1–L6** and for copper complexes **1–6** at 50 and 100 μM concentration: results are expressed respectively as mean percentage inhibition of growth and of aflatoxin production (in comparison with non-treated controls; mean ± SD). Statistical differences between treated and non-treated samples were reported. (*) p-value < 0.001.

During attempts to crystallize **5**, some crystals of the cyclized form of **L5** (indicated as **L5′**) were serendipitously obtained and characterized by X-ray diffraction analyses (see below). The experimental data obtained for **5** and **6** support the proposed structure Cu(I)(cyclized-ligand)Cl.

Slow vapour diffusion of ether in a saturated DMF solution of **5** and **6** led to the isolation of the Cu(II) complexes **5′** and **6′**, whose crystal structures were determined by X-ray diffraction analysis on single crystal, as detailed in the discussion section (Fig. 3). Oxidation undergone by **5** and **6** occurred in solution during recrystallisation. This is confirmed also by X-ray powder diffraction analysis: the traces of **5** and **6**, in fact, do not match with the calculated spectra of **5′** and **6′**, indicating that the powders are different chemical species respect to the ones subsequently obtained by re-crystallisation.

Fungal growth and aflatoxin inhibition. Both ligands **L1–L6** and copper complexes **1–6** were tested at different concentrations (10, 25, 50 and 100 μM) for their ability to inhibit growth and AF accumulation in *A. flavus*. DMSO was used as control. In Table 1 data concerning the effects of 50 and 100 μM treatments on growth and AF inhibition are reported. **L1** and **L4** do not affect growth neither at 50 μM nor at 100 μM concentration. **L3** and **L6** were provided with a scarce fungistatic activity (less than 30% growth inhibition at the higher dose), but **L2** (at 50 μM) and **L5** (at 100 μM) halved the biomass increase.

As far as the effect of the ligands on AF biosynthesis, **L5** and **L6** only were provided with a relevant inhibitory activity. Mycotoxin biosynthesis was nearly halved when fungal cultures were treated with either at 50 or 100 μM doses of **L6**. AF accumulation in the medium was 90% reduced in the 100 μM **L5** amended cultures. The anti-aflatoxigenic efficacy of **L5** was considerable even if its concentration was lowered to 50 μM (76% inhibition). Moreover, **L5** displayed a moderate fungistatic activity (43 and 22% at 100 and 50 μM, respectively).

Generally, the copper complexes showed a better activity profile then uncomplexed ligands: the metal complexes **2**, **3**, **4** and **6** have aflatoxin inhibition ranges from 61 to 80% at 100 μM and from 35 to 62% at 50 μM. Exceptions are represented by **1** and also by **5**, for which a lower AF inhibition percentage respect to the starting

Compound (μM)	Crl1790	Hs27	HFL1	U937
L5	>100	>100	>100	>100
2	31	16	30	27
3	38	17	29	27
5	3	3	1	4
6	1	3	1	3

Table 2. GI_{50} value, concentration of drug that causes a 50% reduction of cell growth, obtained for the most antimycotoxigenic compounds on different human cell lines.

	TA98-S9		TA98 + S9		TA100-S9		TA100 + S9	
DOSE (μM/plate)	mean ± SD	MR	mean ± SD	MR	mean ± SD	MR	mean ± SD	MR
Negative control	19.0 ± 6.4		36.2 ± 6.0		109.5 ± 9.9		127.3 ± 8.1	
0.1	10.0 ± 2.8	**0.5**	34.0 ± 1.4	**0.9**	128.0 ± 14.1	**1.2**	143.0 ± 7.1	**1.1**
1	15.5 ± 7.8	**0.8**	33.5 ± 4.9	**0.9**	116.0 ± 11.3	**1.1**	132.0 ± 9.9	**1.0**
10	17.0 ± 2.8	**0.9**	35.0 ± 4.2	**1.0**	105.5 ± 6.4	**0.9**	132.5 ± 7.8	**1.0**
50	21.0 ± 2.8	**1.1**	36.5 ± 0.7	**1.0**	135.5 ± 20.5	**1.1**	94.5 ± 2.1	**0.7**
100	17.0 ± 4.2	**0.9**	40.0 ± 5.7	**1.1**	105.0 ± 1.4	**1.0**	138.0 ± 5.7	**1.1**

Table 3. Mutagenicity data in *S. typhimurium* TA98 and TA100 strains treated with **L5**, with and without S9 activation. Results are expressed as revertants/plate (mean ± standard deviation) and mutagenicity ratio (MR). Positive controls for TA98 (±S9) and TA100 (±S9): >1000.

L5 (μM)	MCN (mean ± SD)	Mitotic index (%)	Aberration frequencies in different cell cycle phases (%)			
			metaphase	anaphase	telophase	Total cells in division
10	0.6 ± 0.55	9.7	7.1	13.8	1.2	7.5
25	1.2 ± 1.1	9.8	8.3	25.9*	3.1	14.0***
50	0.8 ± 1.3	11.9	1.1	9.0	0.4	2.9
100	tox	8**	11.5*	20.5	0.7	7.9
Negative control	1.6 ± 1.5	11.7	4.6	12.3	1.4	5.7

Table 4. Micronuclei frequency (MCN), mitotic index (MI) and frequency and type of aberration in *A. cepa* roots treated with **L5**. *$p < 0.05$; **$p < 0.01$; ***$p < 0.001$.

ligand **L5** was observed (Table 1). The inhibition activity on aflatoxin production is accompanied for complexes **2–4** also by fungal growth inhibition (from 51 to 72% at 100 μM, Table 1).

Cytotoxicity. Compounds **2**, **3**, **5**, **6** and **L5**, the most promising ones in term of activity, were tested for their cytotoxicity against a panel of human cell lines. Growth inhibition (GI) determination was performed by MTS assay; data are calculated as a mean of four independent experiments and are shown in Table 2. In Figure S10 the representative dose-response curves for **L5** and the copper complex **5** are shown. Unfortunately, all the copper complexes showed important cytotoxicity in the micromolar range, while **L5** has very no effect on cell proliferation. Therefore, only **L5** was chosen for further analysis of mutagenicity and genotoxicity on bacteria, plants and human cells.

Genotoxicological assessment on bacteria, plants and human cells. Three different tests were carried out on **L5** in order to assess its ability to induce genetic damage in target cells of different organisms, i.e. bacteria, plant and human cells. The mutagenic activity (induction of gene mutation) was studied using Ames test with the *S. typhimurium* strains TA100 and TA98, with and without microsomal activation (S9 fraction). **L5** was tested in a dose range from 0.1 to 100 μM/plate and the results of the tests were expressed as Mutagenicity Ratio (MR), obtained from the mean number of revertants colonies per plates for negative controls: it is worth of note that **L5** exhibited no mutagenicity in the bacterial test on *S. typhimurium* TA100 and TA98 strains with or without metabolic activation at all tested doses (Table 3).

A. cepa test showed toxicity on roots at 100 μM, therefore micronuclei analysis at this dose cannot be performed; for lower doses no micronuclei increase was observed (Table 4). The chromosome aberration test in *A. cepa* was carried out on all doses (10, 25, 50 and 100 μM) and statistically significant increase of aberrations was observed only at the dose of 25 μM, but no dose response curve was found. The higher concentration did not induce genotoxic effects, but the highest dose (100 μM) showed a light toxic effect expressed by a lower mitotic index (8% vs 11.7% of negative control), which confirmed the results reported for micronuclei test.

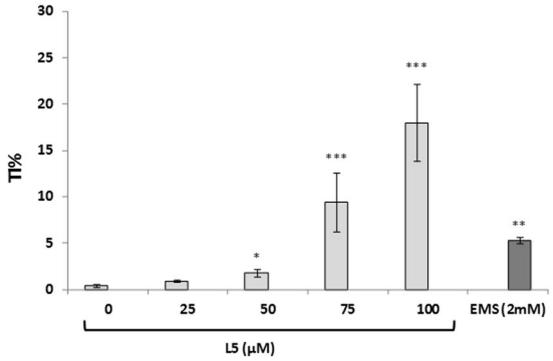

Figure 4. Comet assay: DNA damage induced by **L5** on U937 cells treated for 1 h. Mean and standard deviation of DNA migration, expressed as percentage of tail intensity (TI%) of two independent experiments, are reported. As negative control was used the highest concentration of DMSO, as positive control was used EMS (2 mM). *$p < 0.05$; **$p < 0.01$; ***$p < 0.001$.

Furthermore, to identify if **L5** was able to induce subtoxic DNA alterations on human cells, its DNA damaging activity was assessed through the Alkaline Comet assay. After 1 h of exposure, **L5** produced a dose-dependent DNA migration in the Comet assay, starting from 25 μM, evidencing its genotoxic activity (Fig. 4).

Discussion

Chemistry. In **L1–L6** the substituents on the aromatic ring are modified in order to modulate their physicochemical features, methylation of the NH_2 moiety in **L5** and **L6** was thought in order to modulate the lipophilicity and hydrogen-bonding capabilities. As already mentioned in the Introduction, copper salts have been long used in agriculture for their ability to inhibit the development of pathogens. On the other side, metal chelation could lead to improved bioavailability of the copper ion, facilitating its penetration into lipid membranes and thus resulting, hopefully, in better antimycotic profiles for the metal complexes. With this in mind, **L1–L4** are reacted with $CuCl_2$ leading to the isolation of the copper(I) complexes **1–4**. The ^{1}H-NMR spectra of **1–4**, recorded in DMSO-d_6, support the copper(I) oxidation state for the metal ion: Cu(I), in fact, has a d^{10} electronic configuration and its diamagnetic nature led to sharp signals. In the spectrum of **1**, for example, (Fig. S1) the NH proton was shifted to lower fields, compared to the free ligand, due to the coordination to the metal; the same trend was observed for the chemical shifts of the NH_2 and of the iminic proton. The formation of copper(I) complexes is not completely surprising: it is known that thiosemicarbazones can undergo intramolecular oxidative cyclisation in presence of bases[33], oxidants[34] or redox-active metals like Fe^{3+} or, as in the present case, Cu^{2+} [35]. Copper(II) reduction is a step of a mechanism in which the cyclisation of part of the thiosemicarbazone ligand is also involved[36]. Since thiosemicarbazones possess two nucleophilic centres (N(5) and S) and a C = N double bond, two principal mechanisms are possible, leading to different products: 1,2,4-triazole-3-thione derivatives, formed by intramolecular addition of N(5) to C = N (Fig. 2A), and 1,3,4-thiadiazoline-2-amine derivatives, obtained by the addition of the sulphur atom to the iminic moiety (Fig. 2B). Other oxidative cyclisation mechanisms are reported and desulfurization processes can also occur[37]. However, in the ^{1}H-NMR spectra of **1–4** no signals attributable to the cyclized products could be seen. The signals related to the cyclized ligand can be found in ^{1}H-NMR spectra of a solid obtained by evaporation of the mother liquor after precipitation of the complex (as an example, see Fig. S2). No signals related to the iminic proton are present in this spectrum, as well as peaks attributable to the NH_2 protons, indicating that part of the ligand has undergone a cyclization process according to Fig. 2A. As a consequence of the copper(II) reduction and the cyclization processes, the initial 2:1 ligand to metal stoichiometry is lost and the multimetallic complexes **1–4** are obtained. The formation of these structures could be possible because the thiosemicarbazone ligands possess various coordinative sites: **L1–L4** can coordinate the metal ion as monodentate, *N*,*S*-bidentate or can form bridged structures. The presence of other donor atoms on the phenyl ring could give rise to additional coordination sites. In particular, data analysis suggests 3:2 metal to ligand stoichiometry for compounds **1**, **3** and **4**, and 2:1 metal to ligand stoichiometry for complex **2**. In all the ESI-MS spectra peaks relative to multimetallic species are present, even if with very low intensity (Fig. S3–S6), while base peaks are relative to the 2:1 ligand to metal species. Comparison of the IR spectra of the copper complexes with that of the corresponding ligands made it possible to highlight a shift to slightly higher wavenumbers of the C = N stretching vibration, indicating the involvement of the iminic nitrogen in the coordination to the metal ion. It seems reasonable to conclude that the reactions of **L1–L4** with $CuCl_2$ led to the isolation of multimetallic copper(I) complexes but, unfortunately, hypotheses on the structures of these complexes **1–4** still remain speculative due to the absence of X-ray single crystal diffraction data.

Different is the case of the ligands **L5** and **L6** (Fig. 1), where the NH_2 hydrogens are substituted by two methyl groups. In these cases, in fact, during the reactions with $CuCl_2$, reduction of copper(II) is accompanied by complete cyclisation of the ligands to obtain the Cu(I) complexes **5** and **6**. In their ^{1}H-NMR spectra the aromatic region displayed sharp signals related to the hydrogens of the phenyl ring of the coordinated cyclized thiosemicarbazone. No other signals can be found around 8 or 10 ppm, related respectively to the iminic or NH protons: **L5** and **L6** are cyclized according to Fig. 2B.

X-ray structure analysis. The crystal structure of **L5′**, the cyclized form of **L5**, is represented as an ORTEP view in Figure S7. The molecule is formed by two moieties, the benzene and the thiadiazolic rings. Both fragments are planar but not perfectly coplanar: in fact, the two planes present a slight tilt of 11.12° around the C2-C3 bond. In the aromatic 1,3,4-thiadiazolic ring, the double bonds are fairly localized between C1 = N2 and C2 = N3 (1.321 and 1.304), in contrast with 1.373 Å of the N-N bond and 1.745 and 1.750 of the C-S bonds which are closer to single bond lengths. The packing is mainly determined by pairs of CH…N hydrogen bonds between two aromatic carbon atoms and the two nitrogen atoms of the thiadiazolic ring of a nearby molecule. This system of hydrogen bonds forms ribbons which propagate along the *c* axis direction. The ribbons are in turn packed through an extended network of van der Waals interactions between the methyl groups and the aromatic rings of adjacent molecules.

In the crystal structure of compound **5′** (Fig. 3A) the copper(II) ion lies on a centre of symmetry and is surrounded by two chloride ions and two ligands, bonded through the N2 nitrogen, in a square planar coordination geometry. The ligands are almost perpendicular to the coordination plane forming an angle of 78.30°. Noteworthy are the intermolecular interactions between the terminal methyl groups and the chlorine atoms, which characterize the packing, as shown in Figure S8.

Similarly the crystal structure of **6′** is formed by a copper(II) ion lying on a centre of symmetry in a square planar coordination geometry surrounded by two chloride ions and two ligands (Fig. 3B). Differently from **5′**, the atom bonded to copper is the N3 nitrogen. Also in this case the ligands are almost perpendicular to the coordination plane and form an angle of 87.43°. In this structure the most characterizing feature in the packing is the hydrogen bonds between the oxygens of the methoxy groups and the terminal methyl groups of an adjacent molecule (Fig. S9).

Fungal growth and aflatoxin inhibition. Looking at the results reported in Table 1, it can be seen that among the free ligands, only **L2** (at 50 μM) and **L5** (at 100 μM) halved the biomass increase, while **L1**, **L3**, **L4** and **L6** were provided with no or scarce fungistatic activity.

L5 and **L6** showed the best results in term of inhibition of mycotoxin biosynthesis (Table 1). Interestingly, as reported above, **L5** displayed a moderate fungistatic activity (43 and 22% at 100 and 50 μM, respectively). This is an important aspect to take into consideration: indeed the prevalent economic and sanitary issue posed by *A. flavus* colonization of cereal crops is essentially dependent on mycotoxin release by the mould on the contaminated substrate rather than to a plant pathogenic effect. Specifically targeting the aflatoxin biosynthetic apparatus of *A. flavus*, by using a compound with as low as possible generic fungistatic activity, may have a not secondary beneficial effect of avoiding possible deleterious outcomes due to unwanted modification of the microbiota composition in the environment.

Differences in activity on AF production can be analyzed as a function of the lipophilicity of the compound, as lipophilicity is generally correlated to the ability of the molecule to penetrate through the cell membrane[38,39]. Also in this case, the low activity of **L1–L4** could be correlated to their inability to efficiently penetrate the cell membrane due to their low values of lipophilicity (Table S1); **L5** and **L6** are more lipophilic and an increased activity was observed.

Coordination to copper ions generally increases antiaflatoxigenic activity, resulting in a better activity profile (Table 1).

Cytotoxicity and genotoxicological assessment on bacteria, plants and human cells. Fungal and aflatoxigenic inhibitors have to be used in agriculture and, obviously, they have to be safe for the operators and for the environment. Thus, a screening of the cytotoxicity of the most active compounds in term of aflatoxin inhibition (**2**, **3**, **5**, **6** and **L5**) was performed over a panel of human cell lines. Three normal cell lines were taken into consideration: colon (CRL1790), skin (Hs27), lung (HFL1), and one tumoral cell line (U937). Normal cells were chosen to represent the different routes of exposure by which this kind of chemicals can come in contact and/or enter human bodies: epidermal contact (Hs27), inhalation (HFL1) and ingestion (CRL1790). In addition, we used a tumoral cell line (U937), since it is a good cell model used worldwide to identify cytotoxicity and genotoxic activity of drugs[40]. Looking at the results (Table 2 and Figure S10) it can be seen that only **L5** has a good cytotoxicity profile, while, unfortunately, all the copper complexes showed important cytotoxicity in the micromolar range, and cannot be further evaluated.

L5, instead, was selected for analysis of mutagenicity and genotoxicity on bacteria, plants and human cells. The mutagenic action of a hit compound, in fact, has to be carefully evaluated for the development of new agrochemicals safe for the environment and human health. As reported in Table 3, **L5** exhibited no mutagenicity in the Ames test on *S. typhimurium* TA100 and TA98 strains with or without metabolic activation at all tested doses. However, even if we could not find a clear genotoxic effect of **L5** with *A. cepa* tests, the chromosomal damage that we observed at 25 μM dose suggested a potential clastogenic or aneugenic activity. Moreover, **L5** toxic activity was revealed by the inhibition of cell cycle, showed by decrease of mitotic index at the highest dose (Table 4). Since it is important to establish also the potential ability of a new hit compound to induce damage of human cellular DNA, an Alkaline Comet assay was performed on **L5**. Results reported in Fig. 4 unfortunately confirm the data collected on *A. cepa*, showing a damaging activity of **L5** on DNA that could be correlated to chromosomal aberrations induction.

Conclusions

In the present work, the thiosemicarbazone ligands **L1–L6** have been evaluated for their antifungal and antiaflatoxigenic ability. Effectively, some of these compounds showed relevant aflatoxigenic inhibition (up to 90% reduction of AF accumulation for **L5** at 100 μM), still maintaining a moderate fungistatic activity. This last aspect is

particularly important. In fact, specifically targeting the aflatoxin biosynthetic process, by using a compound with as low as possible fungistatic activity, may avoid possible deleterious outcomes due to unwanted modification of the microbiota composition in the environment. The antifungal and antiaflatoxigenic activities vary considerably along the series **L1–L6**, without apparent connection with the complexing ability of these molecule, an idea that, on the contrary, it is often invoked in the literature[41]. Perhaps, the differences in activity in **L1–L6** could be related to variations in lipophilicity, since an increase of lipophilicity seems to imply an increase in antiaflatoxigenic activity. It is claimed[12] that metal complexation leads to species more active than the corresponding ligand in term of both fungistatic and aflatoxigenic profile. This is also the case of the copper complexes **1–6** here synthesised. However, in the development of crop-protective agents, it is not sufficient to obtain efficient aflatoxigenic inhibitors, but at the same time risks for humans and plants have to be taken into account[42]. Unfortunately, all the metal complexes **1–6** evidenced high cytotoxicity on different human, normal and tumoral, cell lines. On the contrary, **L5** joins interesting fungistatic and antiaflatoxigenic activities, with a good cytotoxic profile and it seems a promising starting point for the development of efficient crop-protective agents. However, further studies are ongoing, because deeper genotoxical assessments on human cells and plants (Comet assay, chromosome aberration test in *A. cepa*) highlighted possible chromosomal aberrations induction for **L5**.

We would like to conclude that: 1) the thiosemicarbazone scaffold seems a promising chemotype for the development of aflatoxin inhibitors, and 2) claims about the individuation of efficient aflatoxin inhibitors, in particular if metal complexes, for further developments as crop-protective agents, have to be combined with deep studies to assess the genotoxic potential risk for environmental and human health.

References

1. Oerke, E. C. & Dehne, H. W. Safeguarding production-losses in major crops and the role of crop protection. *Crop Protection* **23**, 275–285 (2004).
2. Tournas, V. H. Spoilage of vegetable crops by bacteria and fungi and related health hazards. *Critical reviews in microbiology* **31**(1), 33–44 (2005).
3. Gross-Steinmeyer, K. & Eaton, D. L. Dietary modulation of the biotransformation and genotoxicity of aflatoxin B(1). *Toxicology* **299**(2–3), 69–79, doi:https://doi.org/10.1016/j.tox.2012.05.016 (2012).
4. Schatzmayr, G. & Streit, E. Global occurrence of mycotoxins in the food and feed chain: facts and figures. *World Mycotoxin J.* **6**, 213–222 (2013).
5. EFSA Scientific Report vol. 305 (2009).
6. World Health Organization. WHO estimates of the global burden of foodborne diseases: foodborne disease burden epidemiology reference group 2007–2015 (2015).
7. Hüter, O. Use of natural products in the crop protection industry. *Phytochem. Rev.* **10**, 185–194 (2011).
8. Holmes, R. A., Boston, R. S. & Payne, G. A. Diverse inhibitors of aflatoxin biosynthesis. *Appl Microbiol. Biotechnol.* **78**, 559–572 (2008).
9. Ma, Y. T. *et al*. Natural products as sources of new fungicides (I): synthesis and antifungal activity of acetophenone derivatives against phytopathogenic fungi. *Chem. Biol. Drug. Des.* **81**, 545–552 (2013).
10. Gowda, N. K. S., Malathi, V. & Suganthi, R. U. Effect of some chemical and herbal compounds on growth of *Aspergillus parasiticus* and aflatoxin production. *Animal Feed Sci. Technol.* **116**, 281–291 (2004).
11. Cuero, R., Ouellet, T., Yu, J. & Mogongwa, N. Metal ion enhancement of fungal growth, gene expression and aflatoxin synthesis in *Aspergillus flavus*: RT-PCR characterization. *J. App. Microbiology* **94**, 953–961, doi:https://doi.org/10.1046/j.1365-2672.2003.01870.x (2003).
12. Pelosi, G. Thiosemicarbazone Metal Complexes: From Structure to Activity. *Open Crystallogr. J.* **3**, 16–28 (2010).
13. Degola, F. *et al*. *In vitro* evaluation of the activity of thiosemicarbazone derivatives against mycotoxigenic fungi affecting cereals. *Int. J. Food Microbiol.* **200**, 104–111, doi:https://doi.org/10.1016/j.ijfoodmicro.2015.02.009 (2015).
14. Zani, C. *et al*. A new approach using a battery of assays to evaluate the efficacy of thiosemicarbazone derivatives as antifungal and anti-mycotoxigenic agents and their cytotoxic and genotoxic activity. *Food Chem. Toxicol.* **105**, 498–505 (2017).
15. Rogolino, D. *et al*. Investigation of the salicylaldehyde thiosemicarbazone scaffold for inhibition of influenza virus PA endonuclease. *J. Biol. Inorg. Chem.* **20**, 1109–1121 (2015).
16. Betteridge, P. W., Carruthers, J. R., Cooper, R. I., Prout, K. & Watkin, D. J. *J. Appl. Cryst.* **36**, 1487 (2003).
17. SAINT: SAX, Area Detector Integration, Siemens Analytical Instruments Inc., Madison, Wisconsin, USA.
18. Sheldrick, G. *SADABS: Siemens Area Detector Absorption Correction Software*, University of Goettingen, Germany (1996).
19. Altomare, A. *et al*. SIR97: a new tool for crystal structure determination and refinement. *J. Appl. Cryst.* **32**, 115–119, doi:https://doi.org/10.1107/S0021889898007717 (1999).
20. Sheldrick, G. M. A short history of SHELX. *Acta Cryst.* **A64**, 112–122, doi:https://doi.org/10.1107/S0108767307043930 (2008).
21. Farrugia, L. J. WinGX suite for small-molecule single-crystal crystallography. *J. Appl. Cryst.* **32**, 837–838, doi:https://doi.org/10.1107/S0021889899006020 (1999).
22. Degola, F., Berni, E. & Restivo, F. M. Laboratory tests for assessing efficacy of atoxigenic Aspergillus flavus strains as biocontrol agents. *Int. J. Food Microbiol.* **146**, 235–43, doi:https://doi.org/10.1016/j.ijfoodmicro.2011.02.020 (2011).
23. Degola, F., Dall'Asta, C. & Restivo, F. M. Development of a simple and high-throughput method for detecting aflatoxins production in culture media. *Letters in applied microbiology* **55**, 82–9, doi:https://doi.org/10.1111/j.1472-765X.2012.03264.x (2012).
24. Malik, H. S., Eickbush, T. H. & Goldfarb, D. S. Evolutionary specialization of the nuclear targeting apparatus. *Proc. Natl. Acad. Sci. USA* **94**, 13738–42 (1997).
25. Buschini, A. *et al*. Synthesis, characterization and deepening in the comprehension of the biological action mechanisms of a new nickel complex with antiproliferative activity. *J. Inorg. Biochem.* **103**, 666–77, doi:https://doi.org/10.1016/j.jinorgbio.2008.12.016 (2009).
26. Maron, D. M. & Ames, B. N. Revised methods for the *Salmonella* mutagenicity test. *Mutat. Res.* **113**, 173–215 (1983).
27. APHA. Standard Method for the Examination of Water and Wastewater, 22nd ed. American Public Health Association, American Water Works Association, Water Environment Federation, Washington DC, USA ISBN 978-087553-013-0 (2012).
28. Mortelmans, K. & Zeiger, E. The Ames *Salmonella*/microsome mutagenicity assay. *Mutat. Res.* **455**, 29–60 (2000).
29. Fiskesjo, G. The *Allium* test as a standard in environmental monitoring. *Hereditas* **102**, 99–112 (1985).
30. Fiskesjo, G. The *Allium* test – a potential standard for the assessment of environmental toxicity. Environmental Toxicology and Risk Assessment; 2nd Volume, ASTM STP 1216, Gorsuch, J. W., Dwyer F. J., Ingersoll, C. G. & La Point, T. W. Eds, American Society for Testing and Materials, Philadelphia, pp 331–345 (1993).
31. Ma, T. H. *et al*. The improved *Allium/Vicia* root tip micronucleus assay for clastogenicity of environmental pollutants. *Mut. Res.* **334**, 185–195 (1995).

32. Cabaravdic, M. Induction of chromosome aberrations in the *Allium cepa* test system caused by the exposure of cells to benzo(a) pyrene. *Med. Arh.* **64**(4), 215–218 (2010).
33. Addison, A. W., Rao, T. N., Reedijk, J., van Rijn, J. & Verschoor, G. C. Synthesis, structure, and spectroscopic properties of copper(II) compounds containing nitrogen–sulphur donor ligands; the crystal and molecular structure of aqua[1,7-bis(N-methylbenzimidazol-2′-yl)-2,6-dithiaheptane]copper(II) perchlorate. *J. Chem. Soc. Dalton Trans.* 1349–1356 (1984).
34. Korzycka, L., Glowka, M. & Janicka, J. Synthesis and X-ray studies of derivatives of 1,2,4-triazolidine-3-thiones. *Pol. J. Chem.* **72**, 73–77 (1998).
35. Noto, R., Lo Meo, P., Gruttadauria, M. & Werber, G. A quantitative study of substituent effects on oxidative cyclization of some 2-aryl-substituted aldehyde thiosemicarbazones induced by ferric chloride and cupric perchlorate. *J. Heterocycl. Chem.* **36**, 667–674 (1999).
36. Pedrido, R. *et al*. Metal-catalysed oxidation processes in thiosemicarbazones: new complexes with the ligand N-{2-([4-N-ethylthiosemicarbazone]methyl)phenyl}-p-toluenesulfonamide. *Chem. Eur. J.* **14**, 500–512 (2008).
37. Gill-Garcia, R. *et al*. Desulfurization processes of thiosemicarbazonecopper(II) derivatives in acidic and basic aqueous media. *New J. Chem.* **37**, 3568–3580 (2013).
38. Veldman, R. J., Zerp, S., van Blitterswijk, W. J. & Verheij, M. N. Hexanoyl-sphingomyelin potentiates *in vitro* doxorubicin cytotoxicity by enhancing its cellular influx. *Br. J. Cancer* **90**, 917–925 (2004).
39. Price, K. A. *et al*. Mechanisms controlling the cellular accumulation of Copper bis(thiosemicarbazonato) complexes. *Inorg. Chem.* **50**(19), 9594–9605, doi:https://doi.org/10.1021/ic201334q (2011).
40. Sak, K. & Everaus, H. Established human cell lines as models to study anti-leukemic effects of flavonoids. *Curr. Genomics* **18**(1), 3–26 (2017).
41. Veronika Opletalovà *et al*. Identification and characterization of thiosemicarbazones with antifungal and antitumor effects: cellular Iron chelation mediating cytotoxic activity. *Chem. Res. Toxicol.* **21**, 1878–1889 (2008).
42. García-Santamarina, S. & Thiele, D. J. Copper at the fungal pathogen-host axis. *J. Biol. Chem.* **290**(3), 18945–18953 (2015).

Acknowledgements

This study was supported by a grant from "Fondazione Cariplo" (Project N. 2014-0555; http://aflatox.it). "Centro Interdipartimentale Misure Giuseppe Casnati" of the University of Parma is thanked for facilities. Dr. Monica Maffini is thanked for technical assistance in ICP analysis.

Author Contributions

The manuscript was written through contributions of all authors. All authors have given approval to the final version of the manuscript. D.R., A.G., M.C., F.B., G.P.: molecular design and chemical synthesis; G.P.: crystallographic studies; F.M.R., F.D.: fungal growth and aflatoxin inhibition evaluation. A.B., S.M.: cyto- and geno-toxicological assessment on human cells. D.F., C.Z.: genotoxicological assessment on bacteria, and plants.

Additional Information

Supplementary information accompanies this paper at doi:10.1038/s41598-017-11716-w

Competing Interests: The authors declare that they have no competing interests.

Publisher's note: Springer Nature remains neutral with regard to jurisdictional claims in published maps and institutional affiliations.

Journal of Inorganic Biochemistry 179 (2018) 60–70

Contents lists available at ScienceDirect

Journal of Inorganic Biochemistry

journal homepage: www.elsevier.com/locate/jinorgbio

Effects of polar substituents on the biological activity of thiosemicarbazone metal complexes

Franco Bisceglie[a,b], Matteo Tavone[a], Francesca Mussi[a], Simone Azzoni[a], Serena Montalbano[a], Susanna Franzoni[a], Pieralberto Tarasconi[a,b], Annamaria Buschini[a,b,1], Giorgio Pelosi[a,b,*,1]

[a] Department of Chemistry, Life Sciences and Environmental Sustainability, University of Parma, Parco Area delle Scienze 17A, 43124 Parma, Italy
[b] CIRCMSB (Consorzio Interuniversitario di Ricerca in Chimica dei Metalli nei Sistemi Biologici), Parma Unit, University of Parma, Italy

ARTICLE INFO

Keywords:
Thiosemicarbazone
Copper(II)
Nickel(II)
Metal complex
Histosensitivity
Anticancer

ABSTRACT

In this paper, citronellal, vanillin and pyridoxal thiosemicarbazones were modified with polar substituents, namely ethylmorpholine and glucose, to increase their polarity and compare the effects of these moieties on their biological activity. Altogether, nine ligands were synthesized and for each of them also their copper(II) and nickel(II) complexes were prepared and used for the biological tests. Eventually, assays on proliferation inhibition were conducted using leukemic cell line U937, already used as a model for previous citronellal thiosemicarbazone tests. Biological tests were also performed on solid tumor cell line HT29. From the first screenings, two of the metal complexes showed remarkable interesting properties, and, therefore, were also tested for histosensitivity.

1. Introduction

Thiosemicarbazones are biochemically interesting compounds which exert a wide range of biological activities [1–7], and, thanks to this property, are promising, as drugs, in the treatment of many diseases [8–15].

The condensation reaction between an aldehyde or a ketone with thiosemicarbazides that brings to the formation of thiosemicarbazones is straightforward and normally gives high yields of product, but the scarce solubility of the product in water, i.e. the very same driving force that brings to completion these reactions, is one of the major drawbacks of these molecular systems [16,17]. This aspect has a negative impact in the perspective of a clean and green chemistry, which requires the use of aqueous media, but, more importantly, in their potential use as drugs. In fact, the proper balance between a drug hydrophilicity, which favours solubility and bioavailability, and lipophilicity, which allows these molecules to diffuse through the cell membrane lipidic bilayer, is a fundamental prerequisite for an efficient cellular uptake [18,19]. On this basis, the study of the influence of the aromatic/aliphatic nature of the parent aldehyde/ketone on the overall hydrophobicity/hydrophilicity of the molecule, also modulated by the presence of hydrophilic fragments on the terminal amino group, can help improve our understanding of the relationship between the thiosemicarbazone molecular structure and the biological activity exerted.

In this work, we have chosen citronellal, vanillin and pyridoxal as starting aldehydes to prepare the parent thiosemicarbazones.

The first two were selected as representative of aliphatic and aromatic derivatives respectively, while pyridoxal allows us to explore the role of the chelation mode in the activity of these compounds since the corresponding thiosemicarbazone can bind as a terdentate ligand to the metal ion. With the aim to modulate water solubility, two other fragments have been added to the thiosemicarbazide aminic nitrogen to tune the hydrophobicity/hydrophilicity of the whole molecule: N-ethylmorpholine and glucose. These two moieties reduce markedly the molecule hydrophobicity, and glucose was also chosen in the hope that the molecule could be possibly internalized through glucose transport proteins [19–21]. This substituent, being highly polar, should also help cast light on a putative internalization mechanism that assigns to these thiosemicarbazones a role in the transport of metal ions by diffusion through the cell membrane. In principle, these molecules could behave as ionophores. In this perspective, thiosemicarbazones would act by wrapping up the metal ion with their polar heads and exposing the hydrophobic part to the exterior making these complexes prone to cross the hydrophobic lipid bilayer of the cell membrane. The presence of polar groups should prevent or limit this mechanism.

To evaluate the influence of metal ions on the biological activity, copper(II) and nickel(II), two divalent metals of the first transition row, have been chosen to prepare coordination compounds with the above

* Corresponding author.
E-mail address: giorgio.pelosi@unipr.it (G. Pelosi).
[1] AB and GP have equally contributed to the paper and are to be considered co-last authors.

https://doi.org/10.1016/j.jinorgbio.2017.11.009
Received 11 September 2017; Received in revised form 20 October 2017; Accepted 5 November 2017
Available online 21 November 2017
0162-0134/

mentioned ligands.

Altogether, nine ligands have been synthesized and for each of them also their copper(II) and nickel(II) complexes were prepared and used for the biological tests. Eventually, assays on proliferation inhibition were conducted using leukemic cell line U937, already used as a model for previous citronellal thiosemicarbazone tests [22–25]. In this paper, biological tests were also performed on solid tumor cell line HT29. Already from the first screenings, two of the metal complexes showed remarkable interesting properties, and, therefore, were also tested for histosensitivity.

2. Experimental

2.1. General experimental conditions

Dry methanol was prepared according to standard procedures and stored over molecular sieves. TLC's were performed on Silica gel Merck 60 F_{254} aluminium sheets. Flash chromatography was performed on MP Silica 63–200 mesh 60 Å (EchoChrom™), ^{1}H NMR spectra were recorded on Bruker 300 Avance and Bruker 400 Avance spectrometers, at 300 K. The reported *J* values are referred to H,H coupling constants. Chemical shifts are reported as *δ* values in ppm using the solvent residual peak as internal standard. Elemental analysis was recorded on Flash 1112 Series Analyser (CE Instruments) Mass spectra by electrospray ionization (ESI) methods were recorded on LTQ ORBITRAP XL Thermo.

2.2. Crystallographic data collection and crystal structure determination

The X-ray diffraction data were collected on a Bruker-Siemens SMART AXS 1000 diffractometer equipped with a CCD detector and an Mo-Kα (λ = 0.71069 Å) source. The structures were solved by direct methods and refined using SHELXL97 [26]. The drawing were plotted using ORTEPIII [27] and Mercury [28]. CCDC 1571632–1571635 contain the supplementary crystallographic data. These data can be obtained free of charge via http://www.ccdc.cam.ac.uk/conts/retrieving.html, or from the Cambridge Crystallographic Data Centre, 12 Union Road, Cambridge CB2 1EZ, UK; fax: (+ 44) 1223-336-033, or e-mail: deposit@ccdc.cam.ac.uk.

2.3. Syntheses of the ligands

S-citronellal, vanillin and pyridoxal were condensed with three different thiosemicarbazides: thiosemicarbazide, N^4-ethylmorpholine-thiosemicarbazide and N^4-glucosyl thiosemicarbazide (Fig. 2.1) giving rise to nine ligands.

The former two thiosemicarbazides (D, E) were commercially available while the latter (F) was de novo synthesized using D-glucose as starting reagent.

D-glucose was acetylated with pyridine and 4-dimethylaminopyridine in acetic anhydride and then halogenated with HBr 33% in dichloromethane under nitrogen atmosphere to obtain α-acetobromo-D-glucose (Fig. 2.2).

In the presence of potassium thiocyanate and tetrabutyl ammonium chloride, following an S_N2 mechanism, bromide was substituted with an isothiocyanate group [29] giving the precursor of the thiosemicarbazide and its structure was determined by X-ray analysis (see the Experimental section).

Glucosyl thiosemicarbazide was obtained as a white solid by adding dropwise a solution of glucosyl isothiocyanate in ethanol into a cooled solution of hydrazine in ethanol [7].

All the condensation reactions between the functionalized thiosemicarbazide and the selected aldehydes to obtain thiosemicarbazones were carried out refluxing for several hours the reagents in ethanol. Acetylated glucosyl thiosemicarbazones were then deprotected following the Zemplen procedure (MeONa/MeOH dry).

Table 2.1 reports a schematic representation of the synthesized compounds.

Table 2.2 summarizes the synthesized ligands and the acronyms used from here on.

2.3.1. [CitrTSC], (S-citronellal thiosemicarbazone) (1)

The synthesis of compound (**1**) was carried out following a previously described procedure [30]. Briefly, a solution of S-citronellal (0.40 mL, 2.22 mmol) and thiosemicarbazide (0.21 g, 2.22 mmol) in EtOH (10 mL) was refluxed for 60 min under stirring, the mixture was then cooled and the product was isolated as a white powder.

Yield: 95%. **^{1}H NMR** (300 MHz, $CDCl_3$): δ_H (ppm) 9.05 (s, 1H, *NH*), 7.27 (t, 1H, *J* = 6.0 Hz, *CH*=N), 7.08 (2br s, 1H each, *NH*), 5.04 (m, 1H, *CH* = $C(CH_3)_2$), 2.20 (2 m, 2H, CH_2CHCH_3), 1.94 (m, 2H, $CH_2CH = C(CH_3)_2$), 1.76 (m, 1H, CH_2CHCH_3), 1.64 and 1.56 (2 s, 6H, 3H each, $CH(CH_3)_2$), 1.34 (m, 1H, CH_2CHCH_3), 1.34 - 1.28 (2 m, 2H, 1H each, $CH_3CHCH_2CH_2$), 0.94 (3H, d, *J* = 7.0, $CHCH_3$).

2.3.2. [CitrMor], (S-citronellal-4-[2-(4-morpholinyl)ethyl]-3-thiosemicarbazone) (2)

Also the synthesis of compound (**2**) was carried out following a previously described procedure [25]. Briefly, a solution of S-citronellal (0.35 mL, 1.95 mmol) in EtOH 95% (10 mL) was added to a stirred solution of N^4-ethyl morpholine thiosemicarbazide (398 mg, 1.95 mmol) in EtOH 95% (10 mL). The mixture was refluxed until TLC ($AcOEt/C_6H_{12}$ 1:3) revealed starting material consumption. After concentration under reduced pressure, a pale yellow oil was obtained.

Yield: 96%. **^{1}H NMR** (300 MHz, $CDCl_3$): δ_H (ppm) 8.78 (s, 1H,

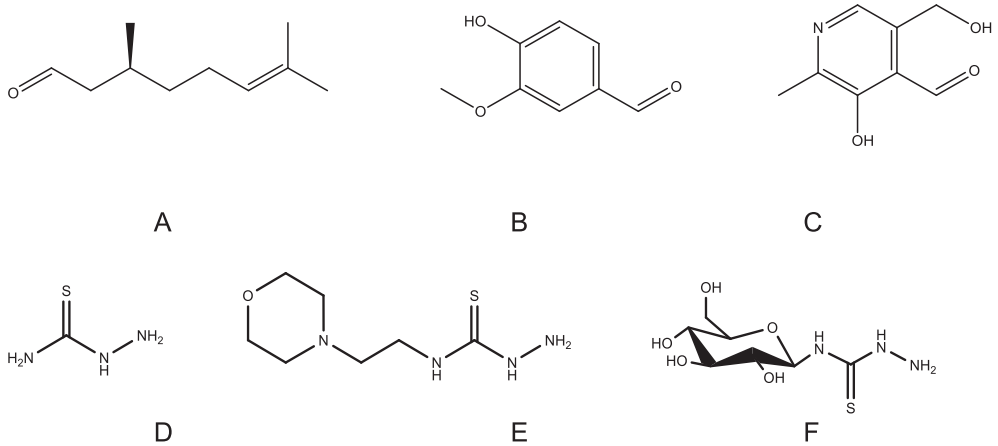

Fig. 2.1. Schematic representation of *S*-citronellal (A), vanillin (B) and pyridoxal (C), thiosemicarbazide (D), N^4-ethylmorpholine-thiosemicarbazide (E) and N^4-glucosyl thiosemicarbazide (F).

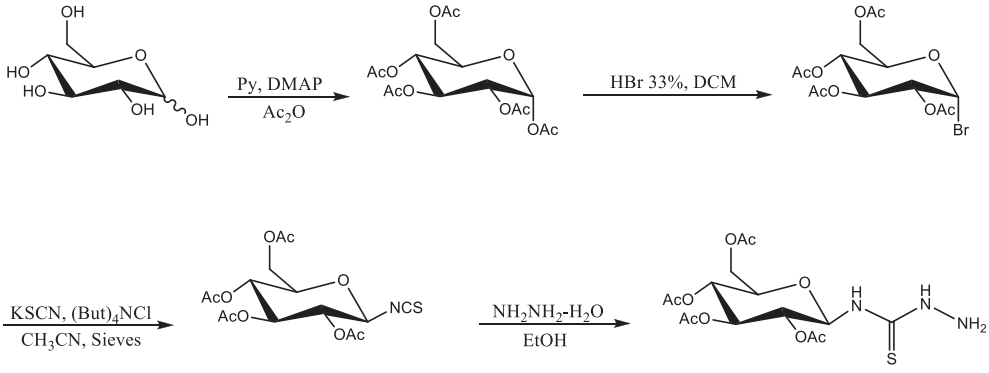

Fig. 2.2. Synthesis of acetylated glucosyl thiosemicarbazide. Py, pyridine; DMAP, dimethylaminopyridine; DCM, dichloromethane.

Table 2.1
Schematic representation of the synthesized ligands and their reaction intermediates.

1	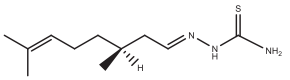	2	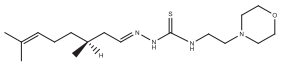
3	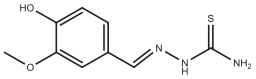	4	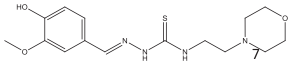
5	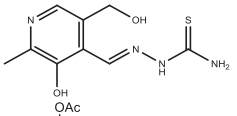	6	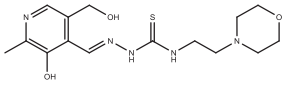
7	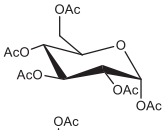	8	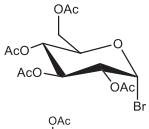
9	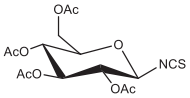	10	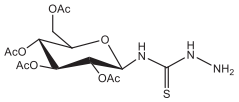
11	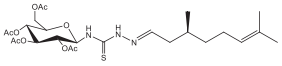	12	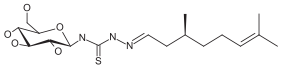
13	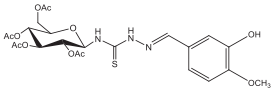	14	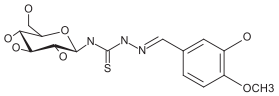
15	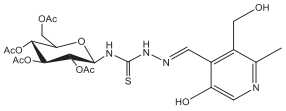	16	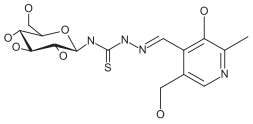

CH_2NHC = S), 7.88 (bs, 1H, *NH*N=C), 7.15 (t, 1H, *CH*=N), 5.04 (m, 1H, *CH* = $C(CH_3)_2$), 3.74 (2 m, 4H, OCH_2CH_2N + CH_2NHCS), 2.65 (t, 2H, OCH_2CH_2N), 2.52 (m, 2H, $NHCH_2CH_2N_{Mor}$), 2.27 (m, 1H, C_3H_2, H-a), 2.0 (m, 4H, OCH_2CH_2N,), 1.94 (m, 2H, $CH_2CH = C(CH_3)_2$), 1.76 (m, 1H, CH_2CHCH_3), 1.70 and 1.62 (2 s, 6H, 3H each, $CH(CH_3)_2$), 1.4 - 1.25 (2 m, 2H, 1H each, $CH_3CHCH_2CH_2$), 0.94 (d, 3H, *J* = 7.0, $CHCH_3$).

2.3.3. [VanTSC], (vanillin thiosemicarbazone) (3)

Compound (**3**) was synthesized modifying a procedure present in the literature [31]. A solution of vanillin (0.2 g, 1.31 mmol) and thiosemicarbazide (0.11 g, 1.31 mmol) in EtOH (20 mL) was refluxed under stirring, and after 60 min was cooled. By slow solvent evaporation, the product was isolated as a yellow crystalline powder.

Yield: 92%. **^{1}H NMR** (300 MHz, $CDCl_3$): δ_H (ppm) 11.38 (s, 1H, *NH*N), 9.72 (s, 2H, NH_2), 7.96 (s, 1H, *CH*=N), 7.33 (d, *J* = 1.59 Hz, 1H, H_5van), 7.13 (dd, *J* = 8.20, 1.59 Hz, 1H, H_2van), 6.81 (d, *J* = 8.20 Hz, 1H, H_3van), 3.83 (s, 3H, OCH_3).

2.3.4. [VanMor], (vanillin-4-[2-(4-morpholinyl)ethyl]-3-thiosemicarbazone) (4)

A stirred solution of vanillin (0.20 g, 1.31 mmol) and N4 ethyl morpholine thiosemicarbazide (0.26 g, 1.31 mmol) in EtOH (15 mL) was refluxed. After a 3 h treatment, the mixture was poured into a crystallizer and the solvent was slowly left to evaporate to afford the product as white crystals apt for X-ray crystallography.

Yield: 90%

^{1}H NMR (300 MHz, $CDCl_3$): δ_H (ppm) 11.38 (s, 1H, *NH*N), 8.29 (t, *J* = 5.29 Hz, 1H, *NH*), 7.96 (s, 1H, *CH*=N), 7.33 (d, *J* = 1.59 Hz, 1H, H_5van), 7.13 (dd, *J* = 8.20, 1.59 Hz, 1H, H_2van), 6.81 (d, *J* = 8.20 Hz, 1H, H_3van), 3.83 (s, 3H, OCH_3), 3.68 (m, 2H, CH_2NH), 3.56 (t, 2H, OCH_2CH_2N), 2.51 (t, *J* = 4.84 Hz, 1H, CH_2 CH_2NH), 2.44 (m, 2H, OCH_2CH_2N)

Crystallographic data: C15H22N4O3S1, Mr. = 338.42, triclinic, space group P-1, a = 7.051(2), b = 8.119(2), c = 15.798(4) Å, α = 82.014(3), β = 79.889(3), γ = 86.463(4)°; V = 881.1(4) $Å^3$, Z = 2, ρcalc = 1.276 Mgm^{-3}, *T* = 298.15 K, F(000) = 210, crystal size = 0.20 × 0.20 × 0.20 mm, index range = −9 < h < 9, −10 < k < 10, −20 < l < 20, collected reflections = 11,561,

Table 2.2
The synthesized ligands and the acronyms used.

	Citronellal (A)	Vanillin (B)	Pyridoxal (C)
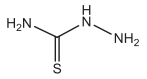	CitrTSC (**1**)	VanTSC (**3**)	PyrTSC (**5**)
(D) 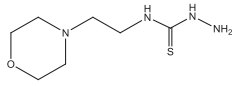	CitrMor (**2**)	VanMor (**4**)	PyrMor (**6**)
(E) 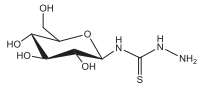	CitrGlu (**12**)	VanGlu (**14**)	PyrGlu (**16**)
(F)			

Table 3.1
Comparison between the polarities (logP) of the new thiosemicarbazones

	logP		logP		logP
CitrTSC (**1**)	3.3	CitrMor (**2**)	3.2	CitrGlu (**12**)	1.5
PyrTSC (**5**)	1.2	PyrMor (**6**)	1.2	PyrGlu (**16**)	− 0.5
VanTSC (**3**)	0.2	VanMor (**4**)	0.2	VanGlu (**14**)	− 1.4

Table 3.2
U937 GI_{50} of Cu and Ni of citronellal and vanillin thiosemicarbazonates

	Complexes	GI_{50} (μM)	Complex	GI_{50} (μM)
Tsc	$Cu(CitrTSC)_2$	14.7	$Cu(VanTSC)_2$	17
	$Ni(CitrTSC)_2$	10	$Ni(VanTSC)_2$	40
Mor	$Cu(CitrMor)_2$	2.3	$Cu(VanMor)_2$	9
	$Ni(CitrMor)_2$	12.3	$Ni(VanMor)_2$	19.5
Glu	$Cu(CitrGlu)_2$	18	$Cu(VanGlu)_2$	> 50
	$Ni(CitrGlu)_2$	44	$Ni(VanGlu)_2$	> 50

Table 3.3
Ligand and complex concentrations that inhibit growth at 50% (GI_{50}, 50% Growth Inhibition), growth at 100% (TGI, Total Growth Inhibition) and that are lethal at 50% (LC_{50}, 50% Lethal Concentration) for cell line U937 (histiocytic lymphoma).

U937			
Compound	GI_{50} (μM)	TGI (μM)	LC_{50} (μM)
CitrTSC	> 50	> 50	> 50
$Ni(CitrTSC)_2$	10	50	> 50
$Cu(CitrTSC)_2$	14.7	> 50	> 50
CitrGlu	> 50	> 50	> 50
$Ni(CitrGlu)_2$	44	> 50	> 50
$Cu(CitrGlu)_2$	18	38	> 50
CitrMor	> 50	> 50	> 50
$Ni(CitrMor)_2$	7.8	20	39.5
$Cu(CitrMor)_2$	2.3	4.6	7
VanTSC	> 50	> 50	> 50
$Ni(VanTSC)_2$	40	> 50	> 50
$Cu(VanTSC)_2$	17	40.5	> 50
VanGlu	> 50	> 50	> 50
$Ni(VanGlu)_2$	> 50	> 50	> 50
$Cu(VanGlu)_2$	> 50	> 50	> 50
VanMor	> 50	> 50	> 50
$Ni(VanMor)_2$	19.5	50	> 50
$Cu(VanMor)_2$	9	35	> 50

Table 3.4
Ligand and complex concentrations that inhibit growth at 50% (GI_{50}, 50% Growth Inhibition), growth at 100% (TGI, Total Growth Inhibition) and that are lethal at 50% (LC_{50}, 50% Lethal Concentration) for cell line HT29 (colon carcinoma).

HT-29			
Compound	GI50 (μM)	TGI (μM)	LC50 (μM)
CitrTSC	> 50	> 50	> 50
$Ni(CitrTSC)_2$	47	> 50	> 50
$Cu(CitrTSC)_2$	10	24.5	40.5
CitrGlu	> 50	> 50	> 50
$Ni(CitrGlu)_2$	> 50	> 50	> 50
$Cu(CitrGlu)_2$	> 50	> 50	> 50
CitrMor	> 50	> 50	> 50
$Ni(CitrMor)_2$	> 50	> 50	> 50
$Cu(CitrMor)_2$	7.5	20.5	37
VanTSC	> 50	> 50	> 50
$Ni(VanTSC)_2$	> 50	> 50	> 50
$Cu(VanTSC)_2$	> 50	> 50	> 50
VanGlu	> 50	> 50	> 50
$Ni(VanGlu)_2$	> 50	> 50	> 50
$Cu(VanGlu)_2$	> 50	> 50	> 50
VanMor	> 50	> 50	> 50
$Ni(VanMor)_2$	> 50	> 50	> 50
$Cu(VanMor)_2$	34	> 50	> 50

unique reflections = 4037, refined parameters = 208, goodness-of-fit = 1.043, final R factor = 0.0407, wR2 = 0.1235, electronic density residues = 0.19 and − 0.16 $eÅ^{-3}$.

2.3.5. [PyrTSC], (pyridoxal thiosemicarbazone) (5)

Compound (**5**) was synthesized modifying a procedure found in the literature [32]. Pyridoxal (0.2 g, 1.31 mmol) and thiosemicarbazide (0.11 g, 1.31 mmol) were dissolved in EtOH (10 mL) and the solution was placed under reflux. After 2 h, the mixture was cooled and the product was isolated as a yellow powder.

Yield: 92%. **^{1}H NMR** (300 MHz, DMSO-d_6): δ_H ppm 11.60 (br s, 1H, *NH*), 9.65 (br s, 1H, *OH*), 8.57 (s, 3H, *CH*Npy + NH_2), 7.99 (s, 1H, *CH*N), 5.25 (s, 1H, OH), 4.57 (s, 2H, CH_2O), 1.76 (s, 3H, CH_3).

2.3.6. [PyrMor], (pyridoxal-4-[2-(4-morpholinyl)ethyl]-3-thiosemicarbazone) (6)

A stirred solution of pyridoxal (0.40 g, 2.39 mmol) and thiosemicarbazide (0.48 g, 2.39 mmol) in EtOH (30 mL) was refluxed and during the process a precipitate separated. After 3 h, the solution was filtered and the product collected.

Yield: 90%. **^{1}H NMR** (300 MHz, DMSO-d_6): δ_H ppm 11.72 (br s, OH), 8.58 (s, 1H, *CH*pyr), 8.30 (br m, 1H, *NH*), 8.01 (s, 1H, *HC*═N), 5.27 (t, J = 5.32 Hz, 1H, CH_2*OH*), 4.61 (d, J = 5.00 Hz, 1H, CH_2OH), 3.68 (m, 1H, CH_2NH), 3.64–3.59 (m, 1H,CH_2CH_2O), 2.53 (t, J = 4.71 Hz, 1H,CH_2N), 2.44 (m, 1H, CH_2*N*mor), 2.41 (s, 3H, CH_3).

Elem. An. $C_{15}H_{23}N_5O_3S$ C = 50.97%; H = 6.56%; N = 19.81%; S = 9.07% Found C = 50.81%; H = 6.38%; N = 19.73%; S = 8.88%.

ESI-MS: m/z = 351.39 $[L + H]^+$

2.3.7. [GluOAc], glucose pentaacetate (7)

Pyridine (7 mL) and a small amount of 4-dimethylaminopyridine were added to a solution containing D-glucose (1 g, 9.24 mmol) dissolved in AcO_2 (7 mL). The solution was stirred in an ice-cold bath for 5 h and then at room temperature for 18 h. Dichlorometane (20 mL) and water (20 mL) were added to the solution, the organic phase was then separated and consecutively washed with a sat. aq. $CuSO_4$ until the dark blue color disappeared and then with water (20 mL). Then dried over Na_2SO_4 and concentrated under reduced pressure to give an oily product, which then crystallized.

Yield: 93%

^{1}H NMR (300 MHz, $CDCl_3$): δ_H (ppm) 6.34 (d, J = 3.68 Hz, H-1), 5.47 (t, J = 10.30, 1H, H-3), 5.15 (m, 1H, H-4), 5.10 (dd, J = 10.30, 3.68 Hz, 1H, H-2), 4.28 (dd, J = 12.58, 4.22 Hz, 1H, H-7), 4.11 (m, 2H H-5, H-6), 2.18 (s, 3H, OAc), 2.10 (s, 3H, Oac), 2.04 (s, 3H, Oac), 2.03 (s, 3H, Oac), 2.02 (s, 3H, Oac).

*2.3.8. [GluOAcBr], acetobromo-α-D-glucose (**8**)*

HBr, dissolved in acetic acid (33%), was added dropwise to a solution of glucose pentaacetate (**7**) (1 g, 2.56 mmol) in dichloromethane (5 mL) under nitrogen atmosphere. The reaction mixture was stirred at room temperature for 2 h, then ice-cold water (10 mL) was added and the mixture was extracted with CH_2Cl_2 (3·20 mL). The combined CH_2Cl_2 layers were washed with a saturated $NaHCO_3$ solution, H_2O, and brine, and the filtrate was evaporated in vacuo to give a thick oil, which subsequently solidified.

Yield: 95%. **^{1}H NMR** (300 MHz, $CDCl_3$): δ_H (ppm) 6.63 (d, J = 4.00 Hz, 1H, *H-1*), 5.58 (t, J = 9.72 Hz, 1H, *H-3*), 5.18 (t, J = 9.85 Hz, *H-4*), 4.85 (dd, J = 9.99, 4.05 Hz, 1H, *H-2*), 4.39–4.27 (m, 1H, *H-5*), 4.13 (m, 2H, *H-6*), 2.08 (4 s, 12H, *OAc*)

*2.3.9. [GluOAcNCS], 2,3,4,6-tetra-O-acetyl-β-D-glucose isothiocyanate (**9**)*

A mixture of potassium thiocyanate (0.200 g, 2 mmol), tetrabutylammonium chloride (0.285 g, 1 mmol) and molecular sieves (4 Å, 1,5 g) in acetonitrile was stirred at room temperature for 3 h. Then acetobromo-α-D-glucose (**8**) (0.423 g, 1 mmol) was added and the mixture refluxed until the reaction was complete as detected by TLC (AcOEt/C_6H_{12} 2:3). Then the solution was filtered and concentrated under pressure to afford a residue, which was purified by flash chromatography (silica gel, AcOEt/C_6H_{12} 2:3).

Yield: 80%

^{1}H NMR (300 MHz, $CDCl_3$): δ_H (ppm) 5.13 (m, 4H, *H-1*, *H-2*, *H-3*, *H-4*), 4.27 (dd, J = 12.45, 4.66 Hz, 1H, *H-6*), 4.17 (dd, J = 12.45, 2.27 Hz, 1H, *H-6*), 3.77 (ddd, J = 10.14, 4.66, 2.27 Hz, 1H, *H-5*), 2.13–2.05 (4 s, 12H, *OAc*)

Crystallographic data: C15H19N1O9S1, Mr. = 389.37, orthorhombic, space group $P2_12_12_1$, a = 5.543(1), b = 14.113(2), c = 25.078(4)Å, V = 1961.8(5)Å^3, Z = 4, ρcalc = 1.318 Mgm^{-3}, T = 298.15 K, F(000) = 816, crystal size = 0.20 × 0.20 × 0.10 mm, index range $-6 < h < 6$, $-17 < k < 16$, $-31 < l < 23$, collected reflections = 11,673, unique reflections = 3939, refined parameters = 255, goodness-of-fit = 0.952, final R factor = 0.0739, wR2 = 0.2415, electronic density residues = 0.51 and −0.47 eÅ^{-3}. The crystal structure is isomorphic with the one of acetylated glucose reported by Jones et al. [33].

*2.3.10. [GluOAcTSC], 2,3,4,6-tetra-O-acetyl-β-D-glucose thiosemicarbazide (**10**)*

A solution of 2,3,4,6-tetra-*O*-acetyl-β-D-glucose isothiocyanate (**9**) (0.67 g, 1.73 mmol) in EtOH (40 mL) was slowly added dropwise to a stirred solution of hydrazine monohydrate (86 μL, 1.76 mmol) in EtOH (25 mL) at 0 °C,. During the addition, a white precipitate formed. The solution was stirred for additional 5′ and the solid product was collected by filtration.

Yield: 76%. **^{1}H NMR** (300 MHz, d_6DMSO): δ_H (ppm) 9.28 (s, 1H, N*H*C═S), 8.20 (s, 1H, N*H*NH_2), 5.78 (t, J = 9.35 Hz, 1H, *H-1*), 5.39 (t, J = 9.35 Hz, 1H, *H-3*), 5.11 (t, J = 9.35 Hz, 1H, *H-2*), 5.09 (t, J = 9.35 Hz, 1H, *H-4*), 4.33 (dd, J = 12.42, 4.41 Hz, 1H, *H-6*), 4.14 (dd, J = 12.42, 2.07 Hz, 1H, *H-6*), 3.89 (ddd, J = 9.35, 4.41, 2.07 Hz, 1H, *H-5*), 2.00 (m, 12H, *OAc*).

Elem. An. $C_{15}H_{23}N_3O_9S$ C = 42.75%; H = 5.50%; N = 9.97%; S = 7.61% Found C = 42.63%; H = 5.37%; N = 9.82%; S = 7.48%.

ESI-MS: m/z = 422.40 $[L + H]^+$

*2.3.11. [CitrGluOAc], (1-S-Citronellal-4-(2,3,4,6-tetra-O-acetyl-β-D-glucosyl)-3-thiosemicarbazone) (**11**)*

A solution of citronellal (0.26 mL, 1.48 mmol) and acetylglucosylthiosemicarbazide (**10**) (0.62 g, 1.48 mmol) in EtOH (25 mL) was refluxed under stirring. After 24 min at reflux temperature, the mixture was cooled and the solution concentrated under reduced pressure. The product was then purified by flash chromatography (AcOEt/C_6H_{12} 1:3).

Yield: 86%

^{1}H NMR (300 MHz, $CDCl_3$): δ_H (ppm) 8.86 (s, 1H, *NH*), 7.13 (t, J = 8.39 Hz, 1H, *HC*═N), 5.95 (t, J = 8.89 Hz, 1H, *H-1*), 5.38 (t, J = 9.37 Hz, 1H, *H-3*), 5.15–5.02 (m, 2H, *H-2*, *H-4*) $H_{4,2}$, 4.33–4,03 (m, 2H, *H-6, H-6′*), 3.87 (m, 1H, *H-5*), 2.17 (m, 1H, *CH_2*CHN), 2.02–1.98 (m, 12H, *OAc*), 1.7 (m, 1H *CH*CH_3), 1.65–1.57 (2 s, 6H, *$(CH_3)_2$*C═), 1.23 (m, 1H, *CH_2*C*H*CH_3), 0.9 (d, 3H, CH*CH_3*)

Elem. An. $C_{25}H_{39}N_3O_9S$ C = 53.84%; H = 7.05%; N = 7.54%; S = 5.75% Found C = 53.77%; H = 6.86%; N = 7.43%; S = 5.60%.

ESI-MS: m/z = 558.62 $[L + H]^+$

*2.3.12. [CitrGlu], (1-S-citronellal-4-(β-D-glucosyl)-3-thiosemicarbazone) (**12**)*

A solution of CitrGluOAc (**11**) (0.37 g, 2.35 mmol) in dry methanol (50 mL) was heated to 50 °C in a Schlenk tube for 8 h in presence of a catalytic quantity of sodium methoxide.

Neutralization of the methoxide by Dowex 50WX4 acid ion-exchange resin, followed by filtration and evaporation of the filtrate, afforded a pure material as evidenced by ^{1}H NMR.

Yield: 98%. **^{1}H NMR** (300 MHz, $CDCl_3$): δ_H (ppm) 8.46 (s, 1H, *NH*), 8.06 (d, J = 8.76 Hz, 1H, *NH*), 7.46 (t, J = 5.84 Hz, 1H, *HC*═N), 5.27 (t, J = 8,74 Hz, 1H, *H-1*), 5,08 (t, J = 7.01 Hz, 1H, *HC* = C$(CH_3)_2$) 3.70–3.00 (m, 6H, *H-2, H-3, H-4, H-5, H-6, H-6′*), 2.23–2.05 (2 m, 1H, *CH_2*CHN),1.97 (m, 1H, *CH_2*CH = C) 1.64 (m, 1H, *CH*CH_3)1.64–1.57 (2 s, 6H, *$(CH_3)_2$*C═), 1.21 (m, 1H, *CH_2*CHCH_3), 0.88 (d, 3H, CH*CH_3*)

Elem. An. $C_{17}H_{31}N_3O_5S$ C = 52.42%; H = 8.02%; N = 10.79%; S = 8.23% Found C = 52.35%; H = 7.89%; N = 10.68%; S = 8.15%.

ESI-MS: m/z = 390.53 $[L + H]^+$

*2.3.13. [VanGluOAc], (1-vanillin-4-(2,3,4,6-tetra-O-aceto-β-D-glucosyl)-3-thiosemicarbazone) (**13**)*

A solution of glucosylthiosemicarbazide (**10**) (1 g, 2.35 mmol) and vanillin (0.37 g, 2.35 mmol) in ethanol (50 mL) was refluxed for 12 h. The solution was then cooled to room temperature, concentrated under reduced pressure, and purified by flash chromatography (AcOEt/C_6H_{12} 2:3). From the solution, crystals apt for single crystal X-ray diffraction determination were isolated.

Yield: 81%. **^{1}H NMR** (300 MHz, $CDCl_3$): δ_H (ppm) 9.88 (s, 1H, *NH*), 8.37 (d, J = 8.45 Hz, 1H, *HC*═N), 7.75 (s, 1H, *NH*), 7.52 (m, 1H, *Hvan*), 7.03 (dd, J = 8.14, 1.63 Hz, 1H, *CHvan*), 6.93 (d, J = 8.10 Hz, 1H, *CHvan*), 5.67 (t, J = 8.95 Hz, 1H, *H-1*), 5.44 (t, J = 9.49 Hz, 1H, *H-3*), 5.18 (td, J = 11.91, 9.58 Hz, 2H, *H-2, H-4,*), 4.43–4,15 (m, 2H, *H-6, H-7*), 4.04 (s, 3H, *CH_3*), 3.95 (m, 1H, *H-5*), 2,2–2,0 (m, 12H, *OAc*).

Crystallographic data: C23H29N3O11S1, Mr. = 553.54, orthorhombic, space group $P2_12_12_1$, a = 9.015 (2), b = 15.221(3), c = 19.882(4)Å, V = 2728.2(10)Å^3, Z = 4, ρcalc = 1.353 Mg·m^{-3}, T = 298.15 K, F(000) = 1168, crystal size = 0.60 × 0.40 × 0.20 mm, index range = $-11 < h < 11$, $-18 < k < 19$, $-25 < l < 19$, collected reflections = 16,954, collected reflections = 6297, refined parameters = 343, goodness-of-fit = 0.856, final R index = 0.0418, wR2 = 0.0898, electronic density residues = 0.25 and −0.16 eÅ^{-3}.

*2.3.14. [VanGlu], (1-vanillin-4-(β-D-glucosyl)-3-thiosemicarbazone) (**14**)*

A solution VanGluOAc (**13**) (0.37 g, 2.35 mmol) in dry methanol (50 mL) was refluxed for 8 h in the presence of a catalytic quantity of sodium methoxyde. Neutralization of the methoxyde by Dowex 50WX4 acid ion-exchange resin, followed by filtration and evaporation of the

filtrate afforded a pure material by ^{1}H NMR.

Yield: 98%. **^{1}H NMR** (300 MHz, D_2O): δ_H (ppm) 8.50 (s, 1H, *NH*), 8.25 (d, *J* = 9.11 Hz, 1H, *NH*), 7.92 (s, 1H, *CH*N), 7.22 (d, *J* = 1.57 Hz, 1H, CHvan), 6.97 (dd, *J* = 8.24, 1.71 Hz, 1H, CHvan), 6.51 (d, *J* = 8.19 Hz, 1H CHvan), 5.36 (t, *J* = 9.07 Hz, 1H, *H-1*), 3.76 (s, 3H, O*CH*$_3$), 3.70–3.00 (m, 6H, H-2-6).

Elem. An. $C_{15}H_{21}N_3O_7S$ C = 46.50%; H = 5.46%; N = 10.85%; S = 8.28% Found C = 46.39%; H = 5.41%; N = 10.73%; S = 8.09%.

ESI-MS: *m/z* = 388.38 $[L + H]^+$

2.3.15. [PyrGluOAc], (1-(pyridoxal)-4-(2,3,4,6-tetra-O-aceto-β-D-glucosyl)-3-thiosemicarbazone) ***(15)***

A solution of tetra-acetyl glucosylthiosemicarbazide (**10**) (1 g, 2.3 mmol) and pyridoxal (0.39 g, 2.3 mmol) in ethanol (50 mL) was refluxed for 12 h. Then the solution was cooled to r.t., concentrated under reduced pressure, and purified by flash chromatography (AcOEt/C_6H_{12} 10:1).

Yield: 81%. **^{1}H NMR** (300 MHz, $CDCl_3$): δ_H (ppm) 8.61 (s, 1H, *CH*pyr), 7.99 (s, 1H, *HC*═N), 5.98 (t, *J* = 9.13 Hz, 1H, *H-1*), 5.41 (t, *J* = 9.50 Hz, 1H, *H-3*), 5.31 (t, *J* = 5.30 Hz, 1H, *H-2*), 5.22 (d, *J* = 8,96 Hz, 1H, *NH*), 4.96 (t, *J* = 9.75 Hz, 1H, *H-4*), 4.58 (d, *J* = 5.26 Hz, 1H, *CH*$_2$Pyr), 4.11 (d, *J* = 9.99 Hz, 1H, *H-5*), 4.15 (m, 2H, *H-6, H-7*), 2.42 (s, 1H, *CH*$_3$), 2.01–1.91 (m, 12H, *OAc*)

Elem. An. $C_{23}H_{30}N_4O_{11}S$ C = 48.42%; H = 5.30%; N = 9.82%; S = 5.62% Found C = 48.39%; H = 5.12%; N = 9.75%; S = 5.45%.

ESI-MS: *m/z* = 571.43 $[L + H]^+$

2.3.16. [PyrGlu], (1-pyridoxal-4-(β-D-glucosyl)-3-thiosemicarbazone) ***(16)***

A solution of PyrGluOAc (**15**) (0.37 g, 2.35 mmol) in dry methanol (50 mL) was refluxed for 8 h in the presence of a catalytic quantity of sodium methoxyde. Neutralization of the methoxyde by Dowex 50WX4 acid ion-exchange resin, followed by filtration and evaporation of the filtrate afforded a pure material by ^{1}H NMR.

Yield: 97%. **^{1}H NMR** (300 MHz, $CDCl_3$): δ_H (ppm) 8.48 (s, 1H, *NH*), 7.89 (d, *J* = 9.32 Hz, 1H, *NH*), 7.48 (s, 1H, *CH*pyr), 7.24 (s, 1H, *HC*═N), 5.41–5.19 (m, 1H, *H-1*), 4.55 (s, 1H, *CH*$_2$OH), 3.70–3.00 (m, 6H, *H-2, H-3, H-4, H-5, H-6, H-6′*) 2.37 (s, 3H, *CH*$_3$).

Elem. An. $C_{15}H_{22}N_4O_7S$ C = 44.77%; H = 5.51%; N = 13.92%; S = 7.97% Found C = 44.61%; H = 5.36%; N = 13.75%; S = 7.80%.

ESI-MS: *m/z* = 403.39 $[L + H]^+$

2.4. Partition coefficient (Pow)

All LogPs were calculated with ALOGPS 2.1 software [34].

2.5. Syntheses of the complexes

Copper(II) and nickel(II) complexes were obtained by refluxing an ethanol solution of the parent thiosemicarbazone to which the inorganic salts were added, and then the reaction products were separated by filtration. A few compounds were obtained in crystalline form by slow evaporation of the reaction solvent. The complexes were characterized by elemental analysis, ESI-MS, and in some cases also by single crystal X-ray diffraction.

2.5.1. [Cu(CitrTSC)$_2$] ***(17)***

The metal complex was synthesized following a reported procedure [35]. A solution of $Cu(OAc)_2{\cdot}H_2O$ (0.05 mg, 0.25 mmol) in H_2O (10 mL) was added dropwise to a solution of CitrTSC (**1**) (0.11 g, 0.5 mmol) in EtOH (20 mL), at room temperature. The complex was isolated as dark red solid by slow solvent evaporation.

Yield: 90% Elem. An. $C_{22}H_{40}CuN_6S_2$: C = 51.18%; H = 7.81%; N = 16.28%; S = 12.42%. Found: C = 51.32%; H = 7.85%; N = 16.32%; S = 12.51%

2.5.2. [Ni(CitrTSC)$_2$] ***(18)***

The metal complex was synthesized following a reported procedure [30]. A solution of $Ni(OAc)_2{\cdot}4H_2O$ (0. mg, 0.044 mmol) in H_2O (10 mL) was added dropwise to a solution of CitrTSC (**1**) (19.98 mg, 0.088 mmol) in EtOH (20 mL), at room temperature. The complex was isolated as dark green crystals.

Yield: 92% **^{1}H NMR** (300 MHz, $CDCl_3$): δ_H (ppm) 6.81 (t, 1H, *J* = 6.0, C2H), 6.20 and 6.17 (2 s, 2H, 1H each, N1H2), 5.14 (m, 1H, C7H), 2.07 (m, 2H,3H2), 1.93 (m, 2H, C6H2), 1.65 and 1.61 (2 s, 6H, 3H each, C9H3 and C10H3), 1.31 (m, 1H, C4H), 1.22 (m, 2H, C5H2), 0.90 (d, 3H,*J* = 7.0, C11H3)

Elem. An. $C_{22}H_{40}N_6NiS_2$: C = 51.67%; H = 7.88%; N = 16.43%; S = 12.54%. Found: C = 51.60%; H = 7.82%; N = 16.57%; S = 12.58%

2.5.3. [Cu(CitrMor)$_2$] ***(19)***

The metal complex was synthesized following a reported procedure [25]. To a solution of ligand CitrMor (**2**) (0.40 g, 0.13 mmol) in EtOH (50 mL), at room temperature with stirring, was added $Cu(OAc)_2{\cdot}H_2O$ (0.13 g, 0.06 mmol). The resulting clear solution, reddish first and brown after a while, was left under stirring at room temperature for 1 h. The complex was isolated after slow evaporation of the solvent in the form of dark red crystals.

Yield: 90% Elem. An. $C_{34}H_{62}CuN_8O_2S_2$: C = 54.99%; H = 8.42%; N = 15.09%; S = 8.64%. Found:C = 55.10%; H = 8.01%; N = 15.48%; S = 8.59%.

2.5.4. [Ni(CitrMor)$_2$] ***(20)***

The metal complex was synthesized following a reported procedure [25]. To a solution of ligand CitrMor (**2**) (0.40 g, 0.11 mmol) in EtOH (50 mL), at room temperature with stirring, solid $Ni(OAc)_2{\cdot}4H_2O$ (0.10 g, 0.05 mmol) was added. The resulting clear solution, which was reddish at first and turned brown after a while, was stirred for 1 h at room temperature. The complex was isolated, after slow evaporation of the solvent, as green crystals.

Yield: 90% **^{1}H NMR** (300 MHz, $CDCl_3$): δ_H (ppm) 6.85 (t, 1H, *CH*═N), 5.39 (bs, 1H, CH_2*NH*CS), 5.08 (m, 1H, *CH* = $C(CH_3)_2$), 3.74 (m, 4H, OCH_2CH_2N + *CH*$_2$NHCS), 3.31 (t, 2H, NCH_2CH_2NH), 2.52 (m, 2H, $NHCH_2CH_2N_{Mor}$), 2.45 (t, 2H, NCH_2CH_2NH), 2.31 (m, 4H, OCH_2CH_2N,), 1.94 (2H, m, *CH*$_2$CH = $C(CH_3)_2$), 1.60 (1H, m, CH_2CHCH_3), 1.70 and 1.62 (6H, 2 s, 3H each, $CH(CH_3)_2$), 1.4–1.2 (m, 2H, $CH3CHCH_2CH_2$), 0.92 (d, 3H, $CHCH_3$).

Elem. An. $C_{34}H_{62}N_8NiS_2O_2$: C = 55.35%; H = 8.47%; N, 15.19%; S = 8.69% Found: C = 54.98%; H = 8.36%; N = 15.28%; S = 8.50%.

2.5.5. [Cu(CitrGlu)$_2$] ***(21)***

$Cu(OAc)_2{\cdot}H_2O$ (0.1 g, 0.51 mmol) was added to a solution of ligand CitrGlu (**12**) (0.40 g, 1.02 mmol) in EtOH (50 mL) and left at room temperature under stirring. After 3 h the solution was poured into a crystallizer and the product was obtained as brown powder after slow evaporation of the solvent. $Cu(CitrGlu)_2$ was obtained as amorphous solid.

Yield: 90% Elem. An: $C_{34}H_{60}CuN_6O_{10}S_2$ C = 48.58%; H = 7.19%; N = 10.00%; S = 7.63%. Found C = 48.36%; H = 7.10%; N = 10.10%; S = 7.59%.

ESI-MS: *m/z* 841.55 $[ML_2 + H]^+$

2.5.6. [Ni(CitrGlu)$_2$] ***(22)***

$Ni(OAc)_2{\cdot}4H_2O$ (0.068 g, 0.38 mmol) was added to a solution of ligand CitrGlu (**12**) (0.30 g, 0.77 mmol) in EtOH (50 mL), at room temperature with stirring. After 3 h of stirring, the solution was poured into a crystallizer and the solvent was left to evaporate slowly. Ni $(CitrGlu)_2$ was obtained as amorphous solid.

Elem. An: $C_{34}H_{60}N_6NiO_{10}S_2$ C = 48.87%; H = 7.24%; N = 10.06%; S = 7.67%. Found C = 48.80%; H = 7.14%; N = 10.01%; S = 7.59%.

ESI-MS: m/z = 836.32 $[ML_2 + H]^+$

2.5.7. [Cu(VanTSC)$_2$] (23)

$Cu(OAc)_2{\cdot}H_2O$ (0.13 g, 0.66 mmol) was added to a stirred solution of VanTSC (**3**) (0.300 g, 1.33 mmol) in EtOH (40 mL). The color immediately turned to green/yellow and a precipitate appeared.

The solution was refluxed for 3 h, then was cooled to r.t. and the green precipitate was collected by filtration.

Yield: 62% Elem. An. $C_{18}H_{20}CuN_6O_4S_2$ C = 42.22%; H = 3.94%; N = 16.41%; S = 12.52%. Found C = 42.53%; H = 3.90%; N = 16.38%; S = 12.37%.

ESI-MS: m/z = 513.13 $[ML_2 + H]^+$

2.5.8. [Ni(VanTSC)$_2$] (24)

$Ni(OAc)_2{\cdot}4H_2O$ (0.137 g, 0.77 mmol) was added to a solution of VanTSC (**3**) (0.350 g, 1.55 mmol) in EtOH (40 mL) under stirring and immediately the color turned to dark green. The solution was refluxed for 3 h, then it was cooled to r.t. and green crystals suitable for X-ray crystallography were obtained by slow solvent evaporation.

Yield: 70%

Elem. An. $C_{18}H_{20}N_6NiO_4S_2$ C = 42.62%; H = 3.97%; N = 16.57% Found C = 42.51%; H = 3.79%; N = 16.53%.

Crystallographic data: C26H44N6NiO8S2, Mr. = 691.50, triclinic, space group P-1, a = 6.859(2), b = 10.644(4), c = 11.797(4) Å, α = 72.869(6), β = 78.656(6), γ = 84.751(6)°; V = 806.5(5)Å^3, Z = 2, ρcalc = 1.423 Mg·m^{-3}, T = 298.15 K, F(000) = 732, crystal size = 0.30 × 0.20 × 0.20 mm, index range = −8 < h < 8, −13 < k < 13, −15 < l < 15, collected reflections = 9823, unique reflections = 3712, refined parameters = 220, goodness-of-fit = 1.018, final R factor = 0.0605, wR2 = 0.1736, electronic density residues = 1.19 and −1.15 eÅ^{-3}.

2.5.9. [Cu(VanMor)$_2$] (25)

$Cu(OAc)_2{\cdot}H_2O$ (0.055 g, 0.28 mmol) was added to a stirred solution of VanMor (**4**) (0.20 g, 0.56 mmol) in EtOH (40 mL), and immediately the color turned to brown and a precipitate formed.

The solution was stirred at r.t. for 3 h and then the precipitate was collected by filtration.

Yield: 64% Elem. An. $C_{30}H_{42}CuN_8O_6S_2$ C = 48.80%; H = 5.72%; N = 15.18% Found C = 49,19%; H = 5,78%; N = 15.4%.

ESI-MS: m/z = 739.25 $[ML_2 + H]^+$

2.5.10. [Ni(VanMor)$_2$] (26)

$Ni(OAc)_2{\cdot}4H_2O$ (0.05 g, 0.28 mmol) was added to a stirred solution of VanMor (**4**) (0.20 g, 0.56 mmol) in EtOH (40 mL). The color immediately turned to green and a precipitate appeared.

The solution was refluxed for 3 h, then it was cooled down at r.t. and the precipitate was collected by filtration.

Yield: 70% Elem. An. $C_{30}H_{42}N_8NiO_6S_2$ C = 49.12%; H = 5.77%; N = 15.28% Found C = 49.21%; H = 5.77%; N = 15.3%.

ESI-MS: m/z 732,579 $[ML_2 + H]^+$

2.5.11. [Cu(VanGlu)2] (27)

$Cu(OAc)_2{\cdot}H_2O$ (0.75 g, 0.38 mmol) was added to a stirred solution of VanGlu (**14**) (0.30 g, 0.77 mmol) in EtOH (40 mL). After 3 h of stirring, the solution was poured into a crystallizer and was allowed to evaporate slowly.

Yield: 65%

Elem. An. $C_{30}H_{40}CuN_6O_{14}S_2$ C = 43.08%; H = 4.82%; N = 10.05% Found C = 43.51%; H = 4.79%; N = 10.53%.

ESI-MS: m/z = 836.12 $[ML_2 + H]^+$

2.5.12. [Ni(VanGlu)$_2$] (28)

$Ni(OAc)_2{\cdot}4H_2O$ (0.137 g, 0.77 mmol) was added to a stirred solution of VanGlu (**14**) (0.350 g, 1.55 mmol) in EtOH (40 mL). After 3 h of stirring, the solution was poured into a crystallizer and was let to evaporate slowly and eventually the $Ni(VanGlu)_2$ compound was collected.

Yield: 70% Elem. An. $C_{30}H_{40}N_6NiO_{14}S_2$ C = 43.33%; H = 4.85%; N = 10.11%; S = 7.71%. Found C = 43.38%; H = 4.52%; N = 10.05%; S = 7.64%.

ESI-MS: m/z = 832.32 $[ML_2 + H]^+$

2.5.13. [Cu(PyrTSC)Cl$_2$]·2H$_2$O (29)

The metal complex was synthesized following a reported procedure. To a stirred solution of PyrTSC (**5**) (0.15 g, 0.62 mmol) in EtOH (40 mL) was added $CuCl_2{\cdot}2H_2O$ (0.106 g, 0.62 mmol) and immediately the color turned to green.

The solution was refluxed for 3 h and then was cooled to r.t., poured into a crystallizer and the product was obtained for slow solvent evaporation.

Yield: 46% Elem. An. $C_9H_{16}Cl_2CuN_4O_4S$, C = 26.32%; H = 3.93%; N = 13.64%; S = 7.81%. Found C = 26,22%; H = 4.08%; N = 13.57%; S = 7.78%.

ESI-MS: m/z = 339.22 $[MLCl]^+$

2.5.14. [Ni(PyrTSC)Cl$_2$] (30)

To a stirred solution of PyrTSC (**5**) (0.15 g, 0.62 mmol) in EtOH (40 mL), $NiCl_2{\cdot}6H_2O$ (0.14 g, 0.62 mmol) was added and immediately the color turned to orange and an orange powder precipitated. The solution was refluxed for 3 h, then it was allowed to cool to r.t. and the brown/orange precipitate was collected by filtration.

Yield: 57% Elem. An. $C_9H_{12}Cl_2N_4NiO_2S$ C = 29.22%; H = 3.27%; N = 15.15%; S = 8.67%. Found C = 29.38%; H = 3.45%; N = 15.01%; S = 8.58%.

ESI-MS: m/z = 334.39 $[MLCl]^+$

2.5.15. [Cu(PyrMor)Cl$_2$] (31)

$CuCl_2{\cdot}2H_2O$ (0.048 g, 0.28 mmol) was added to a solution of ligand PyrMor (**6**) (0.10 g, 0.28 mmol) in EtOH (25 mL), at room temperature with stirring. The solution turned immediately dark. After 3 h of stirring at r.t., the solution was poured into a crystallizer and the solvent slowly evaporated to afford a green powder.

Yield: 57% Elem. An. $C_{15}H_{23}Cl_2CuN_5O_3S$: C = 36.93%; H = 4.75%; N = 14.35%. Found: C = 36.81%; H = 4.85%; N = 14.57%;

ESI-MS: m/z = 452.33 $[MLCl]^+$

2.5.16. [Ni(PyrMor)Cl$_2$] (32)

Solid $NiCl_2{\cdot}6H_2O$ (0.10 g, 0.44 mmol) was added to a solution of ligand PyrMor (**6**) (0.20 g, 0.44 mmol) in EtOH (25 mL), at room temperature under stirring. The resulting brown solution, was stirred at r.t., and a precipitate appeared. After 2 h the brown/orange solid was collected by filtration.

Yield: 61% Elem. An. $C_{15}H_{23}Cl_2N_5NiO_3S$: C = 37.30%; H = 4.80%; N, 14.50%; S = 6.64%. Found: C = 37.26%; H = 4.71%; N = 14.42%; S = 6.59%.

ESI-MS: m/z = 447.50 $[MLCl]^+$

2.5.17. [Cu(PyrGlu)Cl$_2$] (33)

$CuCl_2{\cdot}2H_2O$ (0.12 g, 0.74 mmol) was added to a solution of PyrGlu (**16**) (0.300 g, 0.74 mmol) in MeOH (20 mL). The resulting solution was stirred at r.t. for 4 h and a dark brown powder appeared. This precipitate was then collected by filtration.

Yield 40% Elem. An. $C_{15}H_{22}Cl_2CuN_4O_7S$ C = 33.56%; H = 4.13%; N = 10.44%. Found C = 33.43%; H = 4.47%; N = 10.36%.

ESI-MS: m/z = 464.03 $[ML + H]^+$

*2.5.18. [Ni(PyrGlu)Cl_2] **(34)***

$NiCl_2{\cdot}6H_2O$ (0.17 g, 0.74 mmol) was added to a solution of PyrGlu (**16**) (0.300 g, 0.74 mmol) in MeOH (20 mL). The resulting solution was stirred at r.t. and an orange precipitate appeared. After 4 h the solid was collected by filtration.

Yield: 44% Elem. An. $C_{15}H_{22}Cl_2N_4NiO_7S$ C = 33.86%; H = 4.17%; N = 10.53%. Found C = 33.84%; H = 3.93%; N = 10.61%.

ESI-MS: m/z = 493.07 [ML + H + MeOH] $^+$.

2.6. Biological assays

Cell proliferation determinations were performed by MTS assay on several cell lines: HeLa, HL-60, HT29, Jurkat, K-562, MCF7, SK-N-MC, T-47D, U937.

HL-60, Jurkat, K562 and U937 cells were cultured in RPMI-1640, whereas HeLa, HT29, MCF7, SK-N-MC and T-47D cells in Dulbecco's Modified Eagle Medium (DMEM). All media were supplemented with 10% (v/v) fetal bovine serum, penicillin (100 U/mL), streptomycin (100 μg/mL) and L-Glutamine (2 mM). Adherent cells were grown as a subconfluent monolayer. Flasks and plates were maintained at 37 °C and 5% CO_2 in a humidified atmosphere.

CellTiter 96® Aq_{ueous} One Solution Cell Proliferation Assay was employed to perform MTS assay (Promega Corporation, Madison WI, USA). In brief, 100 μL of a suspension of cells in exponential growth (5×10^4/mL in complete medium without phenol red supplemented with 5% FCS) were added into flat-bottomed 96-well plates (FALCON®, Becton Dickinson, Meylan Cedex, France) 24 h prior to drug treatment. Plates were incubated at 37 °C in a humidified 5% CO_2 incubator. Cells were treated at different drug concentrations (0.5, 1, 5, 10, 50 μM) in quadruplicate for 24 h. Twenty microliters of MTS solution was then added in each well and allowed to incubate at 37 °C in 5% CO_2 for 4 h.

The OD was recorded at 450 nm with microplate reader (Multiskan EX, Thermo Electron Corporation, Vantaa, Finland). The percent growth was measured by the formula:

$$\text{Percent growth} = [1 - (OD_{450}\ \text{treated}/OD_{450}\ \text{control})] \times 100$$

The cytotoxicity response parameters GI_{50} (50% growth inhibition), TGI (total growth inhibition) and LC_{50} (50% lethal growth inhibition) were extrapolated from concentration-response curves.

3. Results and discussion

3.1. Chemistry

The ligands presented in this paper were obtained pure and in good yields and the corresponding metal complexes were isolated with the expected coordination geometry. The substituents on the thiosemicarbazone aminic nitrogen do not affect coordination; consequently, citronellal and vanillin derivatives behave as bidentate ligands [22,23,31], while the pyridoxal ones behave as S,N,O terdentate coordinating agents [14,36]. In all cases the coordination geometry is square planar as confirmed by the X-ray diffraction structure of compound **24** and those of compounds **18** [30], **19** [25], **20** [25] and **29** [36].

3.2. Crystal structure descriptions

*3.2.1. Vanillin-4-[2-(4-morpholinyl)ethyl]-3-thiosemicarbazone [VanMor], **(4)***

The structure of this compound (Fig. 3.1) is formed by three fragments: the thiosemicarbazide, the vanillin and the ethylmorpholine. In spite of the presence of conjugated bonds between the aromatic ring and the thiosemicarbazide fragment the system is not planar, but the two average planes of vanillin and thiosemicarbazide form an angle of 33.97°. The average plane of the morpholine fragment is almost perpendicular to the thiosemicarbazide plane forming an angle of 83.30°. The two dominant interactions that characterize the packing are a strong hydrogen bond between the OH of the vanillin fragment and the morpholine oxygen in position –x − 1, − y + 1, − z + 1 [OH…O 2.694(2)Å], and a weaker one between the sulfur and the hydrazine NH of an adjacent thiosemicarbazide group in position − x, − y, − z [NH… S 3.504(2)Å].

*3.2.2. 2,3,4,6-Tetra-O-acetyl-β-D-glucose isothiocyanate [GluOAcNCS], **(9)***

The ORTEP plot of compound **9** is reported in Fig. 3.2 and the crystal is isostructural with the corresponding non substituted acetylated sugar previously published by Jones et al. [33]

*3.2.3. [VanGluOAc], (1-vanillin-4-(2,3,4,6-tetra-O-aceto-β-D-glucosyl)-3-thiosemicarbazone) **(13)***

Also the structure of the molecule (Fig. 3.3) can be conveniently described as formed of three parts: the acetylated sugar, the thiosemicarbazide and the vanillin aromatic system. Notwithstanding the conjugated double bonds that extend from the vanillin moiety to the thiosemicarbazone fragment, also here the average planes of the two moieties form a remarkably large angle of 20.63°, probably due to packing requirements. The sugar ring is in a chair conformation with puckering parameters of phi2 = − 50.04, theta = 8.57 and QT of 0.59 [37]. The packing is mainly determined by two hydrogen bonds which connect the molecules in the crystallographic *xy* plane and by van der Waals interactions along the *z* direction. One between the hydrazine fragment N2—H and oxygen O7 of a carbonyl group belonging to an acetyl bonded to the sugar [N2···O7(x − 1/2, − y + 1/2, − z + 1) 3.109(5)Å]. This interaction creates a chain of molecules which propagate in the *x*-direction. In the *y*-direction the packing is determined by a hydrogen bond between the vanillin moiety hydroxyl group O1—H and another acetate carbonyl group bound to the sugar O1···O5 3.031 Å (− x + 1/2 + 1,-y, + z-1/2). In the *z*-direction the packing is characterized by van der Waals interactions between the sulfur atom and the methyls of the acetyl groups of the sugar.

*3.2.4. [Ni(VanTSC)$_2$] **(24)***

In the crystal structure (Fig. 3.4), the metal ion lies on a centre of symmetry in a square planar geometry with distances Ni—N and Ni—S of 1.908(4) and 2.1780(9)Å respectively, and a chelation angle of 85.63°. The coordination five-membered ring is slightly puckered, in an envelope conformation. The average plane of the thiosemicarbazide moiety and that of the vanillin aromatic system form an angle of 24.39°. The packing is characterized by the presence of ethanol molecules which take part in two four-centre systems of hydrogen bonds, one involving the terminal NH_2 group of the thiosemicarbazone and the other involving the OH group of the vanillin moiety.

3.3. Partition studies

Octanol/water partition coefficient (P) is the ratio between the concentration of a compound in octanol and its concentration in water ($P = [\text{analyte}]_{Octanol}/[\text{analyte}]_{Water}$). Partition coefficient is extensively used in the pharmaceutical sciences to evaluate the distribution of a molecule in the two phases of a mixture of two immiscible solvents at equilibrium. Hence, the partition coefficient is a measure of how much hydrophilic or hydrophobic a chemical substance is. In medical practice, partition coefficients are useful, for example, in estimating the distribution of drugs within the body [38].

Drugs with higher partition coefficients are distributed preferentially in hydrophobic compartments such as the lipid bilayers of cells, while drugs with lower partition coefficients are preferentially found in hydrophilic media, such as the blood serum. The values reported in Table 3.1 show that the ligands synthesized for the assays possess a wide variety of values that extend from 3.3 (maximum hydrophobicity) to − 1.4 (minimum hydrophobicity).

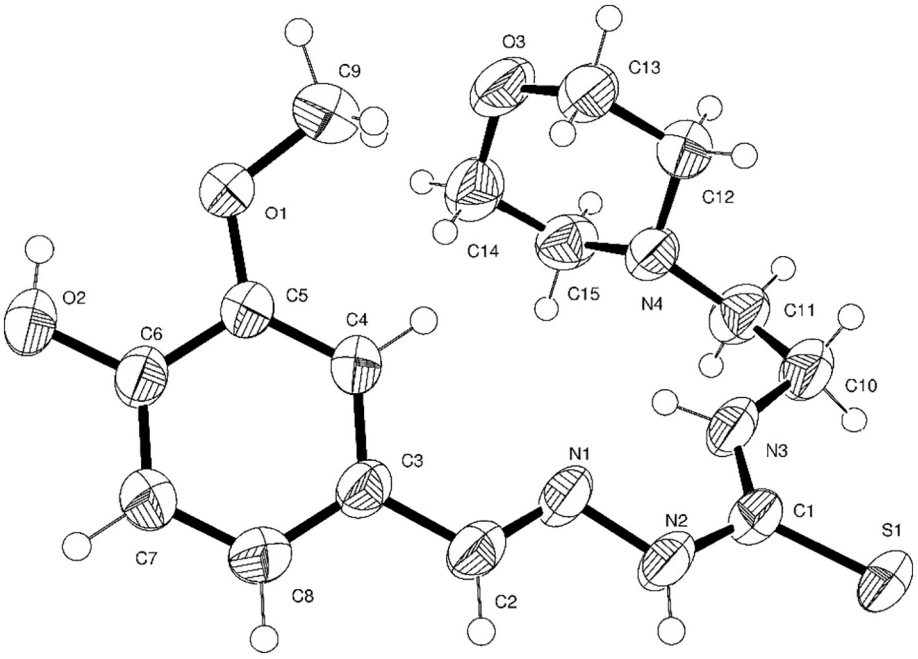

Fig. 3.1. ORTEP drawing of VanMor (50% probability plot).

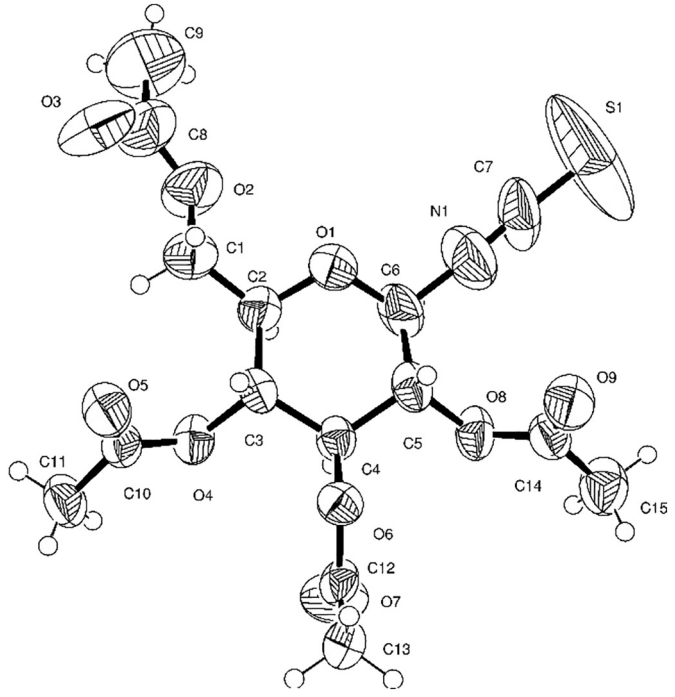

Fig. 3.2. ORTEP drawing of [GluOAcNCS] (50% probability plot).

3.4. Cell growth inhibition of ligands and complexes

All the ligands have shown no significant antiproliferative activity on cell line U937, at least up to 50 μM.

Since our interest was particularly aimed at understanding the role of the hydrophobic and hydrophilic nature of these molecules, biological evaluations were performed with molecules deriving from the ligands showing the higher and lower LogP values, leaving aside the pyridoxal derivatives.

Differently from the ligands, most of their metal complexes possess remarkable activity. From Table 3.2, it is apparent that copper derivatives are more active on U937 cells than those of nickel, but while the non-substituted thiosemicarbazones present activities of the same order of magnitude we observe remarkably low GI_{50} values for the ethylmorpholine copper derivatives. The most striking difference is observable between the copper glucosylated thiosemicarbazones for which the GI_{50} values pass from a 18 μM for the citronellal derivative to a > 50 μM for the vanillin thiosemicarbazone derivatives.

Besides testing the antiproliferative activity on cell lines U937 (histiocytic lymphoma) it has also been possible to extend the biological assays to cell line HT-29 (colon carcinoma). According to the NCI (National Cancer Institute) approach for the "60 human tumor cell line anticancer drug screen" (NCI60), growth inhibiting concentrations at 50% (GI_{50}, 50% Growth Inhibition), growth inhibiting at 100% (TGI, Total Growth Inhibition) and lethal at 50% of the cells (LC_{50}, 50% Lethal Concentration) have been determined. The evaluation has been carried out on a wide range of concentrations (0.5 ÷ 50 μM).

All citronellal and vanillin ligands present no antiproliferative activity up to a concentration of 50 μM. From the reported tables (Tables 3.3 and 3.4) it is apparent that this activity is strongly influenced by metal complexation.

In particular, compounds with $GI_{50} < 20$ μM on cell line U937 are nickel(II) complexes of CitrTSC, CitrMor, VanMor [$Ni(CitrTSC)_2$, $Ni(CitrMor)_2$, $Ni(VanMor)_2$] and copper(II) complexes of CitrTSC, CitrGlu, CitrMor, VanTSC and VanMor [$Cu(CitrTSC)_2$, $Cu(CitrGlu)_2$, $Cu(CitrMor)_2$, $Cu(VanTSC)_2$, $Cu(VanMor)_2$]. Among them the only complexes of Cu (II) having a $GI_{50} < 20$ μM on cell line HT29 are $Cu(CitrTSC)_2$ and $Cu(CitrMor)_2$. The glycosylation of the ligand seems to reduce the antiproliferative activity.

U937 cells have shown the highest sensitivity to both copper(II) and nickel(II) complexes of CitrMor, on the other hand only the Cu complex has been able to drastically reduce the proliferation of HT29 cells (Fig. 3.5).

Based on this results, histosensitivity has been tested for the molecule that resulted to be the most active on the two cell lines: complex $[Cu(CitrMor)_2]$.

All tested cell lines have shown a sensitivity to complex $Cu(CitrMor)_2$ with a $GI_{50} < 10$ μM, a strong antiproliferative effect (GI_{50}) at concentrations lower than 3 μM has been observed on human tumoral cell lines of different origin: HeLa (epitheloid cervix carcinoma); Jurkat (acute T cell leukemia), U937 (histiocytic lymphoma) and SK-N-MC (Neuroepithelioma) (Fig. 3.6).

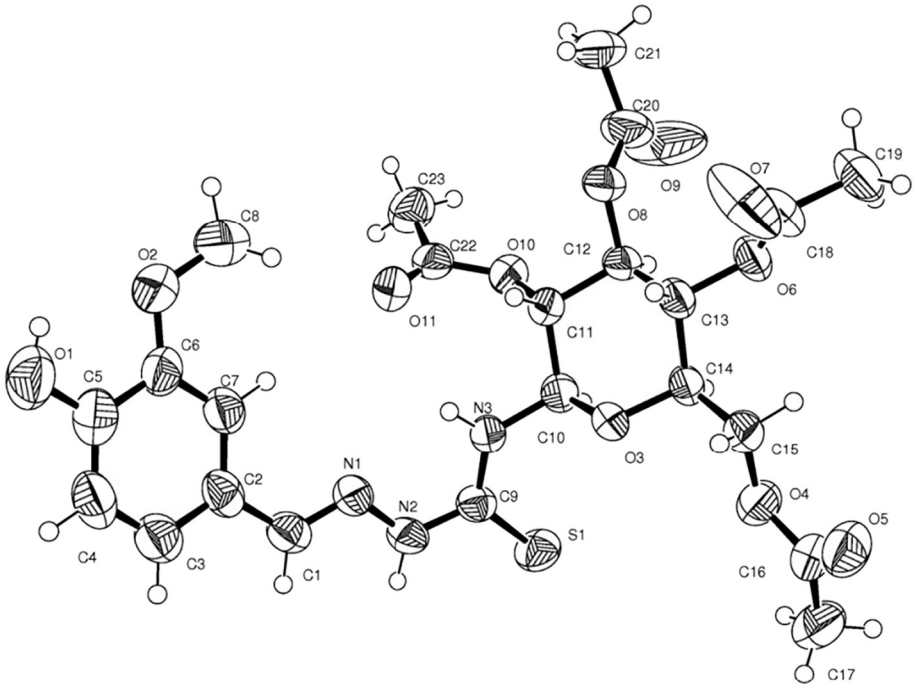

Fig. 3.3. ORTEP drawing of VanGluOAc (50% probability plot).

4. Conclusions

New thiosemicarbazones were synthesized with the aim to study how substituent groups, bringing to significant differences in terms of partition coefficient and metal coordination, influence their biological activity. The free ligands do not show any significant biological activity, independently from the presence or the absence of a substituent on the terminal aminic nitrogen. On the contrary, metal complexes show marked biological activity. In general, copper complexes present a higher proliferation inhibition. In particular, the copper complexes with the morpholine containing ligands exhibit stronger activities than the non-substituted and the glucosylated thiosemicarbazones. Worth of note is that the morpholine ligands are those with the partition coefficient closer to the values required for an effective lipid membrane crossing and this would make it easier for them to diffuse into the cytoplasm. The activity tests on vanillin and citronellal thiosemicarbazones were then extended to cell line HT29 (colon carcinoma). Also in this case, citronellal and vanillin ligands present no antiproliferative activity up to a concentration of 50 μM and the glucosylation of the ligand seems to reduce the antiproliferative activity. This is, once again, an important result, showing on the one hand that the search for an increased water solubility in fact does not increase the bioavailability and the biological activity of a lead compound; on the other hand, we can also note that the glucose residue does not improve the uptake rate and this allows us to exclude that the glucose receptors play a major role in the uptake of the glycosylated molecules.

Histosensitivity has been tested for the molecule that, from a first screening, resulted to be the most active, $Cu(CitrMor)_2$. All tested cell lines have shown a sensitivity to complex $Cu(CitrMor)_2$ with a $GI_{50} < 10$ μM, a strong antiproliferative effect (GI_{50}) at concentrations lower than 3 μM has been observed on cell lines Hela (cervix cancer), Jurkat (leukemia), U937 (leukemia) and SK-N-MC (CNS).

Acknowledgments

This work was supported by the University of Parma. The authors wish to thank the Centro Interdipartimentale Misure “Giuseppe Casnati” (C.I.M.) for the NMR facilities.

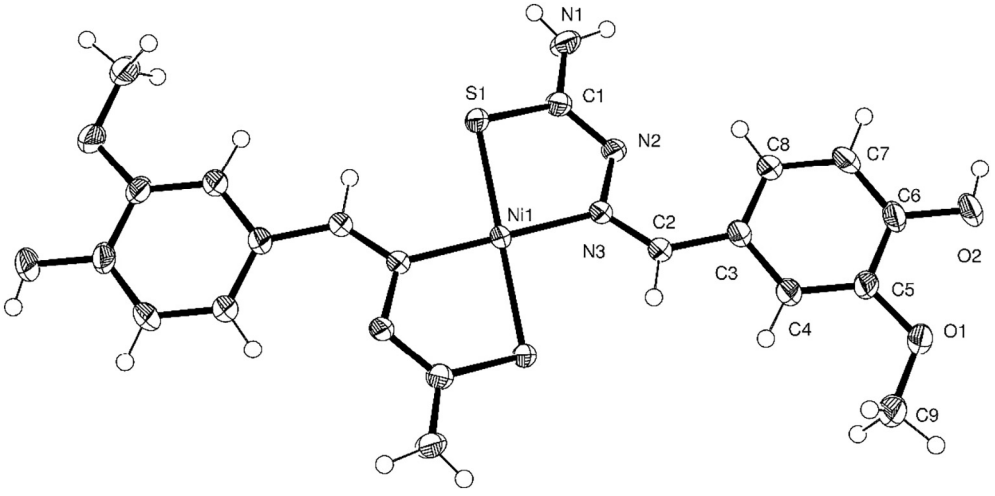

Fig. 3.4. ORTEP drawing of $[Ni(VanTSC)_2]$ (50% probability plot).

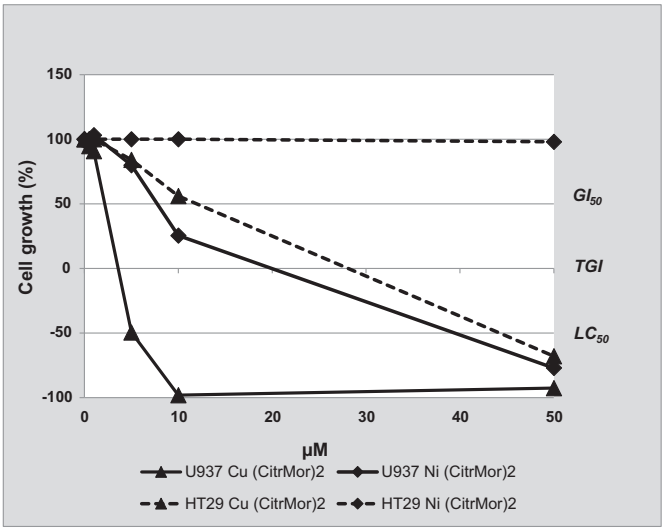

Fig. 3.5. Comparison of the antiproliferative activities of copper(II) and nickel(II) complexes of CitrMor on U937 and HT29 cell lines after 24 h treatment.

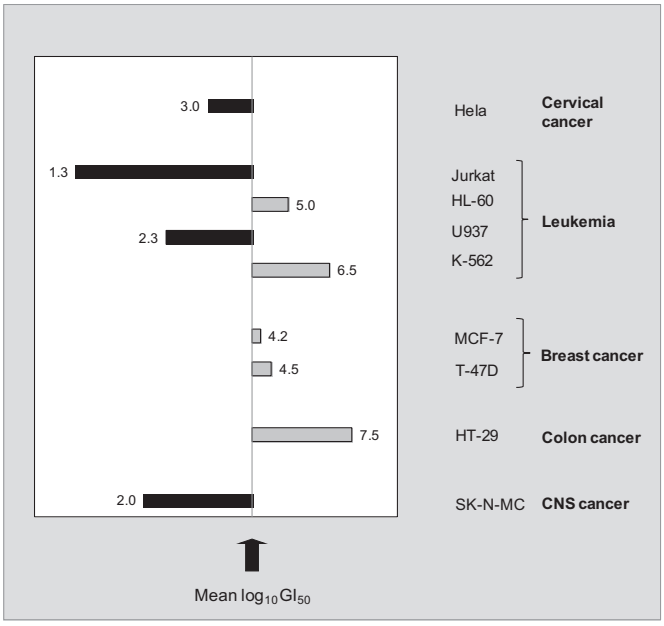

Fig. 3.6. Histosensitivity to complex $Cu(CitrMor)_2$ of the analyzed cell lines. In black the more sensitive lines, in grey the less sensitive. Numbers on the bars represent the relative GI_{50} for each cell line.

Appendix A. Supplementary data

Supplementary data to this article can be found online at https://doi.org/10.1016/j.jinorgbio.2017.11.009.

References

[1] J. Xu, J. Liu, X. Zhu, Y. Yu, S. Cao, Food Chem. 221 (2017) 1530–1538.
[2] M.T. Basha, J. Bordini, D.R. Richardson, M. Martinez, P.V. Bernhardt, J. Inorg. Biochem. 162 (2016) 326–333.
[3] A.E. Stacy, D. Palanimuthu, P.V. Bernhardt, D.S. Kalinowski, P.J. Jansson, D.R. Richardson, J. Med. Chem. 59 (2016) 4965–4984.
[4] J.T. Wilson, X. Jiang, B.C. McGill, E.C. Lisic, J.E. Deweese, Chem. Res. Toxicol. 29 (2016) 649–658.
[5] F. Degola, C. Morcia, F. Bisceglie, F. Mussi, G. Tumino, R. Ghizzoni, G. Pelosi, V. Terzi, A. Buschini, F.M. Restivo, T. Lodi, Int. J. Food Microbiol. 200 (2015) 104–111.
[6] F. Bisceglie, A. Musiari, S. Pinelli, R. Alinovi, I. Menozzi, E. Polverini, P. Tarasconi, M. Tavone, G. Pelosi, J. Inorg. Biochem. 152 (2015) 10–19.
[7] F. Degola, F. Bisceglie, M. Pioli, S. Palmano, L. Elviri, G. Pelosi, T. Lodi, F.M. Restivo, Appl. Microbiol. Biotechnol. 101 (2017) 6683–6696.
[8] K. Pelivan, W. Miklos, S. van Schoonhoven, G. Koellensperger, L. Gille, W. Berger, P. Heffeter, C.R. Kowol, B.K. Keppler, J. Inorg. Biochem. 160 (2016) 61–69.
[9] B.V. Silva, B.N.M. Silva, Med. Chem. 13 (2017) 110–126.
[10] M.T. Huuskonen, Q.Z. Tuo, S. Loppi, H. Dhungana, P. Korhonen, L.E. McInnes, P.S. Donnelly, A. Grubman, S. Wojciechowski, K. Lejavova, Y. Pomeshchik, L. Periviita, L. Kosonen, M. Giordano, F.R. Walker, R. Liu, A.I. Bush, J. Koistinaho, T. Malm, A.R. White, P. Lei, K.M. Kanninen, Neurotherapeutics 14 (2017) 519–532.
[11] J.W. Espíndola, M.V. Cardoso, G.B. Filho, D.A. Oliveira, E. Silva, D.R. Moreira, T.M. Bastos, C.A. Simone, M.B. Soares, F.S. Villela, R.S. Ferreira, M.C. Castro, V.R. Pereira, S.M. Murta, P.A. Sales Junior, A.J. Romanha, A.C. Leite, Eur. J. Med. Chem. 101 (2015) 818–835.
[12] D.S. Kalinowski, P. Quach, D.R. Richardson, Future Med. Chem. 1 (2009) 1143–1151.
[13] N.S.H.N. Moorthy, N.M.F.S.A. Cerqueira, M.J. Ramos, P.A. Fernandes, Mini-Rev. Org. Chem. 13 (2013) 10.
[14] G. Pelosi, F. Bisceglie, F. Bignami, P. Ronzi, P. Schiavone, M.C. Re, C. Casoli, E. Pilotti, J. Med. Chem. 53 (2010) 8765–8769.
[15] G. Pelosi, Open crystallography, Journal 3 (2010) 12.
[16] R.J. Glisoni, D.A. Chiappetta, A.G. Moglioni, A. Sosnik, Pharm. Res. 29 (2012) 739–755.
[17] F. Bacher, É. Enyedy, N.V. Nagy, A. Rockenbauer, G.M. Bognár, R. Trondl, M.S. Novak, E. Klapproth, T. Kiss, V.B. Arion, Inorg. Chem. 52 (2013) 8895–8908.
[18] E. Palma, F. Mendes, G.R. Morais, I. Rodrigues, I.C. Santos, M.P. Campello, P. Raposinho, I. Correia, S. Gama, D. Belo, V. Alves, A.J. Abrunhosa, I. Santos, A. Paulo, J. Inorg. Biochem. 167 (2017) 68–79.
[19] E.A. Akam, E. Tomat, Bioconjug. Chem. 27 (2016) 1807–1812.
[20] H. Pelicano, D.S. Martin, R.H. Xu, P. Huang, Oncogene 25 (2006) 4633–4646.
[21] P. Knapp, A. Chabowski, D. Harasiuk, J. Górski, Horm. Metab. Res. 44 (2012) 436–441.
[22] F. Bisceglie, S. Pinelli, R. Alinovi, P. Tarasconi, A. Buschini, F. Mussi, A. Mutti, G. Pelosi, J. Inorg. Biochem. 116 (2012) 195–203.
[23] F. Bisceglie, R. Alinovi, S. Pinelli, M. Goldoni, A. Buschini, S. Franzoni, A. Mutti, P. Tarasconi, G. Pelosi, Metallomics 5 (2013) 1510–1518.
[24] A. Buschini, S. Pinelli, R. Alinovi, F. Mussi, F. Bisceglie, C. Rivetti, N. Doniselli, G. Pelosi, Metallomics 6 (2014) 783–792.
[25] M. Belicchi-Ferrari, F. Bisceglie, A. Buschini, S. Franzoni, G. Pelosi, S. Pinelli, P. Tarasconi, M. Tavone, J. Inorg. Biochem. 104 (2010) 199–206.
[26] G. Sheldrick, Göttingen, Germany (1997).
[27] L.J. Farrugia, J. Appl. Crystallogr. (2012) 849–854.
[28] C.F. Macrae, I.J. Bruno, J.A. Chisholm, P.R. Edgington, P. McCabe, E. Pidcock, L. Rodriguez-Monge, R. Taylor, J. van de Streek, P.A. Wood, J. Appl. Crystallogr. (2008) 466–470.
[29] M.J. Camarasa, P. Fernández-Resa, M.T. García-López, F.G. De Las Heras, P.P. Méndez-Castrillón, A. San Felix, Synthesis 6 (1984) 2.
[30] A. Buschini, S. Pinelli, C. Pellacani, F. Giordani, M.B. Ferrari, F. Bisceglie, M. Giannetto, G. Pelosi, P. Tarasconi, J. Inorg. Biochem. 103 (2009) 666–677.
[31] D. Rogolino, A. Bacchi, L. De Luca, G. Rispoli, M. Sechi, A. Stevaert, L. Naesens, M. Carcelli, J. Biol. Inorg. Chem. 20 (2015) 1109–1121.
[32] M. Ferrari Belicchi, G. Fava Gasparri, E. Leporati, C. Pelizzi, P. Tarasconi, G. Tosi, J. Chem. Soc. Dalton Trans. 11 (1986) 2461–2465.
[33] P.G. Jones, G.M. Sheldrick, A.J. Kirby, R. Glenn, Z. Krist. Krist. Krist. Krist. 161 (1982) 245.
[34] I.V. Tetko, J. Gasteiger, R. Todeschini, A. Mauri, D. Livingstone, P. Ertl, V.A. Palyulin, E.V. Radchenko, N.S. Zefirov, A.S. Makarenko, V.Y. Tanchuk, V.V. Prokopenko, J. Comput. Aided Mol. Des. 19 (2005) 453–463.
[35] M. Ferrari, F. Bisceglie, G. Pelosi, M. Sassi, P. Tarasconi, M. Cornia, S. Capacchi, R. Albertini, S. Pinelli, J. Inorg. Biochem. 90 (2002) 113–126.
[36] M. Belicchi Ferrari, G. Gasparri Fava, C. Pelizzi, P. Tarasconi, G. Tosi, J. Chem. Soc. Dalton Trans. (1987) 227–233.
[37] D. Cremer, J.A. Pople, J. Am. Chem. Soc. 97 (1975) 1354–1358.
[38] R. Mannhold, G.I. Poda, C. Ostermann, I.V. Tetko, J. Pharm. Sci. 98 (2009) 861–893.